Preface

While books have been written on many topics of Polymer Science, no comprehensive treatise on long-chain branching has ever been composed. This series of reviews in Volume 142 and 143 of Advances in Polymer Science tries to fill this gap by highlighting active areas of research on branched polymers.
Long-chain branching is a phenomenon observed in synthetic polymers and in some natural polysaccharides. It has long been recognized as a major molecular parameter of macromolecules. Its presence was first surmised by H. Staudinger and G. V. Schulz (Ber. 68, 2320, 1935). Interestingly, their method of identification by means of the abnormal relation between intrinsic viscosity and molecular weight has survived to this day. Indeed, the most sophisticated method for analysis of long-chain branching uses size exclusion fractionation with the simultaneous recording of mass, molecular weight and intrinsic viscosity of the fractions.

In the 1940s and 1950s, random branching in polymers and its effect on their properties was studied by Stockmayer, Flory, Zimm and many others. Their work remains a milestone on the subject to this day. Flory dedicated several chapters of his "Principles of Polymer Chemistry" to non-linear polymers. Especially important at that time was the view that randomly branched polymers are intermediates to polymeric networks. Further developments in randomly branched polymers came from the introduction of percolation theory. The modern aspects of this topic are elaborated here in the chapter by W. Burchard.

As polymer science developed, greater control over the architecture of polymer molecules was obtained. In polyolefins synthesis, this was due to the introduction of new catalysts. The development of anionic living polymerization with the concomitant formation of narrow molecular weight distribution polymers and an highly reactive functional end group opened the route not only to block copolymers but also to branched polymers with highly controlled architectures such as stars, combs and graft copolymers. The model polymers allowed us to establish relations between the molecular architecture and the physical properties of the branched polymers. This development has been reviewed by e.g.G.S. Grest et al. Adv. Chem. Phys. 94, 65 (1996).

One chapter in this series deals with the newer use of cationic polymerization to form polymers and copolymers with controlled long-chain branched struc-

tures. Another chapter deals with the use of anionic polymerization to prepare asymmetric star polymers. The asymmetry is introduced when the arms of the polymer differ in molecular weight, chemical composition or in their topological placement. The synthesis of these polymers has led to new insights in microseparation processes of block copolymers. Anionic and cationic living polymerization has also led to macromonomers. Highlights of recent developments in poly(macromonomers) homo, comb and graft copolymers are reviewed by K. Ito. The poly(macromonomers) with their multiple densely packed small linear subchains often lead to monomolecular micelles.

Very recently, highly regular, highly controlled, dense branching has been developed. The resulting "dendrimers" often have a spherical shape with special interior and surface properties. The synthesis and properties of dendrimers has been reviewed (see e.g. G.R. Newkome et al. "Dendritic Molecules", VCH, 1996). In this series, a chapter deals with the molecular dimensions of dendrimers and with dendrimer-polymer hybrids. One possible development of such materials may be in the fields of biochemistry and biomaterials. The less perfect "hyperbranched polymers" synthesized from A_2B-type monomers offer a real hope for large scale commercialization. A review of the present status of research on hyperbranched polymers is included.

The link between the long-chain branch structure and the properties of the polymer has to be established experimentally by means of model branched polymers. This link can also be derived theoretically or through computer modeling. As a result, a large sub-field of study has emerged. The methods and results of this theoretical work are systematically reviewed by J. Freire. Where available, comparisons with experimental results are made.

The final chapter develops the most modern insights in the relation between the rheological properties and the large scale architecture of polymers. Indeed, the largest effects of branching are encountered in their melt relaxation properties. In the absence of reptation, which dominates relaxation processes in linear polymers, a rich variety of other relaxation processes becomes apparent. The control ot the melt properties of polymers by means of their long-chain branch architecture will continue to lead to new industrial applications.

Ottawa, July 1998 J. Roovers

Hyperbranched Polymers

Anders Hult[1], Mats Johansson and Eva Malmström

Department of Polymer Technology, Royal Institute of Technology, SE-100 44 Stockholm, Sweden; [1]*E-mail: andult@polymer.kth.se*

Polymers obtained from the statistical polymerization of A_xB monomers by means of condensation or addition procedures are referred to as hyperbranched polymers. The paper aims to give a brief historical background and to give a survey of hyperbranched polymers in the literature.

Polymerization of A_xB monomers yields highly branched polymers, with a multitude of end groups, which are less prone than linear polymers to form entanglements and undergo crystallization. Hyperbranched polymers are phenomenologically different from linear polymers; for example, the lack of entanglements results in lower viscosity than in linear polymers of the same molecular weight. The thermal properties of hyperbranched polymers have been shown to depend on the nature of the chain ends. The lower the polarity, the lower the glass transition temperature since it is suggested that the glass transition of hyperbranched polymers is due to translational motions.

Hyperbranched polymers are unique in that their properties are easily tailored by changing the nature of the end groups. For some areas, such as coating resins and toughening in epoxy-resins, hyperbranched polymers are foreseen to play an important role. Various applications have been suggested, even though only a few have been commercialized at this time.

Keywords. Hyperbranched polymers, Dendritic, Synthesis, Properties, Application

Advances in Polymer Science, Vol.143

List of Symbols and Abbreviations

ATRP	atom transfer radical polymerization
A_xB	general structure of monomer with one B-functional group and *x* A-functional groups
bis-MPA	2,2-bis(methylol)propionic acid
B_y	y-functional monomer
CMC	critical micelle concentration
D	dendritic units (fully branched A_xB-units) in a hyperbranched polymer
DB	degree of branching
DBTDL	dibutyltin dilaureate

DSC	differential scanning calorimetry
f	total number of functional groups on a monomer
G_{ic}	critical energy release rate
L	linear units (at least one A-group is left unreacted after polymerization) in a hyperbranched polymer
LALLS	low angle laser light scattering
LC	liquid crystalline
M_c	critical molecular weight for the formation of entanglements
M_n	number-average molecular weight
M_w	weight-average molecular weight
NMR	nuclear magnetic resonance
p	fractional conversion of monomer
P_a	reacted fraction of A-groups
P_b	reacted fraction of B-groups
pm V^{-1}	picometer per volt
PVT	pressure-volume-temperature
SCVP	self condensing vinyl polymerization
SEC	size exclusion chromatography
T	terminal unit (all A-functional groups on an A_xB-unit are left unreacted)
TEMPO	2,2,6,6-tetramethyl-piperidinyl-1-oxy
T_g	glass transition temperature
TGA	thermogravimetrical or thermo-gravimetrical analysis
THF	tetrahydrofuran
X_n	number-average degree of polymerization
X_w	mass-average degree of polymerization
z	number of monomers
α	branching coefficient
$[\eta]$	intrinsic viscosity
η^*	complex dynamic viscosity

1 Introduction

At the end of World War II, synthetic polymers started to be utilized for commercial products. Ever since, materials engineers have been trying to improve polymer properties by increasingly ingenious methods. The most common techniques have been either simply to develop a new monomer and synthesize a new polymer, or to modify an existing polymer by some chemical route: modifications are often effected by changing a catalyst or using different co-monomers. For example, short-chain and long-chain branching have been extensively used to modify properties such as crystallinity and viscosity. Various grades of branched polyethylenes play an important role as engineering polymers today. Highly branched polymers have so far mainly been used as oligomers in ther-

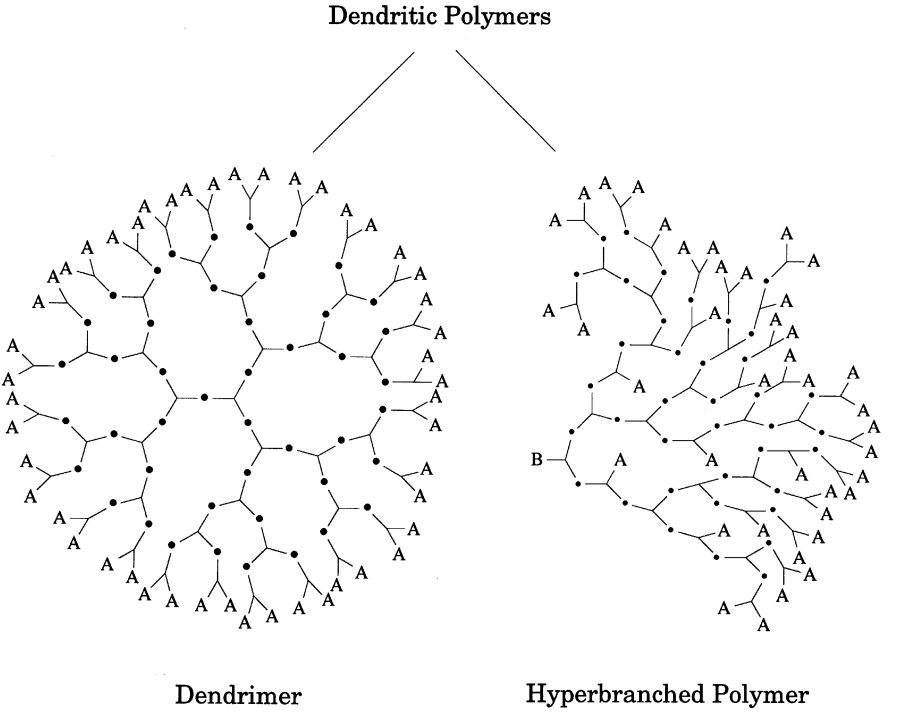

Fig. 1. Schematic description of dendritic polymers comprising dendrimers and hyperbranched polymers

mosets for high solid coating binders, alkyds, and in resins for composites. The most widely used of these is probably etherified hexamethylol melamine.

When Paul Flory wrote his famous book Principles of Polymer Chemistry in 1952, he indicated an alternative scheme for polymer synthesis [1]. He theorized about synthesizing condensation polymers from multifunctional monomers. These polymers were predicted to have a broad molecular weight distribution and to be non-entangled and non-crystalline due to their highly branched structure. However, they were considered to be less interesting since they would provide materials with poor mechanical strength, and at that time Flory did not feel it was worthwhile pursuing this line of research.

A little more than 30 years later, the first papers on synthesis of dendritic polymers emerged (dendron, Greek for "tree") and revealed properties nobody could have foreseen. Dendritic polymers synthesized from A_xB-monomers comprise monodisperse dendrimers with exact branching and irregularly branched, polydisperse, hyperbranched polymers (Fig. 1). The dendritic polymers turned out to have a number of very unique and different properties compared to their linear analogs; for instance, at high enough molecular weight they were found to

be globular. In contrast to linear polymers, the dendritic macromolecules behaved more like molecular micelles [2].

Dendrimers, or arborols, or cascade, or cauliflower, or starburst polymers, were first synthesized in the early 1980s [3, 4]. In 1985 Tomalia et al. [5] and Newkome et al. [6] presented the first papers dealing with dendrimers. A multitude of dendrimers have been presented in the literature ranging from polyamidoamine [7, 8], poly(propylene imine) [9, 10], aromatic polyethers [11–13] and polyesters [14, 15], aliphatic polyethers [16] and polyesters [17], polyalkane [18–19], polyphenylene [20], polysilane [21] to phosphorus [22] dendrimers. Combinations of different monomers as well as architectural modifications have also been presented. For example, chirality has been incorporated in dendrimers [23, 24]. Copolymers of linear blocks with dendrimer segments (dendrons) [25–27] and block-copolymers of different dendrons have been described [28].

The initially published work on dendritic polymers focused on the preparation of perfect monodisperse dendrimers. These well-defined macromolecules have very interesting material properties, but the synthesis is often time-consuming and elaborate. For use as engineering materials they are far too complicated and costly to produce. This was soon realized by researchers at DuPont Experimental Station, from which several publications emerged in the early 1990s [29–31]. Kim and Webster were working on dendritic polymers as rheology control agents and as spherical multifunctional initiators. It was necessary to obtain the material rapidly and in large quantities. This forced them to develop a route for a one-step synthesis of dendritic polyphenylenes [30–32]. These polymers were polydisperse, and had defects in the form of built-in linear segments but they were highly branched dendritic molecules. Kim and Webster named them *Hyperbranched Polymers*. Ever since, a wide variety of hyperbranched polymers have been presented in the literature and some of them will be further described in Sect. 3.

The synthesis of hyperbranched polymers can often be simplified compared to that of dendrimers as it does not require the use of protection/deprotection steps. This is due to the fact that hyperbranched polymers are allowed to contain some linearly incorporated A_xB monomers. The most common synthesis route follows a one-pot procedure where A_xB monomers are condensed in the presence of a catalyst. Another method using a core molecule and an A_xB monomer has also been described.

The lower cost of synthesizing hyperbranched polymers allows them to be produced on a large scale, giving them an advantage over dendrimers in applications involving large amounts of material, although the properties of hyperbranched polymers are intermediate between those of dendrimers and linear polymers [33].

Dendritic polymers are most often reported to be amorphous, which can be anticipated from their highly branched architecture. However, some exceptions are presented in the literature. Percec et al. [34, 35] reported on liquid crystalline (LC) hyperbranched polymers where the LC-phase was achieved by conformational isomerism. Various repeat units of A_2B type have been used where a flex-

ible spacer and a mesogenic unit are combined in the same monomer. Our laboratory has recently reported results on various alkyl-terminated hyperbranched aliphatic polyesters which were shown to be crystalline when analyzed by differential scanning calorimetry and X-ray scattering [36]. Similar results have also been observed for dendrimers with terminal alkyl chains [37].

We will focus on the variety of different hyperbranched polymers that have been synthesized, on the specific properties that hyperbranched polymers exhibit, and hopefully stimulate the reader to find new and unique areas where these novel materials can find future applications.

2
General Concepts

A majority of the hyperbranched polymers reported in the literature are synthesized via the one-pot condensation reactions of A_xB monomers. Such one-step polycondensations result in highly branched polymers even though they are not as idealized as the generation-wise constructed dendrimers. The often very tedious synthetic procedures for dendrimers not only result in expensive polymers but also limit their availability. Hyperbranched polymers, on the other hand, are often easy to synthesize on a large scale and often at a reasonable cost, which makes them very interesting for large-scale industrial applications.

2.1
Polycondensation of A_xB Monomers

In nature, polycondensations of trifunctional monomers having two different functional groups occur under enzymatic control, resulting in tree-shaped, highly branched, but still soluble, macromolecules.

Flory showed great interest in polycondensation reactions and presented one of the first mechanisms for polyesterification reactions [38, 39]. Stockmayer [40–42] was a pioneer in exploring polycondensations leading to branched products. He was closely followed by Flory who also described the condensation reaction of A_xB monomers from a theoretical point of view [1]. The calculations were simplified by assuming that (i) the only allowed reaction is between an A group and a B group, (ii) no intramolecular condensation reactions occur, and (iii) the reactivity of a functional groups is independent of molecular size. Flory predicted that such a polymer will have a highly branched structure and a multitude of end groups (Fig. 2).

If z monomers are coupled together, the resulting molecule will contain only a single B group and (fz–2z+1) A groups, where f is the total number of functional groups on the monomer. For simplicity, the following will concern an $A_{f-1}B$ monomer with f=3. The probability that an arbitrarily chosen A group has reacted is P_a and equals the reacted fraction of A groups. The reacted fraction of B groups, P_b, is $p_b(f-1)$ due to the structure of the monomer. A branching coefficient, α, is defined as the probability that a given functional group on a branch

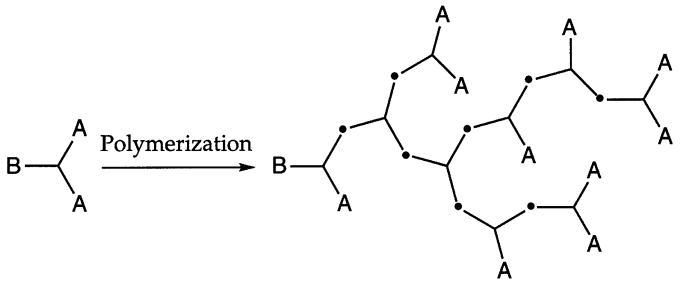

Fig. 2. Principal formation of a condensation polymer based on an A_2B monomer as proposed by Flory

unit is connected to another branch unit. An expression for the branching coefficient is obtained if p_b is replaced with the conversion, p:

$$\alpha = \frac{p}{f-1} . \tag{1}$$

It is possible to derive the number-average degree of polymerization, X_n, as

$$X_n = \frac{1}{1-p} = \frac{1}{1-\alpha(f-1)} \tag{2}$$

and also the weight-average degree of polymerization, X_w, as

$$X_w = \frac{[1-\alpha^2(f-1)]}{[1-\alpha(f-1)]^2} \tag{3}$$

From Eqs. (2) and (3) it is possible to calculate the molecular weight distribution, X_w/X_n, of the system:

$$\frac{X_w}{X_n} = \frac{[1-\alpha^2(f-1)]}{1-\alpha(f-1)} = \frac{(1-\alpha p)}{1-p} \tag{4}$$

From Eq. (4) it can be seen that as the conversion is driven towards completion, i.e., p is close to unity, the molecular weight distribution increases dramatically. Theoretically, polycondensation of A_2B monomers should form an infinite molecule at extremely high conversions, though in practice this is seldom observed. Flory concluded that condensation of A_xB monomers would give randomly branched molecules without network formation [1]. However, the occurrence of unwanted reactions (an A group reacts with an A group, for instance) will eventually give rise to an infinite network. Therefore, side-reactions have to

be suppressed. Intramolecular reactions, on the other hand, reduce the molecular weight and molecular weight distribution.

Since the time of Flory, only a few papers have appeared in the literature in which the kinetics of A_2B condensation reactions are treated. A purely theoretical paper was recently published by Möller et al. where Flory´s theory of A_nB polycondensations was expanded to describe the distribution of molecules containing arbitrary numbers of branching units [43]. In another paper, Hult and Malmström studied the kinetics of a reacting system based on 2,2-bis(hydroxymethyl)propionic acid [44].

2.2 Synthetic Approaches

A wide variety of monomers, such as (3,5-dibromophenyl)boronic acid, 3,5-bis(trimethylsiloxy)benzoyl chloride, 3,5-diacetoxybenzoic acid, and 2,2-dimethylol propionic acid have been used for the synthesis of hyperbranched polymers. A selection of these polymers are described in Sect. 3. The majority of the polymers are synthesized via step-wise polymerizations where A_xB monomers are bulk-polymerized in the presence of a suitable catalyst, typically an acid or a transesterification reagent. To accomplish a satisfactory conversion, the low molecular weight condensation product formed during the reaction has to be removed. This is most often achieved by a flow of argon or by reducing the pressure in the reaction flask. The resulting polymer is usually used without any purification or, in some cases, after precipitation of the dissolved reaction mixture into a non-solvent.

When polymerizing A_2B monomers there is a possibility of losing the unique focal point due to intramolecular cyclization. The loss of the focal point in a hyperbranched polyester based on 4,4-(4´-hydroxyphenyl)pentanoic (Fig. 7) acid was closely examined by Hawker et al. [45]. The study showed no significant occurrence of intramolecular cyclization. One disadvantage of polycondensation polymers is that they are sensitive to hydrolysis, that is depolymerization, which might restrict their use. Some hyperbranched polymers are synthesized via substitution reactions which provide less hydrolytically unstable polymers.

The "second generation" of hyperbranched polymers was introduced a few years ago when Fréchet et al. reported the use of self-condensing vinyl polymerization to prepare hyperbranched polymers by carbocationic systems (Fig. 3) [46]. Similar procedures but adapted for radical polymerization were shortly thereafter demonstrated by Hawker et al. [47] and Matyjaszewski et al. [48].

The solid-phase synthesis of dendritic polyamides was explored by Fréchet et al. [49]. Inspired by the technique used by Merrifield for peptide synthesis, the same strategy was used to build hyperbranched polyamides onto a polymeric support. The idea was to ensure the preservation of the focal point and to ease the purification between successive steps. The resulting polymers were cleaved from the solid support, allowing ordinary polymer characterization. The reaction was found to be extremely sluggish beyond the fourth generation.

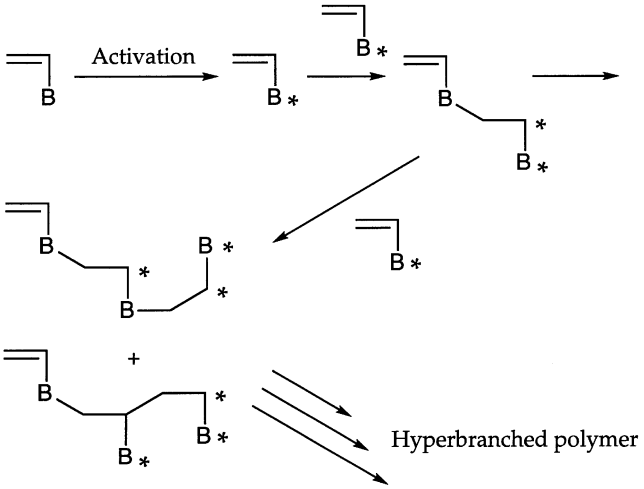

Fig. 3. Schematic description of self-condensing vinyl polymerization used for the synthesis of of hyperbranched polymers based on vinyl monomers as presented by Frechét [52] –(* represents a reactive site which can initiate polymerization)

The idea of using a solid support was further explored by Moore and Bharathi [50].

The concept of constructing hyperbranched polymers (polystyrenes) by a "graft-on-graft" technique was first described by Möller and Gauthier [51, 52] when they performed several functionalization and anionic grafting steps on a linear polystyrene. The concept of building dendritic polymers by sequential growth of end-standing polymer chains (poly(ε-caprolactone)) was further developed by Hedrick and Trollsås [53]. Brenner and Voit explored the use of azo-functional hyperbranched structures as multi-functional initiators [54]. Free radical "grafting from" reactions were carried out using various monomers. The resulting graft copolymers, with a hyperbranched core and linear graft arms, exhibited improved film-forming properties as compared to the ungrafted hyperbranched polymer.

The field of hyperbranched polymers is still young and rapidly growing. The availability of commercial A_xB monomers, however, still limits their potential use.

2.3 Structural Variations

2.3.1 *Degree of Branching*

In a perfectly branched dendrimer, only one type of repeat unit can be distinguished, apart from the terminal units carrying the chain ends (Fig. 4). A more

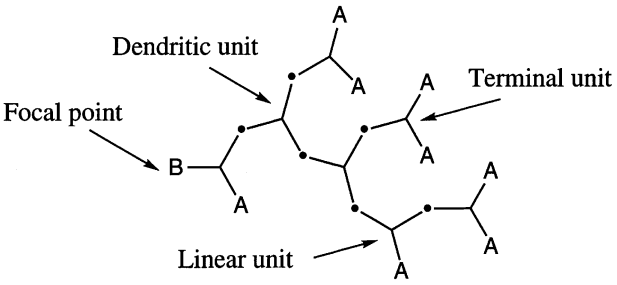

Fig. 4. Different segment types present in hyperbranched polymers

thorough investigation of a hyperbranched polymer (assuming high conversion of B-groups) reveals three different types of repeat units as illustrated in Fig. 4. The constituents are *dendritic units (D)*, fully incorporated A_xB-monomers, *terminal units (T)* having the two A-groups unreacted, and *linear units (L)* having one A-group unreacted. The linear segments are generally described as defects. Fréchet et al. coined the term *degree of branching* (DB) in 1991 [55] and defined it by:

$$DB=(\Sigma D+\Sigma T)/(\Sigma D+\Sigma L+\Sigma T) \quad (5)$$

To date, two different techniques have been used to determine the degree of branching. The first technique was presented by Fréchet et al. [55] and involves the synthesis of low molecular weight model compounds resembling the repeat units to be found in the hyperbranched skeleton. The model compounds are characterized with ^{13}C-NMR. From the spectra of the model compounds, the different peaks in the spectra of the hyperbranched polymers can be assigned. The degree of branching is calculated from the integrals of the corresponding peaks in the spectrum of the polymer.

The second method, based on the degradation of the hyperbranched backbone, was presented by Hawker and Kambouris [56]. The chain ends are chemically modified and the hyperbranched skeleton is fully degraded by hydrolysis. The degradation products are identified using capillary chromatography. Two chemical requirements have to be fulfilled to use this technique successfully. First, degradation must not affect chain ends, and second, the conversion into elementary subunits must be complete.

The expression in Eq. (5) has been used frequently to characterize hyperbranched polymers. The definition leads to high DB values at low degrees of polymerization. Recently, Frey et al. introduced another expression for the degree of branching where the degree of polymerization is also taken into consideration [57]. The same group also published findings from computer simulations of ideal experiments where the monomers are added one by one to a B_y-functional core molecule, keeping the total number of molecules constant throughout the reaction [58]. Increasing the functionality of the core resulted in decreased poly-

dispersity for the final polymer. The degree of branching was found to have a limiting value of 0.66 with slow monomer addition at a high degree of conversion. Some experimental work was carried out in order to verify the simulated results [59].

It is of vital importance to understand how the degree of branching affects the properties of a hyperbranched polymer. One way to obtain polymers with higher degrees of branching is to use preformed dendron-monomers. This concept was used by Hawker and Chu [60] and it was found that the resulting polymers with the highest degree of branching also exhibited the highest solubility in organic solvents. Fréchet and Miravet have also studied this topic by investigating the hyperbranched poly(siloxysilanes) obtained from A_2B-, A_4B-, and A_6B monomers [61].

2.3.2
Copolymerization of A_xB Monomers and B_y Functional Core Molecules

In agreement with Flory´s predictions, hyperbranched polymers based on A_xB monomers reported in the literature exhibit a broad molecular weight distribution (typically 2–5 or more). The polydispersity of a hyperbranched polymer is due to the statistical growth process. A strategy to overcome this disadvantage is to add a B_y-functional core molecule, or a chain terminator, which limits the polydispersity and also provides a tool to control the molecular weight of the final polymer. The concept of copolymerizing an A_2B monomer with a B_3 functional core molecule was first introduced by Hult et al. [62] and more recently also utilized by Feast and Stainton [63] and Moore and Bharathi [64].

2.3.3
End Groups

The influence of the end groups on the properties of a linear polymer is, at a sufficiently high molecular weight, negligible. However, irrespective of what synthetic procedure is used to obtain the hyperbranched polymers, the resulting macromolecules have a large number of end groups. The end groups have been demonstrated to be easily accessible for chemical modifications and the nature of the end groups has been found to determine the thermal and physical properties of the hyperbranched polymers to a great extent. The chain end functionalizations are mainly carried out in solution using reactive acid chlorides as chain terminators.

3
Hyperbranched Polymers

The following aims to give a brief survey of hyperbranched polymers as presented in the literature. However, this section can only be regarded as a selection of the most important classes of hyperbranched polymers. No attempt has been made to include all papers concerning hyperbranched polymers.

3.1 Polyphenylenes

One of the first hyperbranched polymers described in the literature was polyphenylenes, which were presented by Kim et al. [30–32] who also coined the term "hyperbranched". The polyphenylenes were prepared via Pd(0) or Ni(II) catalyzed coupling reactions of various dihalophenyl derivatives such as dibromophenylboronic acid. The polymers were highly branched polyphenylenes with terminal bromine groups which could be further transformed into a variety of structures such as methylol, lithiate, or carboxylate (Fig. 5).

Unlike linear polyphenylenes, the hyperbranched polyphenylenes were soluble in various solvents such as THF with a solubility dependent on the end group. The polyphenylenes even became water soluble when the bromine end groups were transformed into carboxylate groups. Polyphenylenes with bromine end groups exhibited a glass transition temperature (T_g), determined by DSC, of 238 °C which was independent of molecular weight in the examined range (2–35 kg mol^{-1}). The T_g shifted, however, when the end groups were altered – for instance trimethylsilyl end groups gave a T_g of 152 °C. The bromo-functional polyphenylenes were thermally stable up to 550 °C as measured by TGA.

The polyphenylenes were brittle and did not form self-standing films when cast from solution. Therefore, they were considered poor materials. The use of these polymers was instead investigated as additives in polystyrene to improve processing and mechanical properties. A mixture of polystyrene and hyperbranched polyphenylene (5%) was studied and the results showed that the melt viscosity, especially at high temperatures and shear rates, was reduced by up to 80% as compared to pure polystyrene. Also, the thermal stability of polystyrene

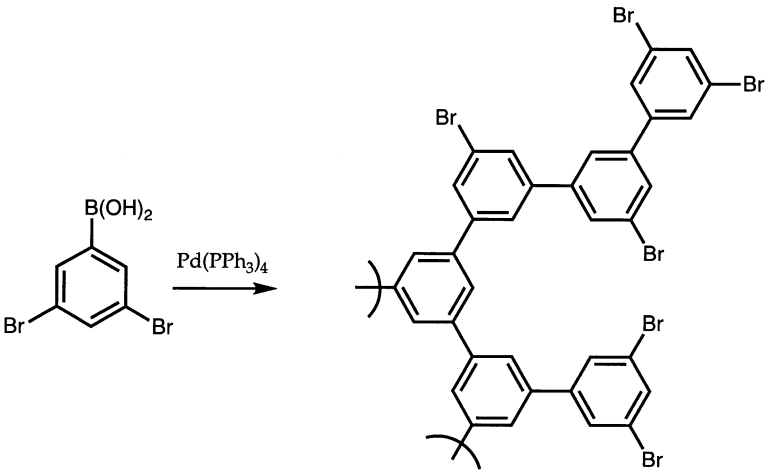

Fig. 5. Example of hyperbranched polyphenylene synthesized by Kim and Webster [31]

was improved and shear induced degradation was reduced. The mechanical properties of the blends were not much affected except for an increase in initial modulus which suggests that weak crosslinking occurred. The hyperbranched polyphenylenes were also shown to be useful as multifunctional macroinitiators for star polymers.

3.2 Polyesters

Polyesters are an important class of condensation polymers, and the availability of a few commercial dihydroxy carboxylic acids has prompted several research groups to look into hyperbranched polyesters in great detail. Several old patents concerning highly branched and hyperbranched polyesters exist. One of the oldest patents, from 1972, concerns the polymers obtained by condensation of polyhydroxy monocarboxylic acids and their use in coatings [65]. The potential use of hyperbranched polymers as rheology modifiers or for drug delivery purposes was described in another patent in 1992 [29]. Two of the most recent patents concern hyperbranched polymers obtained from polyols (chain terminator or core molecule) and A_2B-monomers and their use in coating applications [66, 67].

3.2.1 *Aromatic Polyesters*

Considerable attention has been paid to aromatic hyperbranched polyesters synthesized from monomers derived from 3,5-dihydroxybenzoic acid (DBA). The thermal stability of DBA is not good enough to allow direct esterification of DBA, and therefore chemical modifications are necessary. Some aromatic monomers used for the synthesis of hyperbranched aromatic polyesters are presented in Fig. 6.

Fréchet et al. conducted a systematic investigation of hyperbranched polyesters derived from 3,5-bis(trimethylsiloxy)benzoyl chloride [55, 68–70]. The monomers were condensed at 150–200 °C or by using low temperature esterification procedures. The polymers were found to have a degree of branching close to 0.55 and apparent molecular weights (M_n) in the range of 16–60 kDa as determined by GPC relative to linear polystyrene standards. Several functionalizations were performed on the phenolic end groups in order to investigate how the nature of the end groups affected the glass transition temperature.

Turner et al. [71, 72] also report on hyperbranched polyesters derived from 3,5-bis(trimethylsiloxy)benzoyl chloride and from 3,5-diacetoxybenzoic acid, which both yield phenolic polyesters after hydrolysis of the end groups. The same group investigated the hyperbranched polyesters obtained in the melt condensation of 5-acetoxyisophthalic acid and 5-(2-hydroxy)-ethoxyisophthalic acid respectively. The latter yields a soluble product while the former results in an insoluble polymer due to formation of anhydride bridges.

Kricheldorf and Stöber [73] compared the polyesterification of silylated 5-acetoxyisophthalic acid and of free 5-acetoxyisophthalic acid. The non-silylated

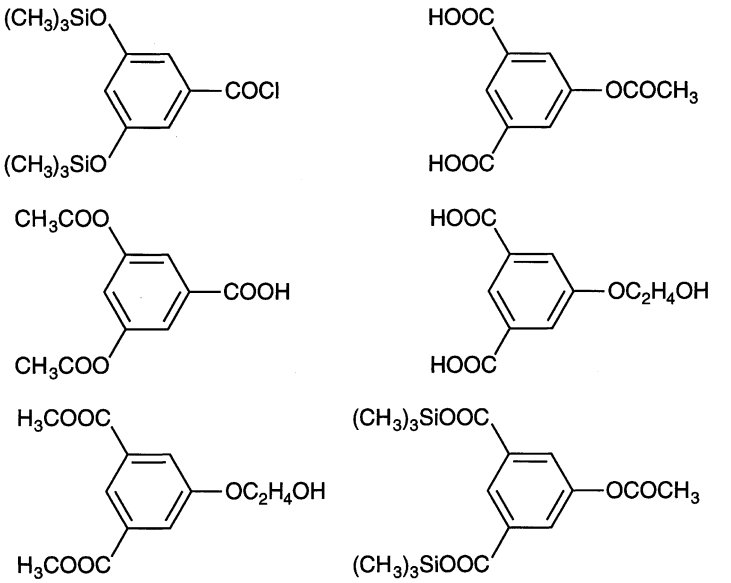

Fig. 6. Examples of A_xB monomers used for the preparation of hyperbranched aromatic polyesters [55, 63, 68, 69, 71–73]

monomer yielded insoluble products, indicating that crosslinked materials were obtained. The degree of branching for these materials was found to be close to 0.6 and independent of reaction conditions. Kricheldorf et al. have also synthesized star-shaped and hyperbranched polyesters by polycondensation of trimethylsilyl 3,5-diacetoxybenzoate [74]. The same authors reported on a number of hyperbranched polymers based on the trimethylsilylester of β-(4-hydroxyphenyl)propionic acid [75]. This is an AB monomer and is strictly speaking not the basis for a hyperbranched polymer.

Feast and Stainton [63] reported on the synthesis of aromatic hyperbranched polyesters from 5-(2-hydroxyethoxy)isophthalate copolymerized with 1,3,5-benzenetricarboxylate (core molecule) as a moderator of the molecular weight. The degree of branching was found to be 0.60–0.67 as determined by ^{13}C-NMR. Apparent molecular weights (M_w) were found to be 5–36 kDa according to SEC characterization using linear polystyrene standards.

Structural variations of hyperbranched polyesters have also been achieved by copolymerizing an A_2B-monomer with an AB-functional monomer, although no properties were reported for these copolymers [71].

A variation of the aromatic polyester structure was utilized by Hawker et al. when they described hyperbranched poly(ethylene glycol)s and investigated their use as polyelectrolyte media [76]. The highly branched structure implies that no crystallization can occur. Linear poly(ethylene) glycols usually crystallize, which has a detrimental effect on their use as polyelectrolyte media.

3.2.2
Aliphatic Polyesters

The use of aliphatic monomers for hyperbranched polyesters has been debated because aliphatic monomers are said to be prone to thermal degradation reactions such as decarboxylation, cyclization, or dehydration [77]. The only commercial hyperbranched polymer is a hydroxy-functional aliphatic polyester, Boltorn, available from Perstorp AB, Sweden.

Essentially one monomer, 2,2-bis(methylol)propionic acid (bis-MPA), shown in Fig. 7, has been used to prepare hyperbranched aliphatic polyesters. Hult et al. described the co-condensation of bis-MPA and a four-functional polyol resulting in hydroxy-functional hyperbranched polyesters [62]. The synthesis was further elucidated, and subsequent papers deal with the materials obtained from bis-MPA and trimethylolpropane [78]. The degree of branching was initially reported to be close to 0.8 but was recently re-evaluated after it was shown that the hydroxy-functional hyperbranched polyesters undergo facile acetal formation during NMR analysis in acetone-d_6. The acetal formation was catalyzed by residual trace amounts of acid remaining in the sample. After re-evaluation in DMSO-d, the degree of branching was close to 0.45, which is in accordance with most other hyperbranched polymers [79].

The hydroxy-functional polyesters had a glass transition temperature close to 35 °C but by end-capping the hydroxyl groups with various alkyl chains it was possible to depress the glass transition to temperatures well below 0 °C. Interestingly, a sufficiently long alkyl chain resulted in a semi-crystalline polymer exhibiting a first-order melt transition as determined by DSC, indicating that side-chain crystallization occurred [36]. Dielectric spectroscopy has been used to investigate how the segmental mobility was affected by various end groups [80, 81]. The influence on various end groups was also investigated using dynamical rheological analysis [36]. Resins for coating applications were obtained by end-capping the hyperbranched skeleton with crosslinkable acrylate groups [82].

Hawker et al. report on the synthesis of a similar hyperbranched polyester based on the corresponding AB_4-monomer; that is, the preformed dendron of the second generation was used in the condensation reaction [79].

Voit also carried out the melt condensation of bis-MPA using a slightly higher reaction temperature, 200 °C, and acid catalysis [83].

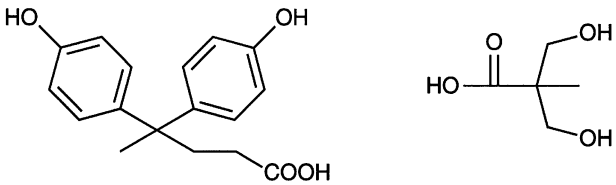

Fig. 7. Examples of A_xB monomers used for the preparation of hyperbranched aliphatic and aromatic-aliphatic polyesters [56, 62, 78]

A somewhat different approach was presented by Rannard and Davis where they first reacted bis-MPA with carbonyl diimidazole, allowing a highly selective base-catalyzed reaction to form a hyperbranched polyester. The resulting polymers were hydroxy-functional and reported to be water-soluble [84].

3.3 Polyethers

Several hyperbranched polyethers have been presented in the literature. Fréchet et al. [85, 86] have described the one-pot synthesis of hyperbranched benzylic polyethers based on the self-condensation of 5-(bromomethyl)-1,3-dihydroxybenzene in solution. The effect of variation of reaction conditions such as monomer concentration, time, and type of solvent was explored and it was concluded that an increased reaction time and polar solvents increased the molecular weight while a change in monomer concentration had less effect. Polymers with molecular weights up to 120 kg mol^{-1}, as determined with LALLS, were obtained under optimum conditions. The desired O-alkylation was accompanied by approximately 30% C-alkylation. Therefore, the degree of branching was difficult to determine. It was also shown that the phenolic end groups could easily be transformed into other moieties such as benzyl, silyl, or acetate end groups with a subsequent change in T_g and solubility of the polymers. One main problem which appeared was, however, that the monomer proved to be extremely allergenic, which limits the use of this structure.

Miller et al. [87, 88] have described the synthesis of hyperbranched aromatic poly(ether-ketone)s based on monomers containing one phenolic group and two fluorides which were activated towards nucleophilic substitution by neighboring groups. The molecular weight and polydispersity of the formed poly(ether-ketone)s could be controlled by reaction conditions such as monomer concentration and temperature. The formed polymers had high solubility in common solvents such as THF.

Hawker and Chu described the synthesis of hyperbranched poly(ether-ketone)s based on A_2B-monomers having either one phenolic and two fluoride groups or two phenolic and one fluoride groups [60]. Polymerization of the two different monomers yielded hyperbranched poly(ether-ketone)s with either phenolic or fluoride end groups. The monomer having two fluoride end groups produced a polymer with a significantly higher degree of branching due to differences in reactivity. The degree of branching could be changed by using A_3B and A_4B monomers with similar chemical structure and it was shown that properties such as T_g were unaffected by the DB. The T_g of the polymers could be greatly varied by changing the structure of the end groups; for example, octoate end groups gave a T_g of 97 °C while carboxylic acid end groups had a T_g of 290 °C. The solubility also changed dramatically with end-group structure ranging from octoate end groups inducing solubility in hexane to carboxylic acid end groups which made the polymers water-soluble. The polymers with carboxylic acid end groups were shown to behave as unimolecular micelles; that is, the pol-

ymer could solubilize hydrophobic compounds in water. The amount of soluble hydrophobic substance was directly proportional to the polymer concentration and no CMC was seen, suggesting the behavior of a unimolecular micelle.

3.4 Polyamides

Fréchet et al. reported on the solid-phase synthesis of dendritic polyamides in 1991 [49]. The intention was to grow dendritic segments from a solid support and thereby enhance the ease of purification between successive steps (Sect. 2.2).

Kim reported on liquid crystalline properties observed for hyperbranched aromatic amides obtained from 3,5-diaminobenzoic acid and derivatives thereof. The resulting polymers exhibited nematic liquid crystalline phases [89].

3.5 Hyperbranched Vinyl Polymers

Recently, self-condensing vinyl polymerization (SCVP) of 3-(1-chloroethyl)-ethenylbenzene was introduced by Fréchet and co-workers [46, 90] (Fig. 3). This reaction involves a vinyl monomer of AB* type in which B* is a group capable of initiating the polymerization of vinyl groups. The chain initiation is the addition of an activated B* group to the vinyl group of another monomer forming a dimer with two active sites and one double bond. Both the initiating center, B*, and the newly created propagating center, * (Fig. 3), can react with the vinyl group of another molecule (monomer or polymer) in the same way. The concept was further developed by Hawker et al. [47], and applied to TEMPO-mediated "living" free radical polymerization of hyperbranched polystyrenes. Matyjaszewski et al. [48] developed ATRP-techniques to obtain hyperbranched polystyrenes. Since then, a number of different approaches, based on vinyl monomers and various initiating systems, have been explored to yield hyperbranched polymers such as poly(4-acetylstyrene) [91], poly(vinyl ether) [92], polyacrylates [93], and polymethacrylates [94].

3.6 Other Hyperbranched Polymers

3.6.1 *Semi-Crystalline and Liquid Crystalline Polymers*

Branching in polymers generally reduces the crystallization tendency for conventional polymers. Therefore, hyperbranched polymers were first believed to behave as amorphous polymers due to the highly branched backbone. Several papers have, however, shown that both liquid crystalline and crystalline hyperbranched polymers can be made from some special A_xB monomers or by attachment of crystallizable end groups.

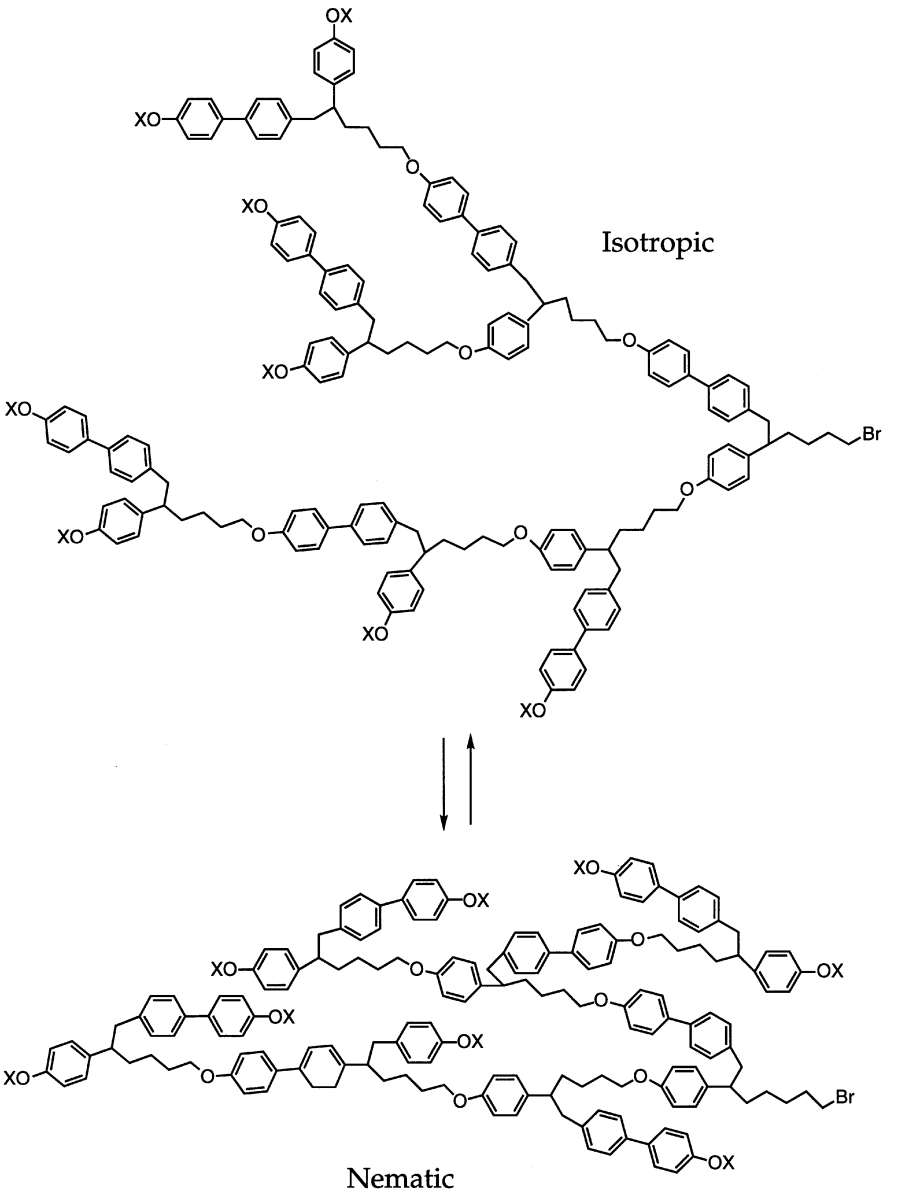

Fig. 8. Isotropic-nematic transformation of a hyperbranched polyether as described by Percec et al. [34, 35]

Percec et al. have described the possibility of making hyperbranched polymers which exhibit liquid crystalline phases [34, 35]. They made hyperbranched polyethers based on an A_xB monomer having both a spacer and a

mesogenic unit incorporated into the monomer structure.The polyethers exhibited a thermotropic nematic liquid crystalline (LC) behavior based on conformational isomerism (Fig. 8). Kim described hyperbranched aromatic polyamides [89, 95] which exhibited a lyotropic liquid crystalline behavior with a nematic mesophase. He suggested that the hyperbranched polymer´s propensity to form aggregates in solution was the reason for the LC-behavior.

Hult et al. [36] have described semi-crystalline hyperbranched aliphatic polyesters where the crystallinity was induced by attachment of long alkyl chains as end groups. The crystallization was affected by several factors such as length of the end groups and the molecular weight of the hyperbranched polyester. The crystallization was proposed as being either intra- or intermolecular depending on the size of the hyperbranched polyester onto which the alkyl chains were attached.

3.6.2 *Polyurethanes*

Polyurethanes are useful in numerous applications such as reaction injection molding, rigid and flexible foams, coatings and adhesives. However, due to the high reactivity of the isocyanate group [96], yielding either dimers, via self-condensation or a carbamate via the reaction with an alcohol, the A_xB-monomers have to be produced in-situ in the reaction vessel.

Spindler and Fréchet used 3,5-bis((benzoxy-carbonyl)imino)benzyl alcohol which decomposed thermally in THF solution containing DBTDL as a catalyst [97]. The resulting polymer was found to be insoluble unless an end-capping alcohol was added from the beginning. The end-capping groups determined the properties of the polymers such as glass transition temperature, thermal stability, and solubility.

Kumar and Ramakrishnan synthesized hyperbranched polyurethanes via the in-situ generation of 3,5-dihydroxyphenyl isocyanate from the corresponding carbonyl azide [98]. The degree of branching was determined as being close to 0.6 using NMR spectroscopy. The hyperbranched polyurethane was completely soluble in common organic solvents while the linear counterpart was completely insoluble.

3.6.3 *Polycarbonates*

Wooley and Bolton recently published a paper concerning hyperbranched polycarbonates obtained by polymerization of a monomer derived from 1,1,1-tris(4´-hydroxyphenyl)ethane [99]. A degradative technique was used to determine the degree of branching, which was found to be close to 0.53. Apparent molecular weights were in the range 16–82 kDa as determined by GPC relative to linear polystyrene standards.

3.6.4
Poly(ester-amide)s

Kricheldorf et al. have investigated several hyperbranched poly(ester-amide)s derived from combinations of 3,5-diaminobenzoic acids and 3,5-dihydroxybenzoic acids and similar monomers [100–102]. The polymers exhibited values of T_g ranging from 160 to 250 °C and were highly soluble in various solvents. They employed diamines as "star centers" in order to control the molecular weight.

Several other papers have appeared in the literature describing hyperbranched poly(siloxysilane)s [103], poly(amine)s [104], poly(phenylene sulfide)s [105], polycarbosilanes [106], phenol-formaldehyde resins [107], poly (aryl ether sulfone)s [108], poly(alkoxysilanes) [109], and poly(lactoside)s [110] but are not further treated in this survey.

4
Properties

The urge of polymer scientists to develop new materials is driven by society's wish to substitute conventional materials by plastics and thereby gain in performance. One reason for the emerging interest in hyperbranched polymers and other macromolecular architectures is their different properties compared to conventional, linear polymers.

Already Flory predicted that the number of entanglements would be lower for polymers based on A_xB monomers, with subsequent reduction in mechanical strength [1].

Changes in properties related to the architecture of hyperbranched polymers rather than the chemical structure have to some extent been evaluated but a full understanding is still lacking. Lately, research in this area has been focused on two questions: why and to what extent the architecture affect the properties.

4.1
Solution Behavior

One of the first properties of hyperbranched polymers that was reported to differ from those of linear analogs was the high solubility induced by the branched backbone. Kim and Webster [31] reported that hyperbranched polyphenylenes had very good solubility in various solvents as compared to linear polyphenylenes, which have very poor solubility. The solubility depended to a large extent on the structure of the end groups, and thus highly polar end-groups such as carboxylates would make the polyphenylenes even water-soluble.

Not only good solubility but also solution behavior differs for hyperbranched polymers compared to linear polymers. For example, hyperbranched aromatic polyesters, described by Turner et al. [71, 72], exhibit a very low α-value in the Mark-Houwink-Sakurada equation and low intrinsic viscosities. This is consist-

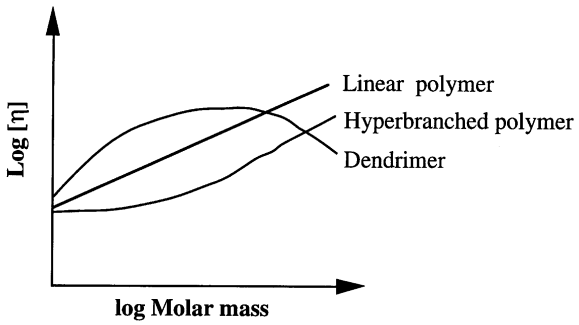

Fig. 9. Generalized description of the intrinsic viscosity as function of molar mass for linear polymers, hyperbranched polymers and dendrimers as described by Fréchet [33]

ent with highly branched and compact structures. Fréchet presented a comparison between linear polymers, hyperbranched polymers, and dendrimers with respect to intrinsic viscosities as a function of molecular weight, which clearly shows the differences induced by variations in the backbone architecture (Fig. 9) [33].

Another special feature of dendritic polymers is the possibility to combine an interior structure with one polarity, with a shell (end groups) having another polarity, for instance a hydrophobic inner structure and hydrophilic end groups. For example, Kim and Webster [30] described their hyperbranched polyphenylenes with carboxylate end groups as unimolecular micelles, where the carboxylate end groups made the polymer water soluble and the hydrophobic interior could host a guest molecule. This has also been described by Hawker and Chu [60] who could solubilize hydrophobic molecules in water by using hyperbranched aromatic poly(ether-ketone)s having acid end groups. They did not observe a critical micelle concentration (CMC) but a steady increase in solubility of the hydrophobic compound with polymer concentration. From this observation they concluded that a unimolecular micelle behavior applied. In a recent review by Uhrich [111] the guest-host possibility is described for various dendritic polymers considered suitable for medical applications such as drug delivery.

The size of dendritic polymers in solution has been shown to be greatly affected by solution parameters such as polarity and pH. Newkome et al., for example, have shown that the size of dendrimers with carboxylic acid end groups in water can be increased by as much as 50% on changing the pH [112].

The dilution properties of hyperbranched polymers also differ from those of linear polymers. In a comparison between two alkyd resin systems, where one was a conventional high solid alkyd and the other based on a hyperbranched aliphatic polyester, the conventional high solid alkyd was seen to exhibit a higher viscosity [113]. A more rapid decrease in viscosity with solvent content was noted for the hyperbranched alkyd when the polymers were diluted.

4.2 Bulk Properties

4.2.1 *Thermal Properties*

Some of the first questions that arise when looking at a new group of polymers such as hyperbranched polymers concern the glass transition temperature – what determines it, what molecular motions determine it, is there a difference in T_g for different parts of the molecule? Since hyperbranched polymers are almost exclusively amorphous materials, the glass transition temperature will be one of the most important features.

The classical visualization of T_g is related to relatively large segmental motions in the polymer chain segments and the fact that the role of the end groups diminishes above a certain molecular weight. This is more difficult to conceive for hyperbranched polymers since segmental motions are affected by the branching points and the presence of numerous end groups. It has instead been proposed that the glass transition for hyperbranched polymers is a translational movement of the entire molecule instead of a segmental movement [31, 32]. Chemical nature also affects the T_g; for example, an aliphatic polyester generally has a much lower T_g than an aromatic one [4].

T_g is one of the properties that has been reported for most of the hyperbranched polymers. The results have been based either on calorimetric or rheological measurements. Values of T_g for a series of hyperbranched aromatic polyesters with different end groups have been presented in a review paper by Voit [4]. T_g shifted as much as 100 °C (from 250 to 150 °C) on going from carboxylic acid to acetate end groups. This and other reports [114] show the large impact of end group structure on the T_g. The T_g for polyether dendrimers has been found to follow a modified Flory equation where the number and structure of end groups are accounted for [115]. However, no complete model to predict the T_g for hyperbranched polymers exists since several other factors such as degree of branching, steric interactions due to crowding, backbone rigidity and polarity in combination also play an important role for the glass transition temperature. The glass temperature of dendritic polymers has been discussed in a paper by Stutz [116].

The thermal stability of hyperbranched polymers is related to the chemical structure in the same manner as for linear polymers; for example, aromatic esters are more stable than aliphatic ones. In one case, the addition of a small amount of a hyperbranched polyphenylene to polystyrene was found to improve the thermal stability of the blend as compared to the pure polystyrene [31].

A study of the PVT properties of hyperbranched aliphatic polyesters by Hult et al. [117] showed that these polyesters were dense structures with smaller thermal expansion coefficients and lower compressibility compared to some linear polymers.

4.2.2
Mechanical and Rheological Properties

The correct mechanical and rheological behavior is essential when introducing new materials onto the market. A material must possess both suitable material and processing properties in order to find an appropriate use.

The rheological properties for hyperbranched polymers are characterized by a Newtonian behavior in the molten state; i.e., no shear thinning or thickening is observed [117], indicating a lack of entanglements for these polymers. The non-entangled state imposes rather poor mechanical properties, resulting in brittle polymers. This has limited the use of these polymers as thermoplastics to applications where the mechanical strength is of minor importance. The large amount of branching also makes most of these polymers amorphous although exceptions exist. Hence, these polymers are mainly suitable as additives or as thermosets when high mechanical strength is required for a certain application.

The melt behavior has been shown to be greatly affected by the structure of the end-groups where an increase in the polarity of the end-groups can raise the viscosity by several orders of magnitude [118] (Fig. 10). This is of great importance in applications where low viscosity is essential for the processing of the material [119].

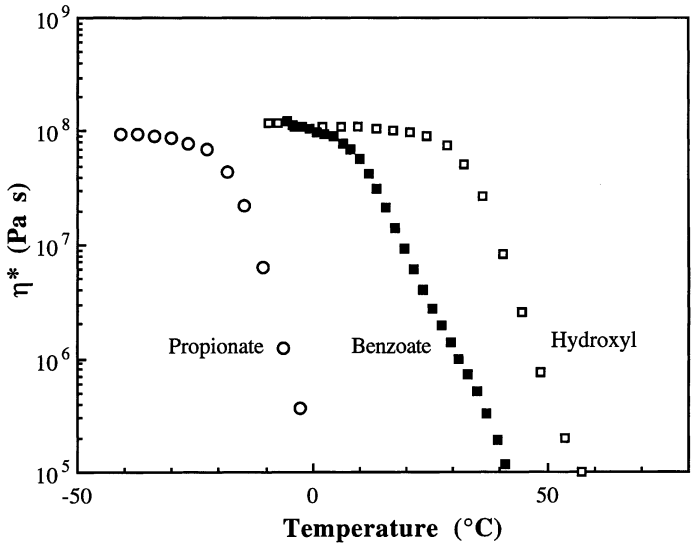

Fig. 10. Complex dynamic viscosity as function of temperature for three different aliphatic hyperbranched polyesters based on bismethylol propionic acid and having different end-group structure – (○) propionate end-groups, (■) benzoate end-groups, (□) hydroxyl end-groups [118]

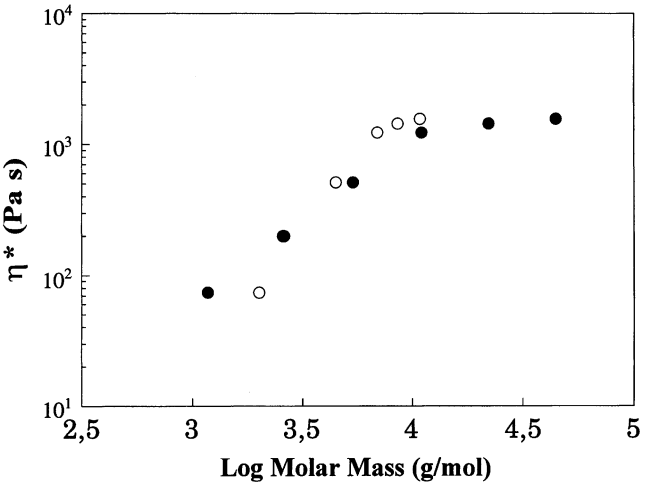

Fig. 11. Melt viscosity at 85 °C vs molar mass for hydroxy-functional hyperbranched aliphatic polyesters based on bismethylol propionic acid. Theoretical molar mass based on core: bis-MPA ratio (●) and Mn determined with SEC relative to linear polystyrene standards (○) [117]

Another very special feature of these polymers is the relationship between molecular weight and melt viscosity. For linear polymers, the increase in melt viscosity with molecular weight is linear with a transition to a 3.4 power law when the molecular weight reaches the critical mass for entanglements, M_c. For hyperbranched polymers, the increase in viscosity follows a different curve: it is less pronounced and levels off at higher molecular weights [117] (Fig. 11).

One application that has been suggested for hyperbranched polymers is as an additive, where the hyperbranched polymers improve a property such as polymer toughness [120–122]. This is possible since the polarity of the hyperbranched polymer can be adjusted to make it either compatible or incompatible with another polymer. Reaction-induced phase separation by adjusting the polarity of a hyperbranched aliphatic polyester relative to an epoxy/amine thermoset system has been demonstrated. The resulting thermoset polymer exhibited a dramatic increase in toughness while retaining the high modulus of the original thermoset. The use of hyperbranched polyphenylenes as a processing aid for polystyrenes has been mentioned [31]. The melt viscosity of polystyrene was reduced without affecting the final properties to any large extent.

Hyperbranched polymers are often referred to as amorphous polymers since the branching of the backbone reduces the ability to crystallize in the same manner as linear polymers. Some exceptions have, however, been presented where the polymers have been modified to induce liquid crystallinity [34, 35] or crystallinity [36] (Sect. 3.6.1).

4.2.3 *Networks*

One area where hyperbranched polymers may find use is in thermoset applications. The low melt viscosity can improve the processing properties while extensive crosslinking can result in sufficient material strength. All or a fraction of the end groups can be functionalized with reactive groups, resulting in a crosslinkable polymer. The remaining non-functionalized end groups are accessible for further modifications. This implies the possibility to tailor the properties of the final network by two different routes, by changing either the crosslink density or the chemical structure of the nonreactive end groups.

Amongst the first studies presenting the use of dendritic polymers for thermoset applications was the work of Hult et al. [62]. They modified hyperbranched hydroxy functional polyesters with various ratios of maleate-allyl ether/alkyl ester end groups. Dependent on this ratio, resins with different vis-

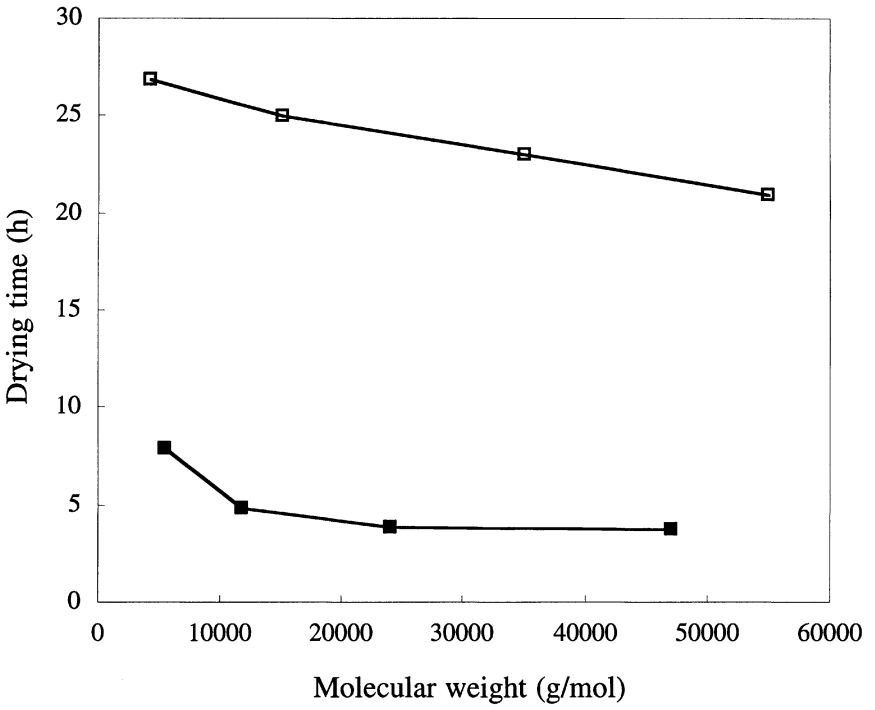

Fig. 12. Comparison between a conventional high solid alkyd coating (□) and an alkyd based on a hyperbranched aliphatic polyester (■). Drying time as a function of molar mass [123]

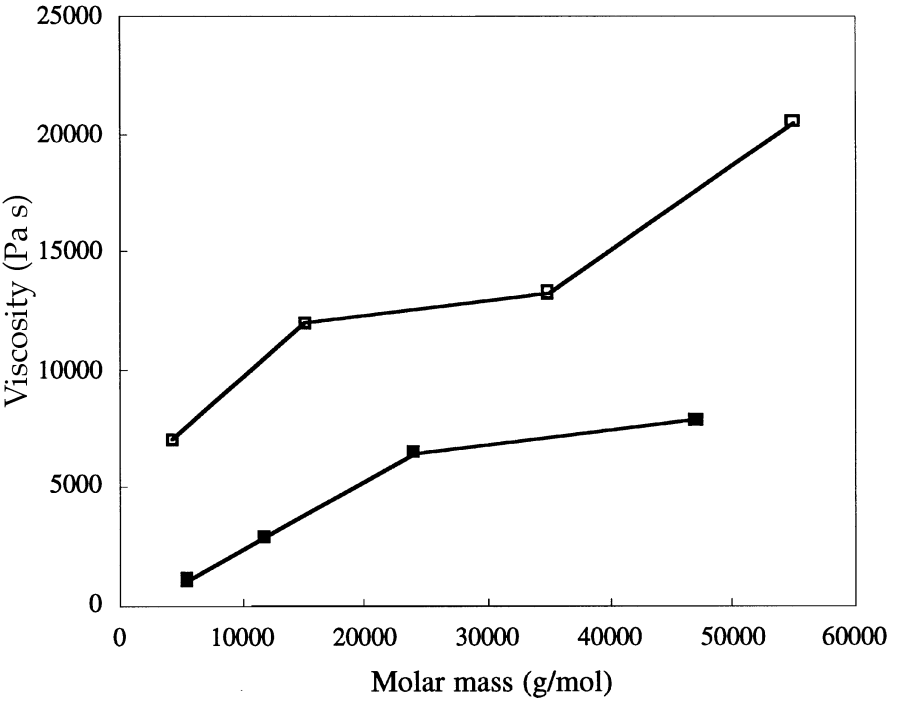

Fig. 13. Comparison between a conventional high solid alkyd coating (□) and an alkyd based on a hyperbranched aliphatic polyester (■). Viscosity as a function of molar mass [123]

cosities (before cure) and different curing rates were obtained. The resins were crosslinked by a free radical mechanism, giving films with final hardnesses depending on the fraction of crosslinkable end groups.

Pettersson and Sörensen have described a number of different thermoset resin structures based on hyperbranched aliphatic polyesters [123]. Their results can best be exemplified by a study on hyperbranched alkyd coating resins. A comparative study was performed between an alkyd resin based on a hyperbranched aliphatic polyester and a conventional high solid alkyd, which is a less branched structure. The hyperbranched resin had a substantially lower viscosity than the conventional resin of comparable molecular weight, that is, less solvent was needed to obtain a suitable application viscosity. The hyperbranched resin also exhibited much shorter drying times than the conventional resin, although the oil content was similar. These achievements would not have been possible without a change in architecture of the backbone structure of the resins (Figs. 12, 13).

Studies on acrylate resins [82, 124, 125] based on hyperbranched aliphatic polyesters have shown that it is possible to vary both the polarity (wetting be-

havior) and T_g of the thermoset by changing either the end-group structure or the crosslink density. These studies showed that it was possible to vary the T_g within a wide range, 50–150 °C, by changing the number of reactive end groups (crosslinkable groups) utilizing the same hyperbranched polyester as a base structure. FT-Raman measurements of the residual unsaturation in these systems also showed that the acrylate functional end-groups are all accessible to polymerization; in other words they are not trapped inside the hyperbranched polyester structure. UV polymerization of the resins also proceeded at a high rate compared to conventional acrylate resins. The structure of the non-reactive end groups affected the T_g to some extent although the crosslink density had a much larger impact on the T_g. The structure of the non-reactive end groups had a much larger effect on other properties such as wetting behavior. Changing these groups from carboxylic acid groups to propionate groups increased the contact angle of water from 10 to 75°.

Overall, it can be concluded that the thermoset properties can be greatly varied within a wide range by changes in the functionality of the end groups while retaining the same backbone structure.

5
Applications

Numerous applications have been suggested for hyperbranched polymers but few or none have yet reached full commercial exploitation. Only a few papers have been published that address certain applications of hyperbranched polymers.

5.1
Surface Modification

Corrosion of metal surfaces is a serious problem worldwide. It has been demonstrated that even rather thin organic layers can passivate and block electrochemical reactions on metal surfaces [126]. Bergbreiter et al. have demonstrated that hydrophobic, fluorinated, hyperbranched poly(acrylic acid) films can block these unwanted electrochemical reactions [127–130]. Hyperbranched films containing acrylic acid were synthesized on mercaptoundecanoic acid self-assembling monolayers on gold via sequential grafting reactions, as shown in Fig. 14. This technique proved to be useful for obtaining thick and homogeneous films. The acid groups were accessible to modifications. Fluorination of these films gave surfaces that were analyzed with cyclic voltametry and a.c.-impedance measurements. These studies showed that the barrier to redox reactions was greatly improved.

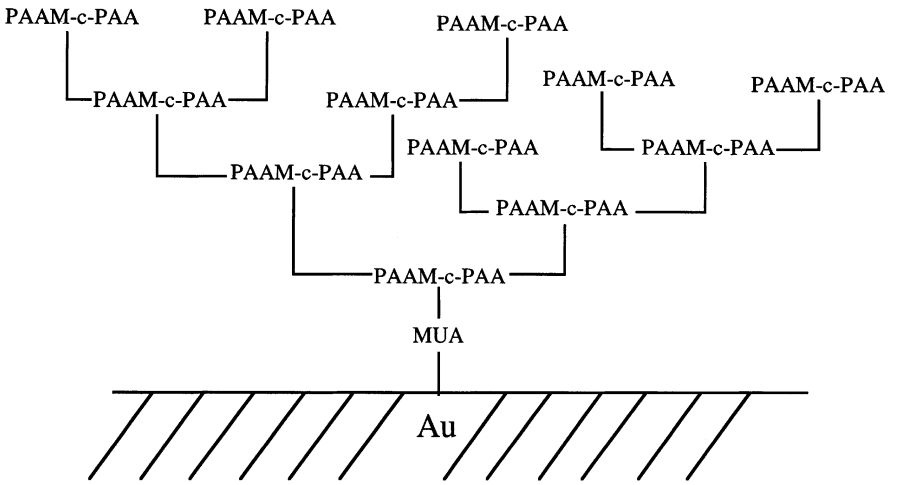

Fig. 14. Hyperbranched polymer grafts prepared on a mercaptoundecanoic acid (MUA) self assembled monolayer confined to a gold substrate. PAAM-c-PAA represents a random copolymer of poly(acrylamide) and poly(acrylic acid) prepared from the poly(acrylic acid) carboxylic acid groups and an amine [129]

5.2 Additives

The lack of mechanical strength for thermoplastic hyperbranched polymers makes them more suitable as additives in thermoplast applications. Hyperbranched polyphenylenes have been shown to act successfully as rheology modifiers when processing linear thermoplastics. A small amount added to polystyrene resulted in reduced melt viscosity [31]. (Sect> 3.1).

5.3 Toughеners for Epoxy-Based Composites

Another demonstrated application is the use of epoxidized hyperbranched polyesters as toughening additives in composites [120–122].

Thermoset resins are widely used in composite materials due to their excellent thermomechanical properties and good impregnation characteristics [121]. However, the toughness, affecting the impact resistance, fatigue behavior and damage tolerance, often limits their applicability. Toughness properties can be greatly improved with various additives. When adding these it is important that the good thermomechanical properties of the thermosetting material are not affected by the toughening system. Månson et al. have demonstrated that by using an epoxy-modified hyperbranched polyester as toughener the critical energy release rate, G_{1c}, of carbon fiber reinforced epoxy was improved from 1400 to

2500 J m^{-2}. This result was obtained by a reaction-driven phase separation. An advantage of this system compared to the more conventional ones is that no filtering of toughener during fiber-impregnation can take place. The phase separation is accomplished by carefully designing the reactivities of the different components as well as the surface polarity of the hyperbranched resin [120–122].

5.4 Coating

The use of hyperbranched polymers as the base for various coating resins has been described in the literature. Different resin types are obtained depending on the reactive end-group structure which is attached to the hyperbranched polymer.

A combination of enhanced reactivity and reduced viscosity for alkyd resins has been achieved by using hyperbranched polyester structures as discussed in Sect. 4.2.3 [123]. This study clearly showed the benefits of using highly branched structures in coating applications to obtain improved properties.

Another type of hyperbranched resins which has been studied is unsaturated polyesters as described in Sect. 4.2.3 [62].

Rånby and Shi also studied hyperbranched methacrylated polyesters and their use in photopolymerizations of films and fiber-reinforced polymer composites. The resins were found to have low viscosities and higher curing rates than those of corresponding linear unsaturated polyesters [131–133].

5.5 Medicine

An important application of polymers in medicine is in advanced drug-delivery systems. These materials control the drug concentration and delivery rate in the body. Hyperbranched polyesters have been suggested for such systems [111]. However, most applications within this field, described in the literature, deal with dendrimers and not with hyperbranched polymers.

An interesting study that was performed on dendrimers is also applicable to hyperbranched polymers. Roberts et al. [134] studied the effect of the dendrimer size when used inside the human body. They found that large dendrimers (M_w ca. 87,000) were passed into the urine and excreted within two days. Smaller dendrimers (M_w ca. 5,000), on the other hand, accumulated mostly in the liver, kidney and spleen with no urine excretion. Since most hyperbranched polymers are polydisperse, this might create a problem for in vivo applications.

5.6 Non-Linear Optics (NLO)

During recent years a number of papers have been presented where a hyperbranched polymer has been designed for a special application. One of the most

recent applications of a hyperbranched polyester, containing 3,6-di-acceptor-substituted carbazole chromophores, was suggested for use in NLO-applications [119, 135]. Wada et al. prepared their hyperbranched polymer from 3,6-diformyl-9-(11-hydroxyundecyl)carbazole via Knoevenagel condensation in a one-pot reaction. Films with good optical quality could be formed from the polymer by spin-coating. After electric corona poling at about 100 °C the films exhibited a second harmonic coefficient (d_{33}) of about 7 pm V^{-1}. The same chemistry was utilized for the synthesis of a similar structure but with a smaller, less stiff polar chromophore, and the second harmonic generation was monitored in thin films. However, the d_{33} was only 2.8 pm V^{-1} [136].

6 Concluding Remarks

New routes, such as variation of the macromolecular architecture, have been increasingly employed for the development of new macromolecular materials during the last few decades. One area of concentration concerns dendritic macromolecules. Numerous polymers with highly branched backbone structures have been synthesized and characterized. Dendritic polymers, comprising dendrimers and hyperbranched polymers, are polymers based on A_xB-monomers, in other words, monomers having one B-functionality and 2 or more A-groups resulting in polymers with a potential branching point in each repeat unit. The difference between dendrimers and hyperbranched polymers is that the former are well defined, layerwise constructed polymers with a branching point in each repeat unit while the latter contain not fully reacted monomers in the polymer backbone. Hyperbranched polymers, having less well-defined architecture than dendrimers, still have properties that differ greatly from conventional linear or moderately branched polymers. One main advantage of hyperbranched polymers over dendrimers is that the synthesis is less tedious, making more material available at a reasonable cost.

Hyperbranched polymers can be synthesized in several different ways, the most commonly used being classical condensation reactions. These reactions are made either in bulk or in solution where the A_xB monomers are condensed by themselves or in combination with a B_y core monomer. The use of a B_y core monomer improves the control over the molecular weight and dispersity of the hyperbranched polymer. Hyperbranched polymers can also be synthesized by self-condensing vinyl polymerization using vinyl-functional monomers. The introduction of this approach has greatly increased the number of possible monomers that can be used for this type of polymer.

A wide variety of hyperbranched polymers have been described in the literature. Initially, these were mainly condensation polymers such as polyesters and polyethers since the required monomers were the most readily available. A number of hyperbranched polymers based on vinyl monomers have been described lately after the introduction of self-condensing vinyl polymerization. One structural variation which has been widely employed for hyperbranched

polymers is modification of the end-group structure. Hyperbranched polymers contain numerous end groups which have been varied from highly polar groups such as carboxylic acids to non-polar end groups. The end groups can also be reactive moieties such as acrylates, giving a crosslinkable hyperbranched polymer.

The properties of hyperbranched polymers have been shown to depend on several parameters, the most important being the backbone and the end-group structure in combination. The glass transition temperature, for example, can be shifted 100 °C simply by changing the polarity of the end groups, while maintaining the same backbone structure. Properties differing from linear polymers are, for example, the solubility which is much higher for hyperbranched polymers but not as high as for dendrimers. Hyperbranched polymers normally exhibit an amorphous, non-entangled behavior, i.e., a Newtonian behavior in the melt. The non-entangled state also makes hyperbranched polymers rather brittle. Attachment of reactive end groups in various amounts leads to thermoset structures where the T_g and crosslink density can be greatly varied for the same hyperbranched polymer. Some examples of crystalline and liquid crystalline hyperbranched polymers have been described although most hyperbranched polymers are considered to be amorphous. The possibility of crystallinity further expands the number of future applications for hyperbranched polymers.

Several applications have already been suggested, related to the special properties of hyperbranched polymers. Several thermoset resin materials have been described where the hyperbranched polymer exhibits a low resin viscosity, thereby reducing the need for solvents to reach the application viscosity. At the same time, rapid curing (high reactivity) and good film properties (high molecular weight of the resin) are obtained. Another successful application of hyperbranched polymers is as toughening additives for composite applications. In this case, the polarity of the hyperbranched polymer was adjusted to give a reaction-induced phase separation in the system, resulting in a dramatic increase in toughness but still retaining the overall good mechanical properties of the system. Another proposed application is in the field of rheological additives where hyperbranched polymers have proved to act successfully as processing aids. Hyperbranched polymers for NLO applications and in medicine have also been described.

Hyperbranched polymers is a young and rapidly growing area within the field of macromolecules. The special properties of these polymers are now clearly described and a number of interesting applications of the hyperbranched polymers will bring them to the marketplace. The future looks bright for these materials.

7 References

1. Flory PJ (1952) In: Principles of polymer chemistry, chap 9. Cornell University Press, Ithaca, New York
2. Zeng F, Zimmerman SC (1997) Chem Rev 97:1681
3. Tomalia DA, Naylor AM, Goddard WA III (1990) Angew Chem Int Ed Engl 102:119
4. Voit BI (1995) Acta Polym 46:87

5. Tomalia DA, Baker H, Dewald J, Hall M, Kallos G, Martin JR, Ryder J, Smith P (1985) Polym J 17:117
6. Newkome GR, Yao Z, Baker GR, Gupta VK (1985) J Org Chem 50:2003
7. Tomalia DA, Baker H, Dewald J, Hall M, Kallos G, Martin S, Roeck J, Ryder J, Smith P (1986) Macromolecules 19:2466
8. Tomalia DA, Hedstrand DM, Ferritto MS (1991) Macromolecules 24:1435
9. de Brabander-van den Berg EMM, Meijer EW (1993) Angew Chem Int Ed Engl 32:308
10. de Brabander-van den Berg EMM, Nijenhuis A, Mure M, Keulen J, Reintjens R, Vandenbooren F, Bosman B, de Raat R, Frijns T, van den Wal S, Castelijns M, Put J, Meijer EW (1994) Macromol Symp 77:51
11. Hawker CJ, Fréchet JMJ (1990) J Am Chem Soc 112:7638
12. Hawker CJ, Fréchet JMJ (1990) J Chem Soc Chem Commun 1010
13. Wooley KL, Hawker CJ, Fréchet JMJ (1991) J Chem Soc Perkin Trans 1:1059
14. Miller TM, Kwock EW, Neenan TX (1992) Macromolecules 25:3143
15. Hawker CJ, Fréchet JMJ (1992) J Chem Soc Perkin Trans 1:2459
16. Buyle Padias A, Hall HK, Tomalia DA, McConnell JR (1987) J Org Chem 52:5305
17. Ihre I, Hult A, Söderlind E (1996) J Am Chem Soc 27:6388
18. Newkome GR, Moorefield CN, Baker GR, Johnson AL, Behera RK (1991) Angew Chem Int Ed Engl 30:1176
19. Newkome GR, Moorefield CN, Baker GR, Saunders MJ, Grossman SH (1991) Angew Chem Int Ed Engl 30:1178
20. Miller TM, Neenan TX, Zayas R, Bair HE (1992) J Am Chem Soc 114:1018
21. van der Made AW, van Leeuwen PWNM (1992) J Chem Soc Chem Commun 1400
22. Launay N, Caminade A-M, Majoral, J-P (1995) J Am Chem Soc 117:3282
23. Lapierre J-M, Skobridis K, Seebach D (1993) Helvetica Chim Acta 76:2419
24. Peerlings HWI, Meijer EW (1997) Chem Eur J 3:1563
25. Gitsov I, Wooley KL, Fréchet JMJ (1992) Angew Chem Int Ed Engl 31:1200
26. Gitsov I, Wooley K L, Hawker CJ, Ivanova PT, Fréchet JMJ (1993) Macromolecules 26:5621
27. Gitsov I, Fréchet JMJ (1993) Macromolecules 26:6536
28. Hawker CJ, Fréchet JMJ (1992) J Am Chem Soc 114:8405
29. Figuly GD (1992) US Pat 5,136,014
30. Kim YH, Webster OW (1990) J Am Chem Soc 112:4592
31. Kim YH, Webster OW (1992) Macromolecules 25:5561
32. Kim YH, Beckerbauer R (1994) Macromolecules 27:1968
33. Fréchet JMJ (1994) Science 263:1710
34. Percec V, Kawasumi M (1992) Macromolecules 25:3843
35. Percec V, Chu P, Kawasumi M (1994) Macromolecules 27:4441
36. Malmström E, Johansson M, Hult A (1996) Macromol Chem Phys 197:3199
37. Van Hest JCM (1996) Ph.D Thesis ISBN 90-386-0277-4
38. Flory PJ (1937) J Am Chem Soc 59:466
39. Flory PJ (1939) J Am Chem Soc 61:3334
40. Stockmayer WH (1943) J Chem Phys 11:45
41. Stockmayer WH (1944) J Chem Phys 12:125
42. Stockmayer WH (1950) J Chem Phys 18:58
43. Beginn U, Drohmann C, Möller M (1997) Macromolecules 30:4112
44. Malmström E, Hult A (1996) Macromolecules 29:1222
45. Chu F, Hawker CJ, Pomery PJ, Hill DJT (1997) J Polym Sci: Part A: Polym Chem 35:1627
46. Fréchet JMJ, Henmi M, Gitsov I, Aoshima S, Leduc M, Grubbs RB (1995) Science 269:1080
47. Hawker CJ, Fréchet JMJ, Grubbs RB, Dao J (1995) J Am Chem Soc 117:10,763
48. Gaynor SG, Edelman SZ, Matyjaszewski K (1996) Macromolecules 29:1079
49. Uhrich KE, Boegeman S, Fréchet JMJ, Turner SR (1991) Polym Bull 25:551
50. Bharathi P, Moore JS (1997) J Am Chem Soc 119:3391

51. Gauthier M, Möller M, Burchard W (1993) Polym Preprint 34(1):60
52. Gauthier M, Möller M (1991) Macromolecules 24:4548
53. Trollsås M, Hedrick JL (1997) Polym Mat Sci Eng 77:208
54. Brenner AR, Voit BI (1996) Macromol Chem Phys 197:2673
55. Hawker CJ, Lee R, Fréchet JMJ (1991) J Am Chem Soc 113:4583
56. Kambouris P, Hawker CJ (1993) J Chem Soc Perkin Trans 1:2717
57. Hölter D, Burgath A, Frey H (1997) Acta Polymer 48:30
58. Hanselmann R, Hölter D, Frey H (1997) Polym Mat Sci Eng 77:165
59. Burgath A, Hanselmann R, Hölter D, Frey H (1997) Polym Mat Sci Eng 77:166
60. Hawker CJ, Chu F (1996) Macromolecules 29:4370
61. Miravet JF, Fréchet JMJ (1997) Polym Mat Sci Eng 77:141
62. Johansson M, Malmström E, Hult A (1993) J Pol Sci: Part A:Polym Chem 31:619
63. Feast WJ, Stainton NMJ (1995) Mater Chem 5:404
64. Bharathi P, Moore JS (1997) Polym Mat Sci Eng 77:111
65. Baker SA, Walbridge DJ (1972) US Pat 3,669,939
66. Hardeman G, Misev TA, Heyenk A (1993) WO 93/18,079
67. Hult A, Johansson M, Malmström E, Sörensen K (1993) WO 93/17,060
68. Wooley KL, Hawker CJ, Lee R, Fréchet JMJ (1994) Polymer J 2:187
69. Wooley KL, Fréchet JMJ, Hawker CJ (1994) Polymer 35:4489
70. Fréchet JMJ, Hawker CJ (1995) React Funct Polym 26:127
71. Turner SR, Voit BI, Mourey TH (1993) Macromolecules 26:4617
72. Turner SR, Walter F, Voit BI, Mourey TH (1994) Macromolecules 27:1611
73. Kricheldorf HR, Stöber O (1994) Macromol Rapid Commun 15:87
74. Kricheldorf HR, Stöber O, Lübbers D (1995) Macromolecules 28:2118
75. Kricheldorf HR, Stukenbrook T (1997) Polymer 38:3373
76. Hawker CJ, Chu F, Pomery PJ, Hill DJT (1996) Macromolecules 29:3831
77. Brenner AR, Voit BI, Massa DJ, Turner SR (1996) Macromol Symp 102:47
78. Malmström E, Johansson M, Hult A (1995) Macromolecules 28:1698
79. Malmström E, Trollsås M, Hawker, CJ, Johansson M, Hult A (1997) Polym Mat Sci Eng 77:151
80. Malmström E, Liu F, Boyd RH, Hult A, Gedde UW (1994) Polym Bull 32:679
81. Malmström E, Liu F, Boyd RH, Hult A, Gedde UW (1997) Polymer 38:4873
82. Johansson M, Hult A (1995) J Coat Techn 67:39
83. Voit BI (1994) Presented at the 35th IUPAC Int. Symp. on Macromolecules, Akron, OHIO, USA
84. Davis N, Rannard S (1997) Polym Mat Sci Eng 77:158
85. Uhrich KE, Hawker CJ, Fréchet JMJ, Turner SR (1991) Polym Mater Sci Eng 64:237
86. Uhrich KE, Hawker CJ, Fréchet JMJ, Turner SR (1992) Macromolecules 25:4583
87. Miller TM, Neenan TX, Kwock EW, Stein SM (1993) J Am Chem Soc 115:356
88. Miller TM, Neenan TX, Kwock EW, Stein SM (1994) Makromol Symp 77:35
89. Kim YH (1992) Adv Mater 4:764
90. Aoshima S, Fréchet JMJ, Grubbs RB, Henmi M, Leduc M (1995) Polym Prepr 36(1):531
91. Lu P, Paulasaari JK, Weber WP (1996) Macromolecules 29:8583
92. Zhang H, Ruckenstein E (1997) Polym Bull 39:399
93. Matyjaszewski K, Gaynor SG, Kulfan A, Podwika M (1997) Macromolecules 30:5192
94. Simon FW, Radke W, Müller AHE (1997) Macromol Rapid Commun 18:865
95. Kim YH (1992) J Am Chem Soc 114:4947
96. Odian G (1981) Principles of polymerization, 3rd edn. Wiley, New York, p 411
97. Spindler R, Fréchet JMJ (1993) Macromolecules 26:4809
98. Kumar A, Ramakrishnan S (1993) J Chem Soc, Chem Commun 1453
99. Bolton DH, Wooley KL (1997) Macromolecules 30:1890
100. Kricheldorf HR, Löhden G (1995) Macromol Chem Phys 196:1839
101. Kricheldorf HR, Löhden G (1995) J M S Pure Appl Chem A32(11):1915
102. Kricheldorf HR, Bolender O, Stukenbrook T (1997) Macromol Chem Phys 198:2651

103. Mathias LJ, Carothers TW (1991) J Am Chem Soc 113:4043
104. Suzuki M, Ii A, Saegusa T (1992) Macromolecules 25:7071
105. Jikei M, Hu Z, Kakimoto M, Imai Y (1996) Macromolecules 29:1062
106. Lach C, Müller P, Frey H, Mülhaupt R (1997) Macromol Rapid Commun 18:253
107. Maciejewski M, Kedzierski M, Bednarek E (1997) Polym Bull 38:613
108. Martínez CA, Hay AS (1997) J Pol Sci Part A Polym Chem 35:2015
109. Muzafarov AM, Golly M, Möller M (1995) 28:8444
110. Roy R, Park WKC, Wu Q, Wang S-N (1995) Tetrahedron Letters 25:4377
111. Uhrich K (1997) Trends in Polym Sci 5(12):388
112. Newkome GR, Moorefield CN, Baker GR, Saunders MJ, Grossman SH (1991) Angew Chem Int Ed Engl 30:1178
113. Hellenius J (1997) MSc Thesis. Dept Polym Techn, KTH, Stockholm, Sweden
114. Voit BI, Turner SR (1994) Angew Makromol Chem 223:13
115. Wooley KL, Hawker CJ, Pochan JM, Fréchet JMJ (1993) Macromolecules 26:1514
116. Stutz H (1995) J Pol Sci Part B: Polym Phys 33:333
117. Hult A, Malmström E, Johansson M (1996) Hyperbranched aliphatic polyesters. In: Salamone JC (ed) The polymeric materials encyclopedia: synthesis, properties and applications. CRC Press, Boca Raton, Florida
118. Ihre H, Johansson M, Malmström E, Hult A (1996) Dendrimers and hyperbranched aliphatic polyesters based on 2,2-bis(hydroxymethyl)propionic acid (Bis-MPA). In: Newkome GR (ed) Advances in dendritic macromolecules, vol 3. JAI Press, London, p 1
119. Zhang Y, Wang L, Wada T, Sasabe H (1996) Macromol Chem Phys 197:667
120. Boogh L, Pettersson B, Japon S, Månson J-A (1995) Proceedings of 10th International Conference on Composite Materials, Whistler, Canada, vol 4, p 389
121. Boogh L, Pettersson B, Kaiser P, Månson J-A (1996). Proceedings of 28th International SAMPE Technical Conference 236, Seattle, USA
122. Boogh L, Pettersson B, Månson J-A (1997) Proceedings of the EPS´97 Conference on Surfaces and Interfaces in Polymers and Composites, Lausanne, Switzerland
123. Pettersson B, Sörensen K (1994) Proceedings of the 21st Waterborne, Higher Solids & Powder Coatings Symposium, New Orleans, Louisiana, p 753
124. Johansson M, Hult A (1996) PRA´s 16th Waterborne, High Solids & Radcure Technologies Conference, Frankfurt, Germany, p 1
125. Johansson M, Rospo G, Hult A (1997) Polym Mat Sci Eng 77:124
126. Laibinis PE, Whitesides GM (1992) J Am Chem Soc 114:9022
127. Zhou Y, Bruening ML, Liu Y, Crooks RM, Bergbreiter DE (1996) Langmuir 12:5519
128. Zhao M, Zhou Y, Bruening ML, Bergbreiter DE, Crooks RM (1997) Langmuir 13:1388
129. Zhou Y, Bruening ML, Bergbreiter DE, Crooks RM, Wells M (1996) J Am Chem Soc 118:3773
130. Bruening ML, Zhou Y, Aguilar G, Agee R, Bergbreiter DE, Crooks RM (1997) Langmuir 13:770
131. Shi WF, Rånby B (1996) J Appl Pol Sci 12:1937
132. Shi WF, Rånby B (1996) J Appl Pol Sci 12:1945
133. Shi WF, Rånby B (1996) J Appl Pol Sci 12:1951
134. Roberts J, Bhalgat M, Zera R (1996) J Biomed Mater Res 30:53
135. Zhang Y, Wang L, Wada T, Sasabe H (1996) J Pol Sci: Part A: Polym Chem 34:1359
136. Zhang Y, Wada T, Sasabe H (1997) Polymer 12:2893

Received: May 1998

Conformational Properties of Branched Polymers: Theory and Simulations

Juan J. Freire

Departamento de Química Física, Facultad de Ciencias Químicas, Universidad Complutense, 28040 Madrid, Spain; *E-mail: juan@hp720.quim.ucm.es*

The prediction and interpretation of conformational properties of branched polymers is difficult, due to the complexity and variety of these structures. Numerical simulations are, consequently, very useful in the investigation of these systems. This review describes the application of numerical simulation techniques to relevant theoretical problems concerning branched polymer systems, taking also into account the related experimental data. Monte Carlo, Molecular Dynamics and Brownian Dynamics methods are employed to simulate the equilibrium and dynamic behavior, and also to reproduce hydrodynamic properties. The simulations are performed on several polymer models. Thus, different Monte Carlo algorithms have been devised for lattice and off-lattice models. Moreover, Molecular Dynamics and Brownian Dynamics can be carried out for detailed atomic or coarse-grained chains. A great amount of investigation has been engaged in the understanding of uniform homopolymer stars as single chains, or in non-diluted solutions and melts, employing this variety of techniques, models and properties. However, other important structures, such as stars with different types of monomer units, combs, brushes, dendrimers and absorbed branched polymers have also been the subject of specific simulation studies.

Keywords. Simulation, Branched, Conformational, Polymers

Advances in Polymer Science, Vol.143

List of Symbols and Abbreviations

a	proportionality constant in the exponent of the dependence of the diffusion coefficient for branched chains (non-dilute conditions)
A	mean asphericity
A	connectivity matrix (Rouse theory)
A_2	osmotic second virial coefficient (in units of volume.mol/mass^2)
b	bead statistical length
B_2	molecular second virial coefficient (in units of volume)
BD	Brownian Dynamics
c	concentration
c*	overlapping concentration
c**	crossover concentration between semi-dilute and concentrate regimes
C(**X**,t)	time-correlation function
C(t*)	stress time-correlation function
d	number of spacial dimensions
d_f	number of dimensions of the tethering object
D	translational diffusion coefficient
D_{ext}	diffusion coefficient of an external blob
D_b	diffusion coefficient of a tethered chain
DMC	Dynamic Monte Carlo
E_{conf}	configurational energy
EV	excluded volume
f	number of arms
f_A	fraction of monomer A in a star copolymer
f^t	translational friction coefficient
$F(R_b)$	end-to-end distance of a branch
F	total frictional force on a chain

$\mathbf{F}_i$	frictional force on unit i
F_{ix}	x component of force on unit i
g	ratio of the quadratic radius of gyration of a branched chain to that of a linear chain of the same molecular weight
g_G	ratio of the quadratic radius of gyration of a Gaussian branched chain to that of a Gaussian linear chain of the same molecular weight
g_n	number of generations in a dendrimer
g'	ratio of the viscosity of a branched chain to that of a linear chain of the same molecular weight
G'	real or storage modulus
G"	imaginary or loss modulus
h	ratio of the translational friction coefficient of a branched chain to that of a linear chain of the same molecular weight
h*	hydrodynamic interaction parameter
H	matrix of preaveraged hydrodynamic interactions
HI	hydrodynamic interactions
I	3×3 unit tensor
k_B	Boltzmann's constant
KR	Kirkwood-Riseman
$\mathbf{l}_i$	bond vector i
LJ	Lennard-Jones potential
M	molecular weight
MC	Monte Carlo
MD	Molecular Dynamics
NVT	canonical ensemble
NPT	isothermal-isobaric ensemble
n-1	number of bonds between two units
n_b	number of beads in a blob
n_{bc}	number of bonds of a given unit
n_c	number of chains in a simulation box
n_{ext}	number of external blobs
n_S	number of units within a dendrimer spacer
N	number of beads in a free chain
N_b	number of beads in a tethered branch or chain
N_L	number of sites in a lattice
N_A	Avogadro's number
p	pressure
P	universal friction parameter
P(q) or P(x)	scattering form factor
q	modulus of the scattering vector
r	distance to the tethering surface, line or point
r_S	lateral distance to the adsorption point in a plane
r_Z	perpendicular distance to the adsorption point in a plane
R	end-to-end distance

R_b	center-to-end distance in a star
R_c	radius of the star core
R_g	mean size of a chain
$R_g{}_b$	mean distance from the tethering point to the chain or branch end
R_h	hydrodynamic radius
$\mathbf{R}_i$	position vector of unit i
$\mathbf{R}_{ij}$	vector joining units i and j
R_S	radius of a rigid sphere
RG	renormalization group
S	radius of gyration
SANS	small angle neutron scattering
SAW	self-avoiding walk
SCF	self-consistent field
t	time
t_0	time zero for correlation
t*	reduced time
T	temperature
$\mathbf{T}$	hydrodynamic interaction (Oseen) tensor
$\mathbf{u}_i$	ith Rouse normal coordinate
U	intramolecular potential
$\mathbf{v}$	center of masses velocity
$\mathbf{v}_i$	velocity of unit i
$\mathbf{v}_i{}^s$	velocity of solvent at unit i
V	volume
$\mathbf{v}^s{}_{i0}$	bulk solvent velocity at unit i
V_w	constant in experimental scattering data
w_{conf}	statistical weight of a configuration
x	chain size-scaled scattering variable
x_b	ideal branch size-scaled scattering variable
$\mathbf{X}$	generic vector
y	exponent in the brush osmotic pressure dependence
y_i	y coordinate of the i unit
y_1	exponent in the empirical dependence of friction
y_2	exponent in the empirical dependence of viscosity
z	excluded volume parameter
z*	reduced excluded volume parameter
ZK	Zimm-Kilb
α	expansion factor
β	reduced bead-bead cluster integral
β_0	reduced bead-bead cluster integral (athermal solvent)
ε	attractive energy (in a lattice or a potential well)
ζ	friction coefficient of a bead
$[\eta]$	intrinsic viscosity
$[\eta(\omega)]$	frequency-dependence complex intrinsic viscosity
η_0	solvent viscosity

θ	theta temperature
$\theta(f)$	exponent in the dependence of the center-to-end distance distribution of a star branch
$\lambda(f)$	exponent for the distance distribution of adsorbed stars
ν	excluded volume mean size critical exponent
ξ	blob size
Π_S	osmotic pressure
ρ	ratio of the radius of gyration to the hydrodynamic radius
ρ_b	bead density
ρ_f	density of tethered chains or branches
ρ_f^*	overlapping density of tethered chains or branches
ρ_S	density of a rigid sphere
σ	repulsive distance parameter in an intramolecular potential
τ_b	relaxation time of a tethered chain
τ_e	elastic relaxation time
τ_k	relaxation time of the kth Rouse mode
τ_D	rotational relaxation time
Φ	universal viscosity parameter
Φ_p	polymer volume fraction
χ	Flory-Huggins thermodynamic interaction parameter
Ψ^*	interpenetration factor
ω	angular velocity of oscillatory shear gradient
$<>$	conformational average
$<>_0$	conformational average in a Gaussian chain
$\approx$	proportional

1 Introduction

Modern synthesis methods, fundamentally based on anionic polymerization [1] have allowed for the preparation of a great variety of polymers with specific branching structures (see Fig. 1) in addition to the random branching that occurs in the polymerization of commercial polymers. Thus, there are architectures with a single polyfunctional branching point containing arms of the same chemical structure with the same or different chain lengths (uniform or non-uniform star chains [2]), and similar structures, but with the arms containing monomers of different compositions (star copolymers and miktoarms). Also, there are structures with a given number of branching points distributed, randomly or uniformly along a backbone (comb chains). Moreover, polymer chains can be grafted onto a surface giving rise to structures generally known as brushes [3, 4]. (Comb chains with branching points of functionality greater than 3 are also sometimes called polymeric brushes [5]). Furthermore, it is possible to build structures possessing regular "treelike" or "dendritic" branching with radial symmetry usually called starburst dendrimers [6, 7]. The multifunctional groups at the ends can react to give a new generation containing an increasingly

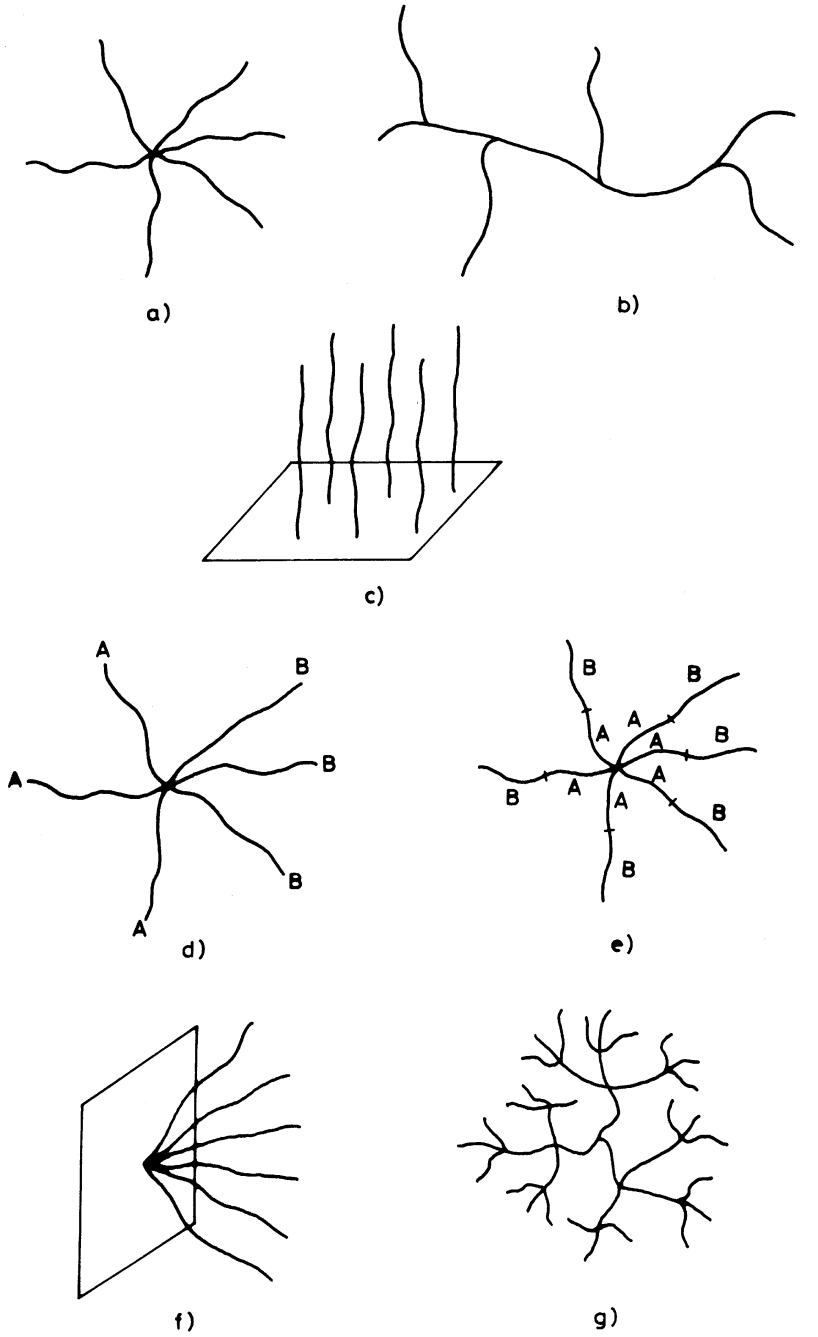

Fig. 1. **a** Star polymer. **b** Comb polymer. **c** Brush. **d** Miktoarm star copolymer. **e** Star copolymer. **f** Star chain center-adsorbed in a plane. **g** Dendrimer

higher number of monomer units. It can be understood that the properties of all these structures can differ remarkably from those of linear polymers of similar chemical composition and molecular weight [8].

Stars, combs with three-functional branching points along a locally rigid backbone, and planar surface-brushes can also be considered as assemblies of linear chains tethered to d_f-dimensional objects [9] (d_f=0, chains tethered to a point, or stars, d_f=1, chains tethered to a line, combs, and d_f=2, chains tethered to a surface, brushes). Excellent introductions and reviews on the molecular properties of these different molecular architectures are contained in [2–4, 6–9].

The interpretation of the physical properties of polymers can be accomplished by means of theories based on molecular models [10]. Often, however, these theories cannot incorporate the complexity necessary to describe branched chains properly. Thus, the presence of a branching point may cause a substantial increase in the density of monomeric units close to it in comparison with other regions of the chain [11]. Some of the idealized polymer models commonly employed in the study of linear chains cannot properly describe this effect. Of course, the heterogeneity in the distribution of polymer units is more important for high functionalities, e.g., the heterogeneity occurring in stars with many branches allows one to distinguish a central region or core of large density of polymer units. Consequently, one of the crucial problems in the study of branched polymers is to formulate a consistent description of the bead density in the different chain regions. The congestion of units close to the branching points also causes difficulties in hydrodynamic and dynamic theoretical treatments. Thus, the popular Rouse [12] and Rouse-Zimm [13] theories, usually employed to describe the dynamics of flexible polymers, makes use of assumptions that can fail to give some of the characteristic features of branched chains. The presence of branching points gives rise to slow relaxation processes that are not described in the Rouse theory [2]. The characterization of different chain relaxations is also an important problem in the study of brushes. Furthermore, the hydrodynamic properties commonly employed for routine polymer characterization depend strongly on the polymer architecture, and the description of these properties by means of the Rouse-Zimm theory is particularly poor in some cases, such as the viscosity of many-arm stars.

Simulation methods have been proved to be useful in the study of many different molecular systems, in particular in the case of flexible polymers chains [14]. According to the variety of structures and the theoretical difficulties inherent to branched structures, simulation work is a very powerful tool in the study of this type of polymer, and can be applied to the general problems outlined above. Sometimes, this utility is manifested even for behaviors which can be explained with simple theoretical treatments in the case of linear chains. Thus, the description of the theta state of a star chain cannot be performed through the use of the simple Gaussian model. The adequate simulation model and method depend strongly on the particular problem investigated. Some cases require a realistic representation of the atoms in the molecular models [10]. Other cases, however, only require simplified coarse-grained models, where some real mon-

omeric or repeating units are engulfed into a single ideal bead [15]. In some cases these beads can be placed on the sites of geometrical lattices. These ideal models allow for a considerable saving of computational time and are able to reproduce the "long-range" or "low frequency" properties, i.e., global properties that do not depend on the local behavior of the chain atoms [16]. There are several types of simulation procedures [14, 17–19]. In the Monte Carlo (MC) methods, different new configurations, i.e., representations of the system, are sampled either randomly (random MC) or after generating a stochastic change in the previous configuration giving rise to a Markov process [18]. The properties of interest (the macroscopic equilibrium conformational averages) are then derived from the values obtained for different configurations in the sample. Some of the Markov processes may actually represent realistic conformational changes in local parts of the chains. With these types of algorithms, it is possible to generate a "Dynamic Monte Carlo" (DMC) trajectory from which some global dynamical properties can be calculated. DMC can even be applied to describe the dynamics of discrete representations of the polymer chains in lattice models. Other simulation algorithms, however, do not rely on stochastic changes, but calculate dynamic trajectories by solving the system equations of motion [19]. Molecular Dynamics (MD) methods use the classical mechanics equations of motions to obtain the positions and velocities of polymer units (and also of solvent molecules if included in the system), while Brownian Dynamics (BD) methods solve the Langevin equation, in which a frictional continuous solvent is represented by a stochastic force acting on each one of the polymer units. MD and BD simulations can be performed on realistic models and also on off-lattice but coarse-grained polymer models.

In this article I review some of the simulation work addressed specifically to branched polymers. The brushes will be described here in terms of their common characteristics with those of individual branched chains. Therefore, other aspects that do not correlate easily with these characteristics will be omitted. Explicitly, there will be no mention of adsorption kinetics, absorbing or laterally inhomogeneous surfaces, polyelectrolyte brushes, or brushes under the effect of a shear. With the purpose of giving a comprehensive description of these applications, Sect. 2 includes a summary of the theoretical background, including the approximations employed to treat the equilibrium structure of the chains as well as their hydrodynamic behavior in dilute solution and their dynamics. In Sect. 3, the different numerical simulation methods that are applicable to branched polymer systems are specified, in relation to the problems sketched in Sect. 2. Finally, in Sect. 4, the applications of these methods to the different types of branched structures are given in detail.

2
Theoretical Background

2.1
Structure

A basic theoretical model for flexible polymers is the Gaussian chain which assumes N ideal beads with intramolecular distance between them following a Gaussian distribution, so that the mean quadratic distance between two beads separated by n-1 ideal and not correlated bonds is given by [15, 20]

$$< R_{ij}^2 >_0 = (n-1)b^2 \tag{1}$$

where b is the statistical length of the beads and the subscript 0 indicates the unperturbed (ideal) character of the Gaussian chain. Therefore, the model predicts that the mean square end-to-end distance of a linear chain can also be written as

$$< R^2 >_0 = (N-1)b^2 \cong Nb^2 \tag{2}$$

and the same proportionally with N also holds for the Gaussian mean quadratic radius of gyration of the chain, $<S^2>_0$. Then, the chain mean size can be estimated as

$$R_g \approx < R^2 >_0^{1/2} \approx < S^2 >_0^{1/2} \approx N^{1/2} \,. \tag{3}$$

The averaged global shape of the chain is represented by a coil with some degree of asphericity. This model is adequate to describe the coarse-grained properties of ideal chains, i.e., chains without intramolecular long-range interaction between units. Therefore, it can be applied in situations where the long-range interactions are effectively canceled. According to Flory [20], this should be the case of a polymer chain in the melt state where intramolecular and intermolecular interactions are indistinguishable, since the density of polymer units is homogeneous and no other types of monomer or solvent molecules are present. Linear chains in dilute solution obey a pseudoideal behavior in the theta state of relatively poor thermodynamic solvent quality, or at the theta (θ) temperature for a given polymer-solvent system [15, 16, 20], where long-range binary polymer-polymer intramolecular interactions are exactly canceled by the polymer-solvent interactions. Deviations from the ideal behavior in theta conditions can be caused by the chain stiffness, in the case of partially rigid chains that are not sufficiently long. The stiffness effects can be incorporated through theoretical models such as the wormlike chain model in terms of a persistence length parameter [15].

For solvents of good thermodynamic quality, the polymer-solvent interactions are preferred over the intramolecular interactions between beads which, therefore, can be effectively considered as repulsive interactions that give rise to

the excluded volume (EV) effects. Then it is possible to define a relevant EV parameter, $z \approx \beta N^{1/2}$, that is proportional to the reduced bead-bead binary cluster integral (relative to the bead volume), β. This integral is assumed to vary with temperature as $\beta=\beta_0(1-\theta/T)$. For $T>>\theta$, the chains tend to expand by including more solvent and form a swollen coil to avoid the repulsive bead-bead interactions. A basic representation of EV is included in the models that consider self-avoiding walk (SAW) chains where the N bonds are not correlated, similarly to the Gaussian chain, but where two beads cannot be in the same position in a given conformation. The EV effect is a many-body type problem. It has been described through two-parameter (b and β or z) perturbation theories [15, 16, 21] that yield universal expressions for the expansion factor

$$\alpha = \left(< S^2 > / < S^2 >_0 \right)^{1/2} = f(z) \tag{4}$$

However, the rigorous expressions obtained in this way are expansions valid only for small values of z. In fact, the theory cannot reach the most interesting limit of very long chains without the use of doubtful approximations, due to the divergence of the EV theory perturbation series for $z \to \infty$. The more recent approach based in formal similarities between the behavior of polymer systems and ferromagnetic materials, and the subsequent application by de Gennes and others of the scaling and renormalization group (RG) theories have allowed for an adequate resummation of the EV effects, which avoids the divergence problem [16]. Thus, it has been proved that the mean size of a long polymer chain of N beads in an athermal ($\beta=\beta_0 \cong 1$) solvent should be proportional to N^{ν}, where ν is a critical exponent whose value is $\nu=0.588 \cong 3/5$. The same result with $\nu=3/5$ is obtained from the mean-field Flory equation [20], which minimizes the free energy obtained as a competition between a cohesive (or entropic) contribution, consistent with the Gaussian distribution of units, and a mean-field evaluation of the monomer-monomer interaction in terms of parameter z. Domb and Barrett [22] have proposed an interpolation formula that takes into account the two-parameter theory expansion, valid for low z, and the EV power-law for high z to describe intermediate values of z. The ν exponent for EV conditions can be compared with the value 1/2, found for the equivalent exponent for the ideal chain, Eq. (3). The RG approach can be related with the two-parameter theory through RG calculations for thermal solvents that yield [23]

$$R_g \approx < S^2 >^{1/2} \approx N^{\nu} \beta^{(2\nu-1)} \tag{5}$$

valid for $z>>1$. On the other hand the chains tend to collapse into a compact globule [24] when they are placed, conveniently diluted, in a very poor solvent (sub-theta regime). Considering a uniform density inside the globule and assuming that the contraction of the chain with respect to the ideal dimensions can be expressed as in Eq. (4), i.e., in terms of a coefficient $\alpha=f(z)$ (now smaller than 1, and corresponding to negative values of β and the variable z) the scaling

law $R \approx N^{1/3}|\beta|^{-1/3}$ is predicted. The transition from the expanded coil to the compact globule can be approximately described by a generalization of the Flory mean-field theory for EV, including a three-body term [24]. A further generalization of this theory to stars has been accomplished by di Marzio and Guttman [25].

It should also be noted that ternary and higher order polymer-polymer interactions persist in the theta condition. In fact, the three-parameter theoretical treatment of flexible chains in the theta state shows that in real polymers with finite units, the theta point corresponds to the cancellation of effective binary interactions which include both two body and fundamentally repulsive three body terms [26]. This causes a shift of the theta point and an increase of the chain mean size, with respect to Eq. (2). However, the power-law dependence, Eq. (3), is still valid. The RG calculations in the theta (tricritical) state [26] show that size effect deviations from this law are only manifested in linear chains through logarithmic corrections, in agreement with the previous arguments sketched by de Gennes [16]. The presence of these corrections in the macroscopic properties of experimental samples of linear chains is very difficult to detect.

Non-dilute solutions also allow for theoretical descriptions based on scaling theory [16, 21]. When the number of polymer chains in the solution is high enough, the different chains overlap. At the overlapping concentration c*, the long-scale density of polymer beads becomes uniform over the solution. Consequently c* can be evaluated as

$$c^* = (M / N_A) / R_g^3 \approx N / R_g^3 \tag{6}$$

where M is the polymer molecular weight (proportional to N) and N_A is the Avogadro number. Since R_g follows the scaling law given by Eq. (3) or Eq. (5) for theta or EV conditions, c* decreases for longer chains and can actually be very small for high molecular weight polymers. Semi-dilute solutions of linear chains are defined as those with polymer concentrations beyond c* but still with a small number of interactions between polymer units. Consequently there are no significant high-order bead-bead interactions, implying correlated fluctuations in the local polymer density.

A semi-dilute solution has an entangled aspect similar to a network. An individual chain can be envisioned as constituted by a series of blobs of size ξ, equal to the transient network mesh size [16], which obviously decreases with increasing concentration. For $c \equiv c^*$, ξ is similar to the chain mean size. For $c >> c^*$, however, the mesh size is independent on the chain length. In a good solvent, according to Eqs. (5) and (6), these conditions are satisfied by:

$$\xi \approx N^{\nu} \beta^{(2\nu-1)} (c / c^*)^{\nu/(1-3\nu)} \tag{7}$$

and, consequently, ξ is approximately proportional to $c^{-3/4}$. Within each one of the blobs the chain does not interact with other chains and, consequently, its be-

havior correspond to the EV regime. The number of units in a blob is obtained from Eq. (5) as

$$n_b \approx \xi^{1/\nu} \beta^{(1-2\nu)/\nu} \tag{8}$$

The whole system is a packed system of blobs, and the distribution of blobs in a chain is similar to the ideal distribution of units in the melt state. For c>>c*, the global size in a good solvent is obtained by considering Eqs. (2), (3), (7) and (8):

$$R_g \approx (N/n_b)^{1/2} \xi \approx N^{1/2} (c/\beta)^{(2\nu-1)/2(1-3\nu)} \approx N^{1/2} (c/\beta)^{-1/8}. \tag{9}$$

If the polymer concentration increases so that the number of high order bead-bead interactions is significant, c>>c**≈β, (when c is expressed as the polymer volume fraction, Φ_p), the fluctuations in the polymer density becomes small, the system can be treated by mean-field theory, and the ideal model is applicable at all distance ranges, independent of the solvent quality and concentration. These systems are denoted as concentrated solutions. A similar description applies to a theta solvent, but in this case, the chains within the blobs remain pseudoideal so that $n_b \approx \xi^2$, $\xi \approx N^{1/2}(c/c^*)^{-1}$ and $R_g \approx N^{1/2}$, i.e., the global chain size is always independent of concentration.

The different regimes of solvent quality and concentration cannot be similarly described in the case of branched chains, due to the higher local density of polymer units around the branching points. Thus, an adequate scaling theory has been applied for the case of a uniform star chain of high functionality (f arms) by Daoud and Cotton [11]. According to this description, the central core is a dense pack of polymer units, similar to that of a melt system, but with all the units belonging to the same chain. Then the polymer core adopts the aspect of globule with uniform density, i.e., with a mass proportional to its volume. Consequently, if the chains are relatively small, the chain size should correspond to

$$R_g \approx N^{1/3} = N_b^{1/3} f^{1/3} \tag{10}$$

(N_b=N/f is the number of beads per branch or arm). For larger chains, however, the solvent can penetrate in outer regions of the star and the situation within these regions is more like a concentrated solution or a semi-dilute solution. These portions of the arms constitute a series of blobs, whose sizes increase in the direction of the arm end. The surface of a sphere of radius r from the star center is occupied by f blobs. Then the blob size ξ is proportional to $rf^{-1/2}$. Most internal blobs are placed in conditions similar to concentrated solutions and, consequently, their squared size is proportional to the number of polymer units inside them as in an ideal chain. This permits one to obtain the density of units inside the blob, n_b/ξ^3, as a function of r:

$$\rho_b(r) = r^{-1} f^{1/2}. \tag{11}$$

A three dimensional integration of this density over values of r ranging from 0 to the mean branch extension, R_g^b (which is also proportional to the global star size R_g), i.e., over the overall chain volume, give the total number of units in the star, N. In this manner the chain mean size is estimated as

$$R_g \approx N_b^{1/2} f^{1/4} . \tag{12}$$

The exponents in Eqs. (10) and (12) agree in the crossover region which, therefore, should correspond to $N_b \cong f^{1/2}$. Consequently, the concentrated solution regime is reached for chains with $N_b >> f^{1/2}$. In a good solvent when the arms are long enough, however, the peripheral blobs behave as in a semi-dilute solution, and they are swollen, i.e., Eq. (8) holds. This new condition leads to

$$\rho_b(r) \approx r^{(1-3\nu)/\nu} f^{(3\nu-1)/2\nu} \beta^{(1-2\nu)/\nu} \cong r^{-4/3} f^{2/3} \beta^{-1/3} \tag{13}$$

$$R_g = < S^2 >^{1/2} \approx R_g^b \approx N_b^{\nu} f^{(1-\nu)/2} \beta^{(2\nu-1)} . \tag{14}$$

The simultaneous agreement of exponents in Eqs. (12) and (14) characterizes the crossover condition. Then it is derived that the validity of Eq. (14) corresponds to $N_b >> f^{1/2}\beta^{-2}$. This means that for an athermal solvent, where $\beta \cong 1$, the intermediate region governed by Eq. (12) disappears, while for a theta solvent Eq. (14) is not applicable.

The distribution of the center-to-end distance, $F(R_b)$, in a star can also be predicted from scaling theory. For EV chains, it is expected to be close to Gaussian [26], except for small R. Applying scaling arguments and RG theory, Ohno and Binder [27] obtained a power-law behavior for small R, $F(R_b) \approx (R_b / < R_b >)^{\theta(f)}$ with the exponent value $\theta(f) \cong 1/2$ for high f. They also considered the case of a star center adsorbed on a planar surface, evaluating the bead density profiles and the distribution of center-to-end distance in the directions perpendicular and parallel to the surface in terms of similar power-laws.

The Daoud and Cotton scaling theory can be considered as a particular case of the general scaling treatment for tethered chains [9]. Thus, combs with three-functional branching points from a locally rigid backbone, and brushes are similarly described by introducing the value of d_f corresponding to the dimensional object to which the chains are tethered. The scaling equations assume that the density of branches (per unit length) or grafted chains (per unit surface), ρ_f, is above the critical overlapping values, $\rho_f^* \approx N^{-\nu}$ and $\rho_f^* \approx N^{-2\nu}$ for EV combs and brushes. Below the overlapping branching or grafting density, the chains hardly interact, they are not stretched, and the branch extension or the brush height does not depends on this density. These conditions are denoted as the mushroom regime. In the overlapping regime, the blob surface can be estimated by assuming that the spherical/cylindrical/planar surface at distance r from the tethering object is shared by the different crossing arms/branches/grafted chains, accordingly to the value of ρ_f (ρ_f=f for stars). Then, the blob size can be written as

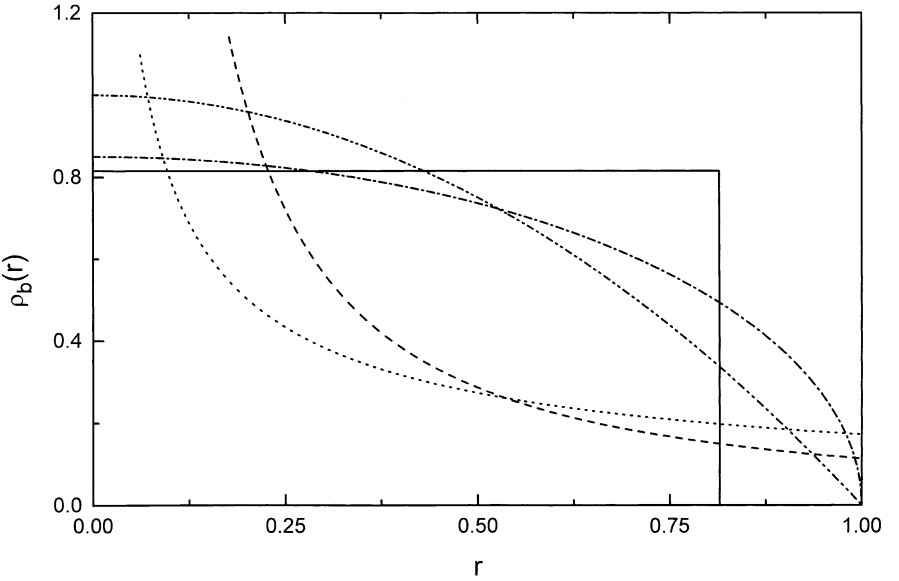

Fig. 2. Bead density profiles. *Solid line* Brushes, mean-field and scaling theory (step function); *dashed-dotted line* generalization of the Milner et al. theory for brushes in the theta state; *dashed-double dotted line* Milner et al. theory for brushes (EV chains); *dashed line* EV stars; *dotted line* EV combs. Variable r is scaled to give zero bead density for the smooth curves of brushes at r=1. The brush curves are normalized to show equal areas (same number of units). The comb and star densities are arbitrarily normalized to show similar bead density per volume unit as the step function and EV curves for brushes at the value of r where these curves intercept

$$\xi \approx r^{(2-d_f)/2} \rho_f^{-1/2}. \tag{15}$$

The density of units as a function of r is given as

$$\rho_b(r) = r^{(1-3\nu)(2-d_f)/2\nu} \rho_f^{(3\nu-1)/2\nu} \beta^{(1-2\nu)/\nu} \tag{16}$$

in a good solvent. Figure 2 illustrates this behavior for the different cases. Integrating the bead density over a d_f-dimensional r variable from zero to the mean extension of the branch or grafted chain gives the number of beads (total number in stars, or the number per unit length/surface for combs/brushes), $N = N_b \rho_f$. This way, the size of a branch or grafted chain is finally estimated as

$$R_g^b \approx N_b^{2\nu/(2-d_f+d_f\nu)} \rho_f^{(1-\nu)/(2-d_f+d_f\nu)} \beta^{(2\nu-1)/2(2-d_f+d_f\nu)} \tag{17}$$

again in a good solvent. Equations (16) and (17) can, in fact, be considered as general results applicable to the theta and sub-theta compact globule regimes, provided that the critical exponent ν is substituted by the adequate 1/2 and 1/3 exponents, and β is respectively ignored or substituted by its absolute value.

Interestingly, scaling theory predicts for brushes that the density of units is independent from the distance to the surface and that the extension of the chain (or the brush height) is proportional to its contour length as if the chains were completely extended. Thus

$$R_g^b \approx N_b \rho_f^{(1-\nu)/2\nu} \cong N_b \rho_f^{1/3} \tag{18}$$

in the EV regime. The same result was obtained by Alexander [28] who applied a theory similar to the Flory treatment of free linear chains, in which the global stretching of a chain, due to mean-field repulsive interactions, is opposed by an entropic contribution. The brush height can be investigated through experimental force measurements between two brushes. The experiments of Auroy et al. [29] confirm its proportionality with the chain length for poly(dimethylsiloxane) chains grafted onto porous silica. More recent experiments [30] have demonstrated that grafted triblock polymer chains are stretched far beyond their equilibrium extension. The collapse or sharp transition to the compact form suffered by individual chains does not apply to brushes in the overlapping regime. Instead, a "weak collapse" is expected, where the brush height decreases but the chain still remain stretched, with its extension proportional to the chain length [31].

An improvement of the approximate Flory approach is given by self-consistent field (SCF) methods, in which the EV interactions are described by a potential field, depending on the segment distribution, which in turn influences this distribution giving rise to a self-consistent procedure. Thus, the Daoud and Cotton scaling prediction for the bead density function of stars has been verified through SCF calculations [32, 33]. The SCF method has also been applied to combs [32], showing that the scaling law gives the correct dependence on ρ_f, but the decay is somehow slower than the $\rho_b(r) \approx r^{(1-3\nu)/2\nu} \cong r^{-2/3}$ prediction. Moreover, the SCF theory for brushes shows that the density of monomers is not uniform, but follows a parabolic decay from a maximum near the surface to zero at the brush height [34]. This result is explained by Milner et al. [35] by assuming that the most favorable configuration of a chain is found by minimizing the sum of local stretching and repulsion terms, allowing that the chain ends are located at any distance from the interface (in contradiction with the Flory-type approach which considers global interactions), and assuming that this configuration is predominant in the long chain limit. Then the extension of the chain is similar to the Alexander result, but a parabolic decay of the bead density is found:

$$\rho_b(r) = C_1 \rho_f^{2/3} - C_2 (r / N)^2 \tag{19}$$

(this decay is also included in Fig. 2). The same theory predicts that the density of end units within the brush is not zero, unless ρ_f is high. This disposition is different in stars, where the ends are preferentially disposed in the outer regions of low bead density. Experimental techniques as neutron reflectivity and small angle neutron scattering (SANS) [36] can probe the inner structure of brushes. The SCF theory predicts [37, 38] that the bead density in the theta state follows an elliptical decrease as a function of the scaled variable $r/N\rho_f^{1/2}$. This is compared with the EV profile in Fig. 2.

Similar theoretical calculations have also been applied to dendrimer molecules of different number of generations, g_n, with a high number of units between functional points, n_S, by de Gennes and Hervet [39], assuming a concentric shell for each generation. The number of monomers in the dendrimer is proportional to n_S and grows exponentially with g_n. Since the available volume grows only as g_n^3, a perfect dendrimer can be grown up to a given generation number limit beyond which only imperfect growth is achieved. According to de Gennes and Hervet, the bead density profile (within the limit generation number) grows parabolically from the core reaching the asymptote value of one at the outer regions. The size of the dendrimer is obtained to be $R_g \approx N^{1/5}$. Recent SCF calculations by Boris and Rubinstein [40] show, however, that the density decreases with r and the ends are distributed in all regions. Biswas and Cherayil [41] performed RG calculations for dendrimers in EV conditions. Their results indicate that exponent ν can also be employed to describe the mean size of starburst molecules.

Freed et al. [42, 43], among others [44, 45] have performed RG perturbation calculations of conformational properties of star chains. The results are mainly valid for low functionality stars. A general conclusion of these calculations is that the EV dependence of the mean size can be expressed as the contribution of two terms. One of them contains much of the chain length dependence but does not depend on the polymer architecture. The other term changes with different architectures but varies weakly with EV. Kosmas et al. [5] have also performed similar perturbation calculations for combs with branching points of different functionalities (that they denoted as brushes). Ohno and Binder [46] also employed RG calculations to evaluate the form of the bead density and center-to-end distance distribution of stars in the bulk and adsorbed in a surface. These calculations are consistent with their scaling theory [27].

The ratio of the squared radius of gyration of a branched polymer to that of the linear polymer having the same molecular weight:

$$g = < S^2 >_{br} / < S^2 >_{lin} \tag{20}$$

is usually employed to analyze the architectural dependence obtained from experimental data. The calculation of g with Gaussian chain model for a uniform star chain, g_G, was performed by Zimm and Stockmayer [47]. They obtained

$$g_G = (3f - 2)/f^2 . \tag{21}$$

This result is valid when the intramolecular interactions are canceled out, i.e., if the mean-field theory is applicable. For a high number of arms, $g \approx f^{-1}$. The same limit also applies to stars with randomly distributed units. Kurata and Fukatsu [48] performed a more general calculation which also included other branched structures as combs (with uniform or random distribution of units in the subchains between branching points and in the branches) and randomly branched chains, all of them with Gaussian statistics. They found that $g_{star} < g_{random} < g_{comb}$ and that the random distribution of units diminishes the contraction of chain size (or increases g) with respect to a uniform chain with the same type of branching. Quantitatively, their results for g can be applied to dilute solutions in the theta state when only low functionality branching points are present, so that core effects around these centers are not significant.

According to the RG calculations, valid for relatively low functionalities, the mean contribution of EV in the numerator and denominator of Eq. (20) should cancel for any branched structure in a good solvent. Therefore, ratio g for a star in a good solvent should be very close to g_G, Eq. (21). Different experimental data included in [49] seem to support this conclusion. Croxton [50] carried out iterative deconvolution theoretical calculations for uniform stars with up to six arms of model lengths that yielded, $g \approx f^{-1}$, a result that is not in agreement with Eq. (21) for the considered range of low functionalities. On the other hand, Eq. (14) shows that the Daoud and Cotton theory gives $g \approx f^{(1-3\nu)}$, or, approximately, $g \approx f^{-4/5}$. A fit of available experimental data for stars in good solvents with f=2–128 is consistent with this scaling law [2, 51].

Contrary to the case of linear chains, the ideal chain cannot generally provide a good representation of a branched chain in the theta state. Thus, the presence of the core in a star chain induces important finite-size effects. These effects are even manifested in the location of the theta point. Since a higher number of branches induces more three-body terms, the compensation of the effective binary interactions (including these three-body terms) is achieved at lower temperatures. This effect is found experimentally for star chains of low molecular weight [49]. Then the theta temperature increases with the molecular weight for relatively short highly-branched chains. For longer chains, however, the number of third-body interactions in the core is relatively small and the theta temperature becomes independent of the chain architecture. The same three-body effects cause an expansion of the branched chains at the theta point with respect to the result expected for an ideal chain [42]. It must be considered that, although the compact distribution of beads within the core is similar to the melt state, the distribution of distances within an arm corresponds, in fact, to an extended conformation. This effect increases remarkably with the degree of branching. Therefore, it is expected from the RG calculations that the values of g of highly branched stars in the theta state, g_θ, are greater than those predicted by the ideal chain, Eq. (21), and, consequently, than those corresponding to the good solvent case. The variation of g_θ with f can be obtained from the scaling theory, Eq. (12) as $g \approx f^{-1/2}$. Fits of experimental data for theta state stars in the range 2–128 presented in [2, 51] yield

$g \approx f^{-0.69}$ and $g \approx f^{-0.64}$. It seems that the exponent depends to some extent on the values of f included.

An increase of g in the theta state with respect to the ideal values is similarly obtained by Ganazzoli et al. [52, 53] through the use of a theoretical approach based on the self-consistent minimization of the intramolecular free energy. Their results indicate a significant expansion of the star arms due to the core effects. The same type of calculations have later been used to describe the star contraction in the sub-theta regime [54]. Guenza et al. [55] described a star chain at the θ point as a semiflexible chain with partially stretched arms that take into account the star core effect. Their results are also consistent with experimental data.

A simple characterization of the chain shape is given by the asphericity, that can be defined and calculated form the eigenvalues of the tensor of quadratic components of the radius of gyration [56]. Branched structures should exhibit clear deviations from the asphericity obtained for linear chains, approaching the zero value corresponding to the sphere limit for very compact structures. The asphericity of ideal uniform star polymers has been theoretically predicted with the Gaussian model by Wei and Eichinger [57]. Wei [58] has also extended the calculations to the case of non-uniform stars. He found a "maximum shape symmetry" effect for stars of two or three different arm lengths at intermediate values of f. This effect is characterized by values of the largest component of the tensor and the prolateness parameter that are higher than for linear chains. Moreover, he has evaluated the asphericity of Gaussian combs with f branches, which exhibit a minimum of asphericity for an intermediate values of f, recovering the result of linear chains for $f \to \infty$. Some RG calculations have also been performed to obtain the asphericity of linear chains with EV [59].

The form factor is an important property of individual chains. This property is expressed as a function of $x = q^2 \langle S^2 \rangle$, where q is the modulus of the scattering vector depending of experimental factors (observed scattering angle and wavelength of the scattering radiation). The form factor of an ideal linear chain is given by the monotonously decreasing Debye function [15]

$$P(x) = (2/x^2)(x - 1 + e^{-x}) . \tag{22}$$

This function also gives an accurate description of the behavior of a linear chain in a good solvent (the expansion of the chain size is scaled by the x variable) except for very high values of x, corresponding to short distances between units. These short distances are dominated by the correlation hole effect due to EV [16, 26].

The calculation of the form factor for an ideal uniform star chain was performed by Benoit [60]. The result can be expressed as

$$P(x) = (2/fx_b^2)\left[x_b - 1 + e^{-x_b} + \frac{f-1}{2}(1 - e^{-x_b})^2 \right] \tag{23}$$

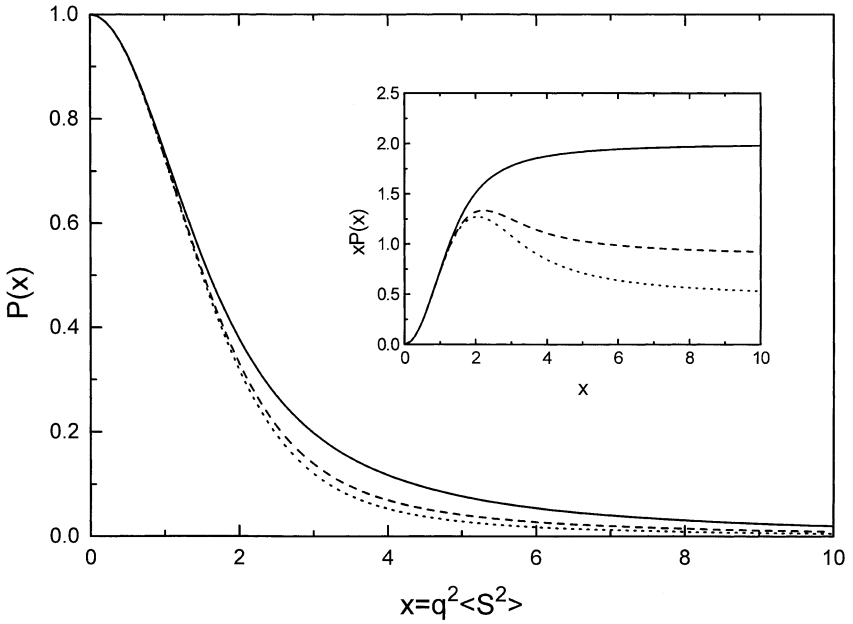

Fig. 3. Form factors. *Solid line* Linear chain; *dashed line* f=6 star chain; *dotted line* f=12 star chain. Inset: Kratky plots (same notation)

where $x_b=(x/g_G)/f$. The shape of the form factors predicted by Eq. (23) differs from the Debye function (Fig. 3). This effect is magnified by means of Kratky plots, in which $P(x)q^2$ is represented vs x. In these plots, the star chains show a maximum which is amplified for higher numbers of arms, while the linear chains exhibit a monotonous increase [61] (see inset at Fig. 3). The Benoit function gives a good description of small angle neutron scattering (SANS) data of 18-arm polyethylene (PE) star melts [62], and the resulting radius of gyration is swollen with respect to the ideal chain prediction. The mean size data of PE stars in the theta state obtained by Boothroyd et al. [63] follow essentially the same behavior, with some additional swelling.

The self-consistent free-energy minimization approach of Ganazzoli et al. [64] yields results for the scattering of stars in the theta point. These functions are compared with the Benoit function, showing some sharpening in the Kratky peak. This feature is attributed to a more uniform density due to intramolecular interactions and describes better experimental data [65] for 12-arm polystyrene (PS), though both theoretical curves fail to give a qualitative description of the high-q region. They also have computed the average angle between arms which decreases from the ideal chain value. Based on these results, the authors have proposed the existence of umbrella-like conformational shapes, though there is no firm evidence of this feature.

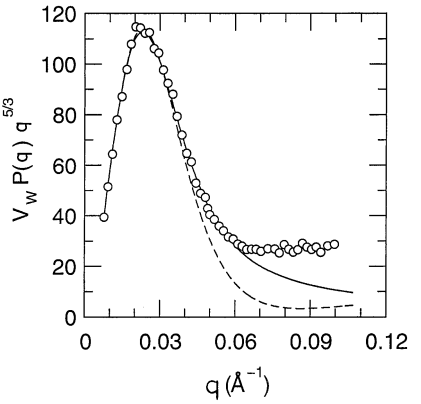

Fig. 4. Generalized Kratky plot of the experimental form factor of an 18-arm PI star (*points*); *solid line* fit to the Benoit function, Eq. (23); *dashed line* fit to the RG curve described in [66]. Reprinted with permission from [67]. Copyright (1994) American Chemical Society

The form factor of a star in a good solvent is better represented by a generalized Kratky plot $P(x)q^{1/\nu}$ vs x. The experimental data show a plateau for high values of q, i.e., at the short-range distance, which correlates with the blob size [11]. Croxton [50] performed calculations of the star form factors with his iterative deconvolution method for relatively short chains that showed significant differences with the Benoit curve. An RG calculation of the form factor of uniform star chains has been carried out by Alessandrini and Carignano [66]. They obtained a complex closed-form expression that can be more simply written by means of a fitted formula. The RG formula qualitatively reproduces the expected plateau, though, like the Benoit curve, cannot be adequately fitted to reproduce the experimental data of an 18-arm polyisoprene (PI) star in a good solvent [67] for high values of q (see Fig. 4).

The experimental data corresponding to one labeled arm in stars of f=12 (good solvent) [68] shows, as expected, Kratky plot ordinates that increase monotonously with q. However, the plateau is only obtained with an apparent critical exponent of 2/3 (i.e., greater than the theoretical value, $\nu \approx 3/5$). This seems an indication of the arm stretching effect, though the scaling and RG theoretical predictions describe this effect only in terms of a pre-exponential factor [11, 42].

In the case of finite star chains with very high functionality, the units are concentrated near and in the star core. Therefore, their theoretical behavior can approximately be described by a rigid sphere [2]. The form factor of a sphere presents a series of oscillations. The experimental data of stars with 128 arms [67] show a smooth function covering the first two oscillations of the sphere, followed by a peak coincident with the third oscillation and the asymptotic behavior for high q previously described for stars of lower functionalities. It seems that the chain resembles a soft spherical core with a peripheral region of considerably smaller density.

The osmotic second virial coefficient A_2 is another interesting solution property, whose value should be zero at the theta point. It can be directly related with the molecular second virial coefficient, expressed as $B_2=A_2M^2/N_A$ (in volume units). For an EV chain in a good solvent, the second virial coefficient should be proportional to the chain volume and therefore scales proportionally to the cube of the mean size [16]. It can, therefore, be expressed in terms of a dimensionless interpenetration factor that is defined as

$$\Psi^* = 2B_2 / (4\pi < S^2 >)^{3/2} . \tag{24}$$

RG calculations in the EV regime have been performed by Freed and Douglas for linear and uniform star chains [69]. The results are expected to be valid only for low functionality stars and, in fact, the comparison with existing experimental data is only reasonable for small number of arms, while the theoretical results for f≥6 clearly exceed the experimental data [49].

Similarly to linear chains, the overlap concentration [16] defines the limit of the semi-dilute regime, and c* has to coincide with the density within the branched chain. However, according to the Daoud and Cotton theory [11], the internal density in a star chain can follow three different regimes depending on the star region. If $f^{1/2}>>N$, the stars only contain their compact internal cores and cannot overlap. In the remaining cases there are two different regions. Inside a region defined by the radius R_c the interactions with other stars are not allowed, and the structure is similar to that of a single star. This radius is obtained by equaling the density within the blobs, $\rho_b(R_c)$, with the system concentration. Then, according to Eq. (13), the result for sufficiently long branches in a good solvent is

$$R_c \approx c^{\nu/(1-3\nu)} f^{1/2} \beta^{(2\nu-1)/(1-3\nu)} . \tag{25}$$

For $r>R_c$, the mesh size of the transient network should be equal to the blob size at distance R_c, i.e.,

$$\xi \approx R_c f^{-1/2} \approx c^{\nu/(1-3\nu)} \beta^{(2\nu-1)/(1-3\nu)} \tag{26}$$

and it coincides with the mesh size of linear chains, as it can be verified from Eqs. (5)–(7) for c>>c*. The same coincidence is also shown for theta solvents. Therefore, the semi-dilute solution of stars has the same aspect as a similar solution of linear chains, but including regions of radius R_c from the chain centers where the star behavior is preserved. The global mean size for c>>c*, is, therefore, given by the same expressions found for semi-dilute solutions of linear chains in a good solvent, Eq. (9), or in theta conditions, Eq. (3).

Recently, Grayce and Schweizer [70] have proposed a liquid-state theory for stars in the melt state, considering only repulsive interactions. They obtained $g \approx f^{-0.64} N_b^{-0.04}$, i.e., the exponent of the f-dependence is bracketed by the scaling theory and the Gaussian chain predictions for theta conditions (exponents –1/2

and –1 respectively). It can be noted that this exponent is also similar to the empirical result obtained from experimental data in theta solvents. The avoidance of the arms by each other is intermediate between the Gaussian model (that ignores this effect) and the scaling theory. This approach seems to be equally applicable in any range of values of f.

2.2 Hydrodynamic Properties

Hydrodynamic properties, such as the translational diffusion coefficient, or the shear viscosity, are very useful in the conformational study of chain molecules, and are routinely employed to characterize different types of polymers [15, 20, 21]. One can consider the translational friction coefficient, f^t, related to a transport property, the translational diffusion coefficient, D, through the Einstein equation, applicable for infinitely dilute solutions:

$$f^t = k_B T / D \tag{27}$$

(k_B is Boltzmann's constant), or the intrinsic viscosity, [η], that is obtained by extrapolating reduced shear viscosities to infinitely dilute conditions. As in the case of the mean size, the experimental data for dilute solutions are expressed in terms of ratios to the equivalent data for linear chains of the same molecular weight. Then, h corresponds to the ratio between the chain friction coefficients

$$h = f^t_{br} / f^t_{lin} \tag{28}$$

and g' corresponds to the ratio of intrinsic viscosities

$$g' = [\eta]_{br} / [\eta]_{lin} . \tag{29}$$

The theoretical prediction of these properties for branched molecules has to take into account the peculiar aspects of these chains. It is possible to obtain these properties as the low gradient limits of non-equilibrium averages, calculated from dynamic models. The basic approach to the dynamics of flexible chains is given by the Rouse or the Rouse-Zimm theories [12, 13, 15, 21]. However, both the friction coefficient and the intrinsic viscosity can also be evaluated from equilibrium averages that involve the forces acting on each one of the units. This description is known as the Kirkwood-Riseman (KR) theory [15, 71]. Thus, the translational friction coefficient, f^t, relates the force applied to the center of masses of the molecule and its velocity

$$\mathbf{F} = f^t \mathbf{v} \tag{30}$$

and **F** is obtained as a sum of the friction forces $\mathbf{F}_i$ exerted on the different units. These forces can be obtained from

$$\mathbf{F}_i = \zeta(\mathbf{v}_i - \mathbf{v}_i^s) = \zeta(\mathbf{v}_i - \mathbf{v}_{i0}^s) - \zeta\sum_{i\neq j}^{N}\mathbf{T}_{ij} \tag{31}$$

where ζ is the friction coefficient of a unit, $\mathbf{v}_i$ is the unit velocity, and $\mathbf{v}^s_i$ is the solvent velocity. This latter quantity differs from the bulk solvent velocity $\mathbf{v}^s_{i0}$ because of the presence of other polymer units. This effect is known as hydrodynamic interactions (HI), and can be described through tensor **T**. As with the EV effects, the HI between blobs are screened out in the semi-dilute regime [21]. For dilute solutions, tensor **T** can be obtained as an approximate solution of the Navier-Stokes equation for incompressible fluids. Its simpler form was derived by Oseen [72] as

$$\mathbf{T}_{ij} = 1/(8\pi\eta_0 R_{ij})\left(\mathbf{I} + \mathbf{R}_{ij}\mathbf{R}_{ij}/R_{ij}^2\right) \tag{32}$$

(η_0 is the solvent viscosity). Vector $\mathbf{R}_{ij}$ connects a pair of units and therefore depends on the particular chain conformation. Furthermore, the HI fluctuate with the fluctuations in the chain conformations. This problem is usually avoided by adopting an orientational and conformational preaverage [15, 21, 71] of **T**:

$$\mathbf{T}_{ij} \cong <\mathbf{T}_{ij}> = 1/(6\pi\eta_0) < R_{ij}^{-1} > \mathbf{I}\,. \tag{33}$$

This leads to a system of N linear equations from which the unit forces can be obtained. The final result can be expressed in the following general expression derived by Horta and Fixman [73], which does not assume any specific form for the distribution of distances between units, or chain model:

$$f^t = \zeta\sum_{i}^{N}\sum_{j}^{N}(\mathbf{H}^{-1})_{ij} \tag{34}$$

where **H** is a HI matrix defined as

$$\begin{aligned} H_{ii} &= 1 \\ H_{ij} &= (\zeta/6\pi\eta_0) < R_{ij}^{-1} > = (3/\pi)^{1/2} bh^* < R_{ij}^{-1} > \end{aligned} \tag{35}$$

h* is the HI parameter [74], whose particular value is not relevant in the non-draining limit, defined as $h^*N\to\infty$, and applicable in many experimental situations. For the free-draining regime, i.e., without HI, h*=0, and

$$f^t = \zeta N\,. \tag{36}$$

This result is applicable to semi-dilute and concentrated solutions [21], and is also useful to check many simulations that do not include HI. For non-draining chains, introducing Gaussian statistics in Eq. (35), and transforming the summations over a large number of units in Eq. (34) into integrals, the translational friction coefficient can finally be written as [15]

$$f^t = 6^{1/2}\eta_0 P < S^2 >^{1/2} \tag{37}$$

where P is a universal parameter for long flexible non-draining linear chains, P= 5.21. Performing a series expansion for the HI tensor, and neglecting higher terms, it is possible to avoid the preaveraging approximation. The result of this approach is known as the double-sum Kirkwood formula [75]

$$f^t = \zeta N^2 / \sum_i^N \sum_j^N H_{ij} = N / \left[1 + (\pi/3) h^* \sum_i^N \sum_j^N < R_{ij}^{-1} > \right] \tag{38}$$

which gives Eq. (37) for a long non-draining Gaussian linear chain but with P= 5.10.

A similar KR approach can be employed for the intrinsic viscosity. In this case it is necessary to assume the presence of a small amount of shear rate, which cancels out in the calculations. Now, the linear equations are used to evaluate an averaged crossed component of the stress tensor on unit i, $<F_{ix}y_i>$. The final result for a long linear non-draining chain is

$$[\eta] = 6^{3/2} \Phi < S^2 >^{3/2} / M \tag{39}$$

in terms of the other universal parameter for long ideal non-draining linear chains, Φ=2.87×10^{23} mol^{-1} (consistent with expressing [η] in cm^3/g and $<S^2>$in cm^2).

Equations (3), (37), and (39) give the scaling laws $f^t \approx N^{1/2}$, $[\eta] \approx N^{1/2}$ for long non-draining linear chains with Gaussian statistics or at the theta point. It can be assumed that the same power laws can also be applied to other types of non-draining flexible chains in ideal conditions. Moreover, it can be argued that Eqs. (37) and (39) can still be employed for other chain architectures in any type of solvent conditions, but with different values of P and Φ as N-independent parameters. Indeed, one can consider a rigid sphere of radius R_S as a limiting case, roughly describing a chain of any architecture collapsed in the sub-theta region [24], or a small star chain with many branches so that it only comprises the core region [11]. The radius of gyration of this compact object is calculated as

$$< S^2 >= (3/5) R_S^2 . \tag{40}$$

This result, together with two well-known hydrodynamic equations, the Stokes law for friction

$$f^t = 6\pi\eta_0 R_s \tag{41}$$

and the Einstein law for viscosity, expressed as

$$\left[\eta\right] = 2.5 / \rho_s \tag{42}$$

where ρ_s is the uniform density inside the sphere, allow for the calculation of the friction coefficient and the intrinsic viscosity as functions of the radius of gyration. The final results are Eqs. (37) and (39), but with P=9.93 and $\Phi = 9.23\times10^{23}$ mol^{-1}. Consequently, it can be assumed that the solvent penetrates in the chain molecule for any other possible situations related with solvent conditions or architecture; then the sphere becomes a coil with some degree of asphericity and with a smaller and non-constant density of polymer units inside it. These changes affect the constants P and Φ, but not the validity of Eqs. (37) and (39). It should also be noted that P is simply related with parameter ρ [76], defined as the ratio of the root mean squared radius of gyration to the hydrodynamic radius, R_h:

$$\rho = < S^2 >^{1/2} / R_h \,. \tag{43}$$

The hydrodynamic radius is the equivalent spherical radius obtained from the Stokes law for the chain friction coefficient, Eq. (41), with R_s substituted by R_h. It is easily verified that

$$\rho = 6^{1/2}\,\pi / P \tag{44}$$

and that the KR value of P for a Gaussian linear chain yield $\rho \cong 1.48$, while $\rho \cong 0.77$ is obtained for a rigid sphere.

If EV effects are incorporated in the radius of gyration, Eqs. (5), (37), and (39) yield $f^t \approx N^{\nu}$ and $[\eta] \approx N^{3\nu-1} \cong N^{4/5}$ for a flexible linear or star polymer in good solvent conditions. Also, the density of polymer units decreases because of the chain expansion. As a result, P and Φ should adopt smaller values than in the ideal chain case (though both the friction coefficient and intrinsic viscosity increase due to the larger chain size). Several approximate ways to introduce the chain expansion according to the two-parameter description in the hydrodynamic theory have been devised [15]. Although all of them describe the decrease of Φ as a function of the EV parameter z, the predicted forms of this variation are not coincident. Freed et al. [77] have performed RG calculations describing the approach to asymptotic values for P and Φ in the long chain limit. The crossover from the theta state to the good solvent region is, however, very slow and dependent on draining effects through the HI parameter h*. This can explain

why many experimental data of hydrodynamic properties in marginal solvents of moderately good quality maintain intermediate scaling law of the types $f^t \approx N_1^y$ and $[\eta] \approx N_2^y$ with exponent values $1/2<y_1<3/5$ and $1/2<y_2<4/5$, which are constant over a broad range of relatively long chain lengths.

Another important problem is related with the validity of the preaveraging treatment of HI, introduced in the KR theory. In the case of rigid objects, modeled as assemblies of beads, it is possible to perform rigorous calculations following the KR approach, but avoiding the orientational preaveraging. According to a numerical method established by García de la Torre and Bloomfield [78] this can be done by solving linear systems of 3 N equations. The conformational preaverage in flexible chains, however, can only be avoided by using approximate approaches. The values $P \cong 6.0$ [79] and $\Phi \cong 2.5 \times 10^{23}$ mol^{-1} [80] are generally accepted as the most accurate results from experimental data of long flexible linear chains in the theta state. The noticeable differences between these values and the KR results for ideal linear chains suggest that the preaveraging approximation has a modest but noticeable influence in the accuracy of the KR predictions for linear chains (together with possible effects of non-canceled three-body interactions in the theta state).

The introduction of branching in the Kirkwood formula and the KR calculations can be accomplished in a relatively easy way if Gaussian statistics corresponding to ideal chains are maintained. This description cannot, however, be very accurate in molecules with centers of high functionality because of the presence of cores with a high density of polymer units, which profoundly perturbs the internal distribution of distances. Stockmayer and Fixman [81] employed the Kirwood formula and Gaussian statistics to calculate h in the case of uniform stars, obtaining an analytical formula. They also performed a KR evaluation of the viscosity and proposed that g' could be evaluated from the approximation

$$g' \cong h^3 \,. \tag{45}$$

This approximation is equivalent to assuming that the differences in internal densities and, consequently, in solvent draining, between a branched chain and the homologous linear chain, when included in their corresponding mean sizes, can describe both the friction coefficient and the viscosity. Besides these theoretical considerations, an empirical correlation in terms of a log-log fit of h vs f was employed by Roovers et al. [51]. Kurata and Fukatsu [48] and Ptitsyn [82] performed a more general Kirwood evaluation of the friction coefficient for different types of ideal branched molecules (uniform and randomly distributed stars, combs and random-branched structures). Their results for different structures are included within the limits $1 \leq h/g^{1/2} \leq 1.39$.

The calculation of g' for Gaussian uniform star chains was carried out by Zimm and Kilb (ZK) [83]. They used a modified version of the dynamic Rouse theory including preaveraged HI (in the non-draining limit) that considers the particular connectivity of units consistently with the star architecture. This ap-

proach will be detailed later in the text. In the context of the present discussion it is sufficient to state that this method is equivalent to preaveraged KR calculations, since both approaches give practically identical quantitative results for hydrodynamic properties of ideal chains [15]. Zimm and Kilb obtained numerical results that, extrapolated to the long chain limit, were consistent with the approximation

$$g' \cong g^{1/2} . \tag{46}$$

A similar numerical calculation with the KR preaveraged formula, Eq. (34) for ideal uniform stars and combs was performed by Prats et al. [84]. For the star chains, they discovered significant differences with respect to the results obtained through the Kirkwood formula, Eq. (38). Thus, the KR values $h/g^{1/2}$ of highly branched stars clearly exceed the Kurata and Fukatsu upper limit. The extrapolated numerical values of h for this type of stars are, however, in better agreement with the experimental data in good solvent or EV conditions (summarized in [49]) which, according to the RG theory arguments [43] should be close to values of ideal chains as in the case of ratio g. Consequently, it seems that employing the KR theory instead of the Kirkwood formula allows for a relatively accurate description of the frictional properties of EV star chains, in spite of the preaverage approximation. Nevertheless. the experimental data of h corresponding to highly branched uniform stars in the theta state are always greater than those obtained with the KR method and ideal statistics. Of course, the presence of the star core, where the arms are expanded in order to avoid repulsions between their units, should be included to explain these differences, as in the previously discussed case of ratio g.

Also, the results for g' from the KR or ZK methods are significantly smaller than the theta solvent data described in [49]. This discrepancy could also be attributed to the use of Gaussian statistics in the theoretical calculations. Nevertheless, the theoretical results are still remarkable higher than the data corresponding to EV conditions (a quantitative analysis of all these results for h and g', together with simulation data will be presented in Sect. 4). The use of preaveraged HI is seemingly responsible for these remaining differences. It is known that the preaveraging treatment of HI gives poorer reproduction of some conformational properties of assemblies or chains with compact distribution of beads. This has been verified for viscosity in the case of rigid structures [85]. Moreover, Burchard et al. [86] investigated the effect of considering preaveraged HI in the calculation of the q-dependent first cumulant, or initial slope, of the dynamic (time-dependant) scattering function for linear chains. They showed that the relative error introduced by the preaveraging approximation becomes as large as 40% for highly branched stars (from 15% in linear chains).

Ganazzoli et al. [53] performed calculations for the hydrodynamic radius (based on the Kirkwood formula), and also for the intrinsic viscosity [87] of uniform stars, using a generalized version of the ZK method that incorporates non-Gaussian intramolecular distances. These distances were obtained according to

their free-energy minimization scheme [52, 53]. They found that the ratios g and h of the ideal chain were slightly smaller but similar to those obtained with EV statistics, in qualitative agreement with the RG theory, and both ratios were significantly smaller than the values obtained at the theta state. For g', however, the EV results were smaller than for the ideal chain. Moreover, these theoretical ratios differ considerably from the available experimental data for h and g'. The approximate way to calculate intramolecular distances and the introduction of preaveraged HI surely explains the deficiencies found in this theoretical description.

2.3 Dynamics

As previously indicated, the Rouse theory is usually employed to describe the dynamics of an ideal chain [12, 15, 21]. Three different types of forces are incorporated. The frictional forces can be set without HI (basic Rouse theory) or with preaveraged HI introduced through matrix **H**, as in the preaveraged KR method (Rouse-Zimm theory [13]). The theory also includes stochastic forces that take into account the random interactions with small solvent molecules (Brownian motion). Finally, the Rouse theory considers intramolecular cohesive forces between units, by means of a system of harmonic springs. (It can be verified that a harmonic spring potential is able to yield the equilibrium distribution corresponding to the ideal chain Gaussian intramolecular distances.) The spring forces are set through a connectivity matrix **A** with elements

$$A_{ii} = n_{bc} \tag{47a}$$

where n_{bc} is the number of bonds in unit i. (1 for end units and 2 for inner units in a linear chain),

$$A_{ij} = -1 \tag{47b}$$

for bonded units i and j (|i-j|=1 for linear chains), and

$$A_{ij} = 0 \tag{47c}$$

for non-bonded units. Diagonalization of the matrix **A** (or **HA** when HI are included) yields a transformation matrix which describes the system N normal coordinates $\mathbf{u}_k$, whose equilibrium and dynamic probabilities are obtained from the Fokker-Planck equation of the chain [15, 21].

Many dynamic properties can be defined as time-correlation functions of a quantity. For vector **X**(t), for instance, in the non-normalized form

$$C(\mathbf{X}, t) = < \mathbf{X}(t_0).\mathbf{X}(t_0 + t) > \tag{48}$$

where the average extends over all the values of t_0. The time-correlation function of each normal coordinate, or Rouse mode, is shown to decay exponentially, giving a relaxation function τ_k. In the basic Rouse model for non-draining chains [13, 21]

$$\tau_k \approx N^{3/2} k^{-2} . \tag{49}$$

Different equilibrium, hydrodynamic, and dynamic properties are subsequently obtained. Thus, the time-correlation function of the stress tensor (corresponding to any crossed-coordinates component of the stress tensor) is obtained as a sum over all the exponential decays of the Rouse modes. Similarly, $M[\eta]$ is shown to be proportional to the sum of all the Rouse relaxation times. In the ZK formulation [83], the connectivity matrix **A** is built to describe a uniform star chain. An (f-1)-fold degeneration is found in this case for the f-independent odd modes. Viscosity results from the ZK method have been described already in the present text.

The incorporation of non-Gaussian effects in the Rouse theory can only be accomplished in an approximate way . For instance, the optimized Rouse-Zimm local dynamics approach has been applied by Guenza et al. [55] for linear and star chains. They were able to obtain correlation times and results related to dynamic light scattering experiments as the dynamic structure factor and its first cumulant [88]. A similar approach has also been applied by Ganazzoli et al. [87] for viscosity calculations. They obtained the generalized ZK results for ratio g' already discussed.

There is an alternative and very direct way to generalize the Rouse-Zimm model for non-Gaussian chains. This approach takes advantage of the expression given by the original theory for the chain elastic potential energy in terms of normal coordinates:

$$U = (3/2) k_B T \sum_k \frac{\mathbf{u}_k^2}{<\mathbf{u}_k^2>} . \tag{50}$$

The approximation consists of assuming that the same expression applies in non-Gaussian chains [21, 89], using for the calculation of $<\mathbf{u}_k^2>$ a general formula in terms of the averages $<\mathbf{R}_i.\mathbf{R}_j>$ ($\mathbf{R}_i$ is the position vector of unit i) and the transformation matrix that diagonalizes **HA**. This approach is consistent with the general relationship

$$\tau_k \approx <S^2>/D \tag{51}$$

that, according to Eqs. (5), (27), and (37), yields $\tau_k \approx N^{3\nu}$ for non-draining chains. Then the sum of relaxation times provides $M[\eta] \approx N^{3\nu}$, which is consistent with the non-draining KR result for the viscosity, Eq. (39). In fact, it has been shown [89] that the proposed approximation leads to the formula derived from the KR theory for the intrinsic viscosity in terms of averages of internal distances [90].

It can also be verified that this formulation is entirely equivalent to the optimized Rouse-Zimm local dynamics approach [55].

The complex viscosity, i.e., the viscosity observed in the presence of an oscillatory shear rate, is a dynamic property that can be straightforwardly obtained from the Rouse, or Rouse-Zimm theory as the Fourier transform of the stress time-correlation function. Thus, these theories give [15]

$$\left[\eta(\omega)\right]^{*} = (\mathrm{N_A}\zeta / 6M\eta_0)\sum_k \tau_k / (1+i\omega\tau_k) \tag{52}$$

where $\omega/2\pi$ is the oscillation frequency, so that $\omega=0$ reproduces the intrinsic viscosity, and, in this particular case, Eq. (52) corresponds to the calculation of this property as a sum of the relaxation times, previously mentioned. The imaginary and real components of the complex viscosity are directly related with the experimental real and imaginary (or storage and loss) parts of the complex modulus G' and G". Of course, Eq. (52) is of limited validity for high frequencies unless the theoretical scheme is modified to include realistic constraints that define practically fixed bond lengths, bond angles, and rotational angles. Sammler and Schrag [91] used the Rouse theory to calculate the complex viscosity and oscillatory flow-birefringence (that can also be derived from the relaxation times) for rings, cyclic and H-shaped combs, and stars. All these calculations were performed with ideal statistics, and preaveraged HI. Ganazzoli [92] has recently incorporated non-Gaussian effects in stars using the same approach employed in his previous calculations of intrinsic viscosities. The results show some special features in the intermediate range of frequencies, due to the effect of the star core. Improved RG descriptions of the HI and EV effects on the calculation of the viscosity properties of a dilute chain undergoing shear flow have been introduced by Öttinger [93] and Schaub [94], and they surely can also be applied to branched structures.

There are some dynamic features due specifically to branching. Thus, in a star chain one can consider the relaxation of the global chain shape, τ_e, obtained from the time-correlation function of the center-to-arm distance. τ_e is clearly conditioned by the interactions in the star core [2, 9]. This relaxation time is distinguishable from the rotational relaxation, τ_D, which should be approximately independent of core effects (τ_D defines the time required for the star to rotate or to translate a distance similar to its size). τ_e can be approximately obtained by applying a relation similar to Eq. (51), but considering the mean size of the arm, $R_g^{\,b}$, given by Eq. (14) and the diffusion of the n_{ext} external blobs. Assuming that most of the arm N_b units are concentrated in these blobs, each one contains N_b/n_{ext} units and their number can be evaluated as $n_{ext}\approx R_g^{\,b}/\xi(R_g^{\,b})$, which is proportional to $f^{1/2}$. In the free-draining regime (consistent with most simulations and prevailing for the semi-dilute conditions within the star), Eqs. (27) and (36) give $D_{ext}\approx(N_b/n_{ext})^{-1}$ and, finally

$$\tau_e \approx (R_g^b)^2 D_{ext} \approx N_b^{(1+2\nu)} f^{(1-2\nu)/2} . \tag{53}$$

Consequently, this relaxation time is predicted to be nearly independent of the number of arms. Dielectric relaxation experiments for stars up to 18 arms by Boese et al. [95] show this behavior. The rotational relaxation time, however, can be considered similar to longest internal modes, i.e., it depends on the overall size and, assuming free draining

$$\tau_D \approx < S^2 > / D \approx < S^2 >_{linear} g / D \approx N^{1+2\nu} f^{1-3\nu} \approx N_b^{1+2\nu} f^{2-\nu} . \quad (54)$$

There is no distinction between τ_e and τ_D in the Rouse description of linear chains. A third relaxation mechanism contemplates the disentangling of two or more intertwined arms. This relaxation is considerably slower and strongly dependent on f. Obviously, this feature cannot be described by the ideal chain model.

The dynamics of a chain molecule in the entangled regime is a fundamental problem in polymer physics. According to the de Gennes tube model [16, 21] a long linear flexible chain moves by reptating along a tube of a given contour length formed by the physical entanglements. This theory predicts relaxation times of the Rouse modes according to $\tau_k \approx N^3/k^2$. Then, considering Eq. (3) for the chain mean size in the non-diluted regime, $c >> c^*$, and Eq. (51), the translational diffusion coefficient should obey the scaling law $D \approx N^{-2}$.

The contour length fluctuations are very important in the case of branched polymers. Obviously, simple reptation cannot explain the dynamics of a star chain. As two arms perform a reptation move along their contour in a tube, other branches have to retract simultaneously from their contours to the branching point and, then, to form new tubes [21, 96]. The time required for the arm motions can be estimated as a mean passage time through a configuration in which the center-to-arm distance is close to zero. Assuming a Gaussian distribution of distances, the activation theory predicts that this time should be exponentially dependent on the arm length. As this process should occur for (f-2) arms simultaneously it is finally found that

$$D \approx e^{-a(f-2)N} . \quad (55)$$

This law reproduces the dependence on the chain length of experimental data of tracer diffusion of three-arm stars in a matrix of long linear polymers [97], though some deviations, attributed to tube renewal effects, are observed for high molecular weights. These results have also been explained with the alternative coupling model of relaxations, employing parameters obtained from viscoelastic data [98]. The experimental variation with f is considerably weaker than in Eq. (55), indicating an alternative mechanism where the star diffuses by retracting just one arm. The experimental self-diffusion of three-arm chains [99] is much faster than the tracer diffusion in the matrix of linear chains. The tube constraint release is apparently much more efficient when the chain is surrounded by other stars of higher mobility.

3
Simulation Models and Methods

Polymer systems can be investigated through numerical simulation procedures [14]. In some cases, it is only necessary to obtain properties of a single isolated chain. Therefore, the simulated configurations correspond to the chain conformations. Exact enumeration techniques can be applied to obtain equilibrium properties for chain models with a discrete number of conformations (which obviously increases very rapidly with chain length), e.g., in the case of a single chain on a lattice. These techniques are based on obtaining exact numerical averages considering all the different conformations for short chains and extrapolating the results to the long chain limit [15].

However, a more general case is the simulation of a many-chain system, for instance a polymer solution. Then a finite volume of the system is defined as the simulation box, and a change in the system configuration corresponds to conformational modifications affecting one or several chains. Usually, interactions with the box walls are avoided by using periodic boundary conditions. Thus, when some polymer units move outside the box, homologous images of these units move inside the box from the opposite wall. Therefore, the size of the box must be sufficiently large to avoid interactions between parts of a chain with its images at the opposite side of the system.

MC techniques randomly sample the configurational equilibrium of a single chain or many-chain system. BD and MD consider mechanical equations of motion and generate dynamic trajectories of positions (and velocities) vs time. The trajectories also sample the system configurations and, therefore, both equilibrium and dynamic properties can be calculated from dynamic methods. The dynamic simulation algorithms only differ between them in the details included in the physical models and in the numerical procedures used for solving differential equations. MC methods, however, must include previously defined rules to change configurations and, therefore, they admit a great variety of algorithms.

3.1
Monte Carlo

Simple MC methods generate randomly chosen independent configurations, and then obtain the required averages of properties by taking into account the equilibrium statistical weights

$$w_{conf} \approx e^{-E_{conf}/k_B T} \tag{56}$$

depending on the configurational energies, E_{conf}, in a canonical, or NVT statistical ensemble where the number of units and molecules, volume and temperature are fixed. (The averages are evaluated as arithmetic means over the accepted configurations, if the model only considers repulsions through the single-occupancy condition, consistent with the hard-spheres potential, in the case of SAW chains.)

These simple methods are, nevertheless, hardly applicable for most physical systems that exhibit a very heterogeneous configurational space, where only a relatively small fraction of configurations are relevant. The enrichment algorithm [100] consists roughly in generating different configurations of SAW chains of N units (or N_b units per branch) by adding randomly a new bond to configurations of N-1 (or N_b-1) units through an adequately chosen number of tries. If all these tries are unsuccessful, further growth of the chain is not attempted, and a new chain generation begins. The averages of properties are calculated over the different configurations generated by the procedure for each chain length.

Many MC algorithms generate Markov chains, in which a configuration is obtained by introducing a randomly generated or stochastic change in the previous configuration. These stochastic processes only have to comply with the conditions of microscopic reversibility and ergodicity along a Markov chain. Therefore they are not required to describe real motions in the simulated system, as far as only equilibrium averages are computed from the simulations. A configuration is accepted or not according to the Metropolis rule [101] based on the consideration of the statistical weights of the new and the previous (old) configuration: It is directly accepted if

$$w_{conf}^{new} > w_{conf}^{old} \tag{57a}$$

If this condition is not met, a random number ranging from 0 and 1, ξ_{ran}, is selected and the new configuration is only accepted if

$$w_{conf}^{new} / w_{conf}^{old} > \xi_{ran} \,. \tag{57b}$$

Otherwise, the previous configuration is again accepted as new. It is easily shown that the resulting configurations constitute an equilibrium ensemble in the canonical ensemble. Other procedures have also been devised to sample the configurational space in an efficient way. For instance, the configurational bias method [102] re-grows a chain from a chosen unit to an end, by placing each one of the successive units, taking into account the relative probabilities of the alternative possible locations. Once the new chain is completed, the Metropolis criterion is employed to accept or not the new chain. In all these Markov methods, the initial chain is built with a moderate energy, and a certain number of configurations is allowed before starting to obtain the system properties in order to allow for the system equilibration. Final results are then obtained as simple arithmetic means over the generated configurations (or a representative sample of them) after this equilibration period.

3.1.1 *Lattice Algorithms*

A basic polymer model is built by attaching successive units along the chain in neighboring sites of a geometrical lattice, with random orientations of the re-

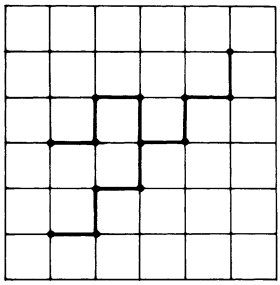

Fig. 5. SAW three-functional star on a squared lattice

sulting chain bonds. In this way the simple and the non-reversal random walk models are defined. With the limit of a high number of units these models reproduce the coarse-grained properties of a Gaussian chain, as any other flexible molecule without intramolecular interactions. The lattice voids represent solvent molecules, and all the lattice sites are assumed to represent the same volume. A certain number of polymer chains, n_c, can be introduced in the system, so that the polymer volume fraction is given by

$$\Phi_p = n_c N / N_L \tag{58}$$

where N_L is the total number of sites in the lattice (or the lattice volume). This basic representation is employed to formulate the mean-field Flory-Huggins theory of polymer solutions [20], where the averaged balance of polymer-polymer, polymer-solvent and solvent-solvent interactions is described by the parameter χ. EV effects can be incorporated by setting the condition that two different units cannot share a common lattice site in a given chain conformation. This restriction defines the SAW chain model on a lattice (Fig. 5). Different degrees of solvent quality can be incorporated by including a reduced attractive parameter, ε/k_BT. Of course, this quantity can be directly related with the Flory-Huggins parameter χ, though this relation depends on the number of neighboring lattice sites, i.e., on the lattice geometry. A term $-\varepsilon/k_BT$ is added to the total energy for a given configuration each time that two non-bonded units, belonging or not to the same polymer chain, are found in neighboring lattice sites. The total configurational energy E_{conf} is calculated from ε/k_BT and the total number of non-bonded neighboring units. Most MC simulations on a lattice consider SAW models with or without configurational energies (corresponding to thermal or athermal solvents).

A variety of rules can be introduced to generate stochastic changes. Local changes (or bead-jump moves) in a chain should include end moves, usually bents of terminal bond, and inner moves [103]. Figure 6 contains illustrations of these moves on a simple cubic lattice. Inner bents (in which a unit between two perpendicular bonds moves to the empty opposite corner) should alternate with crankshafts (moves involving two units and three bonds that take place when the

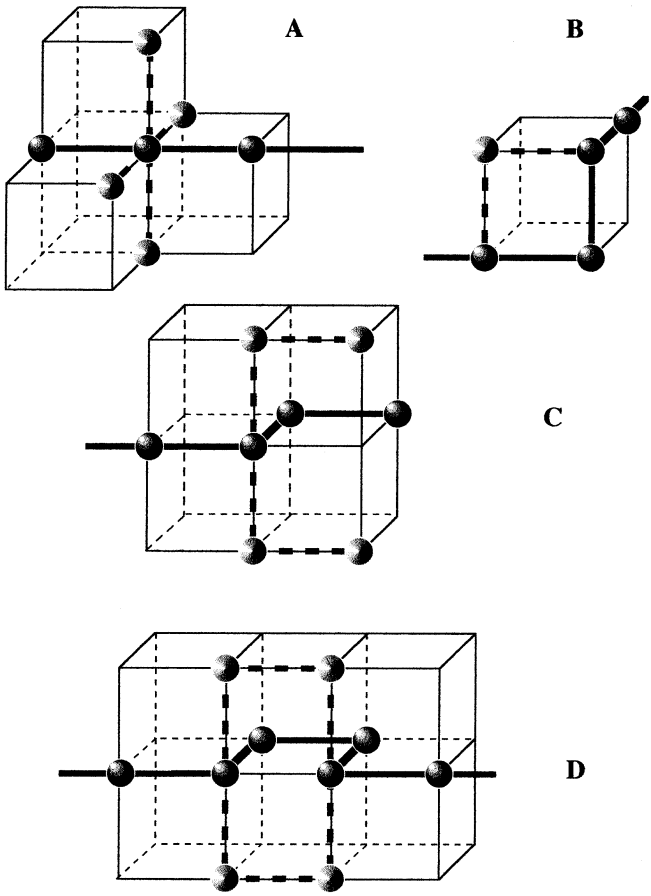

Fig. 6a–d. Scheme of bead-jump moves for a linear chain on a simple cubic lattice: **a** bent (end move); **b** bent (inner move); **c** crankshaft (end move); **d** crankshaft (inner move). *Solid lines* Initial bonds; *broken lines* final bonds (alternative possibilities included)

mentioned corner is not empty) to pratically comply with the ergodicity condition [104]. These bead-jump rules can actually mimic the chain dynamics. They have to be modified in the case of branched chains to include the motion of the branching points. (However, equilibrium simulations for single star chains can consider the central point as a fixed reference.) Linear chains can use the more efficient "reptation" algorithms in which a terminal bonds is removed and added in a random orientation at the other side of the chain.

Other moves are specific for dilute solutions (or single chain simulations) and very congested systems (as melts). Some complex rules involving different chains have been developed for the equilibrium study of melts of linear chains, such as the cooperative motion algorithm [105] where beads are moved cooper-

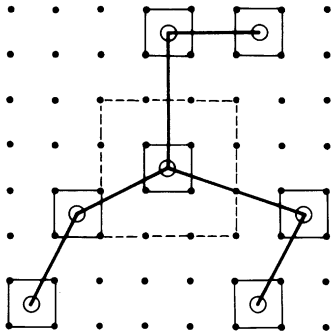

Fig. 7. Fluctuating bond model for a three-functional SAW star on a squared lattice

atively along closed paths in the lattice. For EV single chains, the Pivot algorithm has been shown to be particularly efficient [106]. This algorithm, easily implemented for lattice and non-lattice models, chooses an inner unit and rotates the rest of the chain up to its nearest end (or the branch end) around this pivoting point.

The fluctuating bond model [107] has been developed as an alternative to conventional lattice models, in which the bond lengths can adopt different values similar to the Gaussian segments of a coarse-grained flexible chain. To allow such fluctuations each unit is set to occupy simultaneously a group of neighboring sites in the lattice in order to comply with the SAW condition. The unit is, however, physically placed in one of these sites and, therefore, its distance to a neighboring units is not constant (see Fig. 7). Configurational changes are performed through single unit bead-jumps and, therefore, can also mimic the chain dynamics.

3.1.2 *Off-Lattice Models*

The obvious advantage of lattice models is the simple location of beads in sites which allows for the use of integral numbers in the simulations and also permits a fast identification of interacting neighboring units. The lattice geometry, however, introduces severe constraints at the local level, which can only be smoothed out by generating sufficiently long chains. In the case of branched chains, changes in the branch points can only be included through complex rules. Moreover, there are no simple ways to introduce some physical features such as HI in a lattice model system. Consequently off-lattice models are preferable in many practical cases.

Off-lattice models consider chains composed of interacting units in the free space. Single chains or simulation boxes containing many-chain systems can be investigated. Usually the solvent is only considered according to its quality effects in thermal systems. Therefore it is assumed to fill the remaining space act-

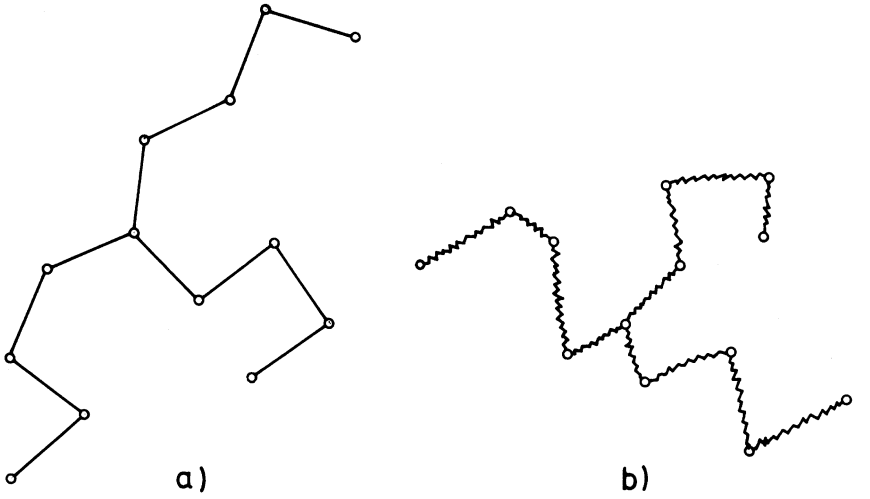

Fig. 8a,b. Off-lattice representations of a three-functional star: **a** Bead and Rod model; **b** Bead and Spring model

ing through a mean-field force. However, more complex, even atomic, representations of chains and solvent molecules are also feasible.

A basic off-lattice model is constituted by hard-sphere beads joined through fixed lengths bonds of random orientations (Bead and Rod models, Fig. 8a). End moves and inner crankshafts are employed in bead-jump algorithms for this model [108]. Reptation moves or Pivot algorithms can also be considered. Energetic interactions between non-bonded units can be introduced by means of distance-dependent potentials. These potentials should include a repulsive part (to mimic the SAW single occupancy condition) and also an attractive well. Provided that these conditions are met, the specific form of the potential is not very important for coarse-grained models. For instance, a 6:12 Lennard-Jones (LJ) potential can be employed. A distance cut-off is sometimes introduced to facilitate the energy computation. The null-interaction distance parameter σ only takes care of the repulsive core of the units and can, therefore, be maintained fixed for many systems. Then the reduced energy in the attractive well, ε/k_BT, is usually the relevant parameter to describe the solvent conditions.

A simple modification of these models may include variable bond lengths, with distribution of lengths usually consistent with those of springs (Bead and Spring models, Fig. 8b). A natural choice is to use a non-perturbed Gaussian distribution of bond lengths [109] so that the model identifies with the ideal or Gaussian chain when ε/k_BT tends to zero (or with the dynamic Rouse model for ideal chains). In these models, inner single bead-jumps can be adequately performed to maintain the intramolecular distance distributions of the bonds linking the bead with its neighbors [110]. Reptations and Pivot algorithms can also be used. A modification of the Pivot algorithm, useful for chains in theta solvent

conditions or for star chains, consists in adding a Gaussianly sampled new bond to the pivoting unit and then simply connecting the rest of the chain up to its end, without performing the prescribed rotation [109]. This procedure will be denoted here as the translational Pivot algorithm.

3.1.3 *Upper and Lower Bounds of Hydrodynamic Properties*

The effect of preaveraging HI in the calculation of friction coefficients or viscosities can be estimated through certain equilibrium MC simulations. Thus, Zimm [90] proposed to estimate a property from its equilibrium average obtained rigorously (i.e., avoiding orientational preaveraging) for the different conformations within an MC sample. This rigid-body approach was shown later to constitute an upper bound of the real value [111]. Following a variational method, Fixman [112] was able to obtain lower bounds both for the friction coefficient and the viscosity. While a first approximation for the lower bound of the friction coefficient is simply given by the KR formula, Eq. (34), and further increases of this limit value are only accomplished through complex and specific procedures [113], a lower bound for the viscosity can be implemented in the form of a relatively simple and general scheme [114] that makes use of certain equilibrium averages. In fact, the calculation of the quantities involved in these averages (essentially 3N×3N double-sum terms) requires a computational effort considerably smaller than working with the rigorous KR equations (which include the inversion of 3N×3N matrices [78]). Since complex computations are always required, the MC samples for these calculations are usually formed by a limited fraction (about 1000 conformations) of the total number of generated conformations.

3.1.4 *Dynamic Monte Carlo*

As we have already mentioned, a stochastic MC sample can be identified with the dynamic trajectory of the system if the rules used in the generation of new conformations somehow describe the perturbations suffered by local regions of a chain. Consequently, it is possible to perform DMC simulations by employing a simple bead-jump algorithm [14]. The unit time for a DMC trajectory is usually defined as composed by the number of bead-jump motions (of any type) needed to give a single chance to every unit to move as average, i.e., it includes $n_c N$, or $\Phi_p N_L$ move attempts. As other dynamic methods, the DMC simulations are employed to obtain different properties through time-correlation functions. Thus DMC for SAW linear chains have been able to reproduce the expected chain length dependence of the Rouse relaxation times in single chain [115] and many-chain [116] systems, which is generally considered as an adequate confirmation of the method validity.

3.2 Molecular Dynamics

Sometimes the required dynamic properties of a single chain or a polymeric system can be investigated by solving the classical mechanics equations of motions of the system. The MD algorithms consider a certain number of simulation steps (with constant forces), obtaining new positions and velocities of the units after each one of these steps [19]. Similar to the MC methods, the initial positions of units are chosen to correspond to an ordered or disordered system configuration of moderate energy. The velocities are sampled from the Maxwellian distribution corresponding to a lower temperature (to avoid local regions of non-relaxing high energy). Then the temperature or the averaged kinetic energy (associated with the mean bead velocities) is progressively raised to the required value (thermalization period). An equilibration period is subsequently observed. Finally the rest of the trajectory is used to collect the observed quantities. Different numerical procedures to solve the differential equations can be employed, differing in their accuracy and complexity, e.g., the simple Verlet or leap-frog algorithms.

Usually, MD methods are applied to polymer systems in order to obtain short-time properties corresponding to problems where the influence of solvent molecules has to be explicitly included. Then the models are usually atomic representations of both chain and solvent molecules. Realistic potentials for non-bonded interactions between non-bonded atoms should be incorporated. Appropriate methods can be employed to maintain constraints corresponding to fixed bond lengths, bond angles and restricted torsional barriers in the molecules [117]. For atomic models, the simulation time steps are typically of the order of femtoseconds (10^{-15} s). However, some simulations have been performed with idealized polymer representations [118], such as Bead and Spring or Bead and Rod models whose units interact through parametric attractive-repulsive potentials.

3.3 Brownian Dynamics

A useful variety of MD simulations permits one to extend considerably the range of time intervals investigated by renouncing to include explicit solvent forces. Then the solvent is considered as a continuous incompressible fluid that exerts stochastic (Brownian) interactions on the frictional chain units. The equation of motion must consider intramolecular forces (including the hard forces associated with constraints present in atomic or Bead and Rod models or the soft cohesive forces corresponding to the Bead and Spring models), together with possible forces induced by external fields. Moreover, the frictional forces, depending on the beads velocities (without or with fluctuating or preaveraged HI), are present. Finally, a stochastic term is included in terms of random quadratic displacements of units whose variance-covariance matrix has to be consistent with

the chain diffusion. A first order algorithm with these specifications was established by Ermak and McCammon [119] and can be applied to the different types of polymer systems. The inclusion of hard potentials (as those consistent with the EV forces or associated with non-bonded intramolecular or intermolecular interactions) presents some difficulties due to the different time range associated with these interactions with respect to the slower motions due to frictional and soft forces. This problem is significant when the simulations include complex calculations, such as those involving fluctuating HI [120].

4 Applications

4.1 Stars

4.1.1 *Global Size and Shape*

The first simulations on the mean size of single branched chains were MC calculations performed on lattice models. Mazur and McCrackin [121, 122] used the SAW model with attraction between non-bonded neighbors in a simple cubic lattice and obtained ratio g, defined in Eq. (20), for uniform star chains (with up to 12 arms) and combs. They estimated the theta conditions by fitting the reduced attraction parameter (inversely proportional to temperature) to reproduce the Gaussian mean size proportionality with the square root of the chain length, Eq. (3). For stars, they found values of g in the theta conditions [122] greater than the results predicted by Zimm and Stockmayer for Gaussian chains, Eq. (21). A similar conclusion was obtained by Kolinski and Sikorski on an investigation into tetrahedral lattices [123], and by Freire et al. [109], who used an off-lattice model of Gaussian beads interacting through a long-range LJ potential without cut-off. In the latter simulation, the translational Pivot algorithm was used. The theta region was estimated by fitting the attractive LJ parameter so that the mean size data of linear chains follow a dependence with the chain length consistent with Eq. (3). This simulation studied chains up to 18 arms, but with only a few beads per arm. The different MC data for g are in reasonable agreement, and they are also close to the available experimental data, summarized in [49]. Batoulis and Kremer [124] have extended the MC calculations to longer chains. They used a biased sampling to study uniform stars with up to 12 arms in an fcc lattice. Their results seems to show that an f-independent value of the reduced temperature at the theta point can be determined by extrapolating to the infinite chain length MC results obtained for sufficiently long chains. Deviations of the mean size with respect to the ideal chain prediction are explained by the effects of three-body interactions in inner regions of the stars. The differences found in the MC (and in the experimental values) for g with respect to the theory predictions, however, are too large to describe the variation of g vs f in

terms of the theoretical scaling law. In fact, the log-log plots of simulation data show slopes bracketed by –0.75 and the scaling theory prediction, –0.5. Batoulis and Kremer proposed the relationship $g \approx (f-3)^{-1/2}$ which is consistent with their data (and those of [109]) and most experimental results for f>6.

Results for g in EV star chains were also reported by the same groups [121, 123, 125] and also by Zimm [126], who performed MC simulations on a lattice for wormlike stars up to six arms. In the case of the off-lattice model [109] the LJ potential was chosen to reproduce adequately the scaling law for the mean size of linear chains vs chain length, according to Eq. (5). Whittington et al. [127] employed exact enumeration and MC calculations for uniform stars on a cubic lattice. They obtained g and also the mean size of arms, showing a similar scaling law as the global size, but with higher pre-exponential factors. The ratios of these factors to that of a linear chain have been predicted in the RG calculation of Miyake and Freed [42] and the simulation data are in good agreement with these estimates. Barrett and Tremain [128] generated uniform stars with up to 24 arms, employing high coordination lattice walks, while Zifferer [129] used a Pivot algorithm to simulate EV stars with up to 12 arms on the tetrahedral lattice. All these investigations revealed that g in the EV is very well described by the Zimm and Stockmayer prediction for ideal chains. Again, the MC data are in agreement with most experimental data reported in [49]. This feature confirms the prediction of the RG calculations [43, 49].

The MC results for stars of different numbers of arms in the EV regime cannot, however, make an accurate distinction between the ideal chain prediction $g \approx f^{-1}$ and the Daoud and Cotton scaling law $g \approx f^{-4/5}$. The verification of the power-law for the dependence of the star mean extension on N, according to Eq. (14) and in terms of the EV critical exponent ν is also difficult for star chains, due to the finite size influence of the star inner regions, which is manifested by residual curvatures in the log-log $<S^2>$ vs N plots. More noticeable curvatures and lower apparent fitted exponents for similar chain length ranges are obtained as the number of arms is increased. Ohno used the enrichment algorithm to generate many-arm star chains with 50 beads per arm [130]. Plots of their data for Rg^b and the mean bead-center distance divided by $N^{3/5}$ vs f reproduce the scaling theory $f^{-2/5}$-dependence, consistent with Eqs. (14) or (17) and $N_b = N/b$.

The distribution of the center-to-end distance has been investigated by Grest [131] through a BD simulation of stars with different solvent qualities. The form of this distribution is close to Gaussian, though some deviations for stars with few arms and poorer solvents are observed (Fig. 9). This is in agreement with SCF calculations for polymers attached to the surface of a highly curved sphere [33]. The width of the distribution decreases for higher f, which is consistent with the reduction of the mean size predicted by the scaling theory. Ohno and Binder [132] used an MC enrichment algorithm to investigate the short distance behavior of this distribution function for EV stars in two dimensions expressed as a power-law dependence on r. Compared to the exponents predicted by the scaling theory [27, 46], the MC results are too low for the different functionalities included in this study.

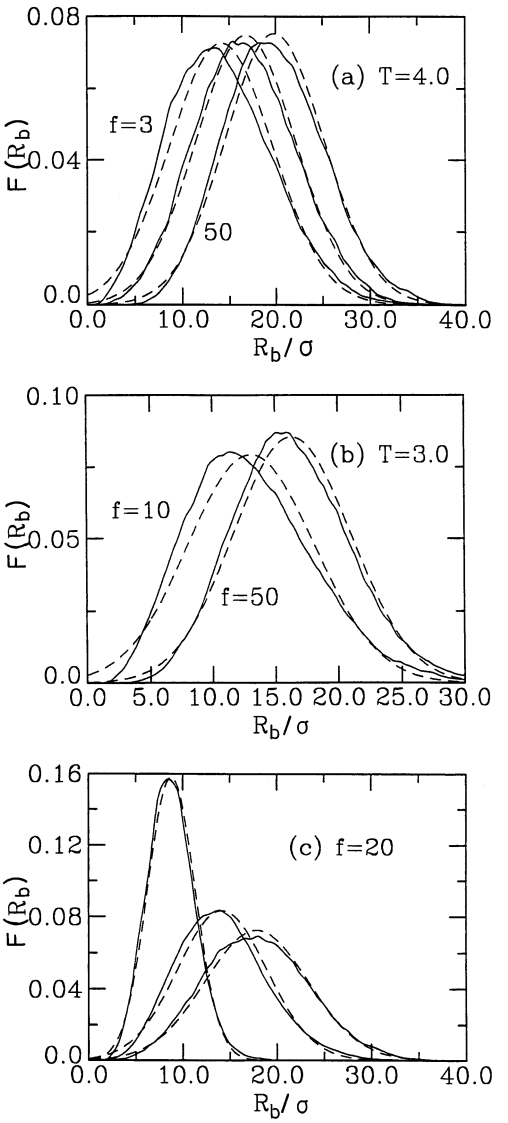

Fig. 9a–c. Scaled distribution function for the center-to-end distances of stars of f=3, 10 and 50 arms (σ is the repulsive distance range of the intramolecular potential): $T=4\varepsilon/k_B$ corresponds to a good solvent; $T=3\varepsilon/k_B$ corresponds to a theta solvent; $T=2\varepsilon/k_B$ (lower temperatures correspond to the curves on the left). *Solid curves* Simulation data; *dashed lines* Gaussian functions. Reprinted with permission from [131]. Copyright (1994) American Chemical Society

The asphericity of uniform stars should decrease with increasing number of arms from the results corresponding to linear chain coils. Highly branched stars present small asphericity values that characterize configurations close to the

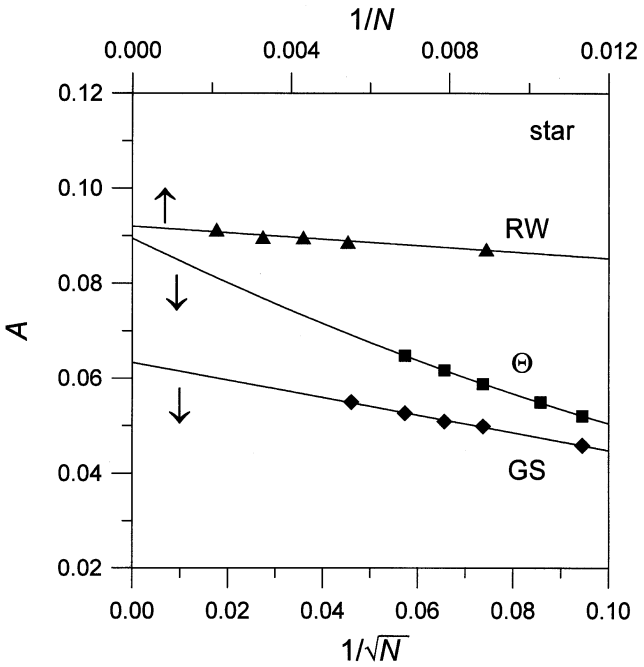

Fig. 10. Dependence of asphericities of stars of 12 arms on chain length corresponding to random walk (RW), θ and good solvent (GS) cases. Reprinted with permission from [140]. Copyright (1997) American Chemical Society

spherical shape. These results depend on the solvent conditions: EV chains show a greater asphericity than ideal chains in the case of linear architectures. Batoulis and Kremer [133] used a dimerization technique to study stars with up to six arms on an fcc lattice, obtaining accurate estimations of this quantity in the EV regime. Bishop and Clarke [134] obtained the asphericity of f=3 uniform stars in different regimes employing BD simulations with a Bead and Spring model and beads interacting through an LJ potential. The asphericity of stars at the theta point is slightly smaller than the result obtained with the Gaussian model. In a later study Bishop et al. used an off-lattice bead model with rigid springs (BD simulation [135]) and with Gaussian springs (MC method with Pivot algorithm [136]) to investigate the EV regime. It is shown that the asphericity of EV stars is always smaller than for ideal (Gaussian) stars (contrary to the result obtained with linear chains). Zifferer [137] obtained asphericities through MC simulations on the tetrahedral lattice. In a similar study [138] with the same model, but with a nearest neighbor attraction term that mimics the theta state, he also found that the asphericities are slightly smaller than for ideal stars. However, the ideal results are practically identical to those obtained with non-reversal random walk chains on the same lattice. He has also carried out an exhaustive simulation with an off-lattice model for random walk stars with up to 96 arms [139].

According to the results, it is determined that the asphericities can be described in terms of polynomials in $f^{-1/2}$. Forni et al. [140] also used an off-lattice model and an MC Pivot algorithm to determine the star asphericity for ideal, theta, and EV 12-arm star chains. They also found that the EV stars chains are more spherical than the ideal and theta star chains. In these simulations the theta chains exhibit a remarkable variation of shape with arm length, so that short chains (where core effects are dominant for all chains with intramolecular interactions) have asphericities closer to those to those found with EV, while longer chains asymptotically approach the ideal chain value(see Fig. 10).

Simulation models with a repulsive-attractive potential can describe the transition from the good solvent (expanded coil) to the collapse of the chain into a compact globule when placed in a very poor solvent [24, 25] (sub-theta regime). This transition has been investigated for star chains in some of the previously mentioned simulations [121, 123, 134] and also by Kajiwara and Burchard [141] (MC calculations on a cubic lattice). Mattice [142] has plotted the expansion curves (above the theta point) obtained for the rotational isomeric state (RIS) model representations of tri-and tetrafunctional polymethylene chains, whose monomers interact through hard spheres. Rey et al. used the bead model with Gaussian springs to perform an off-lattice simulation of the compact state [110] and also of the transition curve [143]. The obvious expected features due to branching correspond to less abrupt transitions, due to the necessarily more compact disposition of units in the star coil. Also, the ratio g should exhibit values closer to 1 for highly branched stars in the sub-theta regime, since both linear and star chains adopt very similar compact conformations. Some simulations [141, 143] have reproduced the approach to the theoretical asymptotic dependence of the mean size with temperature. This dependence can be formulated according to the application of Eq. (14) to the collapse regime, i.e.,

$$< S^2 > \approx \left| 1 - \theta / T \right|^{-2/3} . \tag{59}$$

The approach is slow for stars with higher number of arms, as shown in Fig. 11.

Osmotic second virial coefficients can be obtained through simulation procedures by computing the intermolecular energy between two interacting chains at different conformations, orientations, and distances. Bruns and Carl [144] used the simple cubic lattice model (SAW model with an attractive energy) and determined the values of the reduced attractive energy parameter for which the second virial coefficient vanishes for different chain lengths. Extrapolation of these values to the long chain limit gives the theta point for a particular type of chain. They obtained slightly different extrapolations for stars of different numbers of arms (see Fig. 12) in rough agreement with the conclusion of a single theta point for all the functionalities established from the mean size study of Batoulis and Kremer [124]. Calculations in the EV regime seem easier, since they can be obtained simply by computing the number of intersecting configurations when performed on a lattice. However, this study has only be carried out very

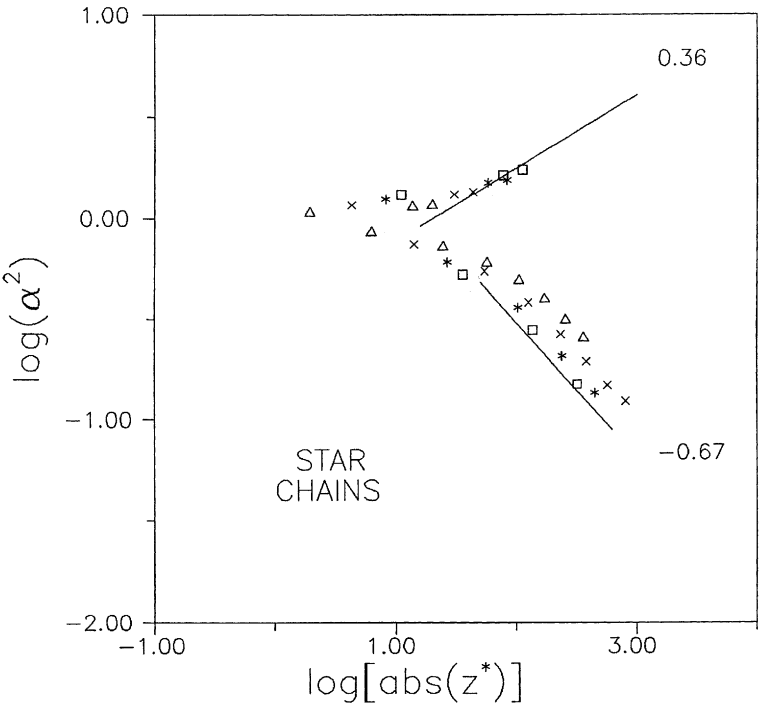

Fig. 11. A log-log plot of the expansion factor, α^2, vs reduced excluded volume, $|z^*|$, for MC data of 12-arms stars with N=25–109 units: *triangles* N=25; *crosses* N=49; *asterisks* N=85; *squares* N=109. The top and bottom *solid lines* and figures represent slopes corresponding to the predicted asymptotic behaviors for the EV and sub-theta regimes, respectively. Reprinted with permission from [143]. Copyright (1992) American Chemical Society

recently. Ohno et al. [145] used an enrichment algorithm with simple MC sampling to study stars with up to six arms on a cubic lattice. Also for the EV regime, Rubio and Freire [146] employed the off-lattice Gaussian bead model and the Pivot algorithm to calculate results for stars up to 18 arms. The values of the interpenetration function, defined in Eq. (24), can be compared to the RG data and experimental data. In Table 1 we give a summary of these data. They should also be compared with $\Psi^* \cong 0.25$, best estimation of the interpenetration factor for linear chains, according to RG theory, numerical simulations, and experimental data [49]. It is observed that the RG theoretical predictions cannot reproduce the simulations for moderately branched stars so that the simulation values constitute the only reliable predictions for chains with more than six arms. The simulation data are in fair accordance with most of the experimental data, summarized in [49], though the different data of highly branched stars exhibit a significant dispersion. It can be noted that the interpenetration factor of 18-arm stars is still very different from the rigid sphere limit, $\Psi^* \cong 1.62$. The MC simula-

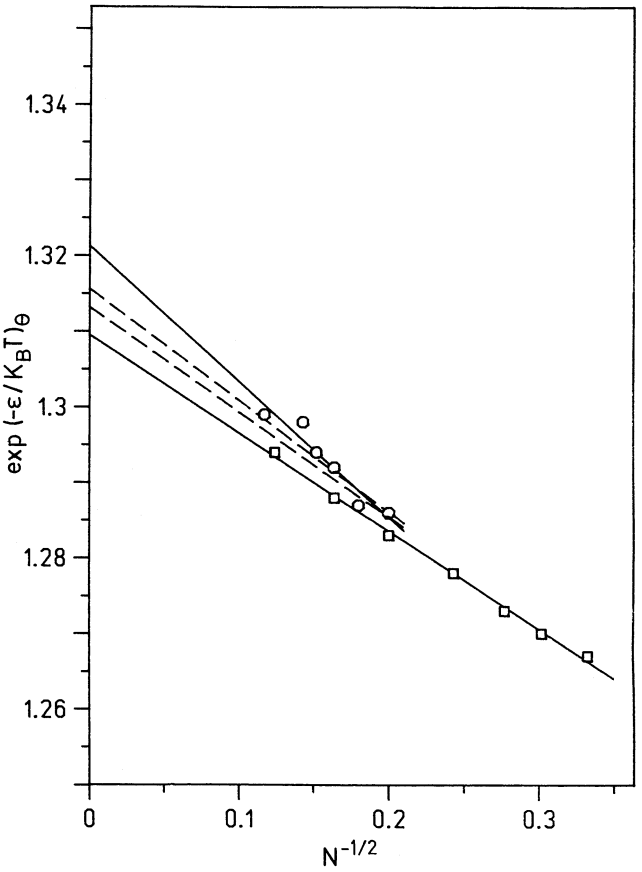

Fig. 12. Inverse of the reduced theta temperature for which the second virial coefficient vanishes from MC calculations on a cubic lattice for linear chains (*squares*) and f=6 stars (*circlelike*); *broken lines* (no symbols) stars with f=4 and 5. Reprinted with permission from [144]. Copyright (1991) American Chemical Society

tion values of Ψ^* for f=4 also agree with recent experimental data of PS in the good solvent benzene [147], while the experimental results in the theta solvent cyclohexane are described through a crossover interpolation formula inspired by the Domb-Barrett approach [22].

Second virial coefficients represent the first approximation to the system equation of state. Yethiraj and Hall [148] obtained the compressibility factor, i.e., pV/k_BTn_c, for small stars. They found no significant differences with respect to the linear chains in the pressure vs volume behavior. Escobedo and de Pablo [149] performed simulations in the NPT ensemble (constant pressure) with an extended continuum configurational bias algorithm to determine volumetric properties of small branched chains with a squared-well attractive potential

Table 1. Comparison of theoretical, simulation and experimental values of factor Ψ*

	Ψ*			
Method	f=4	f=6	f=12	f=18
RG[a]	0.52	0.79	1.35	
Lattice MC[b]	0.43	0.63		
Off-lattice MC[c]	0.44	0.62	1.00	1.21
Experimental[d]	0.46–0.52	0.65–0.67	1.10	1.10–1.26

[a] [23, 49, 69]
[b] [145]
[c] [146]
[d] Range of data within the mean squared deviation among those reviewed in [49]

Table 2. Variation of ratio g of EV chains with concentration

	g					
	Φp[a]					
	0	0.1	0.2	0.3	Gaussian[b]	θ chains[c]
f=3	0.75	0.76	0.77	0.78	0.78	0.81–0.83
f=4	0.61	0.61	0.63	0.62	0.62	0.66–0.68

[a] MC, [154]
[b] Eq. (21)
[c] MC, [122, 123]

(three branches of two beads along a main chain of ten beads). Although the compressibility factors are again similar to those of linear chains, it is observed that the vapor phase density is larger and the liquid density is lower for branched chains. The free energy of mixing of linear and branched chains with solvent was investigated through MC simulation in a cubic lattice by Falsafi and Madden [150]. The branched chain data of this excess thermodynamic quantity are slightly above those of the linear chains and the behavior of the branched chains is closer to the predictions of the lattice cluster theory [151].

Studies of conformational properties through many-chains simulations of star molecules are particularly scarce, since these systems require long equilibration processes without the help of the efficient reptation moves used for linear chains. Moreover, the MC simulations on a lattice must include specific rules to change the star center position. Su and Kovac [152] studied the case of three-arm and four-arm single stars immersed in a bath of linear chains. They used the bond fluctuation model. The increase of concentration causes a decrease of the star mean size. This feature shows the EV screening due to increasing intermolecular bead interactions. This effect is also found in linear chains, though for the stars is less significant, since the star chains suffer a smaller expansion in EV conditions. The Su and Kovac simulation also shows that the asphericity increases slightly for higher concentrations. This is caused by a decrease of the smallest

eigenvalue of the radius of gyration tensor, which means that the molecules tend to be more plate-like as the excluded volume is relieved. Smit et al. [153] performed an MD simulation for a single small three-arm star and varying numbers of solvent (monomer) molecules and found the opposite shape effects.

A many-chain simulation of three- and four-arm stars with up to 400 beads (for the smallest concentrations) on the cubic lattice has recently been carried out [154]. The preliminary analysis of results indicates very small differences for the mean size ratio g of EV star chains corresponding to different concentrations. The values of this ratio are, therefore, always smaller than for the corresponding theta chains, as can be observed in Table 2. This confirms the theoretical argument that EV effects are practically canceled out in this ratio and screened out in concentrated solutions. The swelling of stars in theta conditions with respect to the bulk, revealed by the analysis of scattering data [2, 63], also indicates that g in the melt should be smaller than in the theta state. Higher functionalities would be needed to confirm the intermediate scaling in the bulk predicted by the recent liquid-state theory [70]. According to the simulation, the apparent value of critical exponent ν diminishes from the 3/5 for dilute solutions to values closer to 1/2, the mean-field result. The expected decrease with concentration for chains with a given chain length is found. According to the theoretical scaling arguments, Eq. (9) should apply to describe this variation. The fitted slopes of log-log plots of $<S^2>$ vs the volume fraction Φ_p in the range 0–0.5 yield apparent exponents of –0.24 and –0.21 for the three and four-arm chains of 97 beads, close to the –0.25 value that corresponds to the theoretical prediction. Similar features indicating the EV screening with concentration were previously observed with the same model and similar algorithm for linear chains.

Pakula et al. [155] have used the cooperative motion algorithm to study melts of stars with up to 64 units. They studied the internal bead profiles and the correlations of the star centers of mass. They observed an ordering of the systems of stars with high functionalities.

4.1.2 *Internal Structure and Scattering Form Factor*

The static scattering form factor of stars has also been obtained from simulation. Batoulis and Kremer [133] computed this function from their MC results for linear chains and stars up to six arms in terms of the Kratky plots [61]. The star chains show the expected peaks in the crossover between the regimes governed by distances involving the whole star and distances inside the blobs. This peak increases with f. Croxton [50] has performed a similar MC calculation for the whole scattering of off-lattice star chains with up to six arms with non-overlapping beads, but with a very short number of chain beads, showing significant deviations from the ideal chain prediction due to EV effects. Huber et al. [156] used an RIS model for polymethylene stars without long-range intramolecular potential, but considering adequately restricted bond angles according to the star number of arms. Their MC results were able to reproduce the deviations from

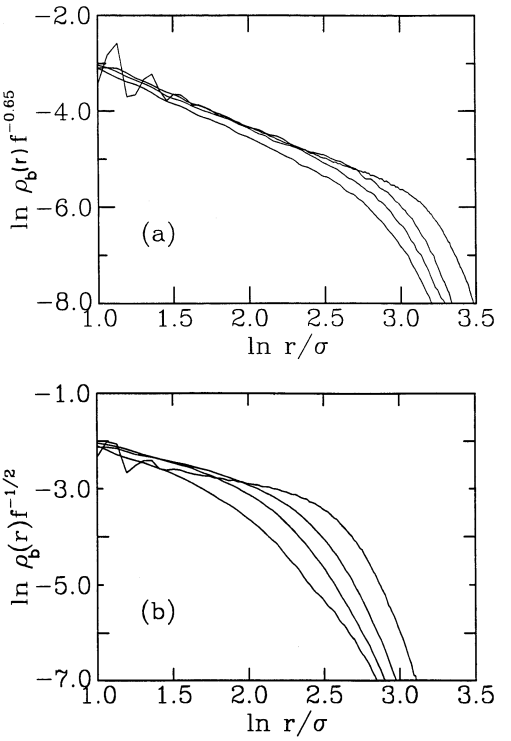

Fig. 13a,b. Scaled bead profiles for star chains of different values of f=4, 10, 20, 50 (higher f, more extended profile): **a** good solvent; **b** theta solvent. According to Eqs. (11) and (13), the profiles should correspond to universal straight lines with slopes –4/3 (case a) and –1 (case b). Reprinted with permission from [131]. Copyright (1994) American Chemical Society

the Benoit behavior, Eq. (23), apparent in the Kratky plots of their SANS experimental data for PS in the theta state [65]. A qualitative description of this effect is also achieved taking into account the stiffness effects within the arms.

The internal distribution of beads in a uniform star predicted by the Daoud and Cotton scaling theory [11] can be tested by computing bead density profiles. These profiles can be compared with the scaling predictions for the density within EV blobs, Eq. (16), that can be explicitly written for EV stars as

$$\rho_b \approx r^{-4/3} f^{2/3} \,. \tag{60}$$

Croxton [50] found some differences with respect to the scaling pictures with discontinuities in the bead density at the central core. These results are in agreement with his theoretical calculations with the iterative convolution technique, also for short chains. However, the main features of the scaling theory prediction for the blobs density has been satisfactorily verified by Grest et al. [157] who performed a BD simulation of stars interacting through an LJ potential. The scaling

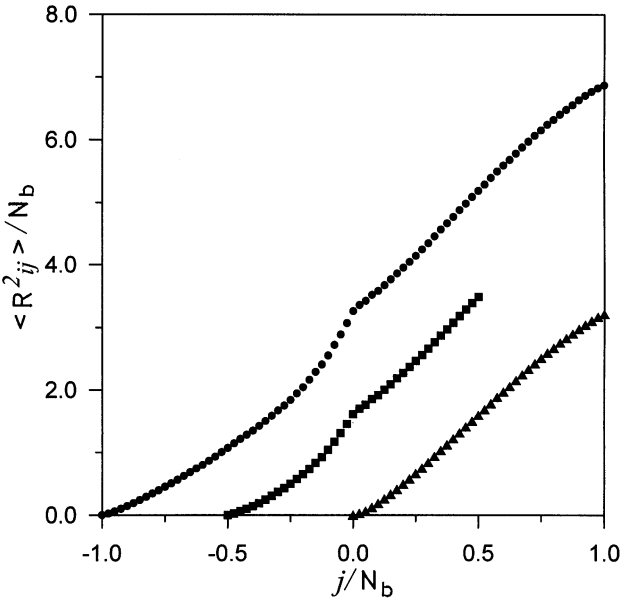

Fig. 14. Normalized averaged intramolecular distances plotted as a function of the position of bead j for a star with 12 arms with a total of 472 bonds. The beads are labeled as negative from $-N_b$ to 0 (the central atom) on the first arm and as positive up to N_b on the second arm. The three locations of the first bead i corresponds to $i=-N_b$, at the free end of the first arm (*circles*); $i=-N_b/2$, at the midpoint of the first arm (*squares*); and i=0, at the central branch point (*triangles*). Reprinted with permission from [158]. Copyright (1997) American Chemical Society

region extends to very small distances, which indicates a small influence of the core region for sufficiently long chains. These data have been confirmed by the BD simulation carried out by Grest [131] for solvents of varying qualities. The agreement with the scaling theory is good for EV chains except for the outer region of the stars (see Fig. 13a). The corresponding scaling for the theta state $\rho_b \approx r^{-1} f^{1/2}$ was similarly verified, though the agreement extended to a narrower range of relatively small values of r, as can also be observed in Fig. 13b. Forni et al. [158] have employed an off-lattice model of 12-arm EV chains, carrying out a detailed analysis of correlations between pairs of units in different regions of the star. Their results emphasize the loss of correlation among beads belonging to different arms, see Fig. 14 and Fig. 15.

The BD simulations by Grest et al. [131, 157] include stars with up to 50 arms. These simulations were also consistent with the f-dependence of ratio g predicted by the scaling theory. However, for the θ state, the simulated data show exponents higher than the theory and in better agreement with experimental data in the range f=2–128, as detailed in [2]. Then it seems that the scaling theory gives a poor description of stars in the theta region, at least in the range of moderately

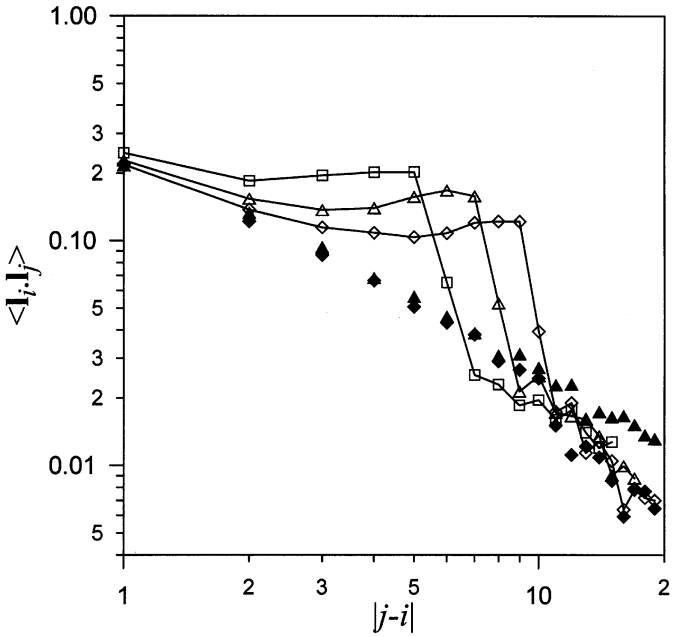

Fig. 15. Correlation of vector bonds. $\mathbf{l}_i$ is fixed, while $\mathbf{l}_j$ can cross the central bead. *Solid diamonds*: linear chain of 40 bonds, with i=11; *solid triangles* linear chain of 80 bonds, i=31. *empty symbols* correspond to a star of 232 bonds and 12 arms (20 bonds/arm). *Diamonds* i=11; *triangles* i=13; *squares* i=15 (the star center is reached after 9, 7 and 5 bonds respectively). Reprinted with permission from [158]. Copyright (1997) American Chemical Society

long chains for which simulations (as well as experimental data) are currently available.

For high f, it is possible to observe in the Kratky plots a sharp transition from the global to the blob regime with some oscillations when the star structure approaches that of a hard sphere. The simulation curves of Grest et al. have been fitted to describe satisfactorily SANS data [2]. Moreover, the same simulations have been used to obtain the partial scattering function of the core and the shell (outer portion of the star) and the corresponding curves have been compared with experimental data obtained for PI stars with a deuterated core [68]. The comparison is satisfactory from the qualitative point of view, since the simulations exhibit the essential features of the experimental data, though some quantitative differences are apparent. At high values of q, the core partial scattering function shows a different scaling law to that of the global chain, indicating the different distribution of intramolecular distances in the star core.

The scattering function can be expanded for low values of q. The expansion coefficients correspond to high moments involving summations of powers of different intramolecular distances (it is well known that the mean quadratic ra-

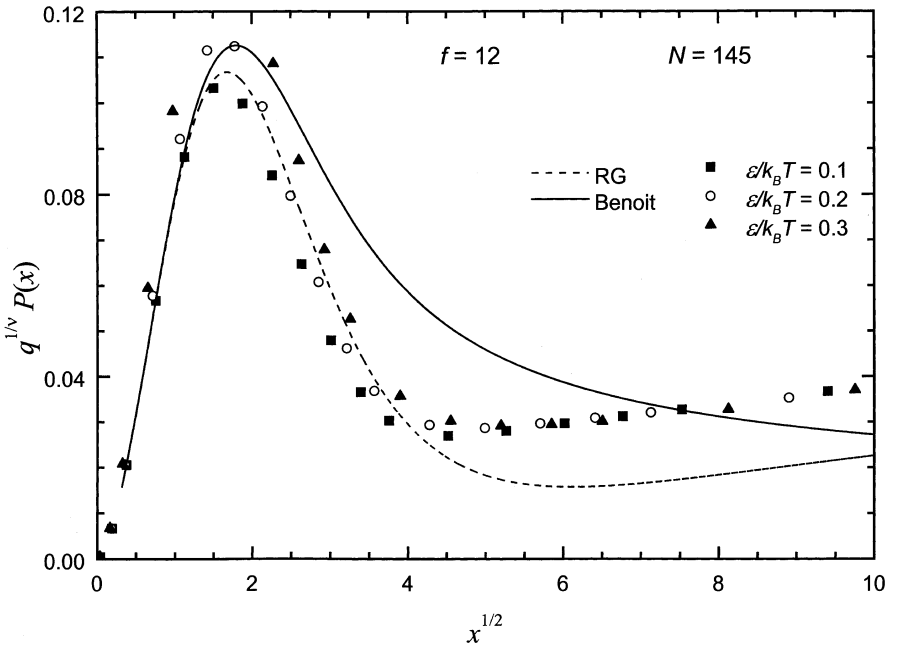

Fig. 16. Generalized Kratky plot of the form factor of a star from numerical data of a MC simulation [161]. $x=q^2<S^2>$. $\varepsilon/k_BT=0.1$ corresponds to EV chains and $\varepsilon/k_BT=0.3$ is close to the theta state

dius of gyrations is, in fact, the second moment corresponding to the first term in this expansion). Bishop et al. [159] have calculated these moments for linear chains and stars using the Gaussian bead model with an LJ potential in the EV regime. The results for linear chains are in good agreement with RG calculations [160]. The moments expansion can, however, reproduce only the low q region of the form factor, even when three or four terms of the expansion are considered. The plot of the simultaneously obtained whole form factor function for stars reveals a closer agreement with the curve obtained by Alessandrini and Carignano [66] (RG calculations) than with the Benoit function [60]. A more detailed study including different solvent conditions introduced through the LJ attraction parameter [161] confirms this conclusion, showing a good qualitative agreement with the RG curve for chains with up to 12 arms, even for chains close to the theta point, as shown in Fig. 16. The solvent quality is only manifested through the different scaling of the curves for low values of x. The appearance of the simulation curves is again different from the theory prediction (Benoit curve) and it seems in better qualitative agreement with the theoretical predictions for the EV regime, obtained with the RG calculations. There is only a significant quantitative disagreement between the RG curve and the simulation results in the asymptotic behavior for high values of x, where the simulation data are shifted up-

wards by a constant value. A similar shift is also found in the comparison of the asymptotic plateau of experimental data corresponding to good solvent conditions with respect to the plateau for high values of q exhibited by the RG curve (Fig. 4). However, a higher value of ν would be required to get a real plateau for the plotted RG and simulation data, instead of the straight lines with small positive slopes shown in Fig. 16, probably due to finite size effects inherent to the relatively small values of N used in the simulations. Moreover, numerical fits of the simulated data to the RG curve in the range of low and moderate q using $<S^2>$ as a single fitting parameter yield numerical estimates of the chain sizes very similar to their actual values (known through direct Monte Carlo evaluation). However, similar fits using the Benoit curve lead to significantly different estimates of the radius of gyration. These types of fits are sometimes used in the interpretation of experimental data [2].

4.1.3
Translational Friction Coefficient and Intrinsic Viscosity

We have previously pointed out that the experimental data for hydrodynamic properties of stars such as the translational diffusion coefficient in the dilute regime and the intrinsic viscosity (expressed in terms of ratios h or g' to the homologous linear chains) are not quantitatively reproduced by approximate theories. The semiempirical relations, Eqs. (45) and (46), also have a limited success in describing existing experimental data. Therefore, it seems that the use of simulation procedures is particularly useful for this purpose. An adequate calculation should consider the following points: (a) to take into account the presence of intramolecular interactions, and (b) to improve the simplistic preaveraged description of HI, employed in the KR or ZK approaches. As previously explained, point (b) is crucial to reproduce viscosity results, which seem particularly affected by the preaveraging approximation in compact structures. Point (a) affects both equilibrium and hydrodynamic properties, especially for chains in the theta conditions, since the ratios of the EV star chains to the corresponding linear chain are always very close to those calculated with Gaussian statistics.

Simple MC calculations with the rigid-body approximation were performed by Zimm [126] for Gaussian and wormlike stars with and without EV up to six arms. Neither the effect of stiffness nor EV effects seem to affect greatly the value of ratios h or g', which are always similar to those obtained with ideal chains. The differences with respect to the KR values are about 7% for h, but they increase to 14% for the ratio g'. These conclusions agree with the general picture given above. A similar calculation on a cubic lattice was carried out by Wilkinson et al. [162]. Freire et al. used the translational Pivot MC algorithm to perform a more extensive rigid-body investigation with the Gaussian bead model with an LJ potential for short stars up to 18 arms. Chains in the theta region [109] and with EV effects [125] were alternatively considered.

Tables 3 and 4 contain extrapolations to the long chain limit of ratios h and g', obtained from rigid-body simulation data, together with similar numerical val-

Table 3. Comparison of theoretical, simulation and experimental values of ratio h

		h				
Model	HI treatment	f=4	f=6	f=8	f=12	f=18
Gaussian	Kirkwood[a]	0.89	0.80	0.73	0.67	0.53
Gaussian	Preaveraged[b]	0.92	0.86	0.81	0.73	0.65
Gaussian	Rigid-body	0.95[c]	0.86[d], 0.90[c]		0.75[d]	0.66[d]
Theta	Rigid-body[d]		0.89		0.82	0.73
EV	Rigid-body	0.94[c]	0.89[c,e]		0.78[e]	0.66[e]
Theta (experimental)[f]		0.94	0.89		0.74–0.85	0.72–0.76
EV (experimental)[f]		0.92–0.93	0.86	0.82	0.70–0.83	0.64–0.68

[a] Eq. (38), [84]
[b] Eq. (34), [84]
[c] [126]
[d] [109]
[e] [125]
[f] Data reviewed in [49]

Table 4. Comparison of theoretical, simulation and experimental values of ratio g'

		g'				
Model	HI treatment	f=4	f=6	f=8	f=12	f=18
Gaussian	Preaveraged[a]	0.81	0.69	0.61	0.51	0.42
Gaussian	Rigid-body	0.71[b]	0.58[b,c]		0.38[c]	0.24[c]
Gaussian	Lower bound[d]				0.33	
Theta	Rigid-body[c]		0.59		0.39	0.28
Theta	Lower bound[d]				0.41	
EV	Rigid-body	0.73[b]	0.56[b],0.58[e]		0.37[e]	0.22[e]
EV	Lower bound[d]				0.33	
Theta (experimental)[f]		0.76–0.77	0.63	0.53	0.42	0.28–0.35
EV (experimental)[f]		0.73	0.58	0.43	0.33–0.35	0.22–0.26

[a] [84]
[b] [126]
[c] [109]
[d] [164]
[e] [125]
[f] Data reviewed in [49]

ues obtained through other models and approaches and a summary of the experimental data reviewed in [49]. The rigid-body EV results for h and g' are similar to those obtained with the same hydrodynamic treatment for ideal chains, in good agreement with the RG theory conclusion that the ratios corresponding

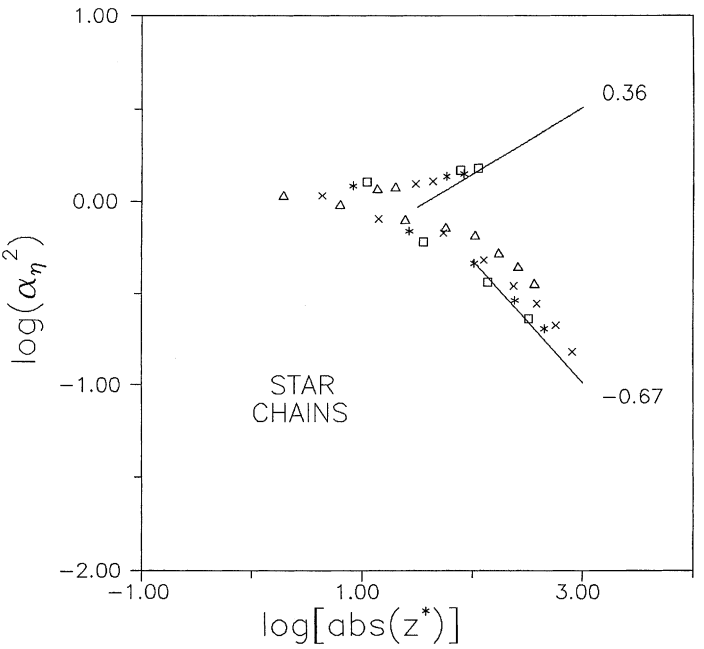

Fig. 17. A log-log plot of expansion factor, α_η^2, (obtained from intrinsic viscosity calculations) vs reduced excluded volume, $|z^*|$, for MC data of 12 arms stars with N=25–109 units (symbols as in Fig. 11). The *solid lines* and figures represent slopes corresponding to the predicted asymptotic behaviors for the EV and sub-theta regimes. Reprinted with permission from [143]. Copyright (1992) American Chemical Society

to ideal and EV chains should be very close. Moreover, these EV and Gaussian results for h are not very different from those obtained with the Gaussian chain with the preaveraged treatment, Eq. (34), though they are always greater than the Kirkwood formula estimations, Eq. (38). However, the rigid-body values of g' for Gaussian and EV stars are smaller than the results from the preaveraged theory, and the differences increase dramatically with the number of arms. It can be verified that the rigid-body MC data give an adequate reproduction of most experimental data corresponding to the investigated architectures for ratios h and g' in the two distinct solvent conditions. These conclusions show that points (a) and (b) enumerated above are the main requirements for a good description of the hydrodynamic properties of stars. Simultaneously, the same rigid-body calculations approximately reproduce the experimental ratios P and Φ. The parameters approach the values for rigid spheres for stars with high numbers of arms [51]. As in the case of linear chains, P and Φ decrease in EV conditions with respect to their values for ideal chains or in theta conditions.

Since the rigid-body approximation gives only an upper bound for the translational friction coefficient and viscosity, MC values of the viscosity for ideal star

chains have also been obtained [163] with the alternative variational method of Fixman [112]. The comparison between both sets of results indicates that the upper and lower bound methods establish a reasonably narrow range for the real value of this property, at least when the comparison is performed from data corresponding to relatively short chains (about 20% in a 12-arm star of 37 beads). Differences due to the bound method are smaller for the ratio g', since both linear and star chains exhibit similar relative deviations in the viscosity results obtained with the upper or with the lower bound procedures. The viscosity was also obtained from the numerical study of the stress tensor time-correlation function calculated from BD trajectories of ideal chains that include fluctuating HI [163]. The latter results can be considered as rigorous and, though affected by higher statistical uncertainties, they were always consistent with the calculated bounds.

The numerical efficiency of the viscosity lower bound method has allowed calculations on considerably longer chains. The long chain limit results for 12-arm stars without intramolecular interactions and with EV (up to 325 beads) and in the theta region (up to 145 beads) [164] are close to the previous estimates with shorter chains (the extrapolated ratio g' obtained in this study is also included in Table 4). The lower bound method has also served to characterize globule-coil transitions of 12-arm star chains from intrinsic viscosity calculations [143], though finite size effects are considerably more important than in the characterization of this transition from the radius of gyration data (see Fig. 17). This is due to the noticeable increase in the solvent permeability associated with the chain expansion in better solvent conditions. However, the permeability effects are smaller in the more compact star chains than in their linear counterparts.

4.1.4 *Dynamics and Relaxation*

Accurate calculations for the real and imaginary components of the complex viscosity function $[\eta(\omega)]^*$ should certainly have to consider the same features required to obtain the intrinsic viscosity. Rey et al. [165] computed the Fourier transforms of the time-correlation function of the stress tensor, obtained from their BD simulation trajectories of ideal chains, to calculate this function. The calculations were performed with preaveraged and fluctuating HI interactions. Although the quantitative differences in these two different estimations of the intrinsic viscosities for highly branched stars are very important (the preaveraged values of the intrinsic viscosity are about 70% above the real values for 12-arm stars), the qualitative aspects of the log-log plots for $[\eta(\omega)]^*$, extended over the useful several decades of frequency values, are not so different. Moreover, the effect of introducing the preaveraging approximation decreases in importance at higher frequencies.

However, the consideration of intramolecular interactions and, therefore, of realistic distributions of intramolecular distances changes the shape of the func-

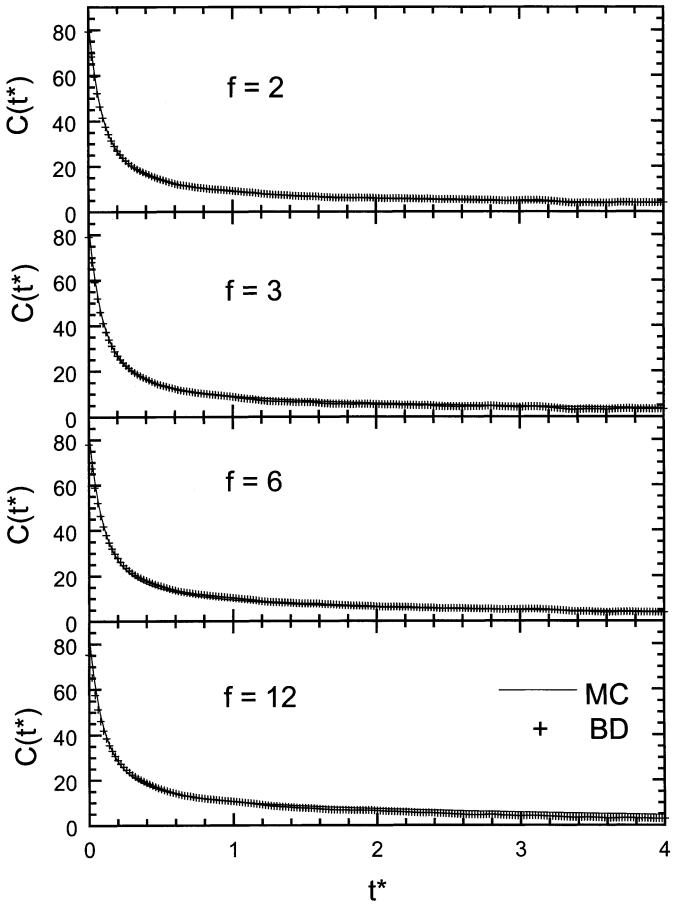

Fig. 18. Stress time-correlation function of EV linear chains and stars with different functionalities. Comparison of Brownian dynamics (*crosses*) and generalized Zimm calculations from MC averages (*solid lines*). Reprinted with permission from [89]. Copyright (1996) American Institute of Physics

tions. This effect was first observed by Rey and Freire [89] by computing Eq. (52) for ideal and EV stars with up to 12 arms, with relaxation times obtained from their generalized Rouse-Zimm model. According to this scheme, the relaxation times can be calculated through the consideration of MC computed equilibrium averages. The stress time-correlation function obtained with this method gives a perfect agreement with the function directly computed from BD trajectories with preaveraged HI (see Fig. 18). This confirms the accuracy of the approximate treatment. The real and imaginary dynamic viscosity curves calculated through this method for EV star chains exhibit features different to the ideal chain curves, as they lie very close and parallel in a limited range of inter-

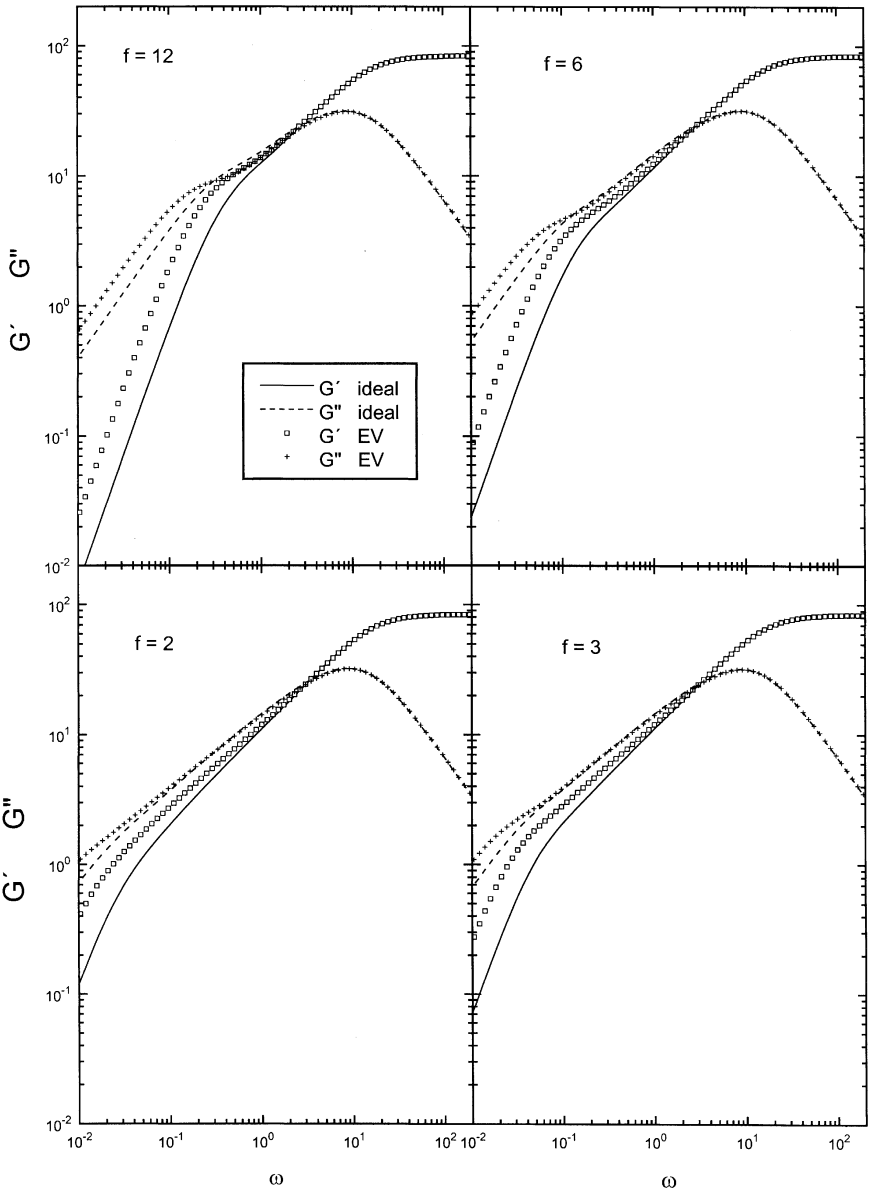

Fig. 19. Complex viscoelastic moduli for linear chains and stars of different functionalities, without intramolecular interactions (ideal) and with a repulsive potential (EV). Reprinted with permission from [89]. Copyright (1996) American Institute of Physics

mediate frequencies, which is broader for higher values of f (in fact, the curves for f=12 cross each other twice in this region) (see Fig. 19). The previously mentioned theoretical calculations by Ganazzoli [92], performed for longer EV chains but with approximate estimations of the intramolecular distances, also show similar curves but without the double crossing. Such double crossings are found for stars [166] and other branched structures in the melt. In any case, the approach of the real and imaginary curves due to non-Gaussian effects in stars is totally missed by the older ideal chain calculations of Sammler and Schrag [91].

Models based on Gaussian beads cannot describe the high frequency region of the dynamic viscosity curves. These models predict a final cross-over of the real and imaginary curves in this region since the storage modulus, G', smaller at low frequencies, tends to an asymptote, while the loss modulus, G", tends to vanish, as can also be seen in Fig. 19. However, the rigid-bond constraints prevent the decrease of the curves for a single chain. This constitutes another failure in the ideal chain calculations. The incorporation of local constraints can be carried out by means of some theoretical schemes [167]. BD simulations can also consider strong harmonic forces or totally rigid bonds, but BD calculations of the complex viscosity functions for multi-bead linear or star Bead and Spring chains have only achieved a modest increase of the frequency of the cross-over [168].

BD and MD simulations can directly describe the dynamic behavior of a chain molecule. Grest et al. [131, 169] studied the relaxation processes, investigating the elastic, rotational, and arm disentanglement mechanism described above. They confirmed the theoretical prediction that the elastic relaxation time is approximately independent of the number of arms. However, the rotation and disentanglement processes, which require longer simulation runs, could not be analyzed through this procedure. The MD simulation of Smit et al. [153] included explicit solvent (monomer) units. They analyzed the time-correlation function of the radius of gyration, together with the diffusion coefficient (from the center of masses displacement and also from the velocity autocorrelation function), but their results show a great dependence on concentration, and a further analysis was not attempted.

MC methods can also be employed to investigate dynamic properties. Ohno et al. [170] applied a Kramers potential (proportional to the product of coordinates xy) to mimic the effect of simple shear flow, and studied the induced change of the averaged size. Therefore they obtained the relaxation time from the analysis of purely static quantities. Their study was performed with the fluctuation bond model. They alternatively applied the enrichment algorithm to SAW star chains with a core on a cubic lattice. Their results confirmed the approximately f-independent behavior of the elastic relaxation. Su et al. [171] used the bond fluctuation model to perform a dynamic MC simulation of three- and four-arm stars. Although their results confirm again qualitatively the scaling law obeyed by the elastic relaxation time, their rotational relaxation functions do not decay as a single exponential.

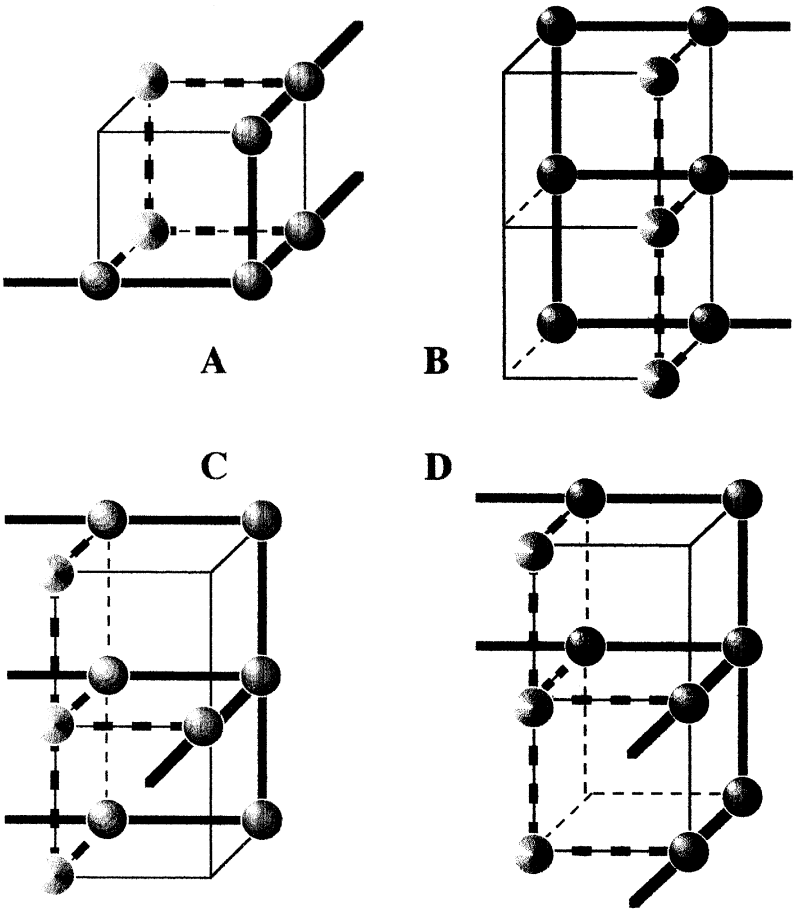

Fig. 20a–d. Rules of bead-jump involving the chain center, employed for a DMC simulations of stars ([154]): **a,b** used for f=3; **c,d** applicable for f=4

Sikorsky and Romiszowski [172, 173] have recently presented a dynamic MC study of a three-arm star chain on a simple cubic lattice. The quadratic displacement of single beads was analyzed in this investigation. It essentially agrees with the predictions of the Rouse theory [21], with an initial $t^{1/2}$ scale, followed by a broad crossover and a subsequent t^1 dependence. The center of masses displacement yields the self-diffusion coefficient, compatible with the Rouse behavior, Eqs. (27) and (36). The time-correlation function of the end-to-end vector follows the expected dependence with chain length in the EV regime without HI consistent with the simulation model, i.e., the relaxation time is proportional to $N^{1+2\nu}$. The same scaling law is obtained for the correlation of the angle formed by two arms. Therefore, the model seems to reproduce adequately the main features for the dynamics of star chains, as expected from the Rouse theory. A sim-

Table 5. MC data of τ_e and τ_D

	f=3					f=4				
	N_b					N_b				
	12	16	24	32	50	12	16	24	32	50
τ_e[a]	15.2	24.2	59.0	118.3	323	21.4	26.9	68	113	319
τ_D[a]	164	318	663	1194	3550	257	403	994	1719	4033

[a] [154] (in DMC step time units)

ilar simulation has been recently applied to the MC investigation of three- and four-arm stars [154]. The different rules employed for the motion of the star center are detailed in Fig. 20. In this case, the relaxation times of the Rouse coordinates have been directly investigated, giving the correct scaling law dependence on the chain length. Moreover, the elastic relaxation times are roughly independent of the number of arms, see Table 5. These simulation results also seem to confirm that the rotational relaxation times, also included in Table 5, depend on the number of arms according to the theoretical scaling law, Eq. (54). However, the arm disentaglement relaxation needs much longer dynamic trajectories, and it is currently very difficult to characterize this mode from any type of simulation algorithm.

Only a few investigations have dealt with star chain dynamics in many-chain systems. Needs and Edwards [174] considered a random walk three-arm chain in a set of fixed obstacles formed by infinitely long rods. With this model they reproduced the exponential dependence of the theoretical diffusion coefficient dependence on chain length. A similar exponential law is predicted for the chain relaxation time. Sikorski et al. have studied star chains up to 1196 units in a matrix of free linear chains of 800 units. [175]. The diffusion coefficient and longest relaxation time follow similar behaviors as in the single chain case, although there is a larger difference between the one-arm and two-arm relaxation times. Some evidence of the arm retraction mechanism was found, though the chains are too short to see the onset of the exponential scaling. The entanglement lengths for stars are somewhat larger than for linear chains.

4.1.5
Copolymers and Miktoarm Stars

Block copolymers have peculiar characteristics due to the coexistence of two or several different parts of different chemical compositions within a chain. They can undergo microphase separation transitions from a homogenous phase to a variety of spatially periodic structures [176]. A distinction should be made between star copolymers, where each arm is composed by two or more blocks, and miktoarm polymers, formed by homopolymer arms of different chemical compositions. Floudas et al. [177] recently performed an extensive study of four-

arms star diblock copolymers which includes a computer simulation. The arms are composed of a block of styrene and a block of isoprene with similar or clearly different number of segments (symmetric or asymmetric compositions). The stars with symmetric compositions exhibit a well-ordered lamellar microstructure at low temperatures. Asymmetric stars of four arms, however, show a succession of phases on heating. Similar theoretical and experimental studies have been carried out for miktoarm stars [178, 179], showing the formation of hexagonally ordered cylinders with a kinetically accessible metastable region broader than in linear diblocks.

The conformational properties of single miktoarm chains have been investigated through MC simulations with the Gaussian bead model with LJ intramolecular interactions by Vlahos et al. [180] for A_2B and A_3B miktoarm stars and different solvent conditions. This study was aimed at characterizing the segregation between the arms due to EV heterointeractions. The results were compared with predictions from RG group calculations and also with intrinsic viscosity data. It is observed that the more compact star structure causes a significantly stronger segregation between chemically distinct blocks than for linear diblock chains.

4.2 Combs

We have previously mentioned that the first MC simulations on comb-like polymers with varying solvent conditions and including the theta point were performed by Mazur and McCrackin [121] on a cubic lattice. In fact, these authors considered the ratio of the molecular weight of a branch to that of the backbone, x_b, to define the comb architecture so that the star chains can be considered as the limit case corresponding to $x_b^{-1} \rightarrow 0$. It is not surprising that the mean size in the theta state is greater than the results given by the general formula of Kurata and Fukatsu [48], who considered Gaussian statistics. The experimental data for chains in the theta state are also greater than the ideal chain statistics, though these data are significantly scattered. Also, as in the star case, the global expansion factors are smaller than those found in linear chains (in contradiction with the two-parameter first-order perturbation theories) due to the smaller values of g for EV chains with respect to the theta state. Their results for the backbone radius of gyration show that this quantity is greater than for the equivalent linear chains, again in variation with the ideal chain model that does not describe such a difference.

Lipson et al. [181] performed an MC study on different types of lattices for three functional comb chains with two branched points, or H-combs, in the excluded volume regime. The variation of the branch mean size with its length follows the expected scaling law in terms of critical exponent, $R_g^b \approx N_b^{\nu}$. This is in accordance with the expected behavior in the low branching (or mushroom) regime, and it is also in agreement with RG calculations [182]. In the Lipson et al. simulations, expansion of the different branches was analyzed by evaluating their amplitudes in this power-law. Thus, the "internal branches" (backbone seg-

ments between two branching points) present a greater expansion than the external branches, due to the higher number of intramolecular interactions between segments. The expansion of the external branches is similar to that of a three-arm star. Their ratio g is similar to that of an ideal chain, in good agreement with the results obtained for EV stars, and also with experimental data and RG calculations [43, 49], as summarized in [49]. A similar study was carried out by Bishop and Saltiel [183] with a BD simulation.

Lipson [184] also carried out an MC simulation of long EV combs with many branches on a tetrahedral lattice. Three different types of branches (of lengths smaller than, equal to, or larger than those of the segments between branching points in the backbone) were considered, while the total number of branches increases linearly with molecular weight. It is evident that, as in other architectures previously analyzed, the scaling law for global dimensions vs chain length is properly described by the critical exponent ν. The presence of finite size effects is, however, larger for the combs with long branches. Moreover, the ratio g, and also an estimation of the ratio h from the friction coefficients obtained through the Kirkwood formula, Eq. (38), are significantly greater than those predicted by the ideal Gaussian model, in contrast to the results obtained for stars and H-combs. These results are consistent with the available experimental data of combs with randomly attached branches but with similar weight fraction of material in the backbone, which seems to be the most relevant characteristic variable. These experimental data correspond to both good and theta solvents [185], which indicates the relative lack of sensitivity of these results to solvent conditions (actually the theta point values of g are slightly greater than the good solvent data, as in the case of stars of low functionalities).

Kosmas et al. [5] performed some MC simulations on a cubic lattice to verify their theoretical calculations for combs with polyfunctional branching points (or "brushes"). They analyzed the expansions of internal branches and found an extra expansion, in agreement with the theory.

Comb polymers may also have a backbone chemical equal to or different from the branches. In many cases this backbone can be stiff or rigid. According to theory [186], this rigidity can be induced by interactions between different branches and depends on ρ_f. One can distinguish between a regime where the backbone only experiences its own EV at low density of branching, ρ_f, an intermediate regime where the EV of branches dominates, and a high ρ_f regime, where the backbone is very rigid. This rigidity effect was confirmed by the simulation of Rouault and Borisov [187]. They use a bond fluctuation MC algorithm, and again the branch extension varies with N_b according to the mushroom regime. The increase of the backbone persistence length due to interactions between branches was also recently simulated by Saariaho et al. [188] with an off-lattice model. Grest and Murat [9] have also presented MD simulations describing the f-dependence of the chain mean size for EV stars and high ρ_f combs, or "bottlebrushes". Although for low ρ_f both types of chains show similar log-log linear behaviors, for high ρ_f the size of bottlebrushes suffers a further increase as they become more elongated.

A limiting case is constituted by many branches grafted to an inflexible line. The scaling theory is pertinent to this case. Then the density of segments is

$$\rho_b(r) \approx (r / \rho_f)^{-1/2} \tag{61}$$

and

$$\rho_b(r) \approx (r / \rho_f)^{(1-3\nu)/2\nu} \cong (r / \rho_f)^{-2/3} \tag{62}$$

in theta and good solvent conditions respectively. The density of segments decreases with r more slowly than in stars (Fig. 2) because the volume available for higher r increases more rapidly in the star case. An MD simulation performed by Murat and Grest [189] for bottlebrushes formed by EV chains attached to cylinders of different curvatures seems to confirm this point for strong curvature, though the simulation results indicate an exponent for the r dependence intermediate between the values –2/3 and –1/2. Recent experimental data [190] for highly-branched combs show an extension of branches proportional to $N_b^{0.71}$, in reasonable agreement with the exponent ≅0.8 predicted from Eq. (17). According to these data, the backbone becomes very stiff, which is attributed to interactions of the branches.

Gauger and Pakula [191] performed an MC simulation of comb polymers on the fcc lattice in dilute and dense media, using the cooperative motion algorithm. It is shown that, unlike linear chains, the EV screening does not appear in the global mean size dependence on N. However, this screening is complete for the branches in the melt, which exhibit ideal behavior.

Branched chains may have an important role in interfacial phenomena. Gersappe et al. [192] studied the behavior of combs constituted by backbones of A monomers and branches, or "teeth", of B units at the interface between immiscible A and B monomers. These teeth are more preferentially located at the interface than the equivalent units in linear chains.

4.3 Brushes

Many different simulations have been performed to test the different features of brushes in different situations. Here we will give only a summary of these results, in the context of the similarities and differences with the features observed in individual branched polymers.

An obvious aim in the simulations is to check the mean-field, and SCF theoretical approaches, which differ in some basic features. Both theories predict the same qualitative relationship for the brush height or the main chain extension in a good solvent (proportional to $N\rho_f^{1/3}$). This result has been confirmed by the MC calculations of Chakrabarti and Toral [193] and Lai and Binder [194] (who

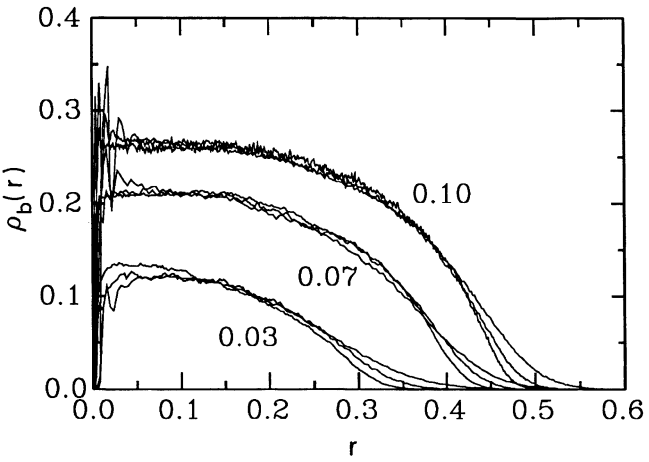

Fig. 21. Bead density profiles in a brush of EV grafted chains with N=50, 100 and 200, and the indicated grafting point densities. Reprinted with permission from [199]. Copyright (1993) American Chemical Society

used the bond fluctuation model) and by the BD simulations of Murat and Grest [195] and Neelov and Binder [196]. Another simulation by Grest [197] has shown that the dependence on the grafting density adopts a higher exponent close to 1/2 for high densities and long chains. This effect is explained by predominant three-body interactions [198] and defines a new range of high grafting densities. Grest and Murat have also checked the predictions for the bead density, ρ_b, through BD [195] or MD [199] simulations. Their results, together with the MC simulations of Chakrabarti and Toral [193] and Lai et al. [200] can roughly be fitted in terms of the parabolic form predicted by the Milner et al. theory [35], allowing for plots of universal (i.e., f-independent) scaling curves except for the end of the brushes (see Fig. 21). Nevertheless, a deviation from the parabolic shape should also be noted near the surface, in the form of a depletion layer, which is more clearly observed for relatively smaller densities. According to the simulations [193, 195, 200] the distribution of free ends follow roughly the behavior predicted in the Milner et al. theory, though it is slightly sharper. This behavior is observed for the adequate range of high grafting density. Clancy and Webber [201] used the Pivot algorithm to compute ρ_b in both the mushroom and high grafting density regimes.

The simulations and theoretical approaches reveal that the density profile is somewhat lost in the presence of polydispersity [193, 202], and special features (including a kink in the profile) are observed for a bimodal chain distribution [195, 203]. The profiles are flatter for the highest grafting densities, due to the influence of high-order terms. Laradji et al. [204] performed an MC simulation with an off-lattice model that uses the Hamiltonian employed in the SCF calculations (i.e., it only considers binary interactions). The parabolic profiles are

found even for high grafting densities. These results demonstrate that the deviations from the parabolic prediction are due to the influence of predominant three-body terms for high densities.

Toral and Chakrabarti [205] used an off-lattice model to study EV chains grafted onto a spherical surface with different radius of curvature. For high values of this radius the bead density profile follows the parabolic behavior. As the radius approaches the brush height, however, the bead density shows a maximum near the surface. Since free ends are located anywhere within a planar brush and they are placed in the outer region of star molecules, it is possible that for finite values of the radius of curvature there is a "dead zone" close to the surface without chain ends. These simulations show that this dead zone only appears for small radii (high curvatures) in relation to the brush height. A similar conclusion is obtained with the MD simulation previously described for a bottlebrush [189]. This is probably due to finite size effects, as the simulation results are in agreement with numerical SCF calculations [206, 207], but not with the analytical results of Li and Witten [208] that predict a dead zone for brushes of long chains in a good solvent. These simulations are also in good agreement with the recent single chain mean-field theory proposed by Carignano and Szleifer [209].

When the brush is immersed in poorer solvents, the theory predicts substantial changes. Thus, the chain extension and the brush height should scale as

$$R_g^b \approx N_b \rho_f^{1/2} \tag{63}$$

for a theta solvent and

$$R_g^b \approx N_b \rho_f \left|\beta\right|^{-1} \tag{64}$$

in the sub-theta compact globule regime. It should be noted that the overlapping density of grafted chains increases, since the chains are not expanded in these solvent regimes. Then $\rho_f^* \approx N^{-1}$ in the theta state and $\rho_f^* \approx N^{-2/3}$ for compact globules. As a result, the system can actually change from the overlapping to the mushroom regime by decreasing the temperature. Consequently, more costly simulations are required to test the theoretical predictions in the high ρ_f regime. Different solvent conditions were contemplated in the bond fluctuation MC calculations of Lai and Binder [210] and the BD calculations of Grest and Murat [199]. Although the Lai and Binder results seem to show a scaled behavior consistent with the theoretical SCF predictions for the first moment of bead density function in the theta state, the profiles obtained in the BD simulations are not in good agreement with the elliptical form predicted by the theory, and they exhibit a significant clear depletion layer close to the grafting surface, as shown in Fig. 22. Moreover, Grest and Murat could not obtain the predicted universal behavior in their scaled plots. In the sub-theta regime at moderately high grafting densities, both simulations found steplike profiles, i.e., with a uni-

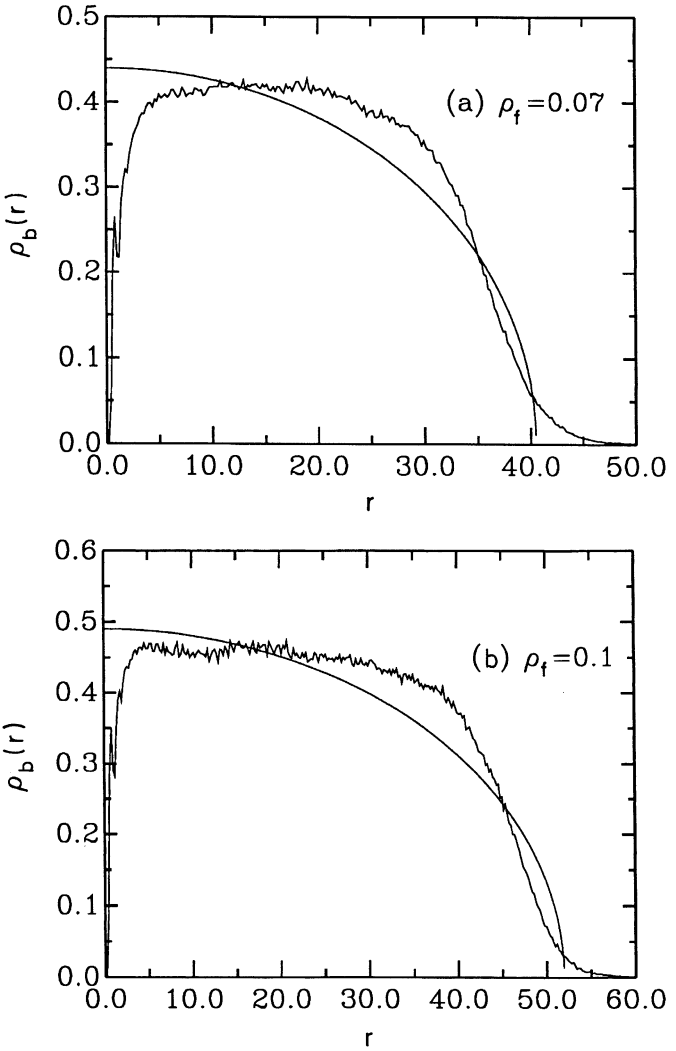

Fig. 22a,b. Bead density profiles in a brush of grafted chains in a theta solvent with N=200, and two different values of the grafting point densities. The *smooth curves* correspond to the elliptical theoretical prediction. Reprinted with permission from [199]. Copyright (1993) American Chemical Society

form bead concentration across the brush (Fig. 23). For grafting densities close to the overlapping value, projections of all the monomers on the surface plane indicate a strong phase separation, with monomer-rich and monomer-poor phases, due to attraction between different chains. This behavior has been confirmed by atom force microscopy experiments [211]. The holes tend to disap-

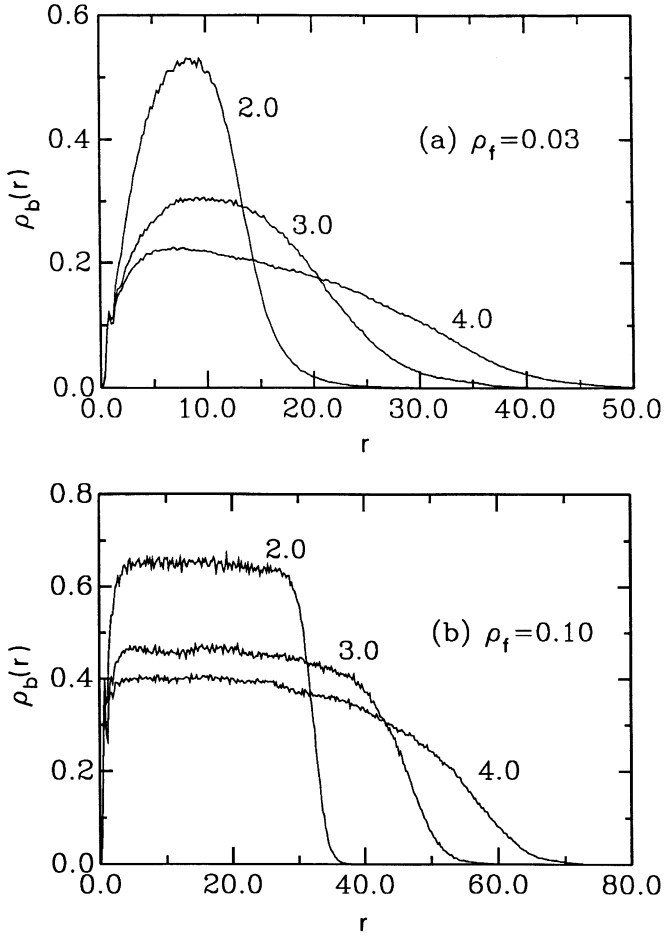

Fig. 23a,b. Bead density profiles of grafted chains with N=50, 100 and 200, and the indicated grafting point densities, and three different values of the temperature (EV, $T_\theta=3\varepsilon/k_B$, and sub-theta). Reprinted with permission from [199]. Copyright (1993) American Chemical Society

pear as the grafting density or the chain length increases, but it is not clear whether a uniform phase should be obtained for very long chains. Weinhold and Kumar [212] used a Bead-Rod model with LJ potential to perform MC simulations of brushes in poor solvent conditions. The significantly homogenous bead density profiles are also in agreement with the theoretical predictions. They also studied the transition between the mushroom and the stretched chain regimes.

Pakula and Zhulina [213] have simulated dry brushes at melt densities in contact with a repulsive wall. They used the cooperative motion algorithm. Their re-

sults were satisfactorily compared with a SCF approach, using a free energy functional, with an energetic part depending on the local stretching and an entropic part derived from the distribution of chain ends. Its minimization, considering uniform bead densities and constant chain lengths, allows them to obtain analytical expressions for these quantities. The chain stretching was found to be larger near the grafted surface.

The surface osmotic pressure, Π_S, can be determined from the first derivative of the free energy per chain with the inverse of the grafting density. Grest [197] performed MD simulations at constant osmotic pressure, studying its variation with ρ_f. The results can be expressed according to the power law $\Pi_S \approx \rho_f^y$, with $y \cong 2.5$. This exponent is significantly higher than the results of the Flory-type and scaling theories, y=5/3 and y=11/6, respectively. However, the simulation value of y is in better agreement with the calculations of Carignano and Szleifer [214] who relate the local osmotic pressure with the conformational distribution of chains, taking into account the bead size. Experimental data by Kent et al. [215] exhibit similarly higher exponents.

The interaction between two parallel brushes in the EV regime has been the object of several BD [216] and MC [217, 218] simulations. When the two surfaces are at a distance of about twice the brush height the brushes begin to overlap and the bead density profiles suffer a deformation. At small distances the bead density becomes uniform, but at moderate compression the profiles still resemble the parabolic form. The ends tend to penetrate into the opposite brush and also migrate into the depletion region near the surfaces where the bead density is small. The forces between the brushes is always repulsive in good solvent conditions. The interaction energies obtained from the simulations can be compared with the theoretical predictions from the scaling and the Milner et al. theories. These predictions are slightly different. The BD simulation data show a good agreement with the scaling theory, and also with distance-force experimental data obtained by Tauton et al. [219] with terminally attached PS chains. A recent generator-matrix calculation on lattices by Ruckenstein and Li [220] also shows good agreement with the experiments of Tauton et al. and Watanabe and Tirrell [221], which constitutes an improvement of the theoretical description.

The dynamics of chains in a brush can also be characterized by means of time-correlation functions of properties such as the grafting point-to-end distance. The Murat and Grest BD simulations [195] for EV chains and the dynamic MC simulations performed by Lai and Binder with the bond fluctuation model for chains in the EV [194] and theta regimes [210] have analyzed this function. The simulation relaxation times for EV chains scale similarly to the prediction of Klushin and Skvortsov [222], which can be roughly explained as Eq. (53) for τ_e, but now considering that not only units belonging to the external blobs (that are of similar size as the rest in the case of brushes) but all units contribute to the free-draining diffusion of the grafted chain. Then Eq. (51) can be considered again, but now in the form $\tau_b \approx (R_g^b)^2/D_b$. Since in the free-draining regime, $D_b \approx 1/N_b$ (consistently with the simulations which ignore HI and with the semi-

dilute conditions in the overlapping regime) and taking into account Eq. (18) it follows that

$$\tau_b \approx N_b^3 \rho_f^{2/3} \tag{65}$$

which is in rough agreement with the simulation data. However, the simulation exponent for the ρ_f dependence obtained by Lai and Binder in the theta point is 1.6, while the argument given yields an exponent of 1 for theta chains.

Lai and Binder also studied the mean quadratic displacement of a given bead in the plane defined by the surface or in the direction perpendicular to it. The displacement in the latter direction in both the EV and the theta regimes follows the typical Rouse $t^{1/2}$ behavior for intermediate times, except for the beads close to the grafted ends. At longer times the displacement increases more slowly to its saturation value due to the grafted nature of the chain. Something similar happens to the displacement parallel to the surface for good solvents. However, the results at the theta point show a slow, proportional to $t^{1/4}$, mean quadratic displacement at intermediate times before saturation. Stronger entanglement of chains in the poorer theta solvent conditions may explain these data.

Similar to the branches in copolymer stars and miktoarms, the grafted chains in brushes can be of different chemical compositions. Brown et al. [223] studied the microphase separation of grafted mixtures of homopolymer chains composed of immiscible A and B units and also [224] of diblock AB copolymers. In the former case, the brushes expand laterally and then experience lateral microphase separation. In the latter case, however, monomers segregate vertically to the surface forming a three layer structure.

4.4 Dendrimers

An MD simulation of dendrimers was performed by Naylor et al. [225]. They employed an atomic model and found open structures which do not support the concentric shells proposed by de Gennes and Hervet [39]. Their method requires long equilibration times and it is not clear that the results describe equilibrium. Lescanec and Muthukumar [226] used an off-lattice kinetic growth algorithm to generate SAW dendrimers. This approach does not ensure a reliable estimation of the true equilibrium configurations, unless a procedure is included to introduce the configuration bias. They obtained a bead density profile monotonously decreasing from the center, in contradiction with the de Gennes and Hervet findings, with substantial chain folding. The mean size data were fitted to an $R_g \approx N^{0.22} n_S^{0.50}$ scaling law. Mansfield and Klushin [227] performed MC simulations of dendrimers up to the eighth generation. The profiles from these simulations show a minimum density for high generation numbers. The monomers corresponding to the last generation are shown at any distance from the center, indicating extensive chain back folding. Also, the different dendrons (or structures contained in a given arm of the first generation) are segregated. Carl

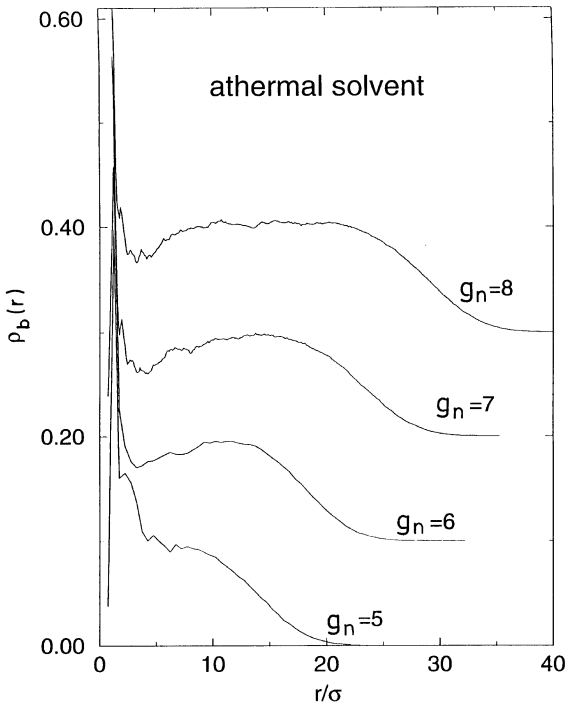

Fig. 24. Bead density profiles in an EV dendrimer with different generation numbers. The curves for g_n=6, 7, and 8 are shifted up by 0.1, 0.2 and 0.3 in the vertical axis. Reprinted with permission from [230]. Copyright (1996) American Chemical Society

[228] employed the Pivot algorithm for a freely-rotating model of Beads and Rods including a hard-spheres potential with several values of the diameter (the value zero corresponds to an ideal chain). He found a mean size $R_g \approx N^{0.25-0.34}$, depending on the bead diameter. Their asphericity values show that the molecules are prolate ellipsoids through all generations. Chen and Cui [229] used a similar algorithm and model, and they found agreement with the profiles obtained by Mansfield and Klushin. Their results for the mean size can be expressed in terms of the total number of units, the generation number, and the length of spacers as $R_g \approx N^{2\nu-1}(g_n n_S)^{1-\nu}$.

Murat and Grest [230] have performed a BD simulation of dendrimers whose beads interact through an LJ potential. Then they have considered different solvent qualities. Including data corresponding to different generations they found $R_g \approx N^{0.3}$ for all the solvent conditions, which suggest a compact globular structure (exponent 1/3). Recent experimental data of poly(amidoamine) dendrimers [231] seem to follow this power-law for the hydrodynamic radius in most solvents, except for the highest generation number. In the simulations of Grest and Murat, the amplitudes of the power-law depend on the solvent condition, as the

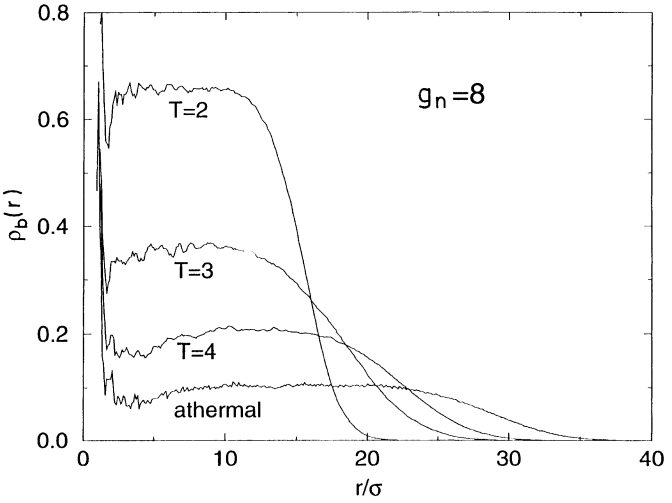

Fig. 25. Bead density profiles in an EV dendrimer with g_n=8 at different temperatures (in units of ε/k_B). Reprinted with permission from [230]. Copyright (1996) American Chemical Society

size decreases for decreasing temperatures. The bead profiles show a sharp decrease from the center, followed by a minimum and a plateau of constant density, when the generation number is higher than 5 (Fig. 24). The density in this plateau does not depend on the generation number. Finally there is a gradual decrease of the density in the outer zone. Narrower plateau regions with higher densities are found for poorer solvents (see Fig. 25). Monomers belonging to the first four generations are localized, but the density is almost constant within the chain for beads corresponding to the sixth or higher generations. Segregation of dendrons is also observed. It decreases for poorer solvent or for higher numbers of generations due to the global increase of the bead density. The internal dynamics of the dendrimer was also analyzed through these simulations. They calculated the time-correlation function of the squared global size. The relaxation times are higher for better solvent conditions and they also seem to increase with increasing number of generations, except at low temperatures. However, this dependence is noisy, perhaps due to the presence of multiple slow disentanglement processes.

Numerical calculations inspired in the ZK method for stars have also been applied for the description of the dynamics of model dendrimers. La Ferla [232] used a freely-rotating model, including a topology-dependence stiffness parameter and preaveraged HI. With this model, he obtained a complex analytical expression for the mean size. Cai and Chen [233] used a Gaussian model without HI and performed a detailed analysis of the relaxation motions. They investigated the diffusion of the center of mass, the relaxation of the center of mass position relative to the core monomer, and also the rotational and internal modes.

They obtained an approximate linear dependence of the intrinsic viscosity with the generation number that, for Gaussian dendrimers without bead overlapping, means a logarithmic dependence with the total number of monomer units. A similar description has been employed for tree-like comb structures [234] showing a power-law of the main relaxation time with chain length whose exponent is the generation number. Then this relaxation time obviously diverges for polymer networks.

4.5 Adsorbed Branched Polymers

According to the generalization of the scaling theory to adsorbed chains [235], the mean size of center-adsorbed stars should depend on the number of units in a way similar to that of free stars with the same functionality. The Ohno and Binder [132] two-dimensional simulations through the MC enrichment algorithm also consider this type of systems, and they have confirmed this point. In a d dimensional space the prediction for the mean size of the adsorbed chain is

$$R_g \approx N_b^{\nu} f^{(1-\nu)/(d-1)} \tag{66}$$

The MC data are in good agreement with this prediction, giving exponents consistent with the value 3/4 corresponding to the critical exponent ν for d=2.

The scaling theory also describes the behavior of the root-mean quadratic end-to-center and bead-center distances in terms of power laws for low values of these distances. Shida et al. [236] have carried out MC simulations of stars with different numbers of arms in three dimensions that are center-adsorbed on a repulsive surface, performing a detailed analysis of these functions. Thus, the distribution functions for the center-to-end parallel and perpendicular to the surface distances, r_s and r_z, were analyzed. For small distances, the results are compatible with the theoretical description of scaling and RG theory in terms of a power law [27, 46]. The logarithmic plot of the decreasing bead density vs r_z shows a clearly defined slope for low r_z, whose value is in good agreement with the theoretical result, $(1/\nu)-d \cong -4/3$ for d=3. However, a similar plot of the distribution profile vs r_S exhibits a strong curvature for small values of r_S. Fits of the intermediate straight regions give slopes that are then compared with the theoretical value, $-d+\lambda(f)$. The data of $\lambda(f)$ obtained in this manner seem to slowly converge to the known limit for $f\to\infty$, $\lambda(f)=1/\nu \cong 5/3$.

Star polymers in a good solvent grafted by one arm on a surface have been investigated through an SCF analysis by Irvine et al. [237]. The chains exhibit significant stretching of the tethering arm which gives rise to a dense region with a peak in the bead density profile, followed by a monotone decrease with the distance from the surface.

Acknowlegments. This work was supported by Grant PB/95–0385 from the DGICYT (Spain). Figs. 6, 16 and 20 were prepared by Dr. Antonio Rey and Dr. Luis A. Molina.

5 References

1. McGrath JE (ed) (1981) Anionic polymerization: kinetics, mechanism and synthesis, vol 166. American Chemical Society, Washington
2. Grest GS, Fetters LJ, Huang JS, Richter D (1996) Adv Chem Phys 94:67
3. Milner ST (1991) Science 251:905
4. Szleifer I, Carignano MA (1996) Adv Chem Phys 94:165
5. Kosmas MK, Gaunt DS, Whittington SG (1989) J Phys A Math Gen 22:5109
6. Tomalia DA (1994) Adv Mater 6:529
7. Service RF (1995) Science 267:458
8. Burchard W (1983) Adv Polym Sci 48:1
9. Grest GS, Murat M (1994) In: Binder K (ed) Monte Carlo and molecular dynamics simulations in polymer science. Clarendon, Oxford
10. Flory PJ (1969) Statistical mechanics of chain molecules. Wiley, New York
11. Daoud M, Cotton JP (1982) J Phys 43:531
12. Rouse PE (1953) J Chem Phys 21:1272
13. Zimm BH (1956) J Chem Phys 24:269
14. Bicerano J (ed) (1989) Molecular level calculations of the structures and properties of non-crystalline polymers. Dekker, New York
15. Yamakawa H (1971) Modern theory of polymer solutions. Harper and Row, New York
16. de Gennes P-G (1979) Scaling concepts in polymer physics. Cornell Univ, Ithaca
17. Catlow CRA, Parker SC, Allen MP (eds) (1990) Computer simulation of fluids, polymers and solids, vol 293, NATO ASI Series C. Kluwer, Dordrecht
18. Baumgärtner A (1984) Annu Rev Phys Chem 35:419
19. Allen MP, Tildesley DJ (1987) Computer simulations in liquids. Clarendon, Oxford
20. Flory PJ (1953) Principles of polymer chemistry. Cornell, New York
21. Doi M, Edwards SF (1986) The theory of polymer dynamics. Clarendon, Oxford
22. Domb C, Barrett AJ (1976) Polymer 17:179
23. Freed KF (1987) Renormalization group theory of macromolecules. Wiley, New York
24. Williams C, Brochard F, Frisch HL (1981) Annu Rev Phys Chem 32:433
25. di Marzio EA, Guttman CM (1989) J Phys Chem 93:7004
26. des Cloizeaux J, Jannink G (1990) Polymers in solution: their modelling and structure. Clarendon, Oxford
27. Ohno K, Binder K (1991) J Chem Phys 95:5444
28. Alexander S (1977) J Phys Paris 38:983
29. Auroy P, Auvray L, Léger L (1991) Phys Rev Lett 66:719
30. Dai L, Toprakcioglu C, Hadziioannou G (1995) Macromolecules 28:5512
31. Halperin A (1988) J Phys Paris 49:547
32. Dan N, Tirrell M (1992) Macromolecules 25:2890
33. Wijmans CM, Zhulina EB (1993) Macromolecules 26:7214
34. Skvortsov AM, Pavlushkov IV, Gorbunov AA (1988) Polym Sci USSR 30:487
35. Milner ST, Witten TA, Cates ME (1989) Macromolecules 22:853
36. Field JB, Toprakcioglu, C, Ball RC, Stanley HB, Dai L, Barford W, Penfold J, Smith G, Hamilton W (1992) Macromolecules 25:434
37. Shim DFK, Cates ME (1989) J Phys Paris 50:3535
38. Zhulina EB, Borisov OV, Pryamitsyn VA, Birshtein TM (1991) Macromolecules 24:140
39. de Gennes P-G, Hervet H (1983) J Phys Lett Fr 44:L351
40. Boris D, Rubinstein M (1996) Macromolecules 29:7251
41. Biswas P, Cherayil BJ (1994) J Chem Phys 100:3201
42. Miyake A, Freed KF (1984) Macromolecules 17:678
43. Douglas JF, Freed KF (1984) Macromolecules 17:2344
44. Vlahos CH, Kosmas MK (1984) Polymer 25:1607

45. Ohno K, Binder K (1988) J Phys Paris 49:1329
46. Ohno K, Binder K (1991) J Chem Phys 95:5459
47. Zimm BH, Stockmayer WH (1949) J Chem Phys 17:1301
48. Kurata M, Fukatsu M (1964) J Chem Phys 41:2934
49. Douglas JF, Roovers J, Freed KF (1990) Macromolecules 23:4168
50. Croxton CA (1988) Macromolecules 21:2269
51. Roovers J, Zhou L-L, Toporowski PM, van de Zwan M, Iatrou H, Hadjachristidis N (1993) Macromolecules 26:4324
52. Ganazzoli F, Allegra G (1990) Macromolecules 23:262
53. Ganazzoli F, Fontelos MA, Allegra G (1993) Polymer 34:2615
54. Raos G, Allegra G, Ganazzoli F (1994) J Chem Phys 100:7804
55. Guenza M, Mormino M, Perico A (1991) Macromolecules 24:6168
56. Solc K (1971) J Chem Phys 55:335
57. Wei G, Eichinger BE (1990) J Chem Phys 93:1430
58. Wei G (1997) Macromolecules 30:2130
59. Diehl HW, Eisenriegler E (1989) J Phys A 22:L87
60. Benoit H (1953) J Polym Sci 11:507
61 Burchard W (1977) Macromolecules 10:919
62. Horton JC, Squires GL, Boothroyd AT, Fetters LJ, Rennie AR, Glinka CJ, Robinson RA (1989) Macromolecules 22:681
63. Boothroyd AT, Squires GL, Fetters LJ, Rennie AR, Horton JC, de Vallêra AMBG (1989) Macromolecules 22:3130
64. Ganazzoli F, Fontelos MA, Allegra G (1991) Polymer 32:170
65. Huber K, Burchard W, Bantle S, Fetters LJ (1987) Polymer 28:1997
66. Alessandrini JL, Carignano MA (1992) Macromolecules 25:1157
67. Willner L, Jucknischke O, Richter D, Roovers J, Zhou L-L, Toporowski PM, Fetters LJ, Huang JS, Lin MY, Hadjichristidis N (1994) Macromolecules 27:3821
68. Richter D, Farago B, Huang JS, Fetters LJ, Ewen B (1989) Macromolecules 22:468
69. Douglas JF, Freed KF (1984) Macromolecules 17:1854
70. Grayce CJ, Schweizer KS (1995) Macromolecules 28:7461
71. Kirkwood JG, Riseman J (1948) J Chem Phys 16:565
72. Oseen CW (1927) Hydrodynamik. Akademische Verlagsgesellschaft, Leipzig
73. Horta A, Fixman M (1968) J Amer Chem Soc 90:3048
74. Osaki K (1972) Macromolecules 5:141
75. Kirkwood JG (1954) J Polym Sci 12:1
76. Burchard W, Schmidt M, Stockmayer WH (1980) Macromolecules 13:1265
77. Freed KF, Wang S-Q, Roovers J, Douglas JF (1988) Macromolecules 21:2219
78. García de la Torre J, Bloomfield VA (1981) Q Rev Biophys 14:81
79. Schmidt M, Burchard W (1981) Macromolecules 14:210
80. Miyaki Y, Einaga Y, Fujita H, Fukuda M (1980) Macromolecules 13:588
81. Stockmayer WH, Fixman M (1953) Ann N Y Acad Sci 57:334
82. Ptitsyn OB (1959) Zh Tekhn Fiz 29:75
83. Zimm BH, Kilb RW (1959) J Polym Sci 37:19
84. Prats R, Pla J, Freire JJ (1983) Macromolecules 16:1701
85. Garcia de la Torre J, Lopez MC, Tirado MM, Freire JJ (1983) Macromolecules 16:1221
86. Burchard W, Schmidt M, Stockmayer WH (1980) Macromolecules 13:580
87. Ganazzoli F, Allegra G, Colombo E, de Viti M (1995) Macromolecules 28:1076
88. Guenza M, Perico A (1993) Macromolecules 26:4196
89. Rey A, Freire JJ (1996) J Chem Phys 104:758
90. Zimm BH (1980) Macromolecules 13:592
91. Sammler RL, Schrag JL (1989) Macromolecules 22:3435
92. Ganazzoli F (1997) J Chem Phys 106:8913
93. Öttinger HC (1990) Phys Rev A 41:4413
94. Schaub B (1990) Z Phys B 81:291

95. Boese D, Kremer F, Fetters LJ (1990) Macromolecules 23:1826
96. Brochard-Wyart F, Ajdari A, Leibler L, Rubinstein M, Viovy JL (1994) Macromolecules 27:803
97. Shull KR, Kramer EJ, Fetters LJ (1990) Nature 345:790
98. Ngai KL, Roland CM (1997) J Polym Sci Polym Phys Ed 35:2503
99. Bartels CR, Crist B, Fetter LJ, Graessley WW (1986) Macromolecules 19:785
100. Wall FT, Erpenbeck JJ (1959) J Chem Phys 30:634
101. Metropolis N, Rosenbluth AW, Rosenbluth MN, Teller AH, Teller E (1953) J Chem Phys 21:1087
102. Siepmann JI, Frenkel D (1992) Molec Phys 75:59
103. Verdier PH, Stockmayer WH (1962) J Chem Phys 36:227
104. Boots H, Deutch JM (1977) J Chem Phys 67:4608
105. Pakula T (1987) Macromolecules 20:679
106. Madras N, Sokal AD (1988) J Stat Phys 50:109
107. Carmesin I, Kremer K (1988) Macromolecules 21:2819
108. Baumgärtner A (1980) J Chem Phys 72:871
109. Freire J, Pla J, Rey A, Prats R (1986) Macromolecules 19:452; ibid 19:457
110. Rey A, Freire JJ, Garcia de la Torre J (1987) Macromolecules 20:2385
111. Wilemski G, Tanaka G (1981) Macromolecules 14:1531
112. Fixman M (1983) J Chem Phys 78:1588
113. Fixman M (1986) J Chem Phys 84:4080
114. Freire JJ, Rey A (1990) Comput Phys Commun 61:297
115. Lax M, Brender C (1977) J Chem Phys 67:1785
116. Kranbuehl DE, Verdier PH (1984) Macromolecules 17:749
117. Ryckaert JP, Ciccotti G, Berendsen HJC (1977) J Comput Phys 23:327
118. Dünweg B, Kremer K (1993) J Chem Phys 99:6983
119. Ermak DL, McCammon JA (1978) J Chem Phys 69:1352
120. Rey A, Freire JJ (1992) Polymer 33:3477
121. Mazur J, McCrackin FL (1977) Macromolecules 10:326
122. McCrackin FL, Mazur J (1981) Macromolecules 14:1214
123. Kolinski A, Sikorski A (1982) J Polym Sci Polym Chem 20:3147
124. Batoulis J, Kremer K (1988) Europhys Lett 7:683
125. Rey A, Freire JJ, Garcia de la Torre J (1987) 20:342
126. Zimm BH (1984) Macromolecules 17:2441
127. Whittington SG, Lipson JE, Wilkinson MK, Gaunt DS (1986) Macromolecules 19:1241
128 Barrett AJ, Tremain DL (1987) Macromolecules 20:1687
129. Zifferer G (1990) Makromol Chem Macromol Chem Phys 191:2717
130. Ohno K (1994) Macromol Symp 81:121
131. Grest GS (1994) Macromolecules 27:3493
132. Ohno K, Binder K (1991) J Stat Phys 64:781
133. Batoulis J, Kremer K (1989) Macromolecules 22:4277
134. Bishop M, Clarke JHR (1989) J Chem Phys 90:6647
135. Bishop M, Smith W (1991) J Chem Phys 95:3804
136. Bishop M, Clarke JHR, Rey A, Freire JJ (1991) J Chem Phys 94:4009
137. Zifferer G (1991) Makromol Chem 192:1555
138. Zifferer G (1994) Macromol Theory Simul 3:163
139. Zifferer G (1995) J Chem Phys 102:3720
140 Forni A, Ganazzoli F, Vacatello M (1997) Macromolecules 30:4737
141. Kajiwara K, Burchard W (1982) Macromolecules 15:660
142. Mattice WL (1984) Macromolecules 17:415
143. Rey A, Freire JJ, Bishop M, Clarke JHR (1992) Macromolecules 25:1311
144. Bruns W, Carl W (1991) J Chem Phys 24:209
145. Ohno K, Shida K, Kimura M, Kawazoe Y (1996) Macromolecules 29:2269
146. Rubio A, Freire JJ (1996) Macromolecules 29:6946

147. Okumoto M, Nakamura Y, Norisuye T, Teramoto A (1998) Macromolecules 31:1615
148. Yethiraj A, Hall CK (1991) J Chem Phys 94:3943
149. Escobedo FA, de Pablo JJ (1996) J Chem Phys 104:4788
150. Falsafi A, Madden WG (1994) Macromolecules 27:3094
151. Bawendi MG, Freed KF (1986) J Chem Phys 85:3007
152. Su S-J, Kovac J (1992) J Phys Chem 96:3931
153. Smit B, van der Put A, Peters CJ, de Swann Arons J, Michels JPJ (1988) J Chem Phys 88:3372
154. Molina LA (1998) Ph D thesis, Universidad Complutense, Madrid
155. Pakula T, Geyler S, Edling T, Boese D (1996) Rheol Acta 35:631
156. Huber K, Burchard W, Bantle S, Fetters LJ (1987) Polymer 28:1990
157. Grest GS, Kremer K, Witten TA (1987) Macromolecules 20:1376
158. Forni A, Ganazzoli F, Vacatello M (1996) Macromolecules 29:2994
159. Bishop M, Clarke JHR, Freire JJ (1995) J Chem Phys 102:5094
160. Witten TA, Schäfer L (1981) J Chem Phys 74:2582
161. Molina LA, Rey A, Freire JJ (1998) Comput Theor Polym Sci 17:243
162. Wilkinson MK, Gaunt DS, Lipson JEG, Whittington SG (1988) Macromolecules 21:1818
163. Rey A, Freire JJ, Garcia de la Torre J (1990) Macromolecules 23:3948
164. Freire JJ, Rey A, Bishop M, Clarke JHR (1991) Macromolecules 24:6494
165. Rey A, Freire JJ, García de la Torre J (1990) J Chem Phys 92:6278
166. Milner ST, McLeish TCB (1997) Macromolecules 30:2159
167. Fixman M, Kovac J (1974) J Chem Phys 61:4950
168. Rey A, Freire JJ (1995) J Chem Phys 102:6900
169. Grest GS, Kremer K, Milner ST, Witten TA (1989) Macromolecules 22:1904
170. Ohno K, Schulz M, Binder K, Frish HC (1994) J Chem Phys 101:4452
171. Su S-J, Denny MS, Kovac J (1991) Macromolecules 24:917
172. Sikorski A, Romiszowski P (1996) J Chem Phys 104, 8703
173. Sikorsky A (1993) Makromol Chem Theory Sim 2:309
174. Needs RJ, Edwards SF (1983) Macromolecules 16:1492
175. Sikorski A, Kolinski A, Skolnick J (1994) Macromol Theory Sim 3:715
176. Fredrickson GH, Bates FS (1996) Ann Rev Matt Sci 26:501
177. Floudas G, Pispas S, Hadjichristidis N, Pakula T, Erukhimovich I (1996) Macromolecules 29:4142
178. Floudas G, Hadjichristidis N, Iatrou H, Pakula T, Fischer EW (1994) Macromolecules 27:7735
179. Beyer FL, Gido SP, Poulos Y, Avgeropoulos A, Hadjichristidis N (1997) Macromolecules 30:2373
180. Vlahos C, Tselikas Y, Hadjichristidis N, Roovers J, Rey A, Freire J (1996) Macromolecules 29:5599
181. Lipson JEG, Gaunt DS, Wilkinson MK, Whittington SG (1987) Macromolecules 20:186
182. Vlahos CH, Kosmas MK (1987) J Phys A Math Gen 20:1471
183. Bishop M, Saltiel CJ (1993) J Chem Phys 98:1611
184. Lipson JEG (1991) Macromolecules 24:1327
185. Roovers J (1979) Polymer 20:843
186. Fredrickson GH (1993) Macromolecules 26:2825
187. Rouault Y, Borisov OV (1996) Macromolecules 29:2605
188. Saariaho M, Ikkala O, Szleifer I, Erukhimovich I, ten Brinke G (1997) J Chem Phys 107:3267
189. Murat M, Grest GS (1991) Macromolecules 24:704
190. Wintermantel M, Gerle M, Fischer K, Schmidt M, Wataoka I, Urakawa H, Kajiwara K, Tsukahara Y (1996) Macromolecules 29:978
191. Gauger A, Pakula T (1995) Macromolecules 28:190
192. Gersappe D, Harm PK, Irvine D, Balazs AC (1994) Macromolecules 27:720

193. Chakrabarti A, Toral R (1990) Macromolecules 23:2016
194. Lai P-Y, Binder K (1991) J Chem Phys 95:9288
195. Murat M, Grest GS (1989) Macromolecules 22:4054
196. Neelov IM, Binder K (1995) Macromol Theory Simul 4:119
197. Grest GS (1994) Macromolecules 27:418
198. Raphaël E, Pincus P, Fredrickson GH (1993) Macromolecules 26:1996
199. Grest GS, Murat M (1993) Macromolecules 26:3108
200. Lai P-Y, Zhulina EB (1992) J Phys II Fr 2:547
201. Clancy TC, Webber SE (1995) Macromolecules 28:2561
202. Milner ST,Witten TA, Cates ME (1989) Macromolecules 22:853
203. Lai P-Y, Zhulina EB (1992) Macromolecules 25:5201
204. Laradji M, Guo H, Zuckermann MJ (1994) Phys Rev E 49:3199
205. Toral R, Chakrabarti A (1993) Phys Rev E 47:4240
206. Wijmans CM, Zhulina EB (1993) Macromolecules 26:7214
207. Dan N, Tirrell M (1992) Macromolecules 25:2890
208. Li H, Witten TA (1994) Macromolecules 27:449
209. Carignano MA, Szleifer I (1995) J Chem Phys 102:8662
210. Lai PY, Binder K (1992) J Chem Phys 97:586
211. Zhao W, Krausch G, Rafailovich MH, Sokolov J (1994) Macromolecules 27:2933
212. Weinhold JD, Kumar SK (1994) J Chem Phys 101:4312
213. Pakula T, Zhulina EB (1991) J Chem Phys 95:4691
214. Carignano MA, Szleifer I (1994) J Chem Phys 100:3210
215. Kent MS, Lee LT, Factor BJ, Rondelez F, Smith GS (1995) J Chem Phys 103:2320
216. Murat M, Grest GS (1989) Phys Rev Lett 63:1074
217. Chakrabarti A, Nelson P, Toral R (1994) J Chem Phys 100:748
218. Toral R, Chakrabarti A, Dickman R (1994) Phys Rev E 50:343
219. Tauton HJ, Toprakcioglu C, Fetters LJ, Klein J (1990) Macromolecules 23:571
220. Ruckenstein E, Li B (1997) J Chem Phys 107:932
221. Watanabe H, Tirrell M (1993) Macromolecules 26:6455
222. Klushin LI, Skvortzov AM (1991) Macromolecules 24:1549
223. Brown G, Chakrabarti A, Marko JF (1994) Europhys Lett 25:239
224. Brown G, Chakrabarti A, Marko JF (1995) Macromolecules 28:7817
225. Naylor AM, Goddard WA, Kiefer GE, Tomalia DA (1989) J Am Chem Soc 111:2339
226. Lescanec RL, Muthukumar M (1990) Macromolecules 23:2280
227. Mansfield ML, Klushin LI (1993) Macromolecules 26:4262
228. Carl W (1996) J Chem Soc Faraday Trans 92:4151
229. Chen ZY, Cui S-M (1996) Macromolecules 29:7943
230. Murat M, Grest GS (1996) Macromolecules 29:1278
231. Stechemesser S, Eimer W (1997) Macromolecules 30:2204
232. La Ferla R (1997) J Chem Phys 106:688
233. Cai C, Chen ZY (1997) Macromolecules 30:5104
234. Schulz M, Reineker P, Möller M (1995) J Chem Phys 103:10,701
235. Ohno K (1989) Phys Rev A 40:1524
236. Shida K, Ohno K, Kimura M, Kawazoe Y (1996) J Chem Phys 105:8929
237. Irvine DJ, Mayes AM, Griffith-Cima L (1996) Macromolecules 29:6037

Received: April 1998

Solution Properties of Branched Macromolecules

Walther Burchard

Albert-Ludwigs-University of Freiburg, Insitute of Macromolecular Chemistry
D-79104 Freiburg, Germany
E-mail: burchawa@ruf.uni-freiburg.de

Dilute and semi-dilute solution properties of several classes of branched macromolecules are outlined and discussed. The dilute solution properties are needed for a control of the chemical synthesis. The molecular parameters also determine the overlap concentration which is an essential quantity for description of the semi-dilute state. This state is represented by a multi-particle, highly entangled ensemble that exhibits certain similarities to the corresponding bulk systems. Because of the rich versatility in branching the present contribution made a selection and deals specifically with the two extremes of regularly branched polymers, on the one hand, and the randomly branched macromolecules on the other. Some properties of hyperbranched chains are included, whereas the many examples of slight deviations from regularity are mentioned only in passing. The treatment of the two extremes demonstrates the complexity to be expected in the general case of less organized but non-randomly branched systems. However, it also discloses certain common features.

The dilute solution properties of branched macromolecules are governed by the higher segment density than found with linear chains. The dimensions appear to be shrunk when compared with linear chains of the same molar mass and composition. The apparent shrinking has influence also on the intrinsic viscosity and the second virial coefficient. Shrinking factors can be defined and used for a quantitative determination of the branching density, i.e., the number of branching points in a macromolecule. A broad molar mass distribution has a strong influence on these shrinking factors. Here the branching density can be determined only by size exclusion chromatography in on-line combination with light scattering and viscosity detectors. The technique and possibilities are discussed in detail.

The discussion of the semi-dilute properties remains confined mainly to the osmotic modulus which in good solvents describes the repulsive interaction among the macromolecules as a function of concentration. After scaling the concentration by the overlap concentration $c^*_{A_2} = (A_2 M_W)^{-1}$ and normalizing the osmotic modulus by the molar mass, universal master curves are obtained. These master curves differ characteristically for the various macromolecular architectures. The branched materials form curves which lie, as expected, in the range between hard spheres and flexible linear chains.

Keywords. Solution properties, Regularly branched structures, Randomly and hyperbranched polymers, Shrinking factors, Fractal dimensions, Osmotic modulus of semi-dilute solutions, Molar mass distributions, SEC/MALLS/VISC chromatography

Advances in Polymer Science, Vol.143

List of Symbols and Abbreviations

α	extent of reaction of a functional group A = probability of reaction of functional group A
M_n	number average molar mass
M_w	weight average molar mass
M_z	z-average molar mass
M_0	molar mass of the repeating unit
f	number of arms in a star macromolecule
$\langle s^2 \rangle_z$	z-average mean square radius of gyration
R_g	radius of gyration
R_T	thermodynamically effective radius
R_h	hydrodynamically effective radius
R_η	viscosity radius
A_2	second osmotic virial coefficient
A_3, A_4	higher osmotic virial coefficients
D_z	z-average translational diffusion coefficient
$[\eta]$	intrinsic viscosity
σ^2	mean square dispersion of a distribution
q	magnitude of the scattering vector
K	contrast factors in LS, SAXS and SANS
θ	scattering angle
$g_2(t)$	intensity time correlation function (TCF)
$g_1(t)$	field time correlation function (TCF)
t	delay time in TCFs

Γ	first cumulant of $g_1(t)$
$D_{app}(q,c)$	apparent diffusion coefficient
k_D	coefficient describing the concentration dependence of the mutual diffusion coefficient
C	coefficient describing the angular dependence of the $D_{app}(q)$
V	volume of a macromolecule
N_A	Avogadro's number
Φ	draining function in $[\eta]$
Ψ^*	asymptotic value of the coil interpenetration function $\Psi(z)$, where z is the thermodynamic interaction parameter
$\rho = R_g / R_h$ $V_T = R_T / R_h$ $V_{A_2\eta} = A_2 M_w / [\eta]$	} generalized ratios
$nu=(M_w/M_n)-1$	non-uniformity
R_Θ	Rayleigh ratio of scattering intensity at scattering angle Θ
$P(q)$	particle scattering factor = normalized molecular structure factor
$\varphi(r)$	segment density distribution
N_K	number of Kuhn segments
ν	exponent in the molar mass dependence of R_g
a_{A2}	exponent in the molar mass dependence of A_2
a_η	exponent in the molar mass dependence of $[\eta]$
d_f	fractal dimension of individual macromolecules
$d_{f,e}$	ensemble average fractal dimension
$w(x)$	weight fraction molar mass distribution
x	degree of polymerization
x_z, x_w, x_n	z-,weight and number averages of x
$f(x/x^*)$	cut-off function
$x^* \cong x_z$	characteristic degree of polymerization defining the cut-off function
$\varepsilon=\lvert p-p_c\rvert/p_c$	critical region within percolation theory is valid
p	occupation probability of a lattice site
p_c	critical value of p where gelation takes place
τ	exponent in the molar mass distribution
$g = \frac{R^2_{gb}}{R^2_{glin}}$	contraction factor of the radii of gyration
$g' = \frac{\eta_b}{\eta_{lin}}$	contraction factors of intrinsic viscosities
a_Φ	exponent describing the molar mass dependence of the draining function Φ
c_i^*	overlap concentration, different definitions are valid for $i=A_2$, R_g, R_h *and* $[\eta]$

π	osmotic pressure
$RT\dfrac{\partial c}{\partial \pi}$	osmotic modulus
$M_{app}(c)$	apparent molar mass
g_a	factor governing the correlation between A_3 and A_2
$\dfrac{1}{RT}\dfrac{\partial \pi}{\partial c}$	reduced concentration

1 Introduction – Why Study Dilute Solution?

Macromolecular chemistry, or more general polymer science, is commonly connected to material science, and here in turn the solid state is often meant. In fact, a typical engineer or physicist is not really interested in the solution properties but in typical materials science parameters, for instance the tensile strength, the glass transition temperature or the degree of crystallinity. Of course, a full set of data can be collected in a list, which is to be consulted when a material has to fulfill special requirements in an application. Certainly, after a while, everybody will start wondering whether all these data in the whole set of parameters are really needed, because some of them are evidently cross-correlated to each other, and furthermore, he will wonder whether all the same data have to be measured again each time when a new product comes on the market. Such suspicions arises for instance when the rubber elasticity is considered which evidently is not a unique property of natural Indian Rubber but appears to be a general feature of all macromolecules when the material is heated beyond a certain temperature.

In such cases it is reasonable to step down to the molecular level of these materials and to think of a conjecture that many of the condensed materials properties may actually be connected to the properties of the individual macromolecules. Pursuing this idea one may follow two approaches. The first consists of molecular modeling of structures on a computer and simulating the material properties of interest. Alternatively, attempts can be made to set up a rigorous basic molecular theory.

Both routes have their limitations. The basic theory of complex structures, which are encountered with macromolecules, often does not allow analytic solutions. Incisive, though reasonable, approximations have to be introduced. On the other hand, rigorous simulations can be made by means of molecular dynamics, but this technique has the limitation that only rather small and fast moving objects can be treated within a reasonable time, even with the fastest computers presently available. This minute scale gives valuable information on the *local structure* and *local dynamics,* but no reliable predictions of the macromolecular properties can be made by this technique. All other simulations have to start with some basic assumptions. These in turn are backed by results obtained from basic theories. Hence both approaches are complementary and are needed when constructing a reliable framework for macromolecules that reflects the desired relation to the materials properties.

The two approaches have been very successfully applied to *linear* and *flexible* macromolecules and have given us a deep understanding of their individual behavior and the correlation to their properties in the condensed phase. Some idealizing assumptions were still necessary to find the desired solid state properties, but as long as only weak van der Waals interactions among the chains are active, these assumptions have led to valuable *qualitative* conclusions [1–7]. *Quantitative* data were obtained by the above-mentioned computer simulations [8]. Unfortunately, the physical basis of these simulation results is often not yet well understood. To give an example, the selective permeation of gases through a membrane can reasonably well be simulated, yet no prediction has been possible by an analytical theory.

The situation becomes drastically more complex when directed, strongly attractive interactions are present, which lead to association [9–11]. Similar problems arise when branched macromolecules are to be considered. Branching and the ensuing gelation and network formation are known almost from the beginning of polymer chemistry, now about 70 years ago [1, 12, 13]. In particular the sol-gel transition has been an intriguing phenomenon, and was initially perceived as a mysterious process. The elucidation has been a matter of intense efforts in research up to the present day. A reliable and quantitative description of the gelation process is, of course, of immense importance. For instance an undesirable gelation in a batch reactor and the laborious cleaning will certainly be costly.

Traditionally, polymer research was concerned with the kinetics of macromolecule formation. A considerable simplification was achieved by Flory [1] when introducing the *extent of reaction of a functional group* that may belong to a monomer or a long chain. This extent of reaction α of a functional group is defined as the ratio of the number of reacted functionalities $[A_t]$ to the total number of reacted and non-reacted functionalities $[A_o]$:

$$\alpha = \frac{No.\ of\ reacted\ functional\ groups}{No.\ of\ all\ functional\ groups} = \frac{[A_t]}{[A_0]} \tag{1}$$

where the subscripts *t* and *o* denote the time of reaction and the starting time of reaction, respectively. Thus the extent of reaction is actually a *probability* of reaction. This concept allows the substitution of the time in kinetics by a probability parameter, and common laws of probability theory can be applied. One important outcome of this probabilistic treatment was the discovery by Stockmayer [14] of a very broad molar mass distribution for random branching processes. The type of this distribution differs fundamentally from all other molar distributions known from the polymerization kinetics of linear chains.

Already in the study of linear chain molecules it has become evident that the *shape of the molar mass distribution* and its width provide a valuable guide to the mechanism of chain formation. Best known are the *most probable* (or Schulz-Flory) distribution and the narrow *Poisson* distribution. The former is often

found in free radical polymerization and linear polycondensation and has a rather broad width (M_w/M_n=2) that does not change with the molar mass. The other distribution is characteristic of living polymerization and has a width that narrows with increasing chain length ($M_w/M_n \cong 1+M_o/M_n$, where M_o is the molar mass of the monomer unit) [15]. The type and width of the molar mass distribution remain extremely important also for branched macromolecules and allow a classification of possible branched molecular architectures. On random branching the polydispersity index M_w/M_n increases almost linearly with the M_w ($M_w/M_n \propto M_w$) [1, 14], but in hyperbranching processes it increases only with the root of the weight average molar mass ($M_w/M_n \propto M_w^{1/2}$) [1, 16, 17].

A broad distribution has undoubtedly a marked influence on the properties of the materials. As a simplifying rule the effects of branching are increasingly counter-balanced by an increasing polydispersity. In some cases the effect can become so pronounced that the branching effects are fully masked by the huge polydispersity. Examples will be given later in this contribution. Because of this influence the immense effort invested in determining these size distributions becomes understandable. However, from the behavior of linear chains we know that it is the molecular structure and the required space which determine the properties in solution as well as in the condensed state. It is not in the first place the molar mass of the macromolecule. This fact becomes intriguing and very complex with branched macromolecules. Grotesque errors are introduced if only standard size exclusion chromatography (SEC) is applied and a calibration curve, obtained with linear polystyrene, is used. This error occurs because the separation in a SEC column proceeds according to the hydrodynamic volume and not according to the molar mass. A linear chain and a branched macromolecule of the same molar mass have however different hydrodynamic volumes.

At this point the following general remark may be appropriate and has to be remembered as an urgent warning. In the last ten years we have gained a comprehensive understanding of the behavior of linear chain molecules. We know that the laws, which govern this behavior, are quite general and in some respect universal. Because of this universality we intuitively tend to believe that the same laws will also hold for all non-linear molecular architectures. This, however, is not the case and it is the basis of many misinterpretations. Branched structures are certainly built up of linear chain segments, but nonetheless they represent new topological classes which differ basically from linear chains. As a new parameter the so called *fractal dimension* d_f has been successfully introduced by which a desirable classification became possible.

The final goal of all attempts is a description, and hopefully also a reliable prediction, of the macromolecular properties in bulk and in moderately concentrated solutions. It may be useful to recall that even the polymerization processes are conducted either in the melt or in fairly concentrated solutions. Under such conditions a complex interplay between the structures of the individual macromolecules with strong mutual interactions takes place. In order to disentangle the complexity it will be helpful to derive at first a precise picture of the structure of *individual* macromolecules. Their properties can most adequately be studied

in the highly diluted regime. Here the distance between macromolecules can be made much larger than the molecular size diameter. Interparticle interactions still have some influence on the measurable parameters, but the concentration is then already sufficiently low that a simultaneous interaction of more than two particles can be considered as negligible. Only the effect of the second osmotic virial coefficient A_2 has to be taken into account.

The second virial coefficient is not a universal quantity but depends on the primary chemical structure and the resulting topology of their architecture. It also depends on the conformation of the macromolecules in solution. However, once these individual (i.e., non-universal) characteristics are known, the data can be used as scaling parameters for the description of semidilute solutions. Such scaling has been very successful in the past with flexible linear chains [4, 18]. It also leads for branched macromolecules to a number of universality classes which are related to the various topological classes [9–11, 19]. These conclusions will be outlined in the section on semidilute solutions.

2
Topological Structures

The set of all phenotypes of molecular branching is evidently very complex; any unit on a linear chain can in principle be a branching point for another chain that again can branch off at a more or less defined position. For a better understanding of the effects of branching it is advantageous to start the study with simple models and to proceed step by step to more complex topologies. This approach does not represent the historical development. Actually for historical reasons the study of branched polymers started with the random polycondensation of *f*-functional monomer units, which might be considered a topological system of highest complexity. Conceptionally the understanding of regular structures appears to be much easier, though the chemical realization has offered great difficulties. Therefore, the presentation of branched models may be opened with some regular structures

2.1
Regularly Branched Systems

2.1.1
Regular Star Molecules

The simplest structure is that of *f* linear chains of exactly the same length attached to an *f*-functional central unit – see Fig. 1

In this model the linear chains become the rays of a star molecule. The rays, consisting of m repeating units, can be considered stiff rods, but in most cases they will be flexible and can be described in a first approximation by Gaussian chain statistics. A star molecule has only one branching unit among $f \times m$ units which belong to linear chains. Their properties can be expected to show a close

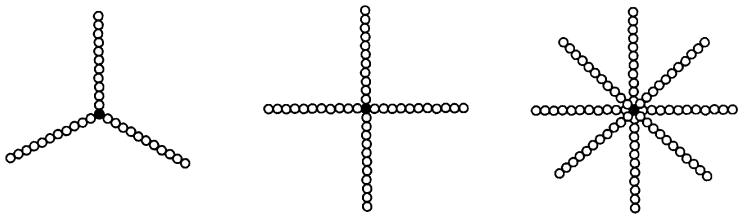

Fig. 1. Regular star macromolecules with f=3, 4, and 8 arms of identical length. The arms or rays can consist of rather stiff chains, but are in most cases flexible chains. The global structure is determined by the overall shape of the whole macromolecule; the internal structure is indicated by a domain that is much smaller than the overall dimension but still larger than a few Kuhn segments

similarity to linear chains. This indeed has been observed when studying the internal and local structure. The global structure, however, deviates considerably from that of linear chains and is determined by tethering the f chains with their end at the branching center [20–37].

A distinction between global and internal or local structures will be repeatedly made in this contribution. The discrimination proved to be helpful when interpreting the properties of branched molecules. It is here defined more explicitly. With global the behavior of a particle is understood as it appears to an observer from a longer distance. Since in solution the particles are in continuous rotational and translational motion they appear on average to have a spherical shape. Thus a mean radius of an equivalent sphere and the domain of interaction among such spheres are the main global parameters. If techniques were available to measure additionally deviations from this equivalent sphere, the shape, i.e., the outer contour of the particle, is also a global structure parameter.

On the other hand, scattering techniques and all types of spectroscopy allow us to get information on the internal structure of the particle. These questions will be considered in a forthcoming review.

2.1.2 *Regular Comb Molecules*

The next higher topological complexities are obtained with flexible regular comb molecules and with so called dendrimers. Regular comb molecules (see Fig. 2) consist of a linear flexible chain of defined length, that forms the backbone, and f flexible side chains of uniform length which are grafted at regular distances onto this backbone.

Again, this structure resembles very much a linear chain, when the side chains are much shorter than the backbone. The other limit is that of a short backbone and long side chains grafted on the backbone in the densest way. This structure will approach the behavior of star molecules. It should be mentioned that a realization of complete regularity will scarcely be possible. It is almost im-

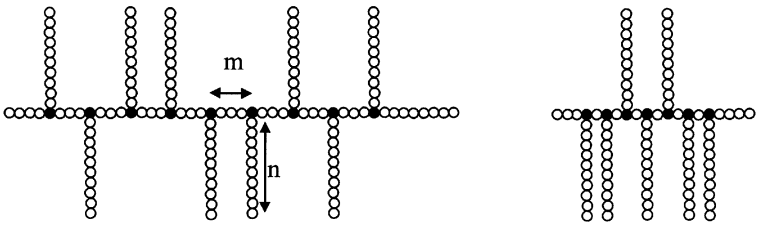

Fig. 2. Two limiting cases of a regular comb molecule. The flexible chain sections between two branching points may consist of m monomer units while the *f* flexible side chains have a length of *n* monomer units. The one structure (*short side chains*) resembles a substituted linear chain, the second one (*short backbone*) has similarity to star molecules

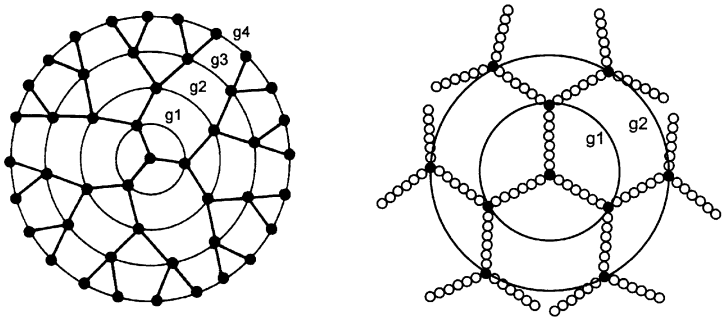

Fig. 3. Dendrimers. The branching units can be directly attached to each other in generations or shells (*left*), but can also be connected via flexible spacers of identical length (*right*)

possible to prepare a comb with a uniform backbone. Imperfections in the spacing of the side chains will often be the result of the chemical synthesis.

2.1.3 *Dendrimers*

Dendrimers, in the generalized form, are obtained when each ray in a star molecule is terminated by an *f*-functional branching unit from which rays of the same length are emanating. A next generation is created when these *f*-1 rays are again terminated by the branching units from which again rays originate etc. Figure 3 shows examples.

If the rays possess ideal flexibility to allow application of Gaussian statistics, the resultant structure will resemble a soft sphere. This was the reason why the present author introduced the soft sphere model [38]. This model reduces to dendrimers in the narrow sense when no spacer chains between the branching units are present.

In recent years the chemistry of preparing dendrimers has become very successful although painfully cumbersome and time consuming [39–47]. This is not the only drawback. Because of space filling it has not been possible to prepare more than five generations. Either the reaction to a higher generation stops completely or, what happens in practice, the outermost shells will develop imperfections. As in the case of comb molecules, corrections have to be made to the properties of this idealized structure.

2.2 Statistical Branching

In most cases no special care is taken in chemistry to achieve regularity: *f*-functional and bifunctional monomer units are mostly just mixed together and left for reaction without any constraints.

2.2.1 *Randomly Branched Systems*

The simplest assumption is that all functional groups have the same reactivity independent of whether they are connected to a monomer or to a macromolecular species. Furthermore, the possibility of ring formation, i.e., the reaction between functional groups belonging to the same macromolecule, has been excluded [1, 13, 14, 48]. Although the visual perception now becomes blurred such fully random systems can be treated analytically by theories of random statistics. Clearly it represents a mean field theory. The whole statistics is based on the extent of reaction α as defined in Eq. (1). The first important conclusion was drawn by Flory [2] who predicted a critical point where gelation takes place. Another important step was the derivation of the molar mass distribution by Stockmayer [14] who showed that this distribution has a hitherto not anticipated extremely broad width. Further progress was made later in the calculation of conformational properties [10, 49–52]. Here the adequate method of representation of the average structure is that of rooted trees. Figure 4 shows three examples of such rooted trees [53]. The treatment of random branching is often called the Flory-Stockmayer (FS) theory. In percolation theory [7] the mean field approach is equivalent to percolation on a Bethe lattice. More details will be given below.

2.2.2 *Deviations from Randomness*

No real system is fully random. Random systems are over-simplified ideal models similar to those of strictly regular structures. Most relevant is the effect of the finite volume of the monomer units which implies that two units can approach each other only up to their diameter. Thus a certain volume is forbidden or excluded for the individual repeating units. For hard sphere monomers this excluded volume is just eight times the monomer volume. This excluded volume

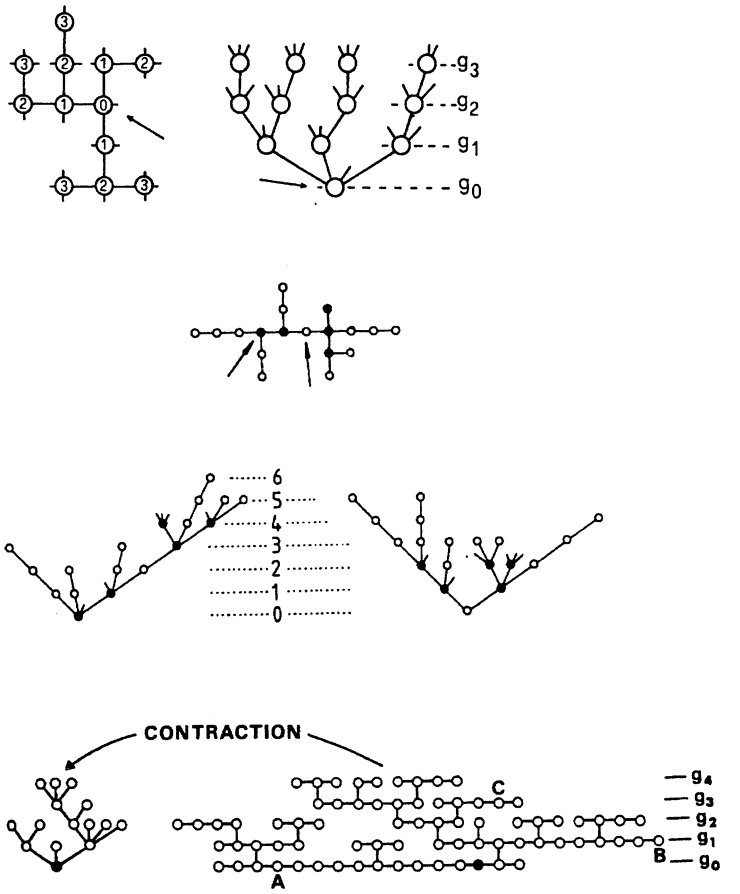

Fig. 4a–c. Rooted trees: **a** for a tri-functional random homo-polycondensation; **b** for the two trees in the copolymerisation with bi functional monomers; **c** for the vulcanization of linear chains. The rooted tree representation brings a clear ordering of the units into generations. Hence the degree of polymerization can be obtained by first deriving a general expression on the population of monomer units in the n-th generation followed by summing over all generations

causes a swelling of the branched structures that significantly perturbs the Gaussian statistics. It can also cause a change in the expected topological architecture, because in a densely branched system the reaction of the various functional groups on a monomer will be influenced by the condition of how many of the f-functional groups had already reacted. This interdependence was called a negative substitution effect by Gordon and Scantlebury [54]. (A positive substitution effect may be observed when there is a local stimulating cooperative reaction, but these cases are rare and mostly less effective than the always existent volume

exclusion.) Clearly these reactions can no longer be adequately described by a mean field approximation. Only crude approximations are at present available to treat this problem [1, 55, 56]

2.2.3 *Hyperbranching*

There exists, however, one special group of branched structures that, in spite of an incisive constraint imposed onto the reaction, can be well described by a mean field approach. This case occurs when a monomer bears two types of functional groups [1, 16, 51], say *A* and *B*, where only group *A* can react with one of the (*f*-1) *B* groups of another monomer unit. Figure 5 shows as examples two cases of an AB_2 polycondensation.

The chemical constraint reduces the number of possible reactions considerably, and consequently it leads to a much narrower molar mass distribution. Furthermore, the extent of reaction α of the *A*-group can cover all values from zero to unity, but the extent of reaction β of the equally reactive *B*-groups cannot become larger than $\beta=\alpha/(f\text{-}1)$. One important consequence of this strict constraint is that gelation can never occur [1, 13]. A much higher branching density than by random polycondensation can be achieved. For this reason one nowadays speaks of hyperbranching.

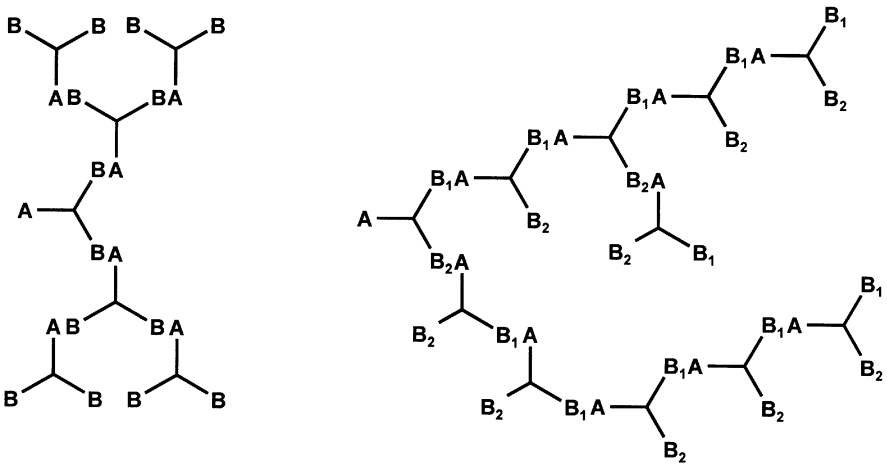

Fig. 5. Polycondensation of $A<\begin{matrix}B\\B\end{matrix}$ and $A<\begin{matrix}B_1\\B_2\end{matrix}$ monomer units (hyperbranching). Much-longer linear chain sections between branching points occur on average when B_2 has a lower reactivity than B_1, and a linear chain is obtained when the reaction of B_2 can be fully suppressed. The structures are called hyperbranched, since due to the chemical constraint a very high branching density becomes possible without gelation

In spite of the many possible structures in branching processes, several similarities, which are specific for branching, can be observed. These similarities are most clearly recognized when the two extremes of strictly regular star molecules and randomly branched macromolecules are compared. The detailed outline in the following sections focuses for this reason mainly on these two structures. The many real systems will be discussed in the light of the knowledge gathered from these two structures.

3
Global Properties of General Macromolecular Architectures in Solution

3.1
Experimental Techniques

The experimental techniques for the study of conformational branched properties in solution are the same as used for linear chains. These are, in particular, static and dynamic light scattering, small angle X-ray (SAXS) and small angle neutron (SANS) scattering methods, and common capillary viscometry. These methods are supported by osmotic pressure measurements and, nowadays extensively applied, size exclusion chromatography (SEC) in on-line combination with several detectors. These measurements result in a list of molecular parameters which are given in Table 1.

As was already mentioned we tend to judge the results on the basis of our knowledge of linear chains. This, however, can be very misleading, and for this reason it will be useful to go back to the basic equations and to recall how these molecular parameters are obtained. Everybody who is familiar with these relationships may omit this section and proceed immediately to the discussion of the results. Whenever questions occur, the basic relationships may be consulted.

All investigations have to start with the determination of the global properties of the macromolecules. In fact, the combination of these data already gives a certain insight in the topological structure and the resulting consequences for the properties. A far more detailed knowledge is obtained when, in addition, the internal structure is studied. Both the experimental techniques and the theoretical

Table 1. Molecular parameters and techniques for their determination

Parameter	Symbol	Technique
molar mass	M_w	static LS
radius of gyration	$R_g \equiv [<S^2>_z]^{1/2}$	static LS
second virial coefficient	A_2	static LS
translation diffusion coefficient	D_z	dynamic LS
intrinsic viscosity	$[\eta]$	viscometry

The indices *w* +and *z* denote the weight and *z*-averages, respectively

relationships needed for such a study are far more complex. For this reason it is advisable to discuss both aspects separately.

The main global parameters are the molar mass and the radius of an equivalent sphere. Because of the often observed large molar mass distribution one has to distinguish between the number and the weight average molar masses M_n and M_w. The former can be measured fairly quickly with dynamic osmometers. In spite of limitations in sensitivity, measurement of the osmotic pressure still provides us with valuable parameters. Most common is the determination of the weight average by means of static light scattering. The ratio M_w/M_n is related to the mean square dispersion, σ^2, (which describes the width of a distribution) by the relationship

$$\frac{M_w}{M_n} - 1 = \frac{\sigma^2}{M_n^2} \tag{2}$$

The next step consists of the determination of the size of the macromolecules in space. Two equivalent sphere radii can be measured directly by means of static and dynamic LS. Another one can be determined from a combination of the molar mass and the second virial coefficient A_2. Similarly, an equivalent sphere radius is obtained from a combination of the molar mass with the intrinsic viscosity. This is outlined in the following sections.

3.2 Special Relationships

3.2.1 *Static Light Scattering*

A relationship for evaluation of static light scattering (LS) data from dilute solutions is given by

$$\frac{K_c}{R_\theta} = \frac{1}{M_w}\left[\left(1 + \frac{1}{3} < S^2 >_z q^2\right) + 2A_2 M_w c\right] \tag{3}$$

$$(qR_g < 2; \qquad A_2 M_w c < 0.5) \tag{3'}$$

In this equation, R_θ is the normalized scattering intensity (Rayleigh ratio) at the scattering angle θ, c is the concentration in g/cm^3, and q is the magnitude of the scattering vector that is related to the scattering angle

$$q = \left(4\pi n_0 / \lambda_0\right)\sin\left(\theta / 2\right) \tag{4}$$

where λ_o is the wavelength of the light used and n_o the refractive index of the solvent. K is a contrast constant that is differently defined in the various scattering techniques. For static LS one has [57]

$$K = \frac{16\pi^2}{\lambda_0^4 N_A} n_0^2 \left(\frac{\partial n}{\partial c} \right)^2 \tag{5}$$

in which $\partial n/\partial c$ is the refractive index increment which, roughly speaking, is the difference in the refractive indices between a solution and the solvent divided by the concentration. The contrast in small angle X-ray scattering (SAXS) is determined by the difference in the electron density [58] and in small angle neutron scattering (SANS) it is given by the difference in the scattering length [59]. The relationships are, for SAXS

$$K = \frac{(\Delta z)^2}{21.0} d \tag{6}$$

with

$$\Delta z = (z_2 - \bar{v}_2 \rho_0) \tag{6'}$$

where Δz represents the difference in the electron density between the solute and the solvent in which is z_2, the molar number of electrons (i.e., $M\,z_2$ is the number of electrons per molecules of molar mass M), $\bar{v}_2$, the specific volume of the polymer in solution, and ρ_0, the mean electron density of the solvent. d denotes the thickness of the scattering cell. The numerical value is $I_e N_A = (7.9 \times 10^{-26})(6.023 \times 10^{24}) = 21.0$, i.e., the product of the Thomson factor and Avogadro´s number, and is given in [58].

For SANS

$$K = \frac{\left(\rho_{b_1} - \rho_{b_0} \right)^2}{c^2} \frac{\bar{v}_1}{N_A} \tag{7}$$

with

$$\rho_b = \frac{\sum \rho_i b_i}{\sum \left(m_i 1.66 \times 10^{-24} \right)} \tag{7'}$$

where b_i is the scattering length of the i-th element in the macromolecule (or solvent molecule, respectively), ρ_i their corresponding densities, and m_i are the masses of the various elements.

The angled bracket in $<S^2>$denotes the average over all possible conformations and the index z indicates that this value is the z-average over the molar mass distribution. For convenience the abbreviation $R_g \equiv (<S^2>_z)^{1/2}$ is used.

Equation (3) is valid when the dimensions of the particle are less than the wavelength of the light and the concentration is sufficiently small. These limits are given in Eq. (3'). Furthermore the light of the primary beam has to be vertically polarized. The scattered light that enters the detector is the sum of the two contributions V_v and V_h which corresponds to the scattered light with an analyzer vertically oriented to the scattering plane (i.e., parallel to the polarization direction of the primary beam) and horizontally oriented, respectively. For branched structures the V_h contribution is very small ($V_h/V_v<10^{-3}$) and can be neglected.

Equation (3) demonstrates that the radius of gyration R_g can unambiguously be measured by static scattering experiments.

3.2.2 *Dynamic Light Scattering*

The equations for dynamic LS require a more detailed outline. Here a time correlation function (TCF) of the scattering intensity is measured that is given as [60]

$$g_2(q,t) \equiv \frac{< i(0) i(t) >}{< i(\infty) >^2} \tag{8}$$

In this relationship $i(0)$ is the scattering intensity at the time zero and i(t) that a short delay time t later. Correspondingly $i(\infty)$ is the scattering intensity at delay time $t \rightarrow \infty$. The brackets < >denote the average over a large number of repetitions ($n>10^5$). If the delay time is of the order of a relaxation time the correlation function decreases from a value of about $g_2(q,0)=2$ to a base line at $g_2(q,\infty)=1$.

The intensity TCF $g_2(q,t)$ is related to the field TCF $g_1(q,t)$, that is accessible to theoretical derivations. Its relationship is in the general case very complex, but as long as the concentration fluctuations of different volume elements in the scattering volume can be assumed to be spatially independent of each other, one can apply the Siegert relationship [61]

$$g_2(q,t) = 1 + \beta \left[g_1(q,t) \right]^2 \tag{9}$$

The coefficient $\beta<1$ depends on the quality of the instrumental set-up but takes a value close to unity when monomodal fibers are used[62].

The field TCF can be calculated on the basis of Brownian motion theory. Its initial time dependence is in every case described by a single exponential decay

$$g_1(q,t) \cong \exp(-\Gamma(q)t); \qquad \Gamma(q)t << 1 \tag{10}$$

This decay time is related to the translational diffusion coefficient as [63]

$$\Gamma(q) = q^2 D_{app}(q,c) \tag{11}$$

where

$$D_{app}(q,c) = D_z(1+k_D c)\left(1+CR_g^2 q^2 - \ldots\right) \tag{12}$$

The relationships follow from considerations of Brownian motions and thermal fluctuations which also influence the internal motions in flexible objects. D_z is the translation coefficient of the particle's center of mass where the subscript indicates the z-average over the molar mass distribution. The first bracket in Eq. (12) describes the concentration dependence which often is well represented by a linear dependence

$$D_c = D_z(1+k_D c) \tag{13}$$

with k_D as a coefficient that depends on the second virial coefficient as well as on the concentration dependence of hydrodynamic friction.

A translational motion can be concentration dependent but it cannot be angular dependent. However, the quantity Γ/q^2 is often found to depend on the scattering angle when the particles are large. Therefore, $\Gamma/q^2 \equiv D_{app}(q,c)$ must be an apparent diffusion coefficient. In fact, if a region of $qR_g > 2$ is covered by dynamic LS the scattering response arises from internal structures, which are much smaller than the radius of gyration R_g. As long as the particles are rigid the mobility of the internal domains will be essentially the same as that of the center of mass, and no angular dependence can be observed. Figure 6 exhibits the result obtained with large latex particles, which indeed shows over a wide angular region no q-dependence of the diffusion coefficient in spite of the strong angular dependence in static LS.

If, however, the various internal domains can move relative to each other they will occur with much faster relaxation times than given by the diffusive translational motion of the center of mass. The motions will become increasingly faster with decreasing size of the domains. Hence, the superimposed internal relaxation spectra must cause an increase of $\Gamma(q)$ as the scattering angle (i.e., q) is increased. For values $qR_g < 2$ this effect could be calculated for flexible chain segments (Gaussian statistics) by a rigorous perturbation theory which resulted in [63]

$$D_{app}(q,c) = D_c\left(1+CR_g^2 q^2 - \ldots\right) \tag{14}$$

with a coefficient C that is essentially determined by the longest internal mode of motion with respect to the center of mass [64]. This coefficient was calculated for various molecular architectures and proved to be a valuable guide for esti-

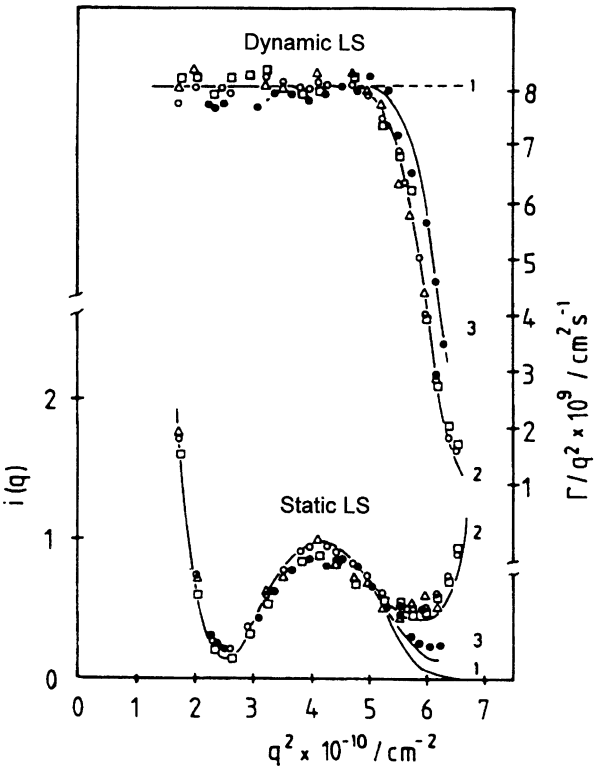

Fig. 6. *Lower part*: angular dependence of the non-normalized static scattering intensity $I(q)$ observerd with latex particles (R=265 nm). *Upper part*: dependence of $\Gamma/q^2 \equiv D$ on the scattering angle in dynamic LS. The sharp downturn at large scattering angles results from a weak back reflection of light on the boundary of the aqueous solution to the index matching bath, that consisted of toluene. This reflection results from the difference in the refractive indices of water (n_o=1.333) and toluene (n_o=1.51). Reprinted with permission from [182]. Copyright [1982] American Society

mating different types of architectures [63]. Details and applications will be discussed later in this contribution. For the moment it is sufficient to remember that one has C=0 for hard spheres, but the value becomes larger with increasing internal flexibility up to a value of $C \cong 0.2$ for linear flexible chains. Branching and cyclization reduce the value again [64, 65].

3.2.3
Stokes-Einstein Relationship

The last point to be made is the famous Stokes-Einstein relationship that was found by Einstein by comparing the Brownian motion with common diffusion processes [66, 67]. Accordingly the translational diffusion was found to depend

on the frictional coefficient f of the particle that again is determined by the hydrodynamically effective radius R_h by the Stokes equation

$$f = 6\pi\eta_0 R_h \qquad \text{(Stokes)} \tag{15'}$$

and gave

$$D = \frac{kT}{f} \qquad \text{(Einstein)} \tag{15''}$$

or

$$D = \frac{kT}{6\pi\eta_0 R_h} \qquad \text{(Stokes-Einstein)} \tag{16}$$

Two remarks have to be added. First, Eq. (16) is a definition for a hydrodynamically effective sphere radius R_h that becomes the actual sphere radius only for spheres with a well defined periphery. Second, R_h actually represents an average over all possible conformations and is given more explicitly by

$$R_h \equiv \left(\left\langle \frac{1}{r} \right\rangle_z \right)^{-1} = \left(\frac{1}{n} \sum_{n=1}^{n} \left\langle \frac{1}{r_n} \right\rangle_z \right)^{-1} \tag{17}$$

in which <>represents the average over all possible reciprocal distances $1/r_n$; the index n denotes the number of monomer units between two segment points in the molecule and the index z indicates that a further averaging with respect to a molar mass distribution (z-average) has to be taken into account. We may say R_h is the z-average of the –1st moment of the sizes distribution. Note: the mean square radius of gyration $R_g^2 \equiv \left\langle S^2 \right\rangle_z$ is the z-average of the 2nd moment of the size distribution. Thus, R_h and R_g are short hand writings of rather complex quantities.

3.2.4 *Intrinsic Viscosity*

The viscosity of the solution is significantly increased when macromolecules are dissolved in a solvent. The specific viscosity of a solution $\eta_{sp}=(\eta-\eta_o)/\eta_o$ can be expected to increase proportionally to the concentration c. The reduced viscosity η_{sp}/c still increases with increasing concentration. The data, however, can be extrapolated to zero concentration and results in the intrinsic viscosity, or the viscosity number $[\eta]$, sometimes also called the Staudinger index

$$[\eta] \equiv \lim_{c \to 0} \left(\eta_{sp} / c \right) \tag{18}$$

Staudinger realized that for macromolecules $[\eta]$ depends characteristically on the molar mass which can be expressed by the Kuhn-Mark-Houwink-Sakurada (KMHS) relationship

$$[\eta] = K_\eta M^{a_\eta} \tag{19}$$

in which K_η and a_η are molecular specific constants which also depend on the solvent quality (i.e., on A_2). Equation (19) has been the subject of many theories. The first result was obtained by Einstein who considered suspensions of hard spheres [68, 69]. He found

$$[\eta] = 2.5 N_a \left(\frac{V}{M}\right)_{sphere} = \frac{10\pi}{3} N_a \left(\frac{R^3}{M}\right) \tag{20}$$

with R the radius of the sphere. Equation (20) can be made more specific by expressing the molecular volume V by the cube of the radius of gyration

$$[\eta] = \Phi \left(\frac{R_g^3}{M}\right) \tag{21}$$

a relationship that is known as the Fox-Flory [70] relationship. The front factor Φ could be calculated for linear flexible chains and was found to approach a constant value when $M_w > 10^4$. However, the magnitude of Φ is influenced by the hydrodynamic interaction (to be defined later), and this in turn depends on the interparticle distance or in other words on the segmental concentration [71]. Since this segment density is larger in branched macromolecules than in linear coils, we have to expect an increase of Φ with branching.

Another interpretation of Eq. (20) is to introduce an equivalent sphere radius R_η by rewriting Eq. (21) as

$$[\eta] = \frac{10\pi}{3} N_A \frac{R_\eta^3}{M} \tag{22a}$$

or

$$R_\eta \equiv \left(\frac{[\eta] M}{(10\pi/3) N_A}\right)^{\frac{1}{3}} \tag{22b}$$

which yields

$$\Phi = \frac{10\pi}{3} N_A \frac{R_\eta^3}{R_g^3} \tag{23}$$

Roughly speaking the Φ-factor describes how deeply a particle is drained by the solvent: a deep draining causes a reduction of the hydrodynamically effective sphere radius and Φ becomes small, if on the other hand only a shallow draining is possible Φ increases and R_η can become much larger than R_g.

3.2.5 *The Second Virial Coefficient A_2*

All measurements, of course, have to be made at a finite concentration. This implies that interparticle interactions cannot be fully neglected. However, in very dilute solutions we can safely assume that more than two particles have only an extremely small chance to meet [72]. Thus only the interaction between two particles has to be considered. There are two types of interaction between particles in solution. One results from thermodynamic interactions (repulsion or attraction), and the other is caused by the distortion of the laminar flow due to the presence of the macromolecules. If the particles are isolated only the laminar flow field is perturbed, and this determines the intrinsic viscosity; but when the particles come closer together the distorted flow fields start to overlap and cause a further increase of the viscosity. The latter is called the hydrodynamic interaction and was calculated by Oseen to various approximations [3, 73]. Figure 7 elucidates the effect.

In all hydrodynamic methods we have the effect of both the hydrodynamic and thermodynamic interactions and these do not contribute additively but are coupled. This explains why the theoretical treatment of $[\eta]$ and of the concentration dependence of D_c has been so difficult. So far a satisfactory result could be achieved only for flexible linear chains [3, 73]. Fortunately, the thermodynamic interaction alone can be measured by static scattering techniques (or osmotic pressure measurement) when the scattering intensity is extrapolated to zero scattering angle (forward scattering). Statistical thermodynamics demonstrate that this forward scattering is given by the osmotic compressibility $\partial c/\partial\pi$ as [74, 75]

$$\frac{R_{\theta=0}}{Kc} = RT\frac{\partial c}{\partial \pi}$$

Since dilute solutions are considered we can expand the osmotic pressure in a virial series that is truncated at the second virial coefficients

$$\frac{K_c}{R_{\theta=0}} = \frac{1}{M_w} + 2A_2c = \frac{1}{M_w}\left[1 + 2A_2M_wc\right] \tag{23'}$$

Actually a dilute solution may be defined by the condition of $A_2M_wc<<1$. The theory of the second virial coefficient has been well developed for flexible chains. The treatment is quite general so that the basic equation can be assumed to hold also for branched structures; see [3]. Accordingly A_2 is expressed in terms of the

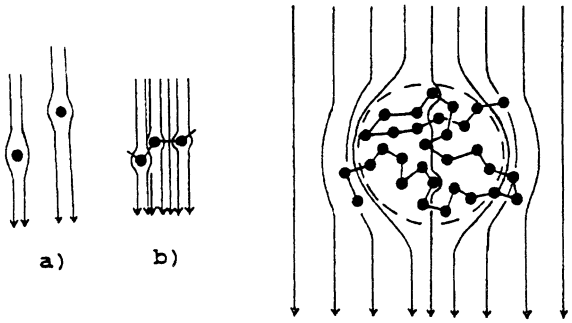

Fig. 7. Schematic representation of laminar flow distortion due to the presence of isolated particles (*left*) and the corresponding effect at higher concentration when the perturbed flow fields start to overlap (*right*). The latter effect causes the hydrodynamic interaction

radius of gyration, the molar mass and a segment-segment interpenetration function Ψ as follows:

$$A_2 = 4\pi^{3/2} N_A \left(\frac{R_g^3}{M^2} \right) \Psi \tag{24}$$

Of course, the interpenetration of two clouds of segments will depend on the repulsive interaction among the various segments, and a certain molar mass dependence of Ψ is to be expected. Surprisingly, in good solvents the Ψ-functions soon approaches a constant value Ψ^* [6]. The magnitude of Ψ^*, however, increases with branching since this causes an increase in the segment density [76–79].

Similar to what was done with the intrinsic viscosity we may compare Eq. (24) with the corresponding equation for hard spheres which is given by [3, 74, 75]

$$A_2 = \frac{16\pi}{3} N_A \frac{R^3}{M^2} \tag{25}$$

This allows us to define a thermodynamically effective equivalent radius R_T by replacing the actual sphere radius of a hard sphere by R_T which gives

$$R_T \equiv \left(\frac{3}{16\pi} \frac{A_2 M^2}{N_A} \right) \tag{26}$$

Together with Eq. (24) this gives a relationship for the interpenetration function Ψ^* in terms of this equivalent radius:

$$\Psi^* = 0.752 \frac{R_{eq}^3}{R_g^3} \tag{27}$$

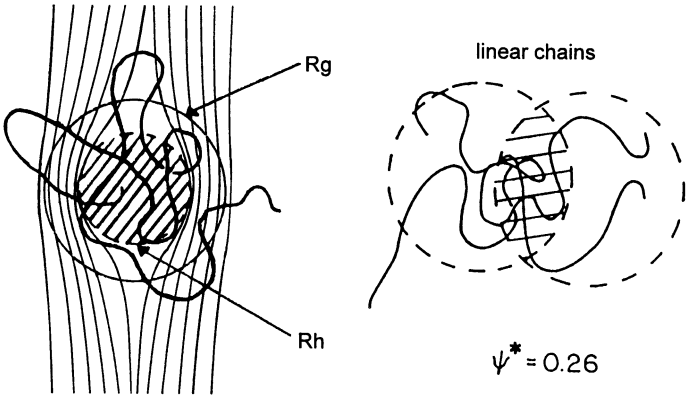

Fig. 8. Representation of the interaction functions Φ and Ψ^* in terms of equivalent sphere radii R_h and R_T, respectively. Both interaction functions depend on the segment density but small solvent molecules can easier penetrate into a coil (*left*) than two of such coils penetrate into each other (*right*)

This equation looks very similar to Eq. (23) for the draining function Φ. The meaning, however, is different: the function Φ is determined by the resistance of the penetration of small molecules (the solvent molecules) into the clouds of connected segments, while the interpenetration function Ψ^* results from the far more inhibited interpenetration of two connected segment clouds. Figure 8 elucidates the difference.

3.3 Synopsis

The results of this consideration may be summarized as follows. The study of global properties of macromolecules in dilute solutions by means of static and dynamic LS and by viscometry allows the determination of the molar mass M_w and four differently defined equivalent sphere radii, R_g, R_h, R_η, and R_T (see Table 2). All the radii have a certain molar mass dependence. The magnitudes of these radii, however, can deviate strongly from each other. These differences result from the fact that they are physically differently defined. The radius of gyration, R_g, is solely geometrically defined; the thermodynamically equivalent sphere radius, R_T, is defined by the domains of interaction between two macromolecules, or in other words, on the excluded volume. The two hydrodynamic radii R_h and R_η result from the interaction of the macromolecule with the solvent (where the latter differs from R_h by the fact that in viscometry the particle is exposed to a shear gradient field).

These differences are of special value for an estimation of the effects of branching.

Table 2. Radii and dimensional ratios formed with the molecular parameters of Table 1

Quantity	Methods
$R_g \equiv [<S^2>_z]^{1/2}$	static LS, angular dependence
$R_T \equiv [(3/16\pi N_A)(A_2 M_w{}^{2/}]^{1/3}$	static LS, concentration dependence
$R_h \equiv kT/(6\pi\eta_0 D_z)$	dynamic LS at c=0 and θ=0
$R_\eta \equiv \{(3/10\pi N_A)[\eta] M_w\}^{1/3}$	viscometry/static LS
$\rho \equiv R_g/R_h$	static LS/dynamic LS
$V_T \equiv R_T/R_h$	static LS/dynamic LS
$A_2 M_w/[\eta]$	static LS/viscometry

For linear chains the relationships between the various parameters are as follows:

$$\psi^*_{lin} = 0.26 = 0.752 \frac{R_T^3}{R_g^3} or \frac{R_T}{R_g} = \sqrt[3]{0.3457} = 0.701$$

Note: The numerical values differ for other architectures

- The interpretation of measured data can be started by examining the molar mass dependence. Here the influence of a broad molar mass dependence has a strong influence, but just this effect can be used for a differentiation between the various mechanisms of their formation and the resulting architectures.
- The various quantities can be compared with that of the linear analogue at constant molar mass. This leads to so called contraction factors, which are significant quantities for a quantitative estimation of the number of branching points per macromolecule.
- Generalized ratios of the four differently defined radii can be written. By this manipulation the molar mass dependence is widely eliminated, and the effects of branching becomes more evident. See Table 2.

The three approaches will now be discussed with some examples. We should however keep in mind that conclusions on the shape and internal structure of the macromolecules can be made only with reservations. For more reliable conclusions the angular dependencies in LS, SAXS, and SANS have to be analyzed. This problem will be outlined separately in a forthcoming review.

4
Molar Mass Dependencies of Global Parameters

4.1
Regular Stars

As already outlined, star branched macromolecules resemble their linear chain analogues. The behavior becomes evident when for a given number of arms f the

length of the arms is varied. A double logarithmic plot of the radius of gyration or of the intrinsic viscosity as a function of the molar mass results in straight lines which run parallel to the corresponding molar mass dependence of the linear chains. This behavior is found in θ-solvents as well as in good solvents. The lines for stars of different arm numbers are, however, increasingly shifted to lower values as the number of arms is increased.

Schaefgen and Flory [79] were the first to observe this effect. They prepared star-branched polyamides by co-condensation of *A-B* types of monomers with central units which carried *f*-functional *A* groups. By this technique star molecules were obtained in which the arms are not monodisperse in length. They rather obeyed the Schulz-Flory most probable length distribution with polydispersity index M_w/M_n=2. However, the coupling of f arms onto a star center leads now to a much narrower distribution that was first derived by Schulz [80]. Later the asymptotic form of this distribution has been extensively used in polymer science of linear chains to characterize the molar mass distributions of their fractions obtained by precipitation procedures. This asymptotic form was obtained by Zimm [81]. For this reason the distribution is often called the Schulz-Zimm distribution.

Elementary probability theory shows [82] that on coupling f polydisperse arms onto a star center (this corresponds to an *f*-fold convolution of a most probable distribution) the polydispersity is reduced: The polydispersity index of the star macromolecules (M_w/M_n) is simply related to the polydispersity index of the arms as [80, 82, 83]

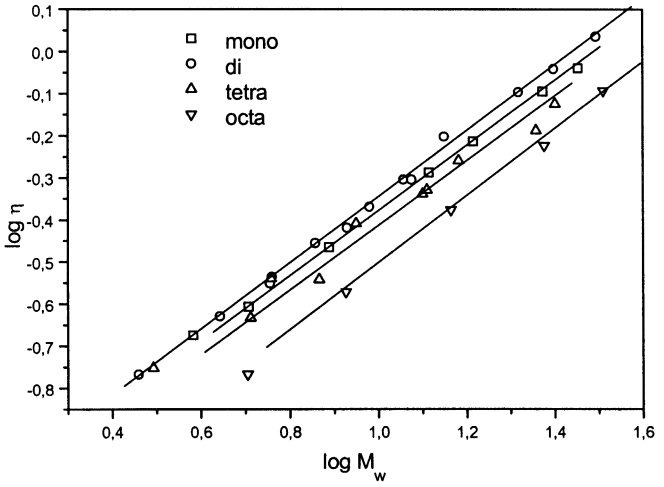

Fig. 9. Molar mass dependencies of the intrinsic viscosity of star-branched polyamides obtained by co-condensation of bifunctional amino acids with f-functional polyacids. The curves appear shifted towards smaller intrinsic viscosities as the functionality of the star center was increased [79]. Reprinted with permission from [79]. Copyright [1948] American Society

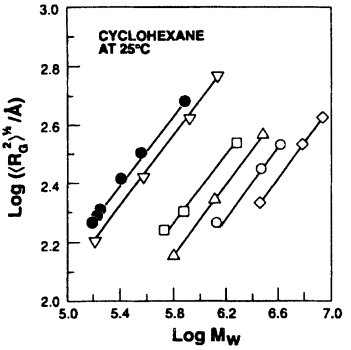

Fig. 10. Molar mass dependencies of the radii of gyration for stars of different functionality in a good solvent [25]. From *top* to *bottom*, linear, 4, 18, 32, 64 and 128-arms. Reprinted with permission from [25]. Copyright [1993] American Society

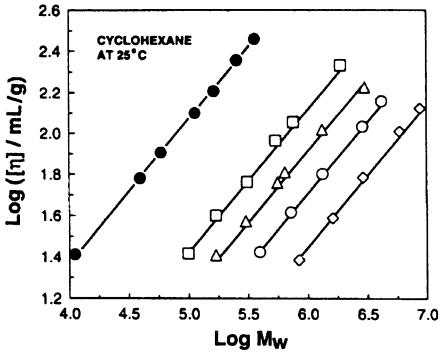

Fig. 11. The same plot as in Fig. 10 but for the intrinsic viscosity of the same samples [25]. Same symbols as in Fig. 10. Reprinted with permission from [25]. Copyright [1993] American Society

$$\frac{M_w}{M_n} = 1 + \frac{1}{f}\left(\frac{M_{w,arm}}{M_{n,arm}} - 1\right) = \left(1 + \frac{nu_{arm}}{f}\right) \tag{28}$$

where for abbreviation the non-uniformity $nu \equiv \frac{M_w}{M_n} - 1 = \frac{\sigma^2}{M_n^2}$ was introduced.

Figure 9 shows the results of the intrinsic viscosity obtained by Schaefgen and Flory.

The fairly broad most probable distribution for the rays may be considered as an undesirable imperfection of regular stars. Corresponding measurements with much narrower arm length distributions were made later, mainly by the research groups of Fetters [20, 30, 31] and Roovers [25, 26] which were obtained by living anionic polymerization of styrene, isoprene and butadiene respective-

ly. Figures 10 and 11 demonstrate some results for the radii of gyration and the intrinsic viscosities, respectively.

Similar effects were also observed for the hydrodynamic radii R_h, obtained by dynamic light scattering, and for the second virial coefficients A_2 [25].

In 1953 Benoit [84] succeeded in the calculation of the particle scattering factor $P(q)$ of regular stars with f-monodisperse arms, which obey unperturbed Gaussian statistics. The particle scattering factor is defined as the ratio of the scattering intensity R_θ at the scattering angle θ to that at the scattering angle θ= 0: $P(q) \equiv (R_\theta / R_{\theta=0})$, where $q=(4\pi n_o/\lambda_o)\sin(\theta/2)$ with n_o the refractive index of the solvent and λ_o the wavelength of the light used. The scattering intensities can be measured by common static light scattering (LS), by small angle neutron scattering (SANS), or small angle X-ray scattering (SAXS). For small values of $qR_g << 1$ the particles scattering factor solely depends on the radius of gyration

$$P(q) = 1 - \frac{1}{3} R_g^2 q^2 + \ldots$$

Therefore the derived equation for the particle scattering factor simultaneously gave an equation for the radius of gyration which is

$$R_{g,star} = b\left(g \frac{DP_{star}}{6} \right)^{1/2} \tag{29}$$

$$R_{g,star} = b\left(\frac{3f-2}{6f} \right)^{1/2} DP_{arm}^{1/2} \tag{29'}$$

$$R_{g,star} = R_{g,arm}\left(\frac{3f-2}{f} \right)^{1/2}; \quad DP_{star} = f(DP)_{arm} \tag{29''}$$

$$R_{g,arm} = b\left(\frac{DP_{arm}}{6} \right)^{1/2} \tag{29'''}$$

Equation (29) was previously derived by Zimm and Stockmayer [49] who used another technique. Figure 12 shows a plot of the theoretical increase of the radii of the stars as a function of the number of arms.

The radius becomes practically independent of the number of arms when f is larger than 8. Inspection of the structure immediately makes clear why this is so; evidently no change is to be expected when one or two more arms are added to a star of, say more than 20 chains. A significant change in the dimensions is only detectable when the number of arms changes between 2 and 6.

Up to this point we have considered only unperturbed chain statistics. However, even under Θ-conditions when A_2=0 unperturbed statistics cannot be

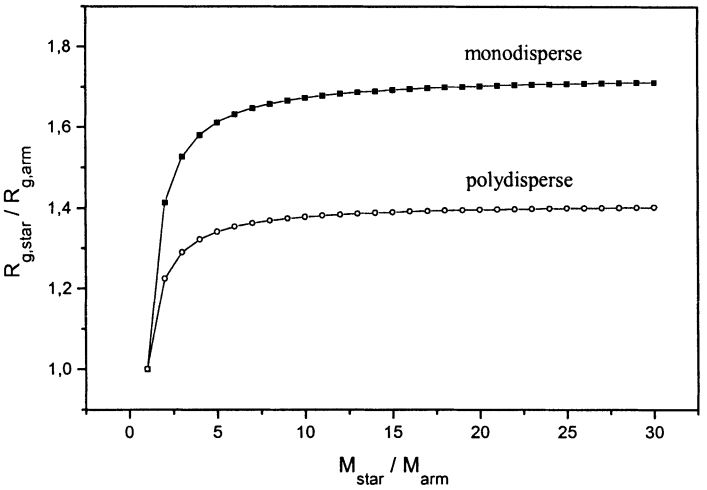

Fig. 12. Change of the radius of gyration $R_{g,star}/R_{g,arm}$ with the number of arms M_{star}/M_{arm} for stars with monodisperse arms and $R_{g(z),star}/R_{g(z),arm}$ as a function of $M_{w,star}/M_{w,arm}$ for stars with polydisperse arm lengths which obey the most probable distribution. (Note that $M_{w,star}/M_{w,arm}=(f+1)/2$ does not represent the number of arms as this is the case for monodisperse arms (see Eq. 28)

strictly obeyed if $f>6$. This conclusion results from the finite volume of the individual monomers. The free space needed for irregular motions of the arm segments remains strongly limited near the star center. As a consequence the arms stretch out, and the decrease of the radius and the intrinsic viscosity (Figs. 10 and 11) will be less pronounced than given by the unperturbed statistics. This effect was observed by Huber et al. [30]. On the other hand, the segment overcrowding quickly vanishes when segments of long arms in the peripheral region of the star are considered. In the limit of long arms the stretching-out effect becomes negligibly small. A quantitative estimation of the segment density distribution was made by Daoud and Cotton [29]. Besides the above-mentioned overcrowding effect they also took account of the excluded volume effect and its shielding in a region near the star center. They found the following results.

(a) A constant density $\varphi(r)\approx 1$ (close sphere packing) is obtained up to a radius $r<r_2\propto f^{1/2}l_K$ where l_K is the Kuhn segment length and f the number of arms.

(b) For $r_2<r<r_1$ the segment density is so high that all excluded volume effects are screened and the chain sections exhibit Gaussian chain behavior. The radius r_1 is given by $r_1\propto f^{1/2}l_K/v$ with v the excluded volume. In between r_1 and r_2 the density decreases as
$\varphi(r)\propto f^{1/2}(l_K/r)$

(c) For sufficiently long arms the segment density is small and volume exclusion can become effective. For $r>r_1$ the density now decreases as $\varphi(r)\propto f^{1/2}(l_K/r)\propto f^{2/3}(l_K/r)^{4/3}v^{-/3}$

Integration over this segment density profile under the condition of $\int_0^R \varphi(r) 4\pi r^2 dr = N f l_K^3$ then leads to a relationship for R as a function of N

$$R \propto \left[N_K f + \frac{1}{10} \frac{f^{3/2}}{\nu^2} + \frac{1}{6} f^{2/3} \right]^{3/5} \nu^{1/5} l_K / f^{2/5} \tag{30}$$

with its asymptote for very large arms of

$$R \propto N_K^{3/5} \nu^{1/5} f^{1/5} l_K \tag{30'}$$

where N_K is the number of Kuhn segments per arm and ν is the excluded volume. Equation (30) suggests that $R \propto f^{1/5}$ rather than independent of f as shown in the Gaussian model of Fig. 12.

Accordingly, in good solvents the curves for R_g and $[\eta]$ become parallel to those of their linear analogues if the arms are sufficiently long. A quantitatively reliable estimation of the magnitude of the shift to lower values could not be made by this theory. A satisfactory answer was given later by Freire et al. [85–87] on the basis of Brownian motion simulations. Experimentally, it was observed that the difference in the decrease for Θ- and good solvents is rather small but measurable. For stars with a small number of arms the Gaussian approximation is met at the Θ-conditions and approximately also at the good solvent condition. Departures are noted only when the molecular weight of the arms are small (large core fraction). However, when the number of arms becomes large (f>20) deviations from Gaussian behavior are observed in good solvents and apparently at the Θ-condition. The Daoud-Cotton-theory [29] would apply, especially in the latter case. The situation at the Θ-condition is not completely clear because of the uncertainty in establishing the Θ-temperature for individual samples.

A further remark has to be made when the stars contain polydisperse arms. The radius of gyration is now based on the z-average of the mean square radius of gyration over the molar mass distribution while the degree of polymerization is the weight average DP_w. Also for this case the molar mass dependence of this radius could be calculated and was found to be [83]

$$R_{g(z),star} = b \left(\frac{f}{(f+1)^2} \right)^{1/2} DP_{w,star}^{1/2} = b \left(\frac{f}{2(f+1)} \right)^{1/2} DP_{w,arm}^{1/2} \tag{31}$$

where an index z in brackets was added, which may remind that actually one has $R_{g(z)} \equiv (\langle S^2_z \rangle)^{1/2}$. Since with Eq. (28)

$$DP_{w,star} = \left(\frac{f+1}{2} \right) DP_{w,arm} \quad \text{and} \quad R_{g(z),arm} = \frac{b}{2} DP_{w,arm}^{1/2}$$

we can also write

$$R_{g(z),star} = \left(\frac{2f}{f+1}\right)^{1/2} R_{g(z),arm} \quad \lim_{f\to\infty} R_{g(z),star} = 1.4142 R_{g(z),arm} \tag{31'}$$

The corresponding curve of $R_{g(z),star}/R_{g(z),arm}$ as function of $M_{w,star}/M_{w,arm}$ is shown for comparison with the strictly regular stars as dashed line in Fig. 12.

The shift in the intrinsic viscosity is easily understood in qualitative terms. Assuming validity of the Fox-Flory relationship also for branched macromolecules one can write

$$[\eta]_{star} = \Phi_{star} \frac{R^3_{g,star}}{M_{star}} \tag{32}$$

This equation suggests a much stronger decrease for $[\eta]$ than for R_g on branching. However, the front factor Φ_{star} is not a universal coefficient but depends on the hydrodynamic interaction among the monomeric units in the macromolecules [3, 88]. Because of the higher segment density compared to the linear chain this hydrodynamic interaction has a stronger effect in branched macromolecules. For this reason an increase of the front factor Φ can be expected with branching which counteracts the decrease in R_g. This point will be discussed in greater detail in the next section.

In earlier experiments the effect of branching on the second virial coefficient was not seriously considered because the accuracy of measurements were not sufficient at that time. With the refinements of modern instruments a much higher precision has now been achieved. Thus A_2 can also now be measured with good accuracy and compared with theoretical expectations. The second virial coefficient results from the total volume exclusion of two macromolecules in contact [3, 81]. Furthermore, this total excluded volume of a macromolecule can be expressed in terms of the excluded volume of the individual monomeric units. In the limit of good solvent behavior this concept leads to the expression [6, 27] as shown in Eq. (24):

$$A_2 = 4\pi^{3/2} N_A \frac{R_g^3}{M^2} \Psi^* \tag{24}$$

where $\Psi(z)$ is a coil interpenetration function that approaches a constant value Ψ^* for interaction parameters of $z>0.75$ [6, 90], a value that is much exceeded for large macromolecules in a good solvent. For linear chains this asymptote is reached for DP>100 [89]. Experiments with branched macromolecules give evidence that this limit may be reached at even lower DP.

Equation (24) indicates a similar decrease with branching for A_2 as already discussed for the intrinsic viscosity. A first quantitative theory was made by Casassa [91] (see also [3]) but the experimentally observed shift to lower values

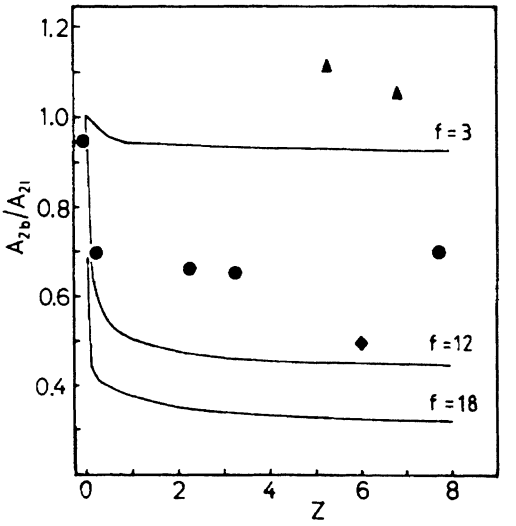

Fig. 13. Chain length dependence of the second virial coefficient A_2 for some star branched macromolecule, according to Casassa (*full line*). The data points correspond to measurements [89] (*triangles* 3-arm, *circles* 12-arm and *rhombus* 18-arm stars. Reprinted with permission from [89]. Copyright [1984] American Society

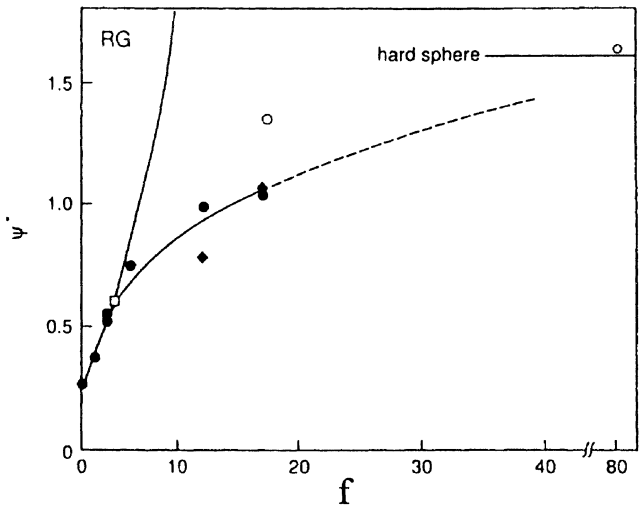

Fig. 14. Dependence of the interpenetration function Ψ^* on the number of arms in star molecules. The *full line* represents the result of the renormalization group theory [90], the *data points* refer to measurements [77]. Reprinted with permission from [77]. Copyright [1983] American Society

was not as large as predicted. This fact results from the difficulty in the correct estimation of the coil interpenetration function. Qualitatively it is obvious that the interpenetration of branched coils will be more strongly inhibited than for linear chains. Figure 13 shows the theoretical result obtained by Casassa [90] and some experimental data [89].

A much better agreement was obtained recently by renormalization group theory (RG), but this theory failed to describe the effect correctly when $f>6$. This is demonstrated by Fig. 14.

4.2 Randomly Branched Macromolecules

Remarkably different molar mass dependencies are obtained with randomly branched or randomly crosslinked macromolecules. Often, below the critical point exponents ν in $R_g \propto M_w^{\nu}$ are found which are close to $\nu=0.5$, and sometimes even lower. Figure 15 shows two typical examples.

These low exponents seem to suggest poor solvent behavior. However, the second virial coefficients are clearly positive and still fairly large and prove good solvent behavior. Surprisingly the molar mass dependencies of R_g and R_h of unfractionated samples are almost indistinguishable from those of their linear analogues.

Also the molar mass dependence of the intrinsic viscosity appears odd at first sight. Here exponents in the KMHS equation of $a_\eta<0.4$ are common, and often the exponent decreases further at large molar masses. Figure 16 shows examples.

Finally the second virial coefficient displays a much faster decrease with M_w than observed with linear chains. Exponents of a_{A_2} in the relationship

$$A_2 = K_{A_2} M_w^{-a_{A_2}} \tag{33}$$

of $0.55 \leq a_{A_2} \leq 0.8$ were found. Figure 17 shows some examples. Evidently branching displays its effect mainly in the behavior of $[\eta]$ and A_2. In the radii R_g and R_h, on the other hand, the branching effect seems to be masked by another property.

These observations require a detailed explanation. After several unsuccessful attempts a satisfying answer was finally found. A first step was made by the ingenious derivation of the molar mass distributions of randomly branched or randomly cross-linked materials [14]. The equation, that was later rederived by Flory [13], will be given in the next section. Here it suffices to point out that the width of the distribution, or the polydispersity index M_w/M_n, increases asymptotically with the weight average degree of polymerization

$$\frac{M_w}{M_n} \cong DP_w \tag{34}$$

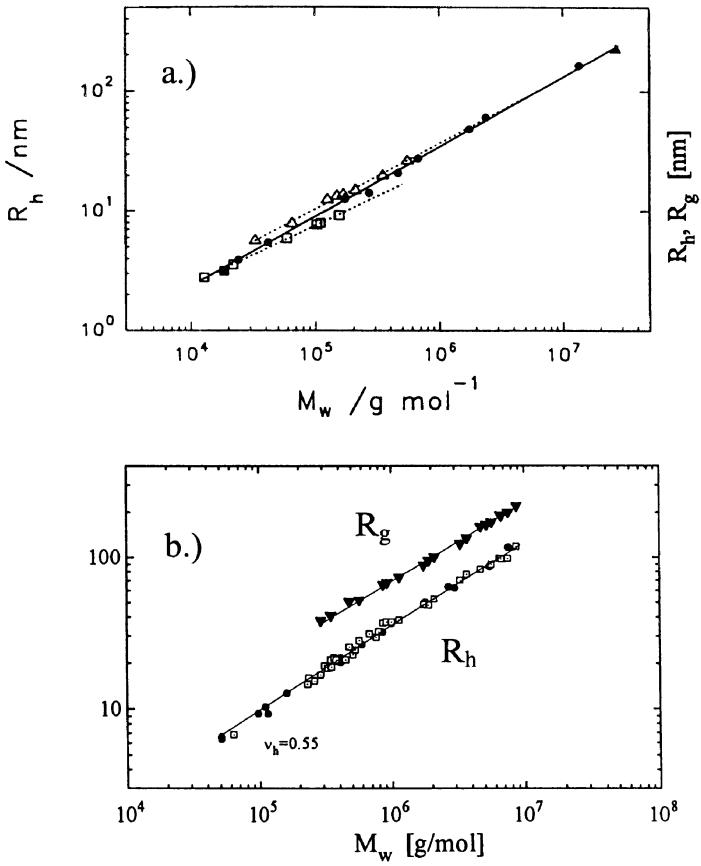

Fig. 15a,b. Molar mass dependencies of the hydrodynamic radius in good solvents for crosslinked polyester chains (obtained by phthalic acid anhydride curing of: **a** phenylglycidyl ethers – linear chains (*open squares*), pregel (*filled symbols*) and postgel (*open triangles*); **b** R_g and R_h of end-linked polystyrene 3-arm star macromolecules [92, 93]. The corresponding exponents areν =0.56±0.03 andν =0.53±0.03, respectively [94]. Reprinted with permission from [94]. Copyright [1995] American Society

The increasing polydispersity, however, represents only one contribution to R_g. As already demonstrated with the regular star-branched macromolecule, branching results in smaller radii than observed with linear chains at the same molar mass. This effect, that corresponds to an apparent contraction, is a general topological property of branching and must also be present for every species in the randomly branched ensemble. Thus, besides the polydispersity this shrinking effect is also operative. Actually, the two effects, shrinking due to branching and polydispersity, counteract and almost compensate each other. This effect was disclosed when the *z*-average of the mean square radius of gyra-

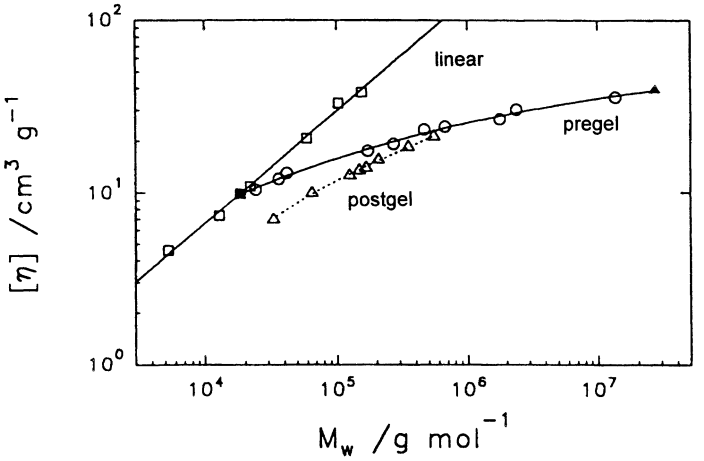

Fig. 16. Molar mass dependencies of the intrinsic viscosity *[η]* for the same samples as shown in Fig. 15 (end-linked PS-stars [94] and randomly crosslinked polyesters [92, 93, 95]

tion $<S^2>_z$ was calculated as a function of the weight average degree of polymerization [50]. For *f*-functional random polycondensation the result was [24]

$$R_{g(z)} = b\left(\frac{f-1}{2f}\right)^{1/2} DP_w^{1/2} \tag{35}$$

where Gaussian statistics were assumed for the chains connecting two segments in the macromolecule. (The *z* in brackets stresses that R_g is based on a *z*-average). This result shows two unexpected effects.

- Compared with their linear analogues the exponent in the power law behavior for R_g is not changed due to branching. This observation also remains valid when excluded volume effects are taken into account.
- The prefactor $[(f\text{-}1)/(2f)]^{1/2}$ increases from 0.5 for linear polycondensates (f= 2) to higher values and reaches asymptotically a value of 0.709 for $f>>1$.

Both effects are the consequence of the difference in averaging R_g and M_w. In fact, a fully different picture is obtained when the radii are calculated for the monodisperse fractions. These calculations were first made by Zimm and Stockmayer [49, 97]. Now the expected strong decrease of R_g with branching was indeed obtained (and also a different molar mass dependence that will be discussed somewhat later).

The peculiarly looking dependence of Eq. (35) is evidently the result of two counteracting effects. The scheme of Fig. 18 may serve as an intuitive explanation. Let us start the consideration with a monodisperse linear chain and a branched species from the ensemble of randomly branched samples. Both mol-

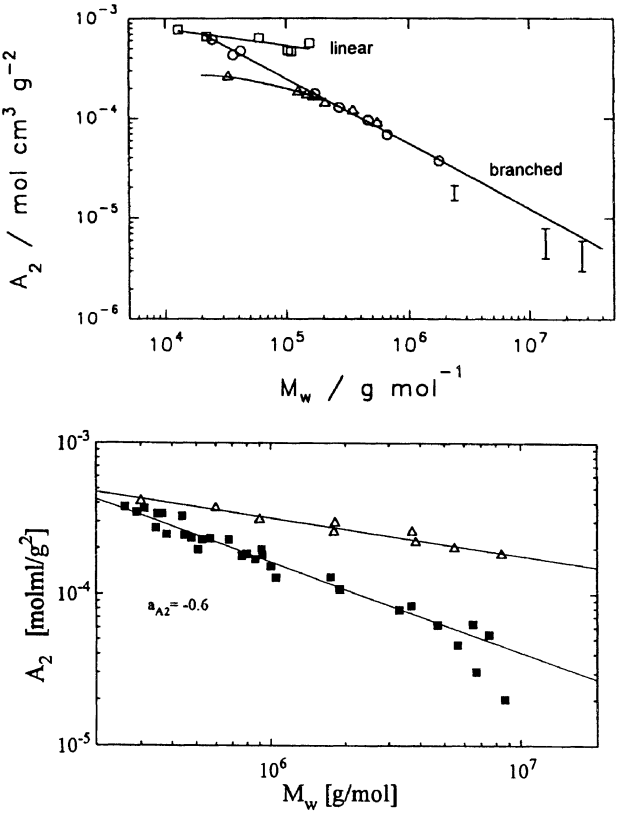

Fig. 17. Molar mass dependencies of A_2 for the same samples as shown in Fig. 16. The *flat curves* correspond to their linear analogues [92–95]

ecules have the same molar mass. Then, due to the Zimm-Stockmayer theory, we would observe a marked decrease in the radius of gyration. However, when the z-average over the molar mass distribution is carried out, the radius is strongly increased by the huge polydispersity. This increase due to polydispersity surpasses the decrease due to branching. Next, we have to take into account that the molar mass also has to be averaged. This too causes a shift of the molar mass to higher values. At the end the point comes to a position which lies only slightly above the curve for the linear chain. If we perform the same procedure with a much higher molar mass, then all corresponding effects are more pronounced, but we end up again with a point that lies only slightly above the linear chain curve.

Now, when measuring the intrinsic viscosity by common capillary viscometry and the molar mass by static light scattering, two quantities are compared which correspond to different types of averages over the size distribution. From light scattering one has $M_{LS}=M_w$, but the average of the intrinsic viscosity is

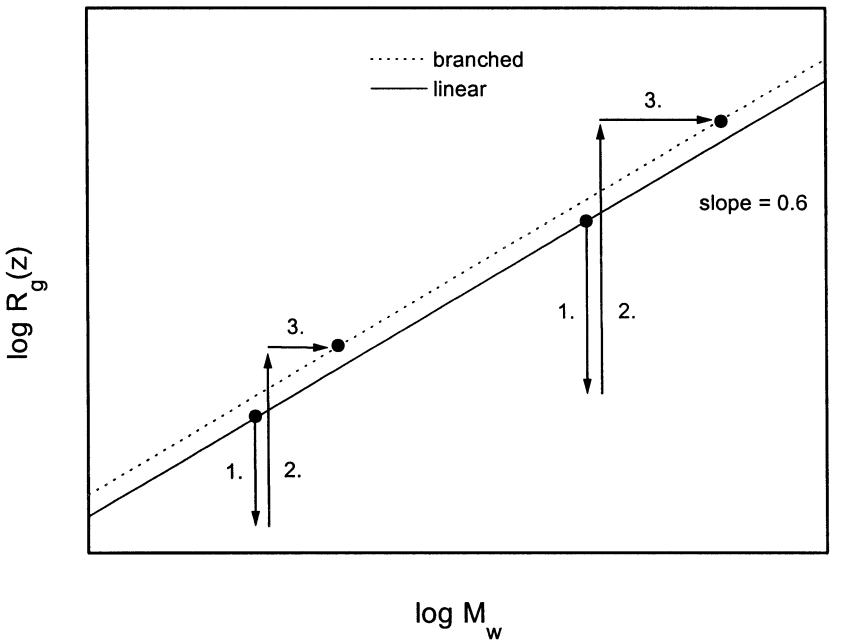

Fig. 18. Schematic explanation why the molar mass dependence of R_g shows no significant change when randomly branched samples are compared with their linear analogues. A decrease due to contraction (1) as a result of branching is overcompensated by the influence of a very broad size distribution (2). Simultaneously the weight average of molar masses in the ensemble causes a shift to the right (3). The final situation remains the same for a higher molar mass sample since both the contraction due to branching and the width of the size distribution increase in similar manner. The indicated points come to lie only slightly above the curve for polydisperse linear chains. The power law remains unchanged and the experimental results lie only slightly above the curve for polydisperse linear chains

much closer to the number average, $M_\eta \cong M_n$. As long as the polydispersity index remains independent of the molar mass this difference in the two averages causes only a parallel shift of the data. But when the polydispersity increases strongly, for instance, as is given by Eq. (34), then the intrinsic viscosities in the M_w plot appear increasingly stretched to larger values of M_w. As a consequence, the curve flattens and shows a lower exponent than expected.

The observed decrease in $[\eta]$ (see Fig. 16) can be understood when recalling that due to Marriman and Hermans [98] the intrinsic viscosity of polydisperse macromolecules is given by the ratio of two number averages

$$[\eta] = \Phi \frac{< R_g^3 >_n}{M_n} \tag{36}$$

The decrease in $[\eta]$ due to contraction as a result of branching is now no longer compensated by performing the number average over the ensemble distribution. Thus the branching effect here becomes apparent also for the non-fractionated samples.

4.3 Fractal Behavior and Self-Similarity

4.3.1 *The Concept of Fractal Dimensions*

The molar mass dependence of the second virial coefficient remains, so far, not fully understood. Why does the exponent a_{A_2} in the relationship

$$A_2 = K_{A_2} M_w^{-a_{A_2}} \tag{33}$$

change so sharply from a value of about a_{A_2} =0.20±0.03 for linear chains to a_{A_2} =0.65±0.15 when random branching occurs? A satisfactory answer to this question was found by new arguments which were introduced by physicists [4, 7, 55, 99, 100].

The starting point was a reconsideration of the molar mass dependence of R_g that is commonly written as

$$R_g = KM^{\nu} \tag{37}$$

The exponent can vary from ν=0.33 for hard spheres up to ν=1.0 for rigid rods. For linear chains ν=0.5 refers to unperturbed coil dimensions in Θ-solvents and ν=0.588 [6] to good solvent conditions. Equation (37) may be re-written by expressing the molar mass as a function of the radius of gyration, i.e.,

$$M = \overline{K} R_g^{d_f} \tag{38a}$$

with

$$d_f = 1/\nu \tag{38b}$$

For solid bodies of hard spheres, flat discs and rigid rods one has
$d_f = d_3 = 3$ for hard spheres
$d_f = d_2 = 2$ for flat discs
$d_f = d_1 = 1$ for thin rods

or in other words, d_f denotes the geometric dimension of the bodies, which in these cases are three-dimensional, two-dimensional, or one-dimensional, re-

spectively. However, when applying Eq. (38b) to the exponents, found with macromolecules, one obtains a fractal number. For instance with ν=0.587 one has the fractal dimension

d_f=1.70 for coils of linear chains in a good solvent

A random coil is clearly a three-dimensional object when looked at from long distance. Locally, however, it resembles more a one-dimensional thread. Therefore it is sensible to describe the coil by a fractal dimension that lies closer to 1 (for other architectures somewhere between 1 and 3). Such disordered objects are called fractals [101, 102].

So far this approach is nothing else than a new way to express a mathematical relationship. But there is more behind this approach. It was proven mathematically that so-called self-similar objects must show power law behavior [103]. The expression self-similarity has the following meaning: independent of the length scale that is used to express the radius of gyration in actual measurements (i.e., whether the bond length b or the Kuhn segment length l_K is chosen), the same exponent ν=1/d_f is obtained [4]. If a change in the exponent ν is observed when passing to very high molar masses, then this is a clear indication that these objects are significantly different from those at lower molar masses. Some examples will be discussed later when the structure of fractions in size exclusion chromatograms is considered.

Simulation of structure formation on a lattice [7, 100] demonstrated that randomly formed branched clusters also fulfill self-similarity conditions and gave fractal dimensions of [7, 104, 105]:

d_f=2.5 for clusters in the reaction bath (e.g. poorly swollen as in the melt)
d_f=2.0 for freely swollen clusters in a good solvent

4.3.1.1 *Molar Mass Dependence of A_2*

We are now ready for an interpretation of the exponents in Eq. (33). Inserting Eq. (38b) into Eq. (24) (that describes the structure dependence of the second virial coefficient) we find

$$A_2 \propto M^{(3/d_f)-2} = M^{-a_{A_2}} \tag{39}$$

or

$$-a_{A_2} = \frac{3}{d_f} - 2 \tag{40}$$

where we have assumed that the interpenetration function Ψ^* does not significantly change with the number of branching points in the macromolecules. With

the fractal dimensions for the freely swollen and the poorly swollen clusters we thus obtain

freely swollen: d_f=2.0; ν=0.5; – a_{A_2} =–0.5; a_η=0.5 (41a)

poorly swollen: d_f=2.5; ν=0.4; – a_{A_2} =–0.8; a_η=0.2 (41b)

Similarly, the values for $a_\eta=(3/d_f)-1$ follow from the Fox-Flory relationship (Eq. 26), again under the condition that Φ_b does not change with the number of branching points per cluster. The assumption of constant Ψ^* and constant Φ_b are not strictly fulfilled. Nonetheless the scaling relationship of Eq. (40), and the corresponding one for the intrinsic viscosity, lead to very reasonable results, which were indeed observed. Here the full power of the fractal concept becomes evident.

4.3.2 *Influence of Polydispersity*

The fractal dimension that is determined from Eq. (38) is not in all cases the true fractal dimension of the individual macromolecules. In a polydisperse ensemble one has to take the ensemble average which yields an ensemble fractal dimension $d_{f,e}$ [7, 92]:

$$M_w \propto R_{g(z)}^{d_{f,e}} \tag{42}$$

Since the mean square radius of gyration requires a z-average but the molar mass a weight average the fractal dimension remains unchanged only if the ratio M_z/M_w is independent of the molar mass or close to unity. These conditions are mostly fulfilled with polydisperse linear chains but not for the randomly branched ones. Here this ratio M_z/M_w increases strongly with the molar mass. The leading parameter that characterizes the distributions of randomly branched samples is an exponent τ that is defined in the next section. The average procedures for the z-average of the mean square radius of gyration and the weight average molar mass results in the relationship [7]

$$d_{f,e} = d_f\left(3-\tau\right) \tag{43}$$

where τ can vary between 2.2 and 2.5. Of course, if the z-average molar mass is known one can determine the true fractal dimension directly from the plot of M_z against R_g. Examples were given by Colby et al. [116] and in [120].

5
Molar Mass Distributions

5.1
Linear and Quasi-Linear Chains

The molar mass distribution of branched materials differ most significantly from those known for linear chains. To make this evident the well known types of (i) Schulz-Flory, or most probable distribution, (ii) Poisson, and (iii) Schulz-Zimm distributions are reproduced. Let x denote the degree of polymerization of an x-mer. Then we have as follows.

5.1.1
Most Probable Distribution [1, 80, 106]

$$w(x) = (1-\alpha)^2 x\alpha^{x-1} \rightarrow \left(\frac{2}{x_w}\right)^2 x\exp(-2x/x_w) \tag{44}$$

$$x_w = \frac{1+\alpha}{1-\alpha};\quad x_n = \frac{1}{1-\alpha};\quad \frac{x_w}{x_n} = 1+\alpha \rightarrow 2;\quad \frac{x_z}{x_w} = \frac{2+\alpha}{1+\alpha} \rightarrow \frac{3}{2} \tag{45}$$

where α is the extent of reaction or in other words the fraction of reacted functional groups to all (reacted+non reacted) functional groups in the polymer.

5.1.2
Poisson Distribution [82, 107]

$$w(x) = \frac{a^{x-1}}{(1+\alpha)(x-1)!} x\exp(-a) \rightarrow \frac{(x_w-1)^{x-1}}{x_w(x-2)!}\exp\left[-(x_w-1)\right] \tag{46}$$

$$x_w = a+1;\quad x_n = a;\ \frac{x_w}{x_n} = 1+\frac{1}{x_n};\quad \frac{x_z}{x_w} = \frac{a+2}{a+1} \rightarrow 1+\frac{1}{x_w} \tag{47}$$

where a is the number average degree of polymerization

5.1.3
Schulz-Zimm Distribution [80, 81]

$$w(x)=\frac{x(x+f-2)!}{(f-1)!(x-1)![fp+1-p]}(1-p)^{(f+1)}p^{x-1} \tag{48a}$$

$$w(x)\rightarrow\frac{x^f}{f!}\left(\frac{f+1}{x_w}\right)^{f+1}\exp\left[\frac{(f+1)x}{x_w}\right] \tag{48b}$$

$$x_w=\frac{f+1}{f(1-p)}=\frac{f+1}{2}x_{wo};\quad x_n=\frac{f}{1-p}=fx_{no};\quad \frac{x_w}{x_n}=1+\frac{1}{f};\quad \frac{x_z}{x_w}=1+\frac{1}{f+1} \tag{49}$$

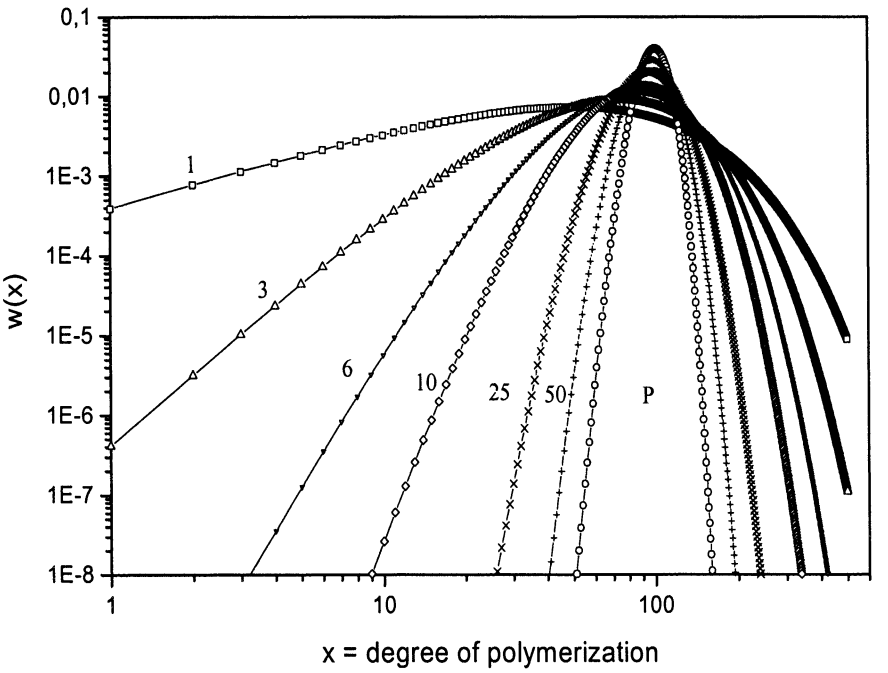

Fig. 19. Weight fraction molar mass distributions *w(x)* of the Schulz-Zimm type for various numbers of coupled chains in a double logarithmic plot. Note: for f=1 the Schulz-Zimm distribution becomes the most probable distribution; in the limit of f>>1 the Poisson distribution is eventually obtained. In all cases the weight average degree of polymerization was x_w=100. The narrowing of the distribution with the number of coupled chains is particularly well seen in the double logarithmic presentation

The exact formula was derived by Schulz [80] and the asymptotic equation is due to Zimm [81]. Schulz derived the distribution for *f* chains that are coupled together, where it has no influence whether one has a head to tail coupling of most probable distributions or whether these distributions are coupled onto a star center. Zimm recognized that the asymptotic form can be efficiently used to describe the distributions of fractions. The index *o* refers to the primary (most probable) chain distribution and *p* is the extent of reaction for this primary chain.

The three types of distributions are plotted in Fig. 19. Actually the molar mass would be increased by the number of chains, but to make the narrowing more evident the curves were normalized to the same weight average degree of polymerization x_w=100.

5.2 Distributions for Branched Chains

5.2.1 *Stockmayer Distribution (Randomly Branched)*

The Schulz-Zimm distribution would be found for *f* end-to-end coupled linear chains which obey the most probable distribution, as well as for *f* of such chains which are coupled onto a star center. This behavior demonstrates once more the quasi-linear behavior of star branched macromolecules. In fact, to be sure of branching, other structural quantities have to be measured in addition to the molar mass distribution.

The other extreme to star molecules are the randomly branched macromolecules. Here the branching process has an immense influence on the shape of the distribution. It was first derived by Stockmayer [14] and later reproduced by Flory [13]. The exact and asymptotic distributions are given by the following two equations:

$$w(x)=\frac{(1-\alpha)^2}{\alpha} f \frac{[(f-1)x]!}{(x-1)![(f-2)x+2]!}\beta^x \tag{50a}$$

with

$\beta=\alpha(1\text{-}\alpha)^{f-2}$

For $\alpha=\alpha_c=1/(f\text{-}1)$ one obtains the asymptotic form [14]

$$w(x)=\frac{(1-\alpha)^2}{\alpha} fx \frac{\exp[-(1-\beta/\beta_c)x]}{2\sqrt{\pi}(f-1)^{5/2}x^{5/2}} \tag{50b}$$

where

$$\beta_c = \frac{(f-2)^{f-2}}{(f-1)^{f-1}}$$

$$x_w = \frac{1+\alpha}{1-(f-1)\alpha};\quad x_n = \frac{1}{1-f\alpha/2};\quad \frac{x_w}{x_n} = \frac{(1+\alpha)(1-f\alpha/2)}{1-(f-1)\alpha} \to \frac{1}{2}\frac{f-2}{f-1}x_w; \tag{51}$$
$$\frac{x_z}{x_w} = \frac{1+3\alpha}{(1+\alpha)^3} + \frac{1-\alpha}{(1-\alpha)^2}\alpha(f-1)x_w \to \frac{(f-1)(f-2)}{f^2}x_w$$

Most remarkable is the immense increase of the polydispersity index x_w/x_n and of the ratio x_z/x_w, which both increase with x_w. This distribution follows asymptotically a power law of $w(x) \propto x^{1-\tau}$ with τ=2.5, when the critical point of gelation is approached. Figure 20 shows some of these distributions for various α, or different x_w.

At this point it is appropriate to emphasize that the above derivation was made under three essential assumptions.

- Intramolecular reactions (ring formation) are excluded.
- Excluded volume effects are neglected.
- All functional groups have the same probability of reaction α, independent of whether the functional group is at the periphery of the branched cluster or whether it might be buried inside of the cluster.

Around 1970 computer simulations of the branching processes on a lattice started to become a common technique. In bond percolation the following assessment is made [7]: whenever two units come to lie on adjacent lattice sites a bond between the two units is formed. The simulation was made by throwing at random n units on a lattice with N^3 lattice sites. Clusters of various size and shape were obtained from which, among others, the weight fraction distribution could be derived. The results could be cast in a form of [7]

$$w(x) = Ax^{1-\tau} f\left(x/x^*\right) \tag{52}$$

in which τ=2.2 was found. The function $f(x/x^*)$ is a cut-off function with a characteristic degree of polymerization x^*. For $x > x^*$ a much stronger decay of the distribution than given by the power law is now obtained. This characteristic degree of polymerization shows critical behavior, i.e., it follows a relationship

$$x^* \propto \frac{1}{|p-p_c|^{1/\sigma}} \tag{53}$$

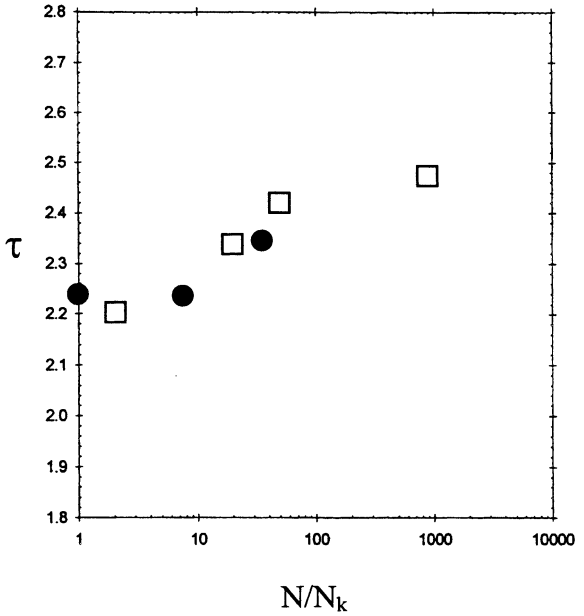

Fig. 20. Plot of the exponent τ as a function of the chain lengths between two branching points. *Open symbols*: results by Colby et al. [118,119] for branched polyesters. The variation of this length was achieved by co-condensation of trifunctional monomers with increasing fraction of bifunctional units. *Filled symbols* refer to polydicyanurates ($N<<N_K$), anhydride cured phenyl monoglycidyl ether with a small fraction of bisphenol A diglycidylether as crosslinker ($N\cong 8\ N_K$) and end-functionalized 3-arm polystyrene stars crosslinked by diisocyanate ($N\cong 40\ N_K$). N denotes the number of repeating units between two branching points

with another exponent σ=0.44. In this equation p represents the occupation ratio of lattice sites and p_c is the critical occupation where for the first time a cluster is formed that extends from wall to wall of the lattice box. Experiments have given much evidence that x^* is close to the z-average degree of polymerization x_z [109]:

$$x^* \cong x_z \tag{53'}$$

The percolation simulations clearly allow ring formation; it also represents self-avoiding statistics, i.e., includes the excluded volume effects in good solvents. Finally, the probability of placing units on lattice sites becomes more and more dependent on whether a site in the neighborhood is already occupied. In other words the percolation experiment becomes a non-mean field approach when the occupation reaches the critical percolation threshold. Therefore, strong deviations were expected between the more accurate percolation and the Flory-Stockmayer mean field approaches. Physicists were of the opinion that the mean field results must be basically wrong.

A careful examination of the Stockmayer and the percolation distributions reveals that both theories gives the same type of distribution [110]. In terms of the two exponents in Eqs. 52 and 53, the percolation calculation yields τ=2.2 and σ=0.44, and the Stockmayer distribution yields τ=2.5 and σ=0.50. These differences in the exponents appear to be small in a double logarithmic plot, but they cause significant differences in the absolute values for $w(x)$ when 3–4 decades in the degree of polymerization are covered. Another point is that the cut-off function could be calculated analytically in the FS-theory to be a single exponential function [110], while the percolation theory could only make a guess about its shape [7].

It took a long time before the percolation theory could be proved to be the better one in most cases. The reason for this delay resulted in part from the fact that until ten years ago the size exclusion chromatography (SEC) with on-line light scattering was not sufficiently well developed. A direct molar mass determination is, however, imperative, since the separation in SEC is due to the hydrodynamic volume of the particles. A branched macromolecule has, however, a significantly higher molar mass than a linear one of the same hydrodynamic volume. Since 1989 a number of results have been reported which all strongly supported the percolation theory [109, 111–116].

Scepticism still remained to some extent, because the FS mean field theory could predict fairly well the point of gelation, while the prediction of the percolation threshold was very poor. Also, the percolation result depended on the type of lattice that was chosen for the simulation. This hidden reservation led de Gennes to suggest [117] that the Ginsburg criterion (known in the theory of critical phenomena) may also be operative in the branching processes. According to Ginsburg the critical range in which percolation can be observed decreases with the chain length between branching points according to [117]

$$\varepsilon \leq AN^{-1/3} \tag{54}$$

where ε is the critical region that is defined as

$$\varepsilon = \frac{\left|p - p_c\right|}{p_c}$$

Accordingly the critical domain will become progressively smaller when the chain length N increases. In these cases a transition towards mean field theory should occur when ε becomes larger than $AN^{-1/3}$. Recently Colby [118] and Lusignan [119] have finished comprehensive studies with polyesters, in which the chain length between branching points was systematically varied. Ginsburg's criterion was applied by interpreting N as N_K, i.e., the number of Kuhn segments. Furthermore, A=1 was assumed. The result is shown in Fig. 20. One realizes that indeed a transition occurs at around N_K=1; at shorter chains the percolation exponent was obtained, at large length on the other hand the FS mean field results were obtained. Similar experiments were performed in the

Freiburg laboratory with three other materials in which the chain length varies from a very small value to a rather large one [93, 110, 113, 115, 120]. The result of the exponents are plotted in Fig. 20 as filled circles. The agreement is very satisfactory.

5.2.2
Distribution of Hyperbranched Samples

A special case of statistical branching occurs when a monomer has one functional group (type *A*) that differs from the *f*-1 other ones (type *B*) such that only groups *A* can react with group *B*, but no reaction between two *A* or two *B* groups are possible. Because of this incisive constraint the reaction is clearly no longer random. This has a stringent influence on the molar mass distribution, which is not immediately recognized by a superficial inspection of the distribution that is given by [1, 13]

$$w(x)=\frac{1-p}{p}\left[1-p(f-1)\right]\frac{\left[(f-1)x\right]!}{\left[(f-2)x+1\right]!(x-1)!}\beta^x \tag{55}$$

with $\beta=p(1\text{-}p)^{f-2}$ and p the probability of reaction of the *B*-groups. Eq. (55) looks very similar to Eq. (50a) for random branching. The intermediate region can be described by a power law as given in Eq.(55'):

$$x(w)_{asymp}=0.395\times\left(\frac{x_w}{x}\right)^{0.5} \tag{55'}$$

However, because of the constraint that *A* can only react with a *B*-group one has for the probability α of the *A*-group

$$\alpha=(f\text{-}1)p \tag{56}$$

i.e., the maximum value for p is by a factor $1/(f-1)$ smaller than the α value in Eq. (50a). This leads to

$$x_w=\frac{1-\alpha^2/(f-1)}{1-\alpha)^2};\ x_n=\frac{1}{1-\alpha};\ \frac{x_w}{x_n}=\frac{1-\alpha^2/(f-1)}{1-\alpha}\rightarrow\frac{f-2}{f-1}x_n=\sqrt{\frac{f-1}{f-2}x_w} \tag{57}$$

$$\frac{x_2}{x_w}=(1-\alpha)\left\{1-2\frac{\left[\alpha^2/(f-1)\right]\left[1-\alpha/(f-1)\right]}{\left[1-\alpha^2/(f-1)\right]^2}\right\}+3\alpha\frac{\left[1-\alpha/(f-1)\right]}{1-\alpha^2/(f-1)}\rightarrow 3$$

where the arrows denote the limit for $x_w>>1$. The limiting relationship results from the condition $\alpha=(f\text{-}1)p\cong 1$.

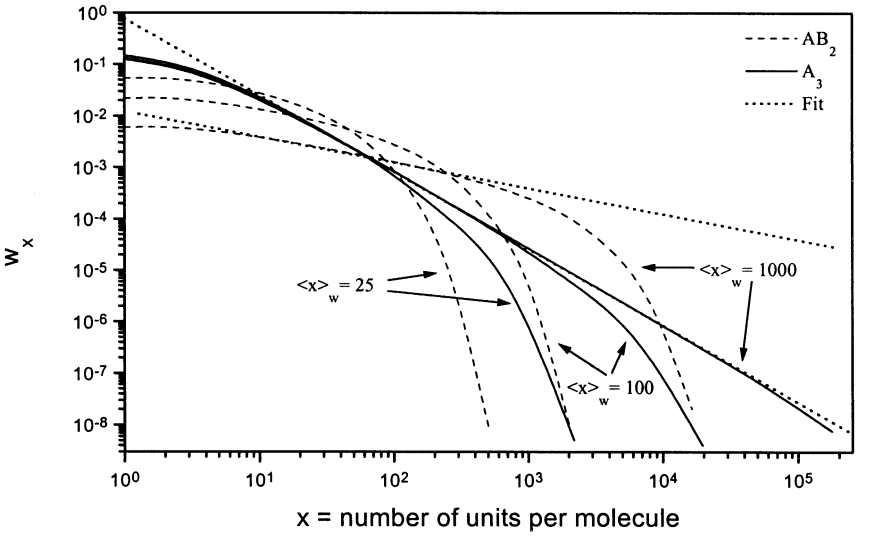

Fig. 21. Comparison of the distributions of randomly branched (*full lines*) and hyperbranched macromolecules (*dashed lines*) for f=3 at x_w=25, 100, and 1000. The *dotted lines* represent fits of the distributions to power laws with exponents (1–τ)=–1.5 (randomly branched) and –0.5 (hyperbranched), respectively. The intermediate region of the hyperbranched distributions can be described by Eq. (55')

Comparison with the corresponding equations for random branching demonstrates that the polydispersity index for hyperbranched materials increases approximately only with the root of x_w while it increases proportional directly with x_w for random branching. Figure 21 shows these distributions for f= 3 and various weight average degrees of polymerization x_w in comparison with the Stockmayer distribution for random branching.

So far all (f–1) B-groups were assumed to have the same reactivity. The generalized case, where, for instance, in a trifunctional unit the second B_2-group has a remarkably lower reactivity than the first one, leads to lower branching densities and eventually to a linear chain. This case was treated by Erlander and French [16], who derived the weight fraction distribution and the various molar mass averages. These derivations allowed the definition of a branching probability and thus the number of branching points per number or weight average degree of polymerization, respectively [17, 24, 52]. Particularly for AB_2 unit the branching probability can never become larger than 0.5. In spite of their importance the distributions are not shown here in a graph, but the lengthy equations are found in [121] and in the Appendix.

One important result may be mentioned in particular. The ratio of x_z/x_w approaches the constant value of 3 [16]. Therefore, the ensemble fractal dimensions becomes identical to the true fractal dimension, i.e. $d_{f,e}=d_f$.

6
Size Exclusion Chromatography

Modern size exclusion chromatography can nowadays be equipped with a multi-angle laser light scattering (MALLS) detector on-line with a viscometer (VISC) in addition to the common refractive index (RI) or ultraviolet (UV) detector. Such a set-up allows the on-line determination of the radius of gyration and the intrinsic viscosity as a function of the molar mass for each of the fractions. The power of this combination is at present not fully used. This is probably for the following reasons. A fraction of the material may sometimes be adsorbed onto the separation gel of the column. Another reason originates from self-association. As long as these particles remain in a metastable region, such that shear forces do not cause a decomposition into smaller units, the aggregates can mostly be recognized via their fractal dimension. Troubles occur, however, when the particles become disaggregated under the influence of shear. These effects can make an interpretation of elution diagrams extremely difficult and the mentioned combination of LS and VISC data are considered as being loaded too much by poorly understood uncertainties. Additional cross-checking with other techniques are indeed imperative.

The following outline assumes ideal conditions in which all these spurious side effects are avoided. Let us assume that the most developed SEC set-up may be available. Then by SEC/RI/MALLS/VISC analysis four elution curves are obtained

1.	$c_j(v_e)$	RI or UV detector	
2.	$c_j M_j(v_e)$	LS detector, (at zero scattering angle)	
3.	$R_{gj(}v_e)$	LS detector (from angular dependence)	
4.	$c_j[\eta]_j(v_e)$	VISC detector	(58)

The index j denotes the measured quantity in the j-th slice at the elution volume v_e. After elimination of the elution volume (as parameter) and by combining the four traces one obtains

1.	c_j	as a function of M_j	
2.	R_{gj}	as a function of M_j	
3.	$[\eta]_j$	as a function of M_j	(59)

6.1
Molar Mass Distribution *w(M)*

The first curve is a histogram of the mass fraction detected in each slice. It is not yet the correct molar mass distribution $w(M)$, because a linear spacing with respect of the elution volume corresponds to a logarithmic spacing in the molar

mass. Hence at small elution volumes the average is taken over a much broader range in the molar mass than it is the case for large v_e. The correct molar mass distribution is obtained by forming first a cumulant distribution $I_k(M)$ which is obtained by the operation

$$I_k\left(M\right) \equiv \sum_{j=1}^{k} \frac{c_j\left(M_j\right)}{c_o} \cong I\left(M\right) \tag{60a}$$

where

$$c_o = \sum_{j=1}^{N} c_j$$

In a second step this cumulant distribution has to be differentiated *linearly* with respect to the molar mass, i.e.,

$$w\left(M\right) = \frac{dI\left(M\right)}{dM} \tag{60b}$$

The step from the discrete $I_k(M)$ to the continuous $I(M)$ often requires some smoothing which has to be made with critical attention.

6.2 Molar Mass Dependence of the Radii of Gyration

The R_{gj} vs M_j curve often gives a straight line in the double logarithmic plot and can be represented by

$$R_{gj} = KM_j^{\nu} \tag{61a}$$

or

$$M_j = \overline{K} R_{gj}^{d_f} \tag{61b}$$

in which d_f is very close to the true fractal dimension of the clusters. Here the data from the histogram can safely be taken. The fractions at small elution volumes are certainly broader than those at large elution volumes, but the polydispersity in the various slices can still be assumed to be very low (probably $(M_w/M_n)_j$<1.05). For such small polydispersities the influence of the ensemble averaging is negligibly small.

When comparing this true fractal dimension with that of the ensemble, which is obtained with a series of non fractionated samples, one finds another possibil-

ity for a determination of the exponent τ in the molar mass distribution of Eq. (52). According to Eq. (43) one has

$$\tau = 3 - \frac{d_{f,e}}{d_f} \tag{43'}$$

The clusters which obey Eq. (61) are self similar to each other. Sometimes, however, the R_g curve flattens at large molar masses and may form another straight line with a different exponent. Such behavior is an indication of a limitation in the separation capability of the column (or some other artifacts) or it is the result of large particles with a different fractal behavior. These particles can be aggregates or clusters of a higher branching density. Similar behavior can be observed also from the molar mass dependence of the viscosity. An example will be shown in the next section.

6.3 Kuhn-Mark-Houwink-Sakurada (KMHS) Equation

The intrinsic viscosity vs molecular weight dependence extracted from the SEC experiments curve of the intrinsic viscosity also often gives a straight line in the double logarithmic plot and can be described by the (KMHS) relationship:

$$[\eta]_j = KM_j^{a_{\eta j}} \tag{19'}$$

In contrast to star-branched macromolecules, this relationship differs now from that of the non-fractionated samples

$$[\eta] = KM_w^{a_\eta} \tag{19''}$$

and this not only in the prefactor K but also in their exponents. A somewhat steeper curve is usually obtained for the fractions. It exhibits power law behavior over the whole molar mass region. For the polydisperse samples such power law behavior is mostly not observed over the whole region, but only at very high molar masses a constant exponent is asymptotically observed. Here again the different averaging procedures have a significant influence as was already discussed in a previous section in qualitative terms. Daoud and Martin [102] and Daoud et al. [121] took account of these differences and derived the following equation:

$$\tau = \frac{2 + a_{\eta j} - 3a_\eta}{1 - a_\eta} \tag{62}$$

which was used for an estimation of the exponent τ of the molar mass distribution from end-linked star-branched polystyrenes [110] and for an epoxy system

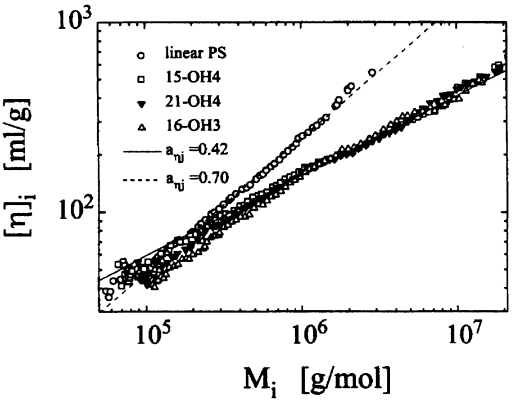

Fig. 22. KMHS relationships for the fractions of end-linked 3-arm star-branched polystyrene molecules and of linear polystyrene fractions. The data refer to three samples of different M_w in the pregel state and one from the sol fraction of a gel. The curves for the branched macromolecules coincide within experimental error in the high molar mass region. The deviations at low M_w result from a different amount of non-reacted end-functionalized stars. The exponents of the end-linked and linear PS chains are $a_{\eta b}$=0.42±0.02 while that of linear chains is $a_{\eta lin}$= 0.70±0.01 [95, 120, 123, 124]. Reprinted with permission from [95]. Copyright [1997] American Society

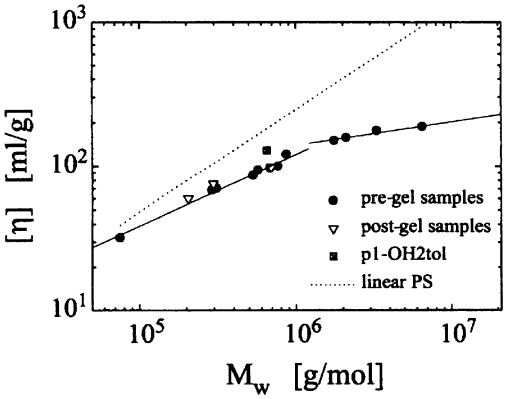

Fig. 23. The intrinsic viscosity of several end-linked PS star molecules as a function of M_w [95]. In the limit of low and high molar masses asymptotic power law behavior may be derived. That at low molar masses is widely controlled by the presence of non-reacted star molecules, that at high molar masses is expected from theory for randomly branched macromolecules. The exponents of the two asymptotic lines are a_η=0.49±0.08 for M_j<0.8×10^6 g/mol and a_η=0.18±0.05 for M_j>2.0×10^6 g/mol. Reprinted with permission from [95]. Copyright [1997] American Society

[120]. Figure 22 shows the results of the fractions from end-linked 3-arm star molecules in comparison to linear polystyrenes in the same solvent and Fig. 23 gives the result of $[\eta]$ as a function of M_w.

6.4 Contraction Factors

At this stage it becomes possible to treat the decrease of R_{gb} and $[\eta]_b$ as a result of branching quantitatively. This was done for the first time by Zimm and Stockmayer [49] for the radius of gyration, and somewhat later by Stockmayer and Fixman [125] for the intrinsic viscosity. They introduced the following shrinking or contraction factors. The radii of gyration can for Gaussian segment distribution in principal be calculated analytically without introducing any physical approximations. For the intrinsic viscosity this is not the case since hydrodynamic interactions among the segments have to be taken into account. So far these can be calculated only under certain approximations whose physical relevance remains not fully understood [3, 88, 126].

$$g = \frac{R_{g,b}^2}{R_{g,lin}^2}\Big|_{\text{at the same M}} \tag{63}$$

$$g' = \frac{[\eta]_{g,b}}{[\eta]_{g,lin}}\Big|_{\text{at the same M}} \tag{64}$$

For the contraction factors g of the mean square radii of gyration for fractions of randomly branched materials Zimm and Stockmayer [49] obtained

$$g_3 = \left[\left(1+\frac{n}{7}\right)^{1/2} + \frac{4n}{9\pi}\right]^{-1/2} \tag{65}$$

$$g_4 = \left[\left(1+\frac{n}{6}\right)^{1/2} + \frac{4n}{3\pi}\right]^{-1/2} \tag{66}$$

The indices 3 or 4 indicate the functionality of the monomeric units, and n denotes the number of branching units in one branched molecule. This number of branching units is related to the degree of polymerization x by the relationship

$$x=(m\times n)$$

where m is the average number monomer units which contains one branching point. For f-functional branching units the following asymptotic relationship was obtained, now expressed in terms of the degree of polymerization x [49]

$$g_f = 3\left(\frac{\pi}{2(f-1)(f-2)x}\right)^{1/2} - \frac{2(6-f)}{(f-1)(f-2)x} \tag{67}$$

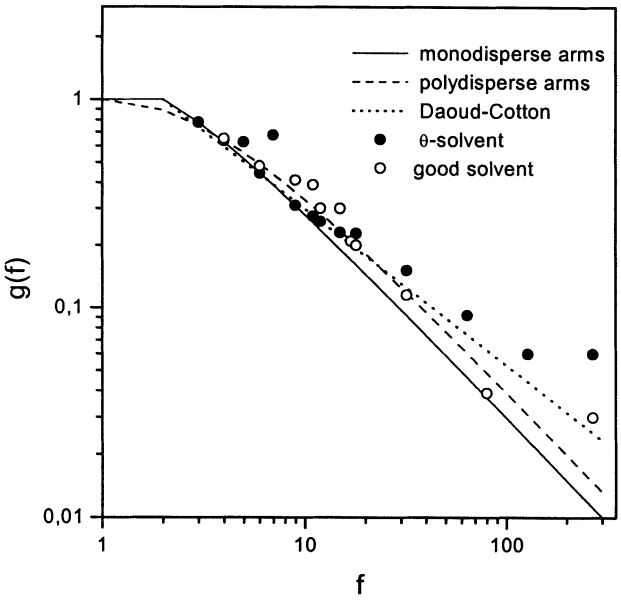

Fig. 24. Contraction factors for star-branched macromolecules as a function of the number of arms. The *full line* represents strictly regular stars, the *dashed line* one that for stars with polydisperse arms (M_w/M_n=2), the *dotted line* according to Daoud and Cotton [29]. The symbols represent the data from the literature. The deviation at large f represents the stretching of the arms due to overcrowding

The calculations were later reproduced by Kajiwara [97] following a different route. For the exact equation the original paper may be consulted.

An experimental verification of Eqs. (65)–(67) has not yet been possible because the MALLS instrument that allows measurement of R_g has only recently become available in laboratories. Furthermore, the combination of the MALLS with the VISC detector is not a trivial problem. Several experiments are, however, in progress. This work is of great importance since a quantitative estimation of the branching density would be possible if the Zimm-Stockmayer equations for the g-factor hold true.

The relationships of Eqs. (65)–(67) are not the same as the g factors for regular stars. This is easily understood since Eqs. (65)–(67) refer to fractions which still remains an ensemble that contains a distribution of isomers of different architecture but the same molar mass. The equation for the stars can be derived from Eqs. (29) and (29'):

$$g = \frac{3f-2}{f^2} \tag{29''}$$

for regular stars with monodisperse arms [49] and from Eqs. (31) and (31') [24,52]:

$$g_{(z)} = \frac{3f}{\left(f+1\right)^2} \tag{31"}$$

for stars with f polydisperse arms.

Figure 24 shows the dependence on the number of arms for the two examples and experimental data from the literature.

Much easier, and with higher precision, on-line intrinsic viscosity measurements are possible. Unfortunately, new problems arise from the insufficiently well known interdependence between g' and g. The relationship between the intrinsic viscosity and the radius of gyration is fairly well settled for linear chains [3, 71] and is satisfactorily described by the Fox-Flory equation (Eq. 21), but for the branched chains the Φ-factor for branched chains may be different. In general one has [49]

$$g' = \frac{\Phi_b}{\Phi_{lin}} \frac{R_{g,b}^3}{R_{g,lin}^3} = \Phi^*\left(g\right) g^{3/2} \tag{68}$$

Thus a simple power law behavior with an exponent of 1.5 would result if $\Phi^* = 1$ [125]. Zimm and Kilb [128] made a first attempt to calculate g' for star branched macromolecules on the basis of the Kirkwood-Riseman approximation for the hydrodynamic interaction. They came to the conclusion that

$$g' \cong g^{1/2} \qquad \text{Zimm \& Kilb} \tag{69}$$

would be a good approximation. Equation (69) suggests the very strong g-dependence of $\Phi^*(g)$ of

$$\Phi^*(g) = g^{-1} \qquad \text{Zimm \& Kilb} \tag{70}$$

Such behavior has not been observed. Kurata et al. [129] developed an empirically based suggestion after comparing the results available in those days for star molecules. He also assumes power law correlation between the two contraction factors as given by

$$g' \cong g^b \tag{71}$$

but with an exponent of b=0.6, which would give

$$\Phi^*(g) = g^{-0.9} \tag{72}$$

Table 3. Experimentally determined contraction factors $g = R^2_{g\,b} / R^2_{g\,lin}$ and $g' = [\eta]_b / [\eta]_{lin}$ for various star molecules in θ- and good solvents

Polymer	θ-solvent		good solvent		Ref.
	g	g'	g	g'	
Polystyrene	Cyclohexane (35 °C)		Toluene		
f=4	0.63	0.76	0.65	0.72	[26, 130, 131]
f=6	0.46	0.63	0.48	0.57	[26, 131]
f=4	0.64	.077	0.65	0.68	[26, 131]
f=6	0.423	0.57	0.48	0.46	
f=3	0.778	0.85			[26, 132]
f=4.75	0.625	0.85			
f=7	0.675	0.514			[26, 133]
f=8.7	0.31	0.41	0.41	0.41	
f=10.7	0.275	0.39	0.39	0.39	
f=12.3	0.26	0.36	0.36	0.36	
f=15.3	0.23	0.30	0.30	0.30	
f=12	0.276	0.41	0.24	0.35	[77]
f=18	0.228	0.35	0.20	0.26	
Polybutadiene	Dioxane (26.5 °C)		Cyclohexane (25 °C)		
f=32	0.151	0.198	0.115	0.154	[108]
f=64	0.092	0.127		0.083	[25]
f=128	0.060	0.0805		0.044	
PS-DVB			THF		
f=17			0.209	0.260	[76]
f=80			0.039	0.133	
Polyisoprene	Dioxane (34 °C)		Toluene		
f=4	0.65	0.772		0.733	[26, 134]
f=6	0.46	0.625		0.589	
Polybutadiene	Dioxane (26.5 °C)		Cyclohexane		
f= 270	0.06	0.045	0.03	0.029	[135]

In the meantime the precision in preparing well defined star molecules and measuring g and g' have been significantly improved. Table 3 gives a list of the data from the literature, and Fig. 25 demonstrates this dependence. Evidently the experimental data cannot be described by a power law. A possible fit curve is given by the equation [110]

$$g' = \left[a + (1-a)g^p\right]g^b \tag{73}$$

with a=1.104; p=7; b=0.906

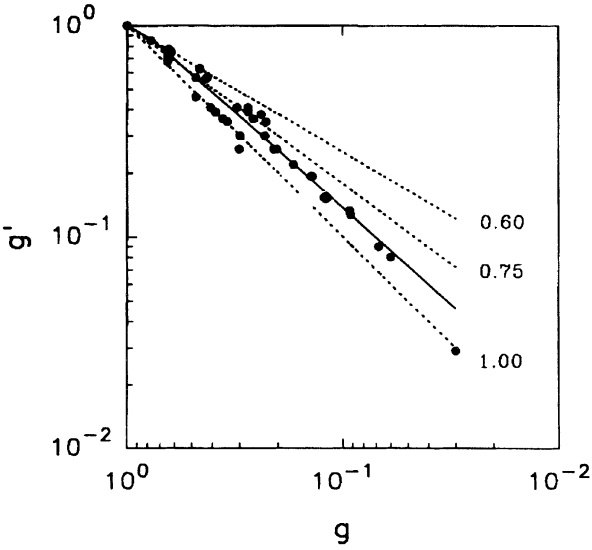

Fig. 25. The viscosity contraction factor g' as a function of the geometric contraction factor g for star-branched macromolecules (f=3–128). No distinction was made between the chemical nature of the various arms and between the thermodynamic quality of the solvents used. See Table 3

This relationship fulfills the condition of $g'=1$ at $g=1$ and attains a power law proportional $g'=a\ g^b$ for very small g. The exponent p defines how quickly the asymptotic power law is obtained.

There seems to exist a certain dependence on the solvent quality, but within the experimental error the difference cannot be described as statistically significant. Therefore, all available data were plotted on Fig. 25 without distinguishing them by special symbols.

6.5
Application to Randomly End Linked Star-Branched Polystyrenes

We come back to the interpretation of the viscosity behavior of the fractions from randomly branched samples. Some examples were given in Figs. 22 and 23. The contraction factors g' from these samples are plotted in Fig. 26. The attempt to describe the curves for the fractions by the Zimm-Stockmayer relationship of Eq. (65) by applying Eq. (73) led to the dashed curve, that evidently gave no agreement with the experimental findings. The fit of the curve with Eq. (73) leaving the exponents p and b and the parameter a free fitting parameters leads to

$$b=0.63, \qquad p\approx 7000, \qquad a=1.04$$

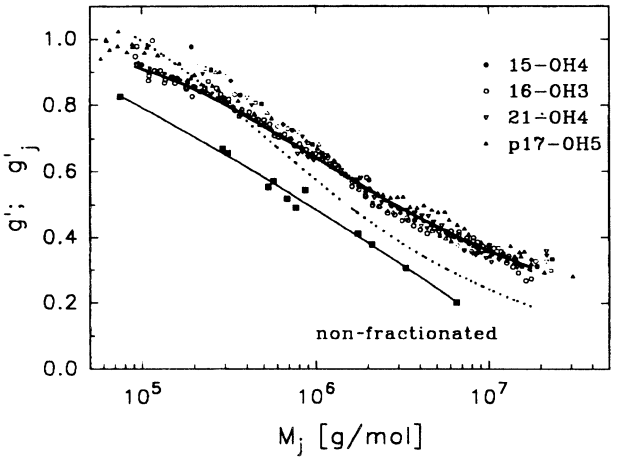

Fig. 26. Molar mass dependence of the g' factor for three pregel and one postgel fraction of end linked PS stars. A good fit was obtained with the Zimm Stockmayer equation (Eq. 69) and an exponent in Eq. (70) of $b \approx 0.63$ [95] which agrees well with Kurata's estimation with $b \approx 0.6$ [129]. Reprinted with permission from [129]. Copyright [1972] American Society

The value of $p \approx 7000$ makes the term $(1\text{-}a)g^p << a$ and thus gives practically the result of Kurata's estimation [129]. This observation leads to the conclusion that it is not the total number of branching units in the branched cluster that defines the type of the g' dependence on g, but very likely it is the functionality of the repeating unit. However, further experiments with $f=4$ have to be made before a well established statement can be made.

A remark had previously been made in various places of the text that the Φ_b parameter will increase with branching or more precisely with the g-factor. This g-dependence must necessarily also result in a molar mass dependence of Φ_b for which a power law behavior was tentatively assumed. From the KMHS-relationship one then finds [95]

$$\left[\eta\right]_b = K_\eta M^{a_\eta} = \Phi_o \left(\frac{M}{M_o}\right)^{a_\Phi} \frac{R_{g,b}^3}{M} = KM^{a_\Phi + \frac{3}{d_f} - 1} \tag{74}$$

or

$$a_\Phi = a_\eta + 1 - \frac{3}{d_f} \tag{75}$$

Thus the molar mass dependence of the Φ-parameter can be estimated when, besides the a_η exponent, the fractal dimension of the clusters could be measured. This fractal dimension can be obtained from the molar mass dependence of the radius of gyration of the fractions, or from the angular dependence of the

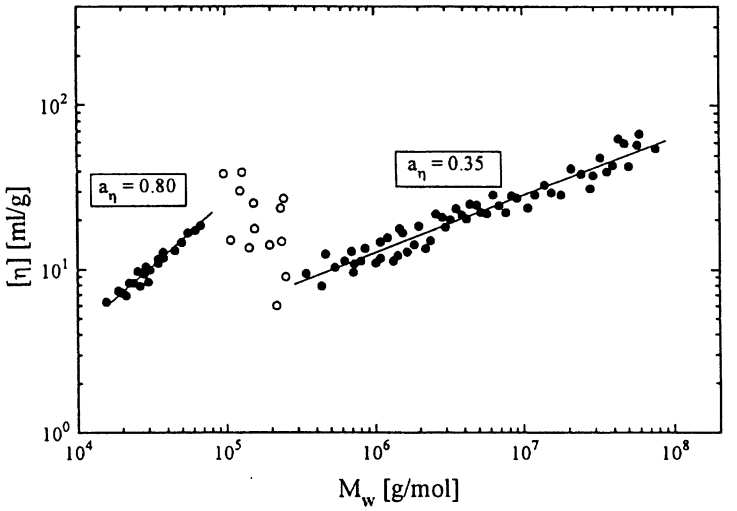

Fig. 27. Molar mass dependence of *[η]* for a fractionated comb macromolecule. The fractionation was made with a SEC/LALLS/VISC set-up. The comb macromolecule consists of a polyimidazole backbone prepared by free radical polymerization. The imidazol side groups acted in a melt with phenylglycidylether and phthalic anhydride as multifunctional initiator for the anionic growth of polyester chains. The straight lines correspond to the behavior of unattached polyester chains and the comb polymers at low and high molar masses respectively [136]

scattered light at large values of $q=(4\pi n_o/\lambda_o)\sin(\theta/2)$ or from the molar mass dependence of the unfractionated samples where then the exponent τ of the size distribution has to be known [95, 110, 129]. In the case of the end-linked PS star molecules the fractal dimension has been estimated to d_f=2.63 and the exponent in the KMHS relationship is a_η=0.40, which gives a_Φ=0.26 and an increase of the Φ_b parameter by a factor of about three in a molar mass region of about two decades. Because of the large experimental error these data can be taken only as a rough estimation. More precise measurements are needed to confirm the results. An increase of the Φ parameter due to branching was already considered by Zimm and Stockmayer as a possibility and was concluded by Roovers and Bywater [130, 131] from early measurements on star molecules.

This section on the contraction factor may be concluded with an example of a comb macromolecule [136]. Due to the route of preparing this comb, unattached side chains also occurred in the system. Figure 27 shows the result of the molar mass dependence of [η] which was obtained from a SEC/LALLS/VISC fractionation. One observes at low molar masses a straight line with an exponent of $a_{\eta,lin}$=0.70 that coincides with the exponents of linear side chains. It follows a chaotic scatter until finally another straight line is formed at large molar masses which has the much lower exponent of $a_{\eta,comb}$=0.34 and which is clearly assignable to the branched structure of the comb molecule. In this case, the occurrence

of two molar mass dependencies within one sample facilitates the determination of the contraction factor.

7
Generalized Ratios

7.1
The $R_g/R_h \equiv \rho$-Ratio

The analysis of the contraction factors g and g' presents a valuable possibility to determine the number of branching units per macromolecule or, in other words, the branching density. The technique has however the disadvantage that the data from linear chains as reference are needed. This reference is in many practical cases not known. Here the use of other universal ratios can be helpful in judging whether branching has occurred. In Sect. 3.3 it has already been mentioned that four different radii can in principle be obtained by the combination of different measurements. All these radii can be expected to show, at least asymptotically, the same molar mass dependence. Therefore, when forming the ratio of two of these radii the molar mass cancels. Since static and dynamic light scattering can in many laboratories now be performed simultaneously, it is reasonable to introduce the ratio [63, 137]

$$\rho \equiv \frac{R_g}{R_h} \qquad \textit{for the same molecule} \tag{76}$$

This ratio ρ_{lin}=1.504 is well known from the Kirkwood-Riseman theory of long linear chains in a Θ solvent with hydrodynamic interactions. (Instead of using the above defined ρ-parameter the reciprocal quantity ξ=1/ρ is sometimes used in the literature [138].) Corrections for the excluded volume were derived by Akcasu and Benmouna [139]. Furthermore, the ratio was also derived for star molecules and randomly branched and hyperbranched unfractionated and fractionated macromolecules, in the latter cases, however, only for particles without excluded volume interaction [24, 63]. Table 4 gives some examples. One realizes that this ratio reflects sensitively the actual segment density as a results of the corresponding hydrodynamic interaction. Unfortunately, the hydrodynamic interaction is not completely correctly treated by the Kirkwood-Riseman approximation [3, 88, 126]. This fact was suspected many years ago but was experimentally proven only several years later [24, 140, 141]. A clarification of the effect was finally given by the simulations of Freire and his coworkers [85–87]. It turns out that the hydrodynamic interaction is somewhat underestimated in the Kirkwood-Riseman approach. The actual hydrodynamic radii are larger and the corresponding ρ-values are smaller by about 10–14%. In spite of this quantitative disagreement the ρ-parameter can be efficiently used as a valuable qualitative measure in judging what architectural structure may be present.

Table 4. The $R_g/R_h \equiv \rho$-ratio and parameter C in Eq. (14) for various polymer architectures. The C-parameter gives information on the internal flexibility (C=0 inflexible particles, C= 0.2 flexible chain behavior)

Architecture	ρ	C	Ref.
Homogeneous (hard) sphere	0.778	0.00	
Random coil, linear chain, monodisperse			[24, 63]
θ-conditions	1.504	0.173	
good solvent	1.78	–	
Random coil, linear chain, polydisperse			[24, 63]
θ-conditions	1.73	0.200	
good solvents	2.05	–	
Regular stars, uniform arm length			[24, 63]
θ-conditions, f=4	1.333	0.148	
θ-conditions, f>>1	1.079	0.098	
Regular stars, polydisperse arms			[24, 63]
θ-conditions f=4	1.534	0.178	
θ-conditions f>>1	1.225	0.133	
Dendrimers n>10 (Gaussian "soft sphere")	0.977	–	[24, 47]
Randomly branched (A_3-monomers)	1.732	0.200	[24, 52, 83]
Hyper-branched (AB_2-monomers), x_w>>10	1.225	0.133	[24, 52]
Cyclic chain, monodisperse	1.253	0.133	[150, 151]
Stiff rings (N>3)	$\propto(1/\pi)\ln N$	–	[150, 151]
Stiff rods (N>3)	$\propto\sqrt{1/3)\ln N}$	–	[150, 151]
Microgels	0.3–0.6	–	[24, 65]

7.2 The Ratio $A_2M_w/[\eta]$

In principle all combinations of universal ratios of the four radii can be formed. A useful combination, however, is the ratio of $R_T/R_{[\eta]}$, where the two radii are related to the second virial coefficient and the intrinsic viscosity as outlined in Eqs. (21) and (22). Likewise one could form the ratio [6, 142–145]

$$V_{A_2\eta} \equiv \frac{A_2 M_w}{[\eta]} = \frac{4\nu_{eq}}{\nu_\eta} = \frac{\pi^{1/2} 6\Psi_b^*}{5\ \Phi_b} \tag{77}$$

This equation has the advantage of being more sensitive than the g- parameter, because volumes are compared rather than radii. It also gives us some information on how the coil interpenetration function Ψ^* changes in comparison to the draining function Φ as a result of the increase in the segment density. There exist at present only a few theoretical considerations of this effect [142–144]. Well documented is the behavior of linear chains. Here an asymptotic constant value is found only at fairly high molar masses that accounts to $V_{A_2\eta,lin} = 1.07 \pm 0.03$ [6]. For hard spheres the corresponding value is $V_{A_2\eta,sphere} = 1.60$. For the other

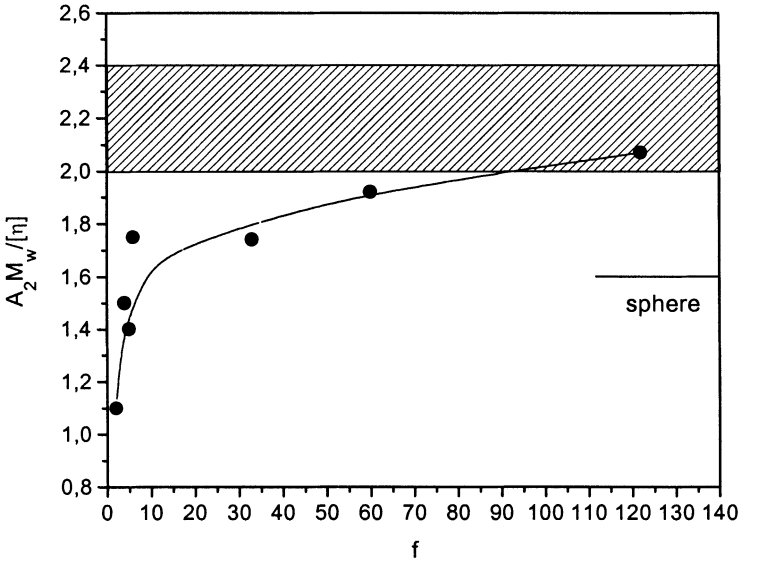

Fig. 28. The ratio $A_2M_w/[\eta]$ at large M_w for star molecules (symbols) and randomly branched structures [25, 26, 108, 130, 131]. The *shaded area* indicates the range of the experimental findings with randomly and hyperbranched samples [144]. The *line* was drawn to guide the eye

structures only experimental data are known. Figure 28 shows some examples. Accordingly, this ratio seems to increase with branching. This result appears to be sensible since the interpenetration of two polymers will be more strongly inhibited than the penetration of small solvent molecules into a coil when the segment density is increased. As a consequence Ψ^* should increase more rapidly than Φ, and the ratio $V_{A_2\eta}$ should increase. In the limit of a hard sphere with an impenetrable periphery no interpenetration of macromolecules and no penetration (draining) of the solvent can occur. Unexpectedly the $V_{A_2\eta}$ ratio of the hard sphere appears to lie below that of randomly branched samples. This effect is not yet understood, but it appears that the not well defined periphery in star molecules is the reason for the wider range of thermodynamic than of hydrodynamic interactions. At this point it is necessary to emphasize that the asymptotes for A_2M_w and $[\eta]$ are not approached in the same manner. For linear chains the asymptote of the ratio $V_{A_2\eta,lin}$ is only slowly approached *from below* [6]. In the case of the end-linked PS star molecules, however, it is approached *from above* [120]. In the former case the intrinsic viscosity evidently approached the asymptotic behavior earlier than the second virial coefficient, whereas for the end-linked PS stars the situation is opposite. The data, plotted in Fig. 28, are assumed to lie already in the asymptotic regime. There are, however, still too few experimental data, or existent data have not yet been evaluated, to ascertain the dependence shown in Fig. 28. A detailed discussion was given in [144].

Another uncertainty arises from the influence of polydispersity. Intrinsic viscosity data were mostly obtained from fractions but the second virial coefficient data were chosen from unfractionated samples. The resulting error is probably not large since A_2 depends only slightly on the width of the distribution [183, 184].

7.3 The Ratio R_T/R_h

This ratio of radii was introduced by Akcasu et al. [146, 147] and discussed in detail for linear chains. It compares the range of thermodynamic interactions with that of hydrodynamic interactions. Although no really satisfactory theory could be derived, this ratio of radii might be a sensitive measure of branching. Experiments mostly demonstrate that the ratio is close to unity which means that the thermodynamic and hydrodynamic interactions act over very similar distances. This observation seems to hold for linear as well as for branched structures [144]. The quantity will not be discussed further as this ratio has not been much used up to now. Two recent result may be mentioned however. Data with polybutadiene star molecules in a good solvent with f=32, 64, and 128 arms respectively yield ratios of 1.18±0.01 for short arms that decreases to 1.06±0.01 for long arms [25, 108]. The second example is related to fractions of end-linked star-molecules [120]. The results are shown in Fig. 29. In the limit of unreacted three-arm starmolecules again a value of R_T/R_h=1.0±0.05 is obtained.

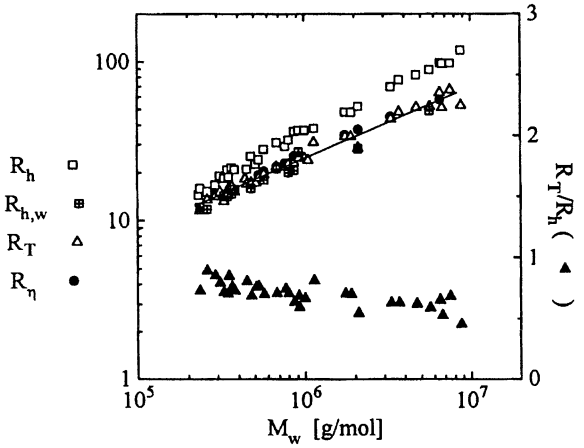

Fig. 29. Molar mass dependence of the radii R_T, R_η, $R_{h,w}$, R_h and of the ratio R_T/R_h. The *straight line* corresponds to the linear regression of the R_T-data and has a slope of 0.46 [120]

8
Semi-Dilute Solutions

8.1
General Remarks

The determination of molecular parameters is bound to very dilute solutions in which on average the macromolecules are widely separated from each other. Due to thermal fluctuations two molecules can still come together, but such occasions will be rare and at most two molecules will have a noticeable chance to collide but a collision of three particles at the same time can be disregarded. This means that only the effects of the second virial coefficient has to be taken into account and all higher terms can safely be neglected. For covalently bound architectures the effect of the second virial coefficient can be eliminated without difficulties by extrapolating the measured quantities towards zero concentration. Besides their academic relevance the molecular parameters are of special interest to all preparative chemists who wish to know whether their synthesis has been successful in the way it was intended. Recently, this question has become increasingly important because of the effort in preparing special supermolecular structures. The branched structures are one of these possible architectures. In this section it will be shown that the various molecular parameters are also necessary prerequisites for the description of semi-dilute solutions in a universal form.

The regime of semi-dilute solutions comprises still a rather dilute concentration regime and exceeds only in rare case a concentration of 10%. Nonetheless there exists a rather incisive boundary between very dilute and semi-dilute solutions which is characterized by the so-called overlap concentration c^* [4, 151, 153]. At this concentration the macromolecules, which require a considerable volume in the solution, start to touch each other. An instructive definition for c^* consists of the point where the weighed-in concentration equals the average segment concentration in a macromolecule. At higher concentrations, $c>c^*$, there remain only two possibilities: either the segment clouds from two or more macromolecules interpenetrate, or the highly swollen macromolecules become compressed. De Gennes [4] and des Cloizeaux [154] claimed that the mutual coil penetration is the dominant effect. Innumerable experiments with linear chains have shown that their predictions are indeed correct. Of course, flexible [18] chains can yield when they collide, and the result will be the above-mentioned overlap of different coils. Because of the repulsive interactions among the segments an appreciable energy is required to accomplish the undesired increase of segment crowding.

Branched polymers can also be dissolved at fairly high concentrations. Because of the higher segment density in the isolated macromolecules the overlap concentration will also be increased. For this reason the semi-dilute regime of branched polymers may in some cases be larger than for linear chains, say about 20% or more. Clearly, however, a full interpenetration, as was assumed for flex-

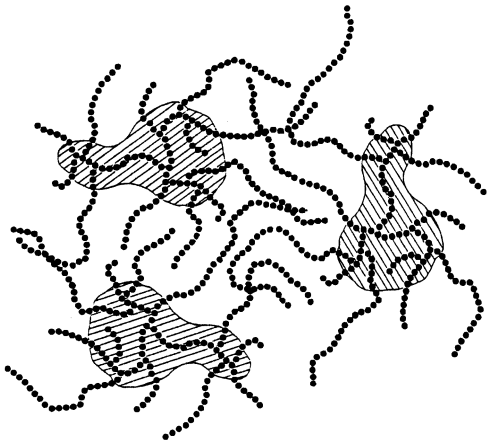

FFig. 30. Schematic representation of branched macromolecules at semi-dilute concentration, $c>c^*$. Only the essentially non-branched chains from the outer shells can interpenetrate. The *shaded area* remains excluded because of the obstacles formed by the branching points [166]. Reprinted with permission from [166]. Copyright [1997] American Society

ible linear chains, can no longer be accomplished with branched macromolecules. The branching points evidently form obstacles which can no longer be circumvented, and the second alternative, i.e., a compression of the macromolecules will occur. Figure 30 demonstrates this effect.

Most important, however, was the discovery by Simha et al. [152, 153], de Gennes [4] and des Cloizeaux [154] that the overlap concentration is a suitable parameter for the formulation of universal laws by which semi-dilute solutions can be described. Semi-dilute solutions have already many similarities to polymers in the melt. Their understanding has to be considered as the first essential step for an interpretation of materials properties in terms of molecular parameters. Here now the necessity of the dilute solution properties becomes evident. These molecular solution parameters are not universal, but they allow a definition of the overlap concentration, and with this a universal picture of behavior can be designed. This approach was very successful in the field of linear macromolecules. The following outline will demonstrate the utility of this approach also for branched polymers in the semi-dilute regime.

8.2
Suitable Choice for the Overlap Concentration

So far, the effects of semi-dilute solutions are qualitatively clear. Ambiguity comes in, however, when the overlap concentration has to be defined quantitatively. This ambiguity arises from the fact that the volume of a macromolecule cannot be uniquely defined. Because of the segment mobility the shape of a macromolecule varies in time such that only a statistical description can be made. As

was already outlined in the beginning of this contribution one can define four different radii which, due to physical processes, are differently weighted with respect to their segment density distribution. Accordingly also four different definitions for the overlap concentration can be given. These are

$$c^*_{R_g} = \frac{M_w}{(4\pi/3)N_A R_g^3} \tag{78a}$$

$$c^*_{Rh} = \frac{M_w}{(4\pi/3)N_A R_h^3} = \frac{\rho^3}{(4\pi/3)N_A}\frac{M_w}{R_g^3} \tag{78b}$$

$$c^*_{A_2} = \frac{1}{A_2 M_w} = \frac{3}{16\pi N_A}\left(\frac{M}{R_g^3}\right) = \frac{1}{4\pi^{3/2} N_A \Psi^*}\left(\frac{M}{R_g^3}\right) \tag{78c}$$

$$c^*_{\eta} = \frac{1}{[\eta]} = \frac{1}{\Phi}\left(\frac{M}{R_g^3}\right) \tag{78d}$$

with

$$\rho = \frac{R_g}{R_h}$$

Even if differences in the averages are neglected one has the following changes when $c^*_{R_g}$ is chosen as reference

$$\frac{c^*_{R_h}}{c^*_{R_g}} = \rho^3 \tag{79a}$$

$$\frac{c^*_{A_2}}{c^*_{R_g}} = \left(3\pi^{1/2}\Psi^*\right)^{-1} = 0.188/\Psi^* \tag{79b}$$

$$\frac{c^*_{\eta}}{c^*_{R_g}} = \left(2.522\times 10^{24}\right)/\Phi \tag{79c}$$

The differences in the overlap concentrations are instructively demonstrated by Fig. 31 for amylopectin fractions [144], which are representatives for hyperbranched structures.

However, the choice of $c^*_{R_g}$ as reference is not advisable, because R_g is a z-average while M_w is a weight average. Even for monodisperse samples the various definitions are not equivalent. Therefore $c^*_{R_g}$ is a quantity that strictly de-

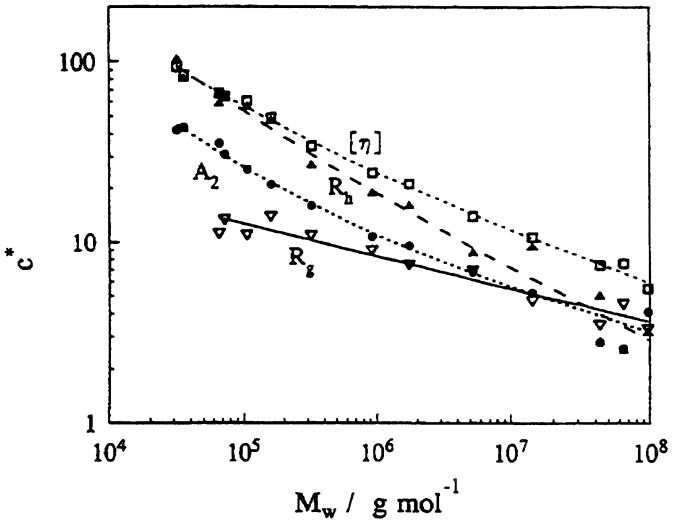

Fig. 31. Molar mass dependencies of four differently defined overlap concentrations c^*(ml/g) for amylopectin fractions in 0.5 mol/l NaOH [144]. Reprinted with permission from [144]. Copyright [1996] American Society

pends on the molecular polydispersity and will give a considerably distorted picture of the actually occurring segment overlap. On the other hand, $c*_{Rh}$ and $c*_{\eta}$ are governed by hydrodynamic interactions. The only consequent and consistent procedure consists in the choice of $c*_{A_2}$ when thermodynamic interactions are considered [6] and $c*_{\eta}$ when rheological properties are discussed [144].

8.3 Osmotic Modulus

As demonstrated in a previous section the osmotic compressibility can be obtained from the forward scattering of light

$$\frac{R_{\theta=0}}{Kc} = RT\left(\frac{\partial c}{\partial \pi}\right) \tag{80}$$

In order to have a suitable connection to the well understood dilute solutions it was suggested by Debye to use the reciprocal of the osmotic compressibility, which for convenience will be called the osmotic modulus

$$\frac{Kc}{R_{\theta=0}} = \frac{1}{RT}\frac{\partial \pi}{\partial c} \equiv \frac{1}{M_{app}(c)} \tag{81}$$

Developing the osmotic pressure in a virial series one obtains

$$\frac{1}{M_{app}(c)} = \frac{1}{M_w} + 2A_2 c + 3A_3 c^2 + \ldots \tag{82a}$$

or

$$\frac{1}{M_{app}(c)} = \frac{1}{M_w}\left[1 + 2A_2 M_w c + 3A_3 M_w c^2 + \ldots\right] \tag{82b}$$

The expression in brackets represents the interparticle interactions. It gives the contribution by which the true molar mass is modified to yield the measurable apparent molar mass $M_{app}(c)$, which is a function of the concentration. A dimensionless quantity can be obtained by multiplying Eq. (78b) with M_w, which will be called the reduced osmotic modulus

$$\frac{M_w}{RT}\frac{\partial \pi}{\partial c} = \frac{Mw}{M_{app}(c)} = 1 + 2A_2 M_w c + 3A_3 M_w c^2 + \ldots \tag{83}$$

The next step is whether the right side can also be transformed in a scaled form. Two observations encourage such an expectation. The first has long been known and states that all higher virial coefficients for hard spheres can be expressed in terms of the second one [74, 75]

$$A_3 M = g_a\left(A_2 M\right)^2 = g_a\left(c / c^*_{A_2}\right)^2 \tag{84a}$$

$$A_3 M = g_{A_4}\left(A_2 M\right)^3 = g_{A_4}\left(c / c^*_{A_2}\right)^3 \tag{84b}$$

etc.where the first five coefficients up to g_{A_7} are exactly known, and for two further virial coefficients good approximations exist [74, 75]. In particular for the first one g_a=0.625 was obtained. The second observation is concerned with flexible linear chains for which des Cloizeaux [154] and de Gennes [4] postulated the asymptotic behavior of

$$\frac{M_w}{RT}\frac{\partial \pi}{\partial c} \propto \left(c / c^*_{A_2}\right)^m \tag{85}$$

with an exponent of m=5/4. This scaling result was subsequently confirmed by renormalization group theory [6], which in addition gave the prefactor and an approximate analytical equation that covered the whole region from the dilute to semi-dilute concentrations. Also for these linear chains a g_a=0.269 could be derived that is close to an earlier estimation of g_a=0.25 by Stockmayer and

Casassa [155] but is different from 0.625 for hard spheres. These two results suggests quite generally for self-similar objects

$$\frac{M_w}{M_{app}(c)} = f\left(X, architecture\right) \tag{86}$$

with

$$X = c / c^*_{A_2}$$

8.4 Star-Branched Macromolecules

This conjecture was found to hold for flexible chains, stiff worm-like chains, star macromolecules, and hard spheres [156]. A few results are shown in Fig. 32.

The architecture dependence is also demonstrated in Fig. 33 by the g_a factors of several star macromolecules, flexible cyclic chains. Randomly and hyperbranched materials show a more complex behavior because of the large width in the molar mass distribution. Table 5 gives the actual values. The plot of Fig. 33 shows nicely how for a large number of arms the factor for hard spheres is approached.

The factors g_a were determined in these cases by a virial expansion that was truncated with the third virial coefficient. In this case one has

$$\frac{M_w}{M_{app}(c)} = 1 + 2X + 3g_a X^2 \tag{87}$$

For a fit of experimental data it is more advantageous to use the scattering intensity itself. In terms of the approximation of Eq. (83) one first obtains

$$\frac{R_{\theta=0}}{K} = \frac{cM_w}{1 + 2X + 3g_a X^2} \tag{88}$$

then multiplying this equation with the second virial coefficient one arrives at

$$\frac{\mathrm{A}_2 R_{\theta=0}}{K} = \frac{X}{1 + 2X + 3g_a X^2} \tag{89}$$

which again is a scaled function. Figure 34 shows the plot for some of the star molecules in comparison to hard spheres, flexible, and stiff linear chains. The curves show a maximum around X=1 whenever g_a is positive. Interestingly for stiff chains the g_a is very small and the corresponding curve displays no maximum.

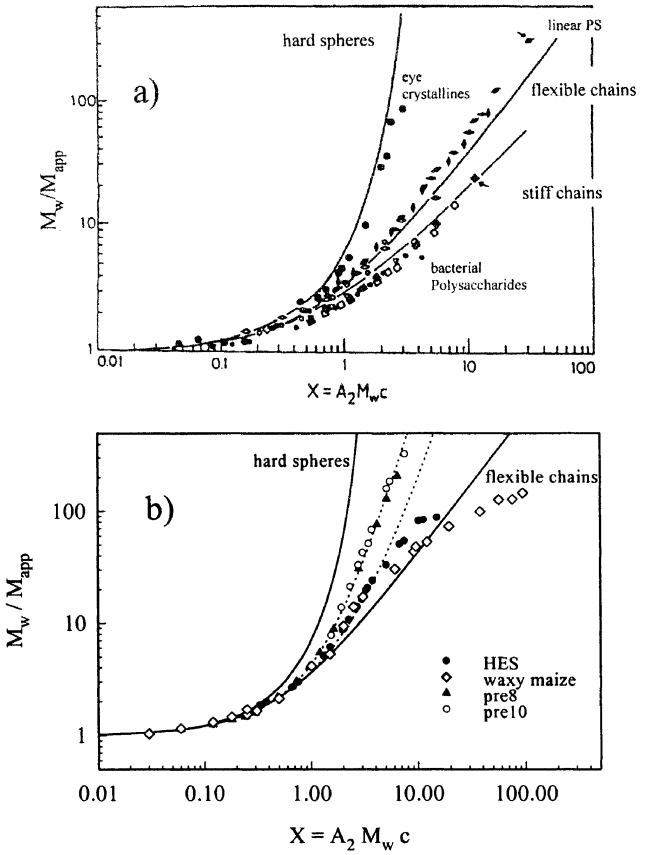

Fig. 32a,b. Plot of the reduced osmotic modulus $M_w/M_{app}(c)$ as a function of reduced concentration $X = A_2 M_W c \equiv \left(c / c^*_{A_2} \right)$. The *solid lines* represent theoretical curves for the osmotic modulus from hard spheres [157], random coils [158] and stiff chains [159].
a Measurements from eye crystallines by Delay et al. [160, 161] as examples for hard spheres, to linear polystyrene samples in toluene for molar masses between M_w=150,000 up about 7×10^6 [156] and to various bacterial polysaccharides, which formed double helices [162–164].
b Randomly branched (pre8, pre10) and to hyperbranched materials (HES and waxy maize). Reprinted with permission from [157]. Copyright [1969] American Society

At this point two essential remarks have to be added. The first is concerned with the reduced concentration $X = A_2 M_W c = c^*_{A_2}$ which is a rather universal scaling parameter. It indicates the fact that the same master curve is obtained whether for a special sample the concentration is changed or the molar mass is varied. Even the solvent can be changed as long as the good solvent condition remains fulfilled, i.e., the coil interpenetration function $\Psi(z)$ should have reached its plateau value Ψ^*. Finally it may be noticed that at no stage of this outline did the chemical nature of the sample have to be introduced. In fact, measurements

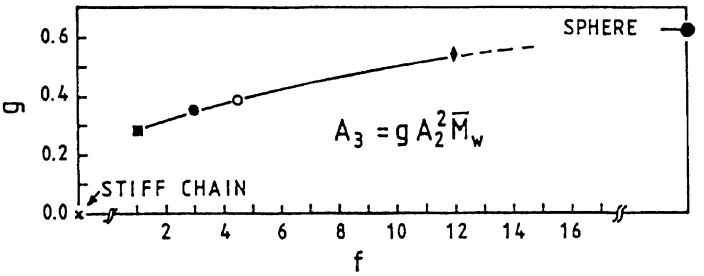

Fig. 33. Plot of the g_a factors against the number of arms for star macromolecules (●), star-branched and stiff macromolecules [156]. The cyclic chain corresponds to stars with f=4.5 (○). Reprinted with permission from [156]. Copyright [1990] American Society

Table 5. Values of the parameters $\hat{g}_a$ and $\hat{h}_a$ in Eq. (91) for linear and cross-linked polyester chains and for various fractions of amylopectin fractions obtained by a controlled acid hydrolysis [177]

Anhydride cured epoxies [165]						
Sample	$M_w \times 10^{-6}$ g/mol	$\hat{g}_a$	$\hat{h}_a$	a_{A_2}	m_{ex}	m_{th} Eq. (96)
Linear	0.103	0.134	0	0.24±0.07	1.50	1.36±0.11
pre5	0.172	0.183	0.067	a	1.70	a
pre8	1.77	0.124	0.211	0.65±0.04	2.40	2.86±0.36
pre10	13.6	0	0.308	0.65±0.04	2.40	2.86±0.36
Starch [144]						
Fractions	$M_w \times 10^{-6}$ g/mol	$\hat{g}_a$	$\hat{h}_a$	a_{A_2}	m_{ex}	m_{th} Eq. (96)
	0.035–5.2	0.18±0.03	0.03±0.01	0.61±0.03	2.2	2.59±0.16

[a] Transition region

from a water soluble polymer (polyvinyl caprolactam) and from cellulose tricarbanilate in dioxane have been included in Fig. 32 (open symbols). They all fall on the curve for flexible linear chains. Similar universality was also found for the stiff chain bacterial polysaccharides which form double helices, no more than five Kuhn segments in length [162–164]. The data from polybutadiene star macromolecules [167] seem to deviate slightly from those of polystyrene stars with the same number of arms. It is difficult to judge whether this is a real effect or whether it is only a question of a systematic error. In spite of improvements in the construction of static light scattering instruments, sometimes it still remains problematic to compare the data from different laboratories.

The second remark concerns the results for the third virial coefficients obtained by Japanese colleagues around Teramoto [168–170]. The authors applied

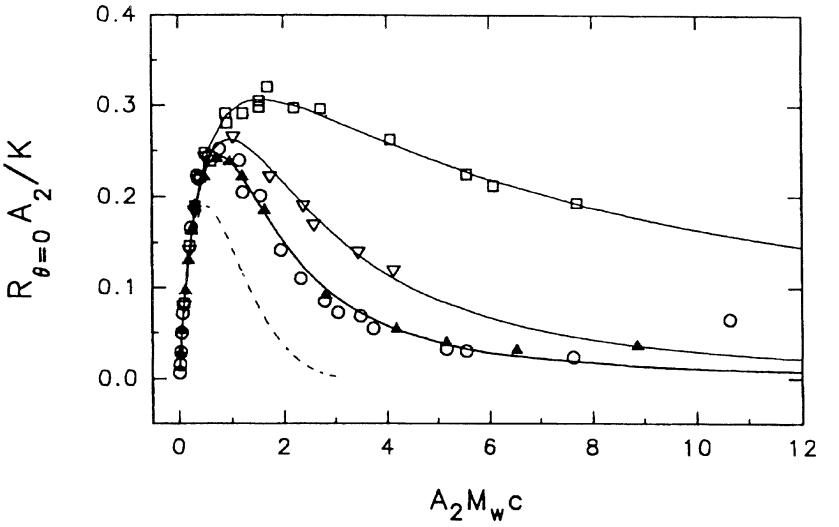

Fig. 34. Plot of the scaled forward scattering intensity (see Eq. 89) as a function of $X=A_2M_wc$ for some selected molecular architectures [165]. ❑ linear polyester; ❍, Δ cross-linked polyesters near the ge-point, ∇ weakly cross-linked polyester (see Table 5)

a different technique that was first suggested by Bawn et al. [171]. Here the slope of the forward scattering between two concentrations is determined and these values are plotted against (c_1+c_2) according to the following relationship:

$$\left[\left(\frac{Kc}{R_{\theta=0}}\right)_{c_2}-\left(\frac{Kc}{R_{\theta=0}}\right)_{c_1}\right]/\left(c_2-c_1\right)=A_2+A_3\left(c_1+c_2\right) \tag{90}$$

A straight line is expected if all virial coefficients larger than A_3 are neglected. The slope gives the third virial coefficient and the intercept the second one. The Japanese group found essentially the same values for g_a with the exception that for very high molar masses a continuous increase of about 25% was found. The plot is essentially equivalent to a suggestion by Stockmayer and Casassa [155]. Roovers et al. [172] checked the Bawn procedure with the conventional one and found no difference between the various techniques.

Possibly the increase in the g_a factor at high molar masses contains a hidden systematic error. Inspection of the curves in Fig. 34 reveals that the fit with the truncated Eq. (89) holds only for values of $X<2$ and sometimes up to $X=4$. At larger concentrations a fit becomes possible only when a further term in Eq. (89) is added:

$$\frac{R_{\theta=0}}{K}=\frac{cM_w}{1+2X+3\hat{g}_aX^2+4\hat{h}_aX^3} \tag{91}$$

Here now both coefficients $\hat{g}_a$ and $\hat{h}_a$ vary with the molar mass in a manner such that $\hat{g}_a$ decreases while $\hat{h}_a$ increases. This mutual dependence of the two parameters clearly demonstrate that the new parameters no longer correspond to true virial coefficients. Equation (91) has now to be considered as a semi-empirical fit relationship. For an accurate determination of the correct g_a factor the fit should be restricted to a region of $X<1$, Roovers even demands $X<0.5$ [172]. The influence of higher virial coefficients may not be easily detected in the Bawn treatment, and a weak curvature may look within experimental errors like a straight line. Unfortunately, the Japanese authors avoided scaling arguments and did not check whether their points of measurements from different molar masses would form one common master curve. It may be noted, however, that very similar results were also obtained by the Japanese authors when the high molar mass region is disregarded.

8.4.1
Randomly Branched and Hyper-Branched Macromolecules

At present, there are only a few experimental results known on the osmotic modulus of randomly branched macromolecules or randomly cross-linked chains in the semi-dilute regime. One possible explanation for this lack of data may be based on the prejudice that the universality predicted by de Gennes [4] for linear chains will hold in the same manner also for branched materials. In particular it is expected that the individual characteristics of the macromolecules are lost due to the strong overlap of the segments from different macromolecules. The following data, mainly from the author's own research group, revealed however, that the characteristics of the special architectures are not lost.

Figure 35 shows the result for the scaled forward scattering from randomly cross linked polyester chains which were prepared by anhydride curing of phenylglycidylether in the presence of bisphenol A diglycidylether [173–175]. The data could be fitted with Eq. (91) with values for $\hat{g}_a$ and $\hat{h}_a$ which are collected in Table 5.

For low extents of crosslinking the curves lie between the limits of the curve near the gel point and that for linear chains. This behavior is understood when recalling that at low crosslinking the system mainly consists of linear chains. The highly crosslinked chain on the other hand approaches a molar mass independent master curve that, as expected, lies in the region of hard sphere behavior.

The results for the osmotic modulus from amylopectin fractions are shown in Fig. 32b. The curves could be fitted by the $\hat{g}_a$ and $\hat{h}_a$ parameters as given in Table 5. Interestingly, the same curve was obtained with the non-degraded native waxy maize (pure amylopectin) in water, with the amylopectin fractions from potato starch in 0.5 mol/l NaOH and with hydroxyethyl starches (from amylopectin) again in water. Amylopectin has a branching density of 4–5% and is a typical representative of hyperbranching polymers. Unexpectedly, the curve for these samples runs below that of the crosslinked polyester chains. The hyperbranched materials have a much larger number of branching units than the ran-

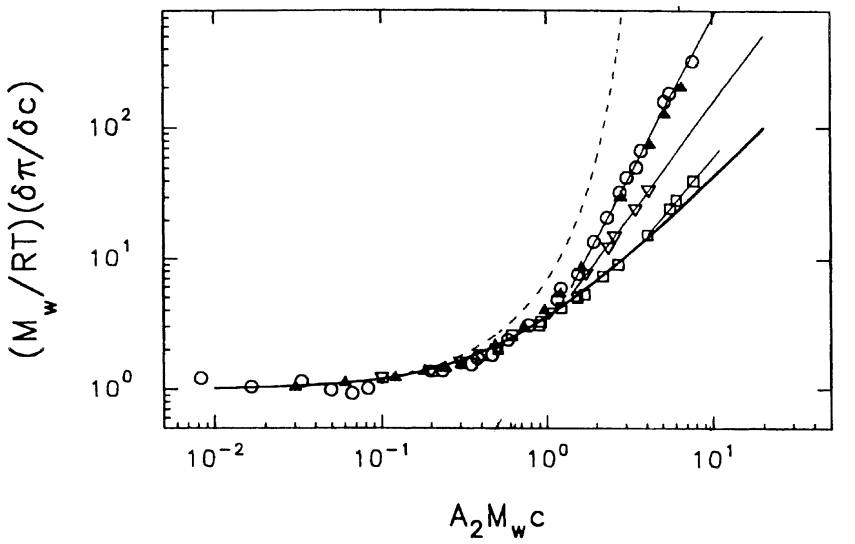

Fig. 35. Plot of the reduced osmotic modulus from anhydride cured linear and cross-linked phenylglycidylethers [165, 173–175]

domly crosslinked chains and should thus show more similarity to hard sphere behavior. The reason for the unexpected findings is not yet clear. One may speculate that not the *number* of branching units would be the essential parameter but rather the *functionality* of the branching units. This functionality is four in the crosslinked chains and three for the amylopectins. However, further results have to be collected before more definite conclusions can be drawn.

8.5 Asymptotes for the Reduced Moduli

Des Cloizeaux [154] and de Gennes [4, 176] suggested an asymptotic power law for linear chains when $X>>1$

$$\frac{1}{RT}\frac{\partial\pi}{\partial c} \rightarrow \frac{1}{M_w}X^m = \frac{1}{M_w}\left(A_2M_wc\right)^m \tag{92}$$

The exponent was determined from two conditions (Eqs. 93, 94):

- $\frac{1}{RT}\frac{\partial\pi}{\partial c} \propto M^0$ (independent of molar mass M_w) (93)
- $A_2 \propto M_w^{-a_{A_2}}$ (fractal behavior) (94)

Table 6. Relationship between the fractal dimension d_f the exponent a_{A_2} for the molar mass dependence of the second virial coefficient and the expected exponent m for the osmotic modulus when the scaling assumptions of Eqs. (93)–(96) are made. The experimental data were derived from the exponents for the second virial coefficient

d_f	a_{A_2}	m	Comments
		Theoretictal values	
1.70	0.235	1.30	linear chains
2.00	0.500	2.00	branched chains, fully swollen
2.50	0.800	5.00	branched chains, in melt
3.00	1.000	∞	hard sphere
		Experimental values	
2.16±0.05	0.61±0.03	2.56±0.11	starch fractions in 0.5 mol/l NaOH [144]
2.22±0.07	0.65±0.04	2.86±0.32	anhydride cured epoxies [93, 165]
2.14±0.08	0.60±0.05	2.50±0.41	end-linked star molecules in THF [120]

where

$$-a_{A_2} = \frac{3}{d_f} - 2 \tag{95}$$

with the fractal dimension d_f. The two conditions lead to

$$m = \frac{1}{1 - a_{A_2}} = \frac{d_f}{3 - d_f} \tag{96}$$

Table 6 gives a list of d_f, a_{A_2} and the asymptotic exponent m for various theoretical models and experimental examples.

One realizes that the limiting values are correctly predicted for the hard spheres and reasonably well for the linear chains according to the theory of Ohta and Oono [4, 158]. The corresponding asymptotes for the two branched examples in Fig. 35 are also in reasonable agreement with the experimental data at high X.

8.6 Behavior at $X=A_2M_wc>5$

The asymptotic value of Eq. (92), however, will never be reached in realistic experiments, since the physical conditions for this behavior will have changed when a certain overlap concentration is exceeded. Often strong deviations from the expected behavior are observed. The osmotic modulus no longer increases with the concentration, but it fairly suddenly passes through a maximum and starts to decay sharply towards very small values until either gelation takes place or a strong turbidity makes further light scattering measurements impossible.

The reasons for this peculiarly looking behavior become clear when writing Eq. (92) is a slightly different manner:

$$\frac{1}{M_{app}(c)} = \frac{1}{M_w(c)}\left[1+2A_2M_w(c)c+3A_3M_w(c)c^2+\ldots\right] = \frac{1}{M_w(c)}\left\{1+2\left[A_2M_w(c)\right]c+3g_a\left[A_2M_w(c)\right]^2c^2+\ldots\right\} \tag{97}$$

This means that association is taken into consideration which would cause an increase of the true molar mass when the concentration is enlarged. For hard sphere interaction the term $A_2M_w(c) \propto (R_g^3 / M_w(c))$ remains independent of the molar mass and does not change with the concentration. Thus a situation may be possible where $M_w(c)$ increases stronger than the repulsive force, given by the expression in curled brackets. Such a situation occurs for instance when gelation takes place at a critical concentration c_{crit} which is lower than that for close sphere packing. At the gel point the molar mass increases beyond all limits but the repulsive interaction among the associates still remains finite. Such a case has been observed with β-galactosidase in a phosphate buffer [177, 178]. In most cases the repulsive interaction is slightly weaker, i.e., $A_2M_w(c)$ increases slightly according to the fractal property as

$$A_2M_w(c) = K\left(M_w(c)\right)^{\left(3-d_f\right)/d_f} \tag{98}$$

This makes the 'catastrophic' break-down of the osmotic modulus somewhat softer.

A second reason for the 'turn-over' in the osmotic modulus may arise from a decrease in A_2 until it becomes zero or even negative. This would be the classical situation for a phase separation. The reason why in a good solvent such a phase separation should occur has not yet been elucidated and remains to be answered by a fundamental theory. In one case the reason seems to be clear. This is that of starches where the branched amylopectin coexists with a certain fraction of the linear amylose. Amylose is well known to form no stable solution in water. In its amorphous stage it can be brought into solution, but it then quickly undergoes a liquid-solid transition. Thus in starches the amylose content makes the amylopectin solution unstable and finally causes gelation that actually is a kinetically inhibited phase transition [166]. Because of the not yet fully clarified situation this 'turn-over' will be not discussed any further.

In some case, however, only a flattening of the osmotic modulus curve is observed. Such a case is found with star-branched macromolecules. This observation has rather comprehensively been investigated by Roovers et al. with stars of 64 and 128 arms [172]. The authors give the following explanation. At the point of coil overlap and at somewhat higher concentrations the stars feel the interaction as a quasi colloidal particle. Hence, a steeper increase of the osmotic mod-

ulus than for flexible linear chains occurs. Once, however, most of the star molecules are involved in mutual interpenetration, only the interaction among linear chain section (from the arms) will be operative. Therefore the curve should approach the asymptotic slope of the flexible linear chains. These arguments appear convincing and are essentially in agreement with the model that was presented by Daoud and Cotton [29].

A similar flattening of the osmotic modulus curve was also observed with native amylopectin from waxy maize starch. In contrast to the star macromolecules this hyperbranched macromolecule is multiply branched. A deep coil interpenetration of the fairly short non-branched outer chains is not possible. In this case a screening of excluded volume interaction was assumed [179], which causes a shrinking of the molecular volume and thus a shift of the overlap concentration to higher values. When making a scaling assumption similar to that given by Daoud [176], the flattening of the osmotic modulus could indeed be well described. A closer inspection of the radii of gyration, which have been measured simultaneously, also reveals, however, a strong increase of the dimension. Thus an association has to be taken into consideration. The increase of the molar mass could be calculated via a fractal assumption. The required fractal dimension of the associates was known from previous measurements [180, 181]. Also in this case a screening of excluded volume interaction, or a compression of the swollen particles, has to be assumed. The shrinking of the particle radius was found to follow a power law with an exponent of approximately –0.19, a value that is close to that derived for linear chains [18].

Acknowledgements. The author is indebted to Professor Ralph Colby, Pennsylvania State University for giving him the as yet unpublished data for the exponents τ shown in Fig. 20. He also wishes to express his thanks to Dr. Jacques Roovers, for the many useful suggestions which made this contribution readable and easier to understand. The manuscript would have not been possible without the technical help of Dipl. Chem. Juergen Schmidt to whom the author owes his sincere thanks.

9 Appendix: Some Relationships of the $A<_{B}^{C}$-Polycondensation Model

The model goes back to Flory [1] and more specifically to Erlander and French [16]. Further derivations concerning the mean square radius of gyration and the hydrodynamic radius were made by the author [17]. The following calculations are based on the $A<_{B}^{C}$ model which is related to the condensation of the glucose ring. The reactive groups A, B, and C are related to the OH groups at the C_1 (reducing end group), C_4, and C_6 positions of the glucose ring. Because of enzymatic specificity bonds can be formed only between $C_1 \rightarrow C_4$ and $C_1 \rightarrow C_6$; all other reactions are excluded. The corresponding extents of reaction (probability of reaction) are p_1, p_4, and p_6 with the obvious constraint

$$p_1 = p_4 + p_6 \tag{A1}$$

This model corresponds to the general case of hyperbranching and reduces the *common hyperbranching process* if

$$p_4 = p_6 = \frac{p_1}{2} \tag{A2}$$

In amylopectin and glycogen $p_6=p$ is the branching probability, which does not depend on the molar mass of the branched polysaccharides.

According to the common (mean field) theory of branching processes, one has

$$M_n = \frac{M_0}{1-p_1} \tag{A3}$$

$$M_w = M_0 \frac{1-p_4^2-p^2}{(1-p_4-p)^2} \tag{A4}$$

$$\frac{M_z}{M_0} = \frac{\left[(1-p_1)(1-p_4^2-p^2)-2(1-p_1)\left[p_4^2(1-p_4)+p^2(1-p)\right]\right]}{\left[(1-p_1)^2\left(1-p_4^2-p^2\right)\right]} + \frac{3\left(1-p_4^2-p^2\right)\left[p_4(1-p_4)+p(1-p)\right]}{\left[(1-p_1)^2\left(1-p_4^2-p^2\right)\right]} \tag{A5}$$

$$\frac{M_w}{M_n} = 1+\left[1+2p(1-p)DP_w\right]^{1/2} = 2(1+B_n) \tag{A6}$$

$$B_n = p(1-p)DP_n$$

$$\frac{R_g}{R_h} \equiv \rho = \left(\frac{3(1+2B_n)}{4(1+B_n)}\right)^{0.5}\left(\frac{2+B_n}{1+B_n}\right) \tag{A7}$$

$$C_h = \frac{1}{6}\frac{1+B_n}{1+2B_n}\left(1+\frac{1}{5}\frac{2+3B_n}{2+B_n}+\frac{B_n}{(1+2B_n)(2+B_n)}\right) \tag{A8}$$

where

$$B_n = p(1-p)DP_n \tag{A9}$$

$$B_w = p(1-p)DP_w \tag{A10}$$

$$D_{app}(q) = D_z\left(1+C_h R_g^2 q_2 - \ldots\right) \tag{A11}$$

10 References

1. Flory PJ (1953) Principles of polymer chemistry. Cornell University Press, Ithaca, NY
2. Flory PJ (1969) Statistical mechanics of chain molecules. Wiley, New York
3. Yamakawa H (1971) Modern theory of polymer solutions. Harper and Row, Evanstone, Il
4. De Gennes P-G (1979) Scaling concepts in polymer physics, Cornell University Press, Ithaca, NY
5. Doi M, Edwards SF (1986) The theory of polymer dynamics. Clarendon, Oxford
6. Freed KF (1987) Renormalization group theory of macromolecules. Wiley, New York
7. Stauffer D (1985) Introduction to percolation theory. Taylor & Francis, London
8. Freire JJ (1998) Chapter in this book; there a list of relevant literature on the techniques of simulation
9. Burchard W (1988) Makromol Chem Macromol Symp 18:1
10. Burchard W (1993) TRIP 1:192
11. Burchard W (1966) Adv Colloid Interface Sci.64:45
12. Flory PJ (1941) J Am Chem Soc 63:3083
13. Flory PJ (1946) Chem Revs 39:137
14. Stockmayer WH (1943) J Chem Phys 11:45
15. See textbooks on polymer science, eg [1] and more recent ones
16. Erlander SR, French D (1956) J Polymer Sci 20:7
17. Burchard W (1972) Macromolecules 5:604
18. Daoud M, Cotton J-P, Farnoux B, Jannink G, Sarma G, Benoit H, Duplessix R, Picot C, de Gennes P-G (1975) Macromolecules 8:804
19. Burchard W, Lang P, Schulz L (1992) Makomol Chem, Macromol Symp 58:21
20. Willner L, Jucknischke O, Richter D, Roovers J, Zhou L-L, Toporowski PM, Fetters LJ, Huang JS, Lin MY, Hadjichristidis N (1994) Macromolecules 27:3821
21. Allegra G, Colombe E, Ganazzoli F (1993) Macromolecules 26:330
22. Benoit H, Joanny JF, Hadziioannou G, Hammouda B (1993) Macromolecules 26:5790
23. Alessandrini JL, Carignano MA (1992) Macromolecules 25:1157
24. Burchard W (1983) Adv Polym Sci 48:1
25. Roovers J, Zhou L-L, Toporowski PM, van der Zwan M, Iatrou H, Hadjichristidis N (1993) Macromolecules 26:4324
26. Bywater S (1979) Adv Polym Sci 30:89
27. Cherayil BJ, Bawondi MG, Miyake A, Freed KF (1986) Macromolecules 19:2770
28. Douglas JF, Roovers J, Freed KF (1990) Macromolecules 23:3168
29. Daoud M, Cotton J-P (1982) J Physique (Paris) 43:531
30. Huber K, Burchard W, Bantle S, Fetters LJ (1987) Polymer 28:1997
31. Richter D, Farago B, Huang JS, Fetters LJ, Even B (1989) Macromolecules 22:468
32. Douglas JF, Freed KF (1984) Macromolecules 17:7461
33. Freed KF, Wang Q-S, Roovers J, Douglas JF (1988) Macromolecules 21:2219
34. Horton JG, Squires GL, Boothoyd AT, Fetters LJ, Rennie AR, Glinka CJ, Robinson RA (1989) Macromolecules 22:681
35. Grest GS, Fetters LJ, Huang JS, Richter D (1996) Adv Chem Phys 94:67
36. Ganazzoli F, Allegra G (1990) Macromolecules 23:262
37. Ganazzoli F, Fontelos MA, Allegra G (1993) Polymer 34:2615
38. Burchard W, Kajiwara K, Nerger D (1982) J Polym Sci Phys Ed 20:157
39. Voit BI (1995) Acta Polym 46:87
40. Tomalia DA, Durst HD (1993) Top Curr Chem 165:194
41. Tomalia DA, Naylor A, Goddard W (1990) Angew Chem In Ed 29:138
42. Tomalia DA, Hedstrand DM, Wilson LR (1990) In: Encyclopedia of polymer science and technology. Wiley, New York, pp 46–92

43. Mekelburger H-B, Jaworek W, Vögtle F (1992) Angew ChemInt Ed 31:1571
44. Newkome GR, Morrefield CN, Baker GR (12992) Aldichim Acta 25:31
45. Fréchet JMJ (1994) Science 263:1710
46. Wooley KL, Hawker CJ, Fréchet JMJ (1991) J Am Chem Soc 113:4252
47. Wooley KL, Hawkers CJ, Fréchet JMJ (1994) Angew Chem Int Ed 33:82
48. Stockmayer WH (1944) J Chem Phys 12:125
49. Zimm BH, Stockmayer WH (1949 J Chem Phys 17:1301
50. Kajiwara K, Burchard W, Gordon M (1970) Brit Polymer J 2:110
51. Burchard W (1972) Macromolecules 5:604
52. Burchard W (1977) Macromolecules 10:919
53. Gordon M (1962) Proc Roy Soc (London) 51:240
54. Gordon M, Scantlebury GR (1964) Trans Fard Soc 60:604
55. Isaacson J, Lubensky TC (1980) J Physique (Paris) 41:L469
56. Boris D, Rubinstein M (1996) Macromolecules 29:7251
57. Huglin MB (1972) Light scattering from polymer solutions. Academic Press, London
58. Glatter O, Kratky O (1982) Small angle X-ray scattering. Academic Press, London
59. Higgins JS, Benoit H (1994) Polymers and neutron scattering. Clarendon Press, Oxford
60. Berne BJ, Pecora R (1976) Dynamic light scattering. Wiley, New York
61. Siegert AJF (1943) MIT Rad Lab Report 465; see also [60]
62. Flammer J, Ricka J (1997) Apl Optics 36:508
63. Burchard W, Schmidt M, Stockmayer W (1980) Macromolecules 13:1265
64. Schmidt M, Stockmayer WH (1984) Macromolecules 17:509
65. Burchard W, Schmidt M, Nerger D (1979) Polymer 20:582
66. Einstein Q (1905) Ann Phys 17:549
67. Einstein A (1906) Ann Phys 19:371
68. Einstein A (1906) Ann Phys 19:289
69. Einstein A (1911) Ann Phys 34:591
70. Flory PJ, Fox TG (1951) J Am Chem Soc 73:1904
71. Krigbaum WR, Carpenter DK (1955) J Phys Chem 59:1166
72. McMillan WG, Mayer JE (1945) J Chem Phys 13:276
73. Oseen CW (1927) Hydrodynamik. Akademie Verlag, Leipzig
74. McQuarrie DA (1973) Statistical mechanics. Harper and Row, New York
75. Friedman HL (1985) A course in statistical mechanics. Prentice Hall, Englewood, NJ
76. Lang P, Burchard W, Wolfe MS, Spinelli HJ, Page L (1991) Macromolecules 24:1306
77. Roovers J, Hajichristidis N, Fetters LJ (1983) Macromolecules 16:214
78. Douglas JF, Freed KF (1984) Macromoleules 17:1854
79. Schaefgen JR, Flory PJ (1948) J Am Chem Soc 70:2709
80. Schulz GV (1939) Z Phys Chem B39:25
81. Zimm BH (1948) J Chem Phys 16:1099
82. Feller W (1957) An introduction to probability theory and its applications, 3rd edn. Wiley, New York
83. Burchard W(1974) Macromolecules 7:841
84. Benoit H (1953) J Polymer Sci 11:507
85. Freire JJ, Pla J, Rey A, Prats R (1986) Macromolecules 19:452
86. Freire JJ, Rey A, Garcia de la Torre J (1986) Macromolecules 19:457
87. Rey A, Freire JJ, Garcia de la Torre J (1987) Macromolecules 20:342
88. Kirkwood JG, Riseman J (1948) J Chem Phys 16:565
89. Huber K, Burchard W, Fetters LJ (1984) Macromolecules 17:54
90. Douglas JF, Freed KF (1984) Macromolecules 17:1854; 2344
91. Casassa EF (1962) J Phys Chem 37:2176
92. Trappe V, Bauer J, Weissmüller M, Burchard W (1997) Macromolecules 30:2365
93. Trappe V, Burchard W (1994) Polymer Preprints (Am Chem Soc, Div Polymer Chem) 36:1
94. Weissmüller M, Burchard W (1995) Macromol Symp 93:301

95. Weissmüller M, Burchard W (1997) Acta Polym 48:571
96. Burchard W, Kajiwara K, Gordon M, Kalal J, Kennedy JW (1973) Macromolecules 6:642
97. Kajiwara K (1971) Polymer 12:57
98. Marriman J, Hermans JJ (1961) J Phys Chem 65:385
99. De Gennes P-G (1980) Compt Rend 291:17
100. Stauffer D, Coniglio A, Adam M (1982) Adv Polym Sci 44:103
101. Mandelbrot BB (1982) The fractal geometry of nature. Freeman, San Francisco
102. Daoud M, Martin JE (1989) In: Avnir D (ed) The fractal approach to heterogeneous chemistry. Wiley, New York
103. Stanley HE (1972) Introduction to phase transition and critical phenomena. Clarendon Press, Oxford
104. Schaefer DW, Martin JE, Hurd AJ, Keefer KD (1985) In: Boccora N, Daoud M (eds) Physics of finely divided matter. Springer, Berlin Heidelberg New York
105. Schaefer DW (1989) Science 243:1023
106. Flory PJ (1936) J Am Chem Soc 58:1877
107. Flory PF (1940) J Am Chem Soc 62:1561
108. Zhou LL, Hadjichristidis N, Toporowski PM, Roovers J (1992) Rubber Chem Tech 65:303
109. Schossler F, Benoit H, Grubisic-Gallot Z, Strazielle C, Leibler L (1989) Macromolecules 22:400
110. Weissmüller M, Burchard W (1997) Polymer Internat 44:380
111. Adam M, Delsanti M, Munch JP, Durand D (1988) Phys Rev Lett 61:706
112. Patton EV, Wesson JA, Rubinstein M, Wilson JC, Oppenheimer LE (1989) Macromole cules 22:1946
113. Bauer J, Burchard W (1992) J Physique II (France) 2:1053
114. Burchard W, Schulz L, Auersch A, Littke W (1990) Polymer Preprints 31(2):131
115. Trappe V, Richtering W, Burchard W (1992) J Physique II (France) 2:1453
116. Colby RH, Rubinstein M, Gillmor JR, Mourey TH (1992) Macromolecules 25:7180
117. De Gennes P-G (1977) J Physique (Paris) 38L:355
118. Colby R (1998) Personal communication, manuscript in preparation
119. Lusignan C P (1998) PhD Thesis. Pensylvania State University
120. Weissmüller M (1996) PhD Thesis. University of Freiburg, Germany
121. Daoud M, Family F, Jannink G (1984) J Physique Lett (Paris) 45:199
122. Martin JE, Adolf D, Wilxcoxon JP, Luck JM (1987) Phys Rev Lett 61:2620
123. Bhatt M, Jamieson AM (1988) Macromolecules 21:3015
124. Meyerhoff G, Appelt B (1979) Makromol Chem 12:968
125. Stockmayer WH, Fixman M (1953) Ann NY Acad Sci 57:334
126. Kirkwood JG (1954) J Poly Sci 12:1
127. Zimm BH (1956) J Chem Phys 24:269
128. Zimm BH, Kilb RW (1959) J Polymer Sci 37:19
129. Kurata M, Abe M, Imwama M, Matsushima M (1972) Polym J 3:729
130. Roovers JEL, Bywater S (1972) Macromolecules 5:384
131. Roovers JEL, Bywater S (1974) Macromolecules 7:443
132. Berry GC (1971) J Polym Sci 9:687
133. Zilliox JG (1972) Makromol Chem 156:121
134. Hadjichristidis N, Roovers JEL (1974) J Polymer Sci, Phys Ed 12:2521
135. Roovers JEL, Toporowski PM, Martin J (1989) Macromolecules 22:1897
136. Leukel J (1997) Ph D Thesis. University of Freiburg, Germany
137. Schmidt M, Nerger D, Burchard W (1979) Polymer 20:528
138. Tanford C (1967) Physical chemistry of macromolecules. Wiley, New York, p 344
139. Akcasu AZ, Benmouna M (1978) Macromolecules 11:1187
140. Schmidt M, Burchard W (1981) Macromolecules 14:370
141. ter Meer H-U, Burchard W (1980) Colloid Polym Sci 258:657
142. Douglas JF, Freed KF (1984) Macromolecules 17:2344

143. Douglas JF (1996) Personal communication
144. Galinsky G, Burchard W (1996) Macromolecules 29:1498
145. Bauer J, Burchard W (1993) Macromolecules 26:3103
146. Akcasu AZ, Benmouna M (1978) Macromolecules 11:1193
147. Huber K, Burchard W, Akcasu AZ (1985) Macromolecules 18:2743
148. Kratky O, Porod G, Kahovec L (1951) Z Elektrochem 55:53
149. http://ne43neuiucedu/n-scatter/n-lengths/listhtml
150. Burchard W, Schmidt M (1980) Polymer 21:745
151. Burchard W (1986) In: Semlyen JA (ed) Cyclic polymers. Esevier, London
152. Simha R, Zakin JL (1960) J Chem Phys 33:1791
153. Utracki L, Simha R (1963) J Polym Sci A1:1089
154. Des Cloizeaux J (1975) J Physique (Paris) 36:281
155. Stockmayer WH, Casassa EF (1952) J ChemPhys 20:1560
156. Burchard W (1990) Makromol Chem, Macromol Symp 39:179
157. Carnahan NF, Starling KE (1969) J Chem Phys 51:635
158. Ohta T, Oono Y (1983) Physics Lett 79:339
159. Cotter MA, Martire DC (1970) J Chem Phys 52:1909
160. Delay M, Tardieu A (1983) Nature 30L:415
161. Delay M, Gromiec A (1983) Biopolymers 22:1203
162. Coviello T, Kajiwara K, Burchard W, Dentini M, Crescenzi V (1986) Macromolecules 19:2826
163. Dentini M, Coviello T, Burchard W, Crescenzi V (1988) Macromolecules 21:3312
164. Coviello T, Burchard W, Dentini M, Crescenzi V, Morris VJ (1995) J Polym Sci, Phys Ed 33:1833
165. Trappe V (1994) PhD Thesis. University of Freiburg
166. Aberle T, Burchard W (1997) Starch 49:215
167. Merkle G, Burchard W, Lutz P, Freed KF, Gao J (1993) Macromolecules 26:2736
168. Sato T, Norisuye T, Fujita H (1987) J Polym Sci, Phys Ed 25:1
169. Nakamura Y, Akasaka K, Katayama K, Norisuye T, Teramoto A (1992) Macromolecules 25:1134
170. Okumoto M, Nakamura Y, Norisuye T, Teramoto A (1998) Macromolecules 31:1615
171. Bawn CEH, Freeman RFJ, Kamaliddin AR (1950) Trans Farad Soc 46:862
172. Roovers J, Toporowski PM, Douglas J (1995) Macromolecules 28:7064
173. Trappe V, Burchard W, Steinmann B (1991) Macromolecules 24:4738
174. Trappe V, Richtering W, Burchard W (1992) J Phys II (Paris) 2:1453
175. Trappe V, Bauer J, Weissmüller M, Burchard W (1997) Macromolecules 30:2365
176. Daoud M (1976) PhD Thesis. Paris CEN Saclay
177. Auersch A, Littke W, Lang P, Burchard W (1991) J Cryst Growth 110:201
178. Burchard W, Lang P, Schulz L, Coviello T (1992) Makromol Chem, Macromol Sympos 58:21
179. Aberle T, Burchard W (1997) Comp Theor Polym Sci 7:215
180. Hanselmann R, Burchard W, Ehrat M, Widmer HM (1996) Macromolecules 29:3277
181. Andres-Köksal K (1996) PhD Thesis. University of Freiburg (manuscript in preparation)
182. Bantle S, Schmidt M, Burchard W (1982) Macromolecules 15:1604
183. Burchard W, Dolega R, Stockmayer WH (1995) Collect Czech Chem Commun 60:1653
184. Bareiss R, Jung B, Khokhov AR (1996) Macromol Theory Simul 5:57

Received: June 1998

Entangled Dynamics and Melt Flow of Branched Polymers

Tom C.B. McLeish[1], Scott T. Milner[2]

[1] IRC in Polymer Science and Technology, Department of Physics and Astronomy, University of Leeds, Leeds, LS2 9JT, UK *E-mail: t.c.b.mcleish@leeds.ac.uk*
[2] Exxon Research and Enginering Company, Route 22 East, Annandale, New Jersey 08801, USA

One of the most puzzling properties of branched polymers is their unusual viscoelasticity in the melt state. We review the challenges set by both non-linear experiments in extension and shear of polydisperse branched melts, and by the growing corpus of data on well-characterised melts of star-, comb- and H- molecules. The remarkably successful extension of the de Gennes/Doi-Edwards tube model to branched polymers is treated in some detail in the case of star polymers for which it is quantitatively accurate. We then apply it to more complex architectures and to blends of star-star and star-linear composition. Treating linear polymers as "2-arm stars" for the early fluctuation-dominated stages of their stress-relaxation successfully accounts for the relaxation spectrum and "3.4-law" viscosity-molecular weight relationship. The model may be generalised to strong flows in the form of molecular constitutive equations of a structure not found in the phenomenological literature. A model case study, the "pom-pom" polymer, exhibits strong simultaneous extension hardening and shear softening, akin to commercial branched polymers. Computation with such a constitutive equation in a viscoelastic flow-solver reproduces the large corner vortices in contraction flows characteristic of branched melts and suggests possible future applications of the modelling tools developed to date.

Keywords. Viscoelasticity, Molecular rheology, Branched polymers, Tube model, Non-Newtonian flow

Advances in Polymer Science, Vol.143

List of Symbols and Abbreviations

a	tube diameter
b	Kuhn step length
c_j	number concentration of object labelled j
CR	constraint release
D_e	diffusion constant of an entanglement length
D_{mon}	monomeric diffusion constant
D_R	curvilinear diffusion constant of a polymer chain
E	deformation tensor (non-linear)
f	free energy density
f_{eq}	equilibrium Brownian tension along an entangled chain
$f(\mathbf{u},s,t)$	distribution function of segments of orientation **u** at co-ordinate s and time t
$f(m)$	distribution of segment priorities in an ensemble of branched polymers
G_0	plateau modulus
$G(t)$	relaxation modulus
$G^*(\omega)$	complex modulus
HDPE	high density polyethylene
$h(\gamma)$	shear damping function
k	Boltzmann's constant
$\boldsymbol{k}$	scattering wavevector
K	velocity gradient tensor
L	primitive path length along tube
LCB	long chain branching
LDPE	low density polyethylene
M	molecular weight
M_a	molecular weight of a star polymer arm
M_b	molecular weight of a comb backbone or pom-pom cross-bar
M_c	critical molecular weight
M_e	entanglement molecular weight
M_x	molecular weight between branch points in a tree polymer
N	degree of polymerisation
NMR	nuclear magnetic resonance
NSE	neutron spin echo
p	probability of branching in a stochastic tree
p_c	critical branching probability at onset of gelation in a stochastic tree
$p(s,t)$	survival probability of tube segment labelled s at time t
PB	polybutadiene
PS	polystyrene
q	number of branches on a comb or on each end of a pom-pom polymer
Q	Doi-Edwards strain tensor
$<r^2>$	mean square displacement of a monomer
R	average end-to-end distance of a chain

R	ideal gas constant
$\boldsymbol{R}(s,t)$	chain configuration at time t
R_g	radius of gyration
RPA	Random Phase Approximation
SANS	small angle neutron scattering
$S(\boldsymbol{k},t)$	dynamic structure factor
$\mathbf{S}(t)$	time-dependent second orientation moment of a pom-pom cross-bar ensemble
T	absolute temperature
u	dynamic exponent for power-law relaxation
$\mathbf{u}$	unit vector
$U(z)$	free energy potential for fluctuations in primitive path length
$U_{eff}(s)$	renormalised effective potential for path length fluctuations
$U_{s<},U_{s>}$	effective potentials for the star arm before and after the reptation time in a star-linear blend
$v(s)$	relative curvilinear velocity of tube and chain at co-ordinate s
x	normalised contour variable along an entangled arm
z	functionality of branch points on a tree polymer
α	dilution exponent for M_e; $\alpha=\beta-1$
β	dilution exponent for the plateau modulus
$\dot{\gamma}$	shear rate
γ	shear strain
$\delta(\boldsymbol{r})$	Dirac delta function in three dimensions
$\dot{\varepsilon}$	extension rate
ε	extensional strain
ε	strain tensor (linear)
ϕ	volume fraction of a polymeric component in a solution or blend
$\phi_p(s,t)$	eigenmodes of tube relaxation equation
$\boldsymbol{\Phi}$	entangled unrelaxed volume fraction
η	viscosity
$\lambda(t)$	time-dependent average stretch of a pom-pom cross-bar ensemble
$\mu(t)$	stress relaxation functions (dimensionless)
ν	dimensionless number 15/8
ρ	density
τ_{arm}	longest relaxation time of a dangling arm
τ_b	orientational relaxation time of a pom-pom cross-bar
τ_e	Rouse relaxation time of an entanglement length
τ_i	relaxation time of the i-th level in a tree polymer
τ_k	relaxation time of concentration fluctuation of wavenumber k
τ_k	shortest time for time/strain factorability (in this context – see above for scattering)
τ_{max}	longest relaxation time
τ_{mon}	orientational relaxation time of a monomer
τ_0	attempt time for path length fluctuations
τ_{rep}	reptation time

τ_R	Rouse time of a chain
τ_s	stretch relaxation time of a pom-pom cross-bar
$\tau(s)$	relaxation time of a tube segment with arc co-ordinate s
σ	stress tensor
ζ	monomeric friction coefficient
ζ_{br}	effective friction constant of a long chain branch point
θ	topological dynamical exponent

1 Introduction

One of the most fascinating and rapidly moving areas of polymer science at present concerns the rôle played by large-scale molecular structure in the dynamics and rheology of bulk polymer fluids. The technological aspects of this highly interdisciplinary field are increasingly important: in this context the subject becomes the role of polymer synthesis in determining the processing characteristics of an industrial polymer melt or solution. Polymer chemistry is playing a vital role in providing model materials for the fundamental science, as well as new catalysts for controlled industrial synthesis. Yet paradoxically many of the relevant properties in polymer rheology are dependent on local (monomer) chemistry via only a few scaling parameters – much of the behaviour is universal among polymer chemistries. Far greater variation is found within the structural parameters of long chain branching (LCB). So the role of branch structure in polymer melts is becoming vital as a key to our understanding of their molecular dynamics as well as the highly practical control of processing properties. Hence the addition of theoretical and experimental physics to the techniques brought to bear upon branched polymer melts. Not only careful rheological experiments, but also molecular probes such as neutron scattering are providing further information for the remarkable theoretical models which have recently shed considerable light on this tangled tale.

1.1 Evidence for Topological Interaction

It has long been realised that the key physics determining the rheology of high molecular weight polymers in the melt state arises from the *topological* interactions between the molecules [1, 2]. This is deduced from observations on many different monodisperse materials that:

(i) above a critical molecular weight, M_c the viscosity η rises steeply with M as approximately $M^{3.4}$;

(ii) at high molecular weight the rheological response of polymer melts *at high frequency* is similar to that of a cross-linked rubber network with a molecular weight M_e between cross-links (it exhibits an elastic modulus G_0 nearly independent of frequency);

(iii) $M_c \sim 2M_e$ for all amorphous melts independent of their chemistry, which determines purely the value of G_0.

This conclusion has been supported for over a decade by the remarkable contrast in the rheological behaviour of polymer melts whose molecules themselves differ topologically. In the sphere of commercial materials the presence of "long chain branching" has been invoked to explain the radically different rheology of (branched) Low Density Polyethylene (LDPE) from that of (linear) High Density Polyethylene (HDPE) [3]. A fascinating example is well-known from flow-visualisation experiments. These two polyethylenes with matched viscosities (and of course identical local chemistry) exhibit quite different flow-fields when driven from a larger into a smaller cylinder (Fig. 1). The "contraction flow" for the linear polymer resembles that of a Newtonian fluid, while that of the branched polymer sets up large vortices situated in the corners of the flow field. The understanding of a link between such differences in molecular topology and a macroscopic change in flow represents a considerable challenge.

The rheology of LDPE is puzzling in a deeper way in that none of the panoply of phenomenological constitutive equations in the rheological literature seems able to account for all its properties with a single set of adjustable parameters, no matter how large. For example, even the highly flexible integral equations cannot reproduce softening in shear together with hardening in both planar and

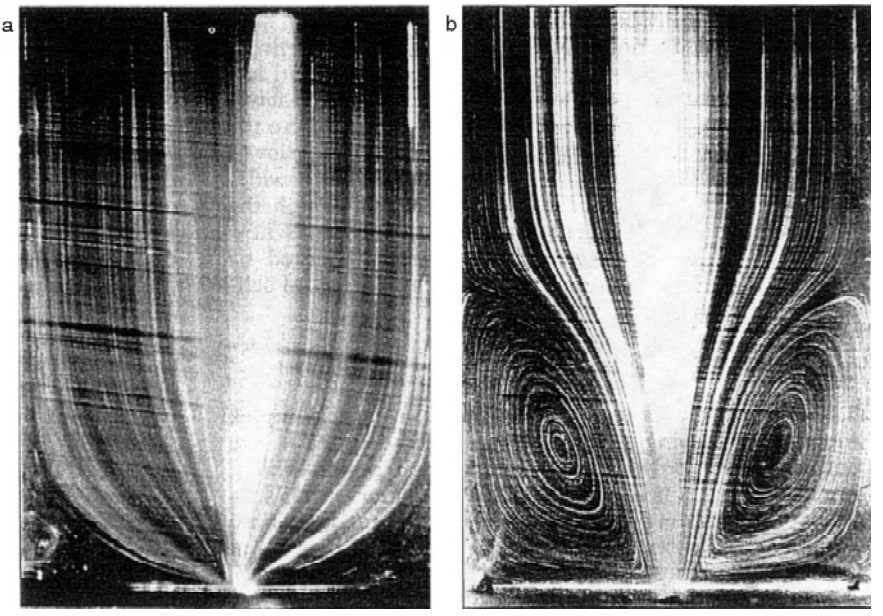

Fig. 1 . Flow-visualisation of molten polyethylenes into a contraction: *left* HDPE (linear); *right* LDPE (branched). (Courtesy of B Tremblay)

uniaxial extension (see Sect. 6.2.2 below). Other differential constitutive equations have difficulty with the structure of stress-transients in "startup flow". Might a molecular understanding of the role of LCB and topology assist in identifying what is missing from traditional approaches?

More discriminating experiments have been possible with small amounts of tailored model materials that possess nearly monodisperse molecular weight and topology. These have typically been anionically synthesised polyisoprenes, polystyrenes and polybutadienes [4]. Branching is achieved in a controlled way by reacting living chain ends at multi-functional coupling agents such as chlorosilanes. For some years the remarkable distinction in rheology between linear and multi-arm star polymer melts has been exhaustively investigated [5]. Fewer, but very significant, studies have been made on H-shaped [6], comb-shaped [7] and the important case of blends containing branched components [8].

1.2 The Tube Model

The most successful theoretical framework in which the accumulating data has been understood is the *tube model* of de Gennes, Doi and Edwards [2]. We visit the model in more detail in Sect. 2, but the fundamental assumption is simple to state: the topological constraints by which contingent chains may not cross each other, which act in reality as complex *many-body* interactions, are assumed to be equivalent for each chain to a tube of width a surrounding and coarse-graining its own contour (Fig. 2). So, motions perpendicular to the tube contour are confined while those curvilinear to it are permitted. The theory then resembles a dynamic version of rubber elasticity with local dissipation, and with the additional assumption of the tube constraints.

The theoretical framework is economic in that the number of free parameters required to make predictions is very limited: as well as the Kuhn step length b,

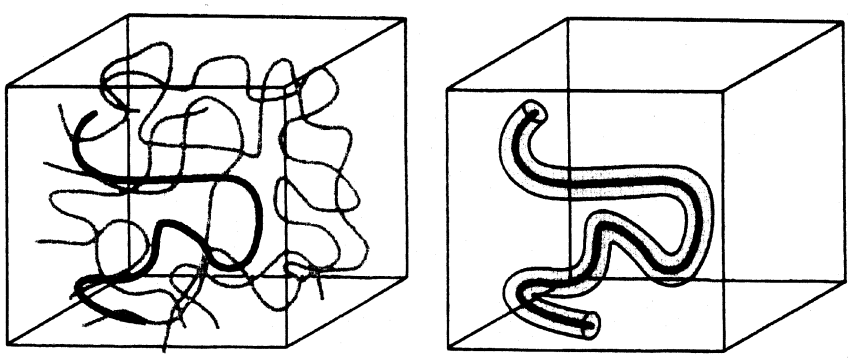

Fig. 2. The tube model replaces the many-chain system (*left*) with an effective constraint on each single chain (*right*). The tube permits diffusion of chains along their own contours only

one more static parameter is needed in the tube diameter, a (or equivalently the plateau modulus G_0) and one dynamic parameter – the monomeric friction coefficient ζ (or equivalently the Rouse time of an entanglement length). Once these parameters are determined for a polymer of specified chemistry, quantitative predictions for the linear rheology, as determined by the stress relaxation modulus[1] $G(t)$ or its Fourier transform $G^*(\omega)$ are in principle calculable. Because the model is a molecular one, albeit coarse-grained on the level of Gaussian sub-chains, it also provides predictions for other, more direct probes of the molecular dynamics such as the dynamic structure factor $S(\mathbf{k},t)$ (see Sect. 2.4 below). This very important advantage of molecular theories has yet to be fully exploited experimentally in the context of polymers, mainly because the associated timescales are so long. However we will see below how single-chain and bulk structure-factors may be calculated within the theory alongside the rheological response.

A second appealing feature of tube model theories is that they provide a natural hierarchy of effects which one can incorporate or ignore at will in a calculation, depending on the accuracy desired. We will see how, in the case of linear polymers, bare reptation in a fixed tube provides a first-order calculation; more accurate levels of the theory may incorporate the co-operative effects of "constraint release" and further refinements such as path-length fluctuation via the Rouse modes of the chains.

Third, the theory contains the implicit claim that entangled polymer dynamics are dominated at long times by the *topological* interactions of the chains. If true, then the rheological behaviour of polymer melts should show a high degree of universality. For example, two monodisperse melts of different chemistries but with the same number of entanglements per chain (M/M_e equal for both) should exhibit stress relaxation functions $G(t)$ which may be superimposed by simple scaling in modulus and time. This is a stronger requirement than simply demanding that the molecular weight scaling of the viscosity is universal for all linear polymers (see (i) above). However, the viscosity is just the integral of the stress relaxation function:

$$\eta = \int_0^\infty G(t)dt \tag{1}$$

which contains much more information than η alone. Figure 3 shows such shifts on published data on three anionically polymerised linear polymers: polystyrene (PS), polybutadiene (PB) and polyisoprene (PI) [1]. The three have similar degrees of entanglement. We plot the functions $G'(\omega)$ and $G''(\omega)$ – the one-sided Fourier transforms of the stress-relaxation function $G(t)$. These are the in-phase and out-of-phase stresses measured in an oscillatory shear experiment,

1 The experiment here is a small rapid shear-strain at time zero – after this the shear stress in a viscoelastic liquid will not vanish instantaneously, but decay as a characteristic function with time. When normalised by the strain to yield the dimensions of modulus, this is $G(t)$.

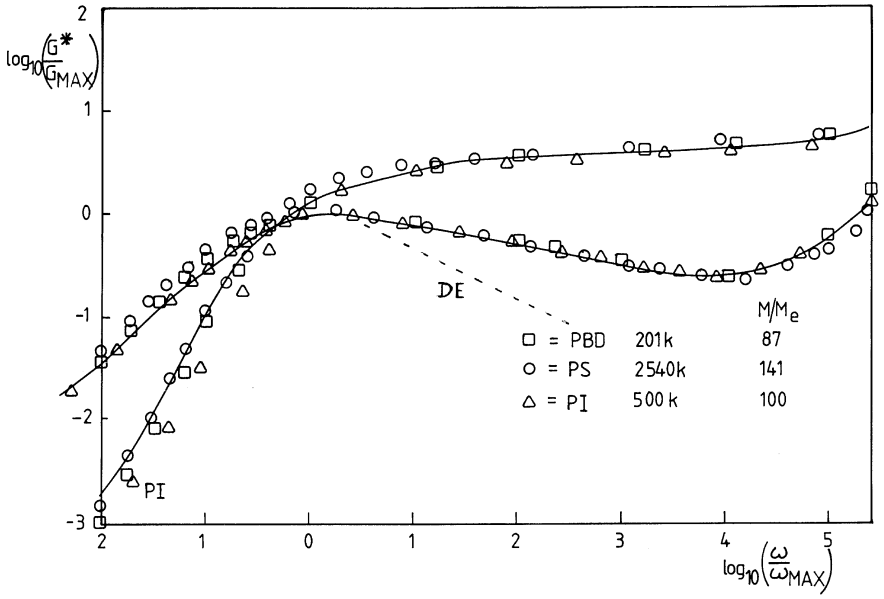

Fig. 3. *G'(ω)* and *G"(ω)* for monodisperse linear polymers of PI, PB and PS. The curves have been shifted so that the plateau moduli and terminal times coincide. The *dashed line* indicates the Doi-Edwards prediction for *G"(ω)* in the absence of path-length fluctuations

and reveal more structure than *G(t)* [1]. Both the shape of the peak around the dominant relaxation time τ_{max}^{-1} and the frequency range before the minimum in the curve are very similar providing values of M/M_e are matched.

This is strong support for theories based on universal aspects of polymer structure. In particular, a purely *topological* theory of dynamics leads naturally to the conjecture that changes in the *molecular topology* itself will radically alter the motions of entangled molecules. The simplest change one can imagine is to introduce a single branch-point into the linear molecule, creating a "star polymer". So there are compelling theoretical as well as chemical reasons to synthesise and characterise melts of monodisperse star polymers with controlled numbers of arms. We shall see that star polymers do indeed have very striking rheological behaviour. How these and more complex molecular architectures may be treated within the tube model will be dealt with in Sects. 3 and 4.

Fourth, it is possible to extend the model to make predictions of response in highly non-linear deformations and flows [2]. This is naturally of great interest in applications, since most of polymer-processing involves extremely large and rapid deformations, but is also proving of value as a strong experimental test of theoretical assumptions and of polymer structures such as branching. For many years the response of polymer melts in strong flows has been approached phenomenologically: rather complex and subtle mathematical "constitutive equa-

tions" containing variable phenomenological parameters or functions have been fitted to restricted sets of data in the attempt to predict further data sets [9], or flows in complex geometries [10]. The mathematics incorporates the necessary features of strain-history-dependence, elastic response at short times and viscous flow at long times, but is not derived from any molecular physics. Much of this work has been directed at the important branched polymer LDPE using very adaptable integral equations [11]. However, as we noted above, even these constitutive equations fail to describe the rheology of LDPE even qualitatively when data from the challenging *planar extension* geometry is added to that of shear and uniaxial extension [12]. We will see what inroads a tube model for highly-branched polymers in shear and extensional flows can make into this problem in Sect. 6.

2 Monodisperse Linear Polymers

The fundamental example of the tube model's application is the simplest one of linear chains of identical molecular weight M or degree of polymerisation N. It will provide the starting point for more complex applications.

2.1 Reptation

The tube model was first invoked by de Gennes as a dynamic constraint to model the motion of a single free chain in a *network* of crosslinked chains [13]. The idea was extended later to polymer melts by Doi and Edwards [2]. The curvilinear motion along the tube contour is the only unrestricted type of motion at times longer than an average monomer takes to diffuse a tube-diameter a. The motion is a form of unbiased one-dimensional diffusion which has become known as *reptation*. Central sections of the chain must follow their neighbours along the tube contour, but the chain ends are free to explore the melt isotropically, so creating new tube (see Fig. 4). Such constrained dynamics gives rise to a characteristic timescale: the time taken on average for the chain to diffuse one tube-length by reptation (or equivalently one radius of gyration in space). This is the reptation time τ_{rep} and is given by the single-particle diffusion scaling:

$$\tau_{rep} \approx \frac{L^2}{D_R} \tag{2}$$

where L is the curvilinear distance along the tube, and D_R the curvilinear diffusion constant for the chain. The tube can be thought of as a chain of N/N_e entanglement sections of diameter a (N_e is the degree of polymerisation of an entanglement segment of molecular weight M_e), so $L \approx aN/N_e$. So the tube *coarse-grains* the path of the chain at the length-scale a. This coarse-grained path was termed the *primitive path* by Doi and Edwards [2], who identified it with the path of

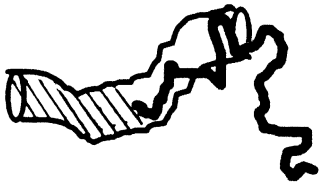

Fig. 4. By curvilinear diffusion a chain evacuates its original tube and creates new tube segments from an isotropic distribution. "Forgotten" portions of the original tube are shown *shaded*

shortest distance through the melt which honoured all the topological interactions of the defining chain.

The other important physical assumption is that the friction is *local* (hydrodynamic interactions are screened in the melt [2]) so that $D_R \approx (N_e/N) D_e$ with D_e the diffusion constant in the melt of an unentangled chain of N_e segments. Now the characteristic relaxation (Rouse) time of an entanglement segment τ_e is just a^2/D_e so that

$$\tau_{rep} \approx \tau_e \left(\frac{N}{N_e} \right)^3 = \tau_{mon} \frac{N^3}{N_e} \tag{3}$$

The second relation arises from the unentangled (Rouse) scaling of τ_e with N_e^2 in terms of a fundamental monomer timescale τ_{mon}.

This simple argument can yield the expected molecular weight dependence of both the single chain diffusion constant (in three dimensions) D and the viscosity η. For in one reptation time the chain has moved on average one chain end-to-end distance $R \approx (N/N_e)^{1/2} a$, so

$$D \approx \frac{R^2}{\tau_{rep}} \sim D_{mon} \frac{N_e}{N^2} . \tag{4}$$

The viscosity scales, from Eq. (1), as $\eta \approx G_0 \tau_{rep}$ since G_o and τ_{rep} are the characteristic modus and relaxation times appearing respectively in the integral. The plateau modulus is independent of molecular weight for highly entangled polymers [1] but inversely proportional to N_e, so

$$\eta \sim G_0 \tau_{rep} \sim \frac{N^3}{N_e^2} . \tag{5}$$

The prediction for the diffusion constant at Eq. (4) is in very good agreement with measurements of the self-diffusion constants of polymer melts [14] while results on the viscosity have consistently given a stronger dependence of the characteristic times and viscosities on molecular weight of approximately $N^{3.4}$. The investigation of these discrepancies in the context of linear polymers has de-

veloped into quite an industry, alongside the extensions to branched polymers which we discuss below. There is a consensus now appearing that the answer can be found in a proper treatment of the internal modes of entangled chains in addition to the centre-of-mass reptation mode. But first we must consider the application of the theory to stress-relaxation and other rheological experiments.

2.2 Expression for the Stress

The first ingredient in any theory for the rheology of a complex fluid is the expression for the stress in terms of the microscopic structure variables. We derive an expression for the stress-tensor here from the *principle of virtual work*. In the case of flexible polymers the total stress arises to a good approximation from the entropy of the chain paths. At equilibrium the polymer paths are random walks – of maximal entropy. A deformation ε_{ij} induces preferred orientation of the steps of the walks, which are therefore no longer random – the entropy has decreased and the free energy density f increased. So

$$\sigma_{ij} = \frac{\partial f}{\partial \varepsilon_{ij}} \tag{6}$$

which is valid for timescales longer than those contributing to the sampling of microstates in f but shorter than the slow degrees of freedom. In a polymer melt, the free energy density can be expressed in terms of subchains of (arbitrary) degree of polymerisation N of Kuhn segments of length b; the chain has an end-to-end distance R. If these subchains have a number density c_N in the melt, we have from the properties of Gaussian chains [2]

$$f = 3kTc_N \frac{\left\langle R^2 \right\rangle}{2Nb^2} \tag{7}$$

where the angular brackets denote an average over configurations of subchains. The tube model provides a *specific choice* of the scale of subchain (R and N) which couples to the bulk imposed strain: assuming that the tubes themselves deform affinely with the bulk, then chains confined within them are constrained to deform at length scales larger than the tube diameter a but not at smaller scales. These are the "slow degrees of freedom" in this case. So choosing $Nb^2 = R^2 = a^2$ and carrying out the differentiation in Eq. (6) leads to the simple form:

$$\sigma_{ij} = \frac{3kT}{a} c_a \left\langle a u_i u_j \right\rangle = 3kTc_a \left\langle u_i u_j \right\rangle \tag{8}$$

where $\boldsymbol{u}$ is the unit vector tangent to the tube axis containing a segment of chain end-to-end length a, and c_a is the number concentration of such segments. As in

rubber elasticity, the stress arises from the anisotropic orientation of the elastically-active segments, and is dominated by the entropy associated with this orientation. In contrast to a cross-linked rubber, however, it is the deformed tube (deforming affinely with the bulk by assumption) which confers the orientation on any chain which occupies it, rather than permanent crosslinks.

2.3 Stress Relaxation

The curvilinear diffusion along the contour of the tube gives an immediate theory for stress relaxation, once the special physics of the free ends of the chains are accounted for. The usual assumption is that the chain ends can explore the melt in any direction. They create new tube segments for the chain which follows them, but this new tube is chosen isotropically, so as time proceeds after a small step-strain there are two populations of occupied tube segments: a decaying fraction of anisotropically oriented segments and a growing fraction of isotropic segments (Fig. 4).

If we assume that the anisotropic part of the stress is now just proportional to the fraction of chain segments still constrained by the original (and deformed) tube segments, then we just need to calculate the fraction of original tube surviving at time t to calculate the stress relaxation function $G(t)$. The easiest way to do this is to recognise an equivalence between a picture in which the chain diffuses curvilinearly along the tube and one in which the *tube segments* diffuse curvilinearly along the *chains*. In this frame in which the chain is fixed, a tube segment from the population at $t=0$ ceases to exist when it reaches a chain end. So if $p(s,t)$ is the probability that a tube segment situated a curvilinear distance s from the end of a chain at time t is one of the original population, then p will satisfy a linear one-dimensional diffusion equation – the physics is identical to that of diffusion in one dimension if we map the population of original tube segments onto diffusing particles. The disappearance of original tube segments at the ends of the chain corresponds to absorbing boundary conditions for the diffusing particles, so finally

$$\begin{aligned} &\frac{\partial}{\partial t} p(s,t) = D_R \frac{\partial}{\partial s^2} p(s,t); \\ &p(0,t) = p(L,t) = 0 \end{aligned} \quad . \tag{9}$$

As in Sect. 2.1, D_R is the curvilinear centre-of-mass diffusion constant of the chain, and is given in terms of the monomeric friction constant ζ by the Einstein relation $D_R=kT/N\zeta$. L is as before the length of the primitive path, or tube length of the chain, which is Nb^2/a. Finally, we need the initial condition on $p(s,t)$, which is just that at $t=0$ the survival probability is unity everywhere on the domain $(0,L)$. A standard method of solving a partial differential equation set such as this is to expand in eigenfunctions of the spatial operator $\partial^2/\partial s^2$ and its bound-

ary conditions. These are the Fourier sine modes $\phi_p(s,t)=\sqrt{(2/L)}\sin(p\pi s/L)\exp(-p^2\pi^2 D_R t/L^2)$, in terms of which the full solution is given by a linear expansion

$$p(s,t)=\sum_{p=1}^{\infty} a_p \phi_p(s,t) \tag{10a}$$

with

$$a_p=\begin{cases}\sqrt{\dfrac{8L}{p^2\pi^2}} & p \text{ odd}\\ 0 & p \text{ even}\end{cases} \tag{10b}$$

The relaxation modulus $G(t)$ is just the plateau modulus multiplied by the fraction of remaining tube, which in turn is just the integral of the survival probabilities $p(s,t)$ over the tube co-ordinate s:

$$G(t)=G_0\int_0^L p(s,t)ds \tag{11}$$

Substitution of Eq. (10) into Eq. (11) gives the well-known "Doi-Edwards" relaxation spectrum:

$$G(t)=G_0\mu(t);\qquad \mu(t)=\sum_{p \text{ odd}}\frac{8}{p^2\pi^2}e^{-p^2 t/\tau_{rep}} \tag{12}$$

The sum over weighted relaxation times is heavily dominated by the longest time (the reptation time) $\tau_{rep}=L^2/\pi^2 D_R$. Because of this the frequency-dependent dissipative modulus, $G''(\omega)$ is expected to show a sharp maximum[1]. The higher modes do modify the prediction from that of a single-mode "Maxwell" model, but only to the extent of reducing the form of $G''(\omega)$ to the right of the maximum from $\sim\omega^{-1}$ to $\sim\omega^{-1/2}$. In fact, experiments on monodisperse linear polymers show a still broader maximum, with $G''(\omega)\sim\omega^{-1/4}$ to the right of the peak, as shown in Fig. 3, where data on well-entangled linear polymers is compared to the Doi-Edwards spectrum. The power law to the right of the peak weakens for less well-entangled chains [15]. These observations form the experimental starting point for the additional effects of path-length fluctuations and cooperative constraint-release of entanglements [16]. A version of the tube model due to Cates [17], which treats the case of reptating *living* polymers (such as solutions of self-assembled wormlike surfactant micelles or liquid sulphur) gives a pure Maxwell model when the recombination reactions are fast enough – a result confirmed accurately by experiment [17].

1 It is a simple exercise to show that in a fluid for which the stress-relaxation is single-exponential, $G(t)=G_0 exp(-t/\tau)$, the viscous modulus $G''(\omega)$ has the simple peaked form $G_0\omega\tau/(1+\omega^2\tau^2)$.

2.4
Neutron Scattering and the Single Chain Structure Factor

There is a vast and continually growing collection of data on the rheological response of entangled polymeric fluids. This is due both to the relative ease with which this data is obtained and to the sensitivity of the data to structural features such as polydispersity and branching (see below). However, the molecular theory for polymer dynamics makes predictions of other quantities which can provide much more specific checks on the behaviour at the molecular level than the macroscopic rheological response. A common example is the scattering structure factor [18]. In the case of polymers, the ability to replace hydrogen atoms selectively with deuterium allows wide application of the technique of neutron scattering [18]. If uncorrelated single chains are deuterated in a melt of chemically identical but hydrogenous chains, scattering can measure the *single chain structure factor S(**k**,t)*:

$$S(\mathbf{k},t)=\frac{N}{L^2}\int_0^L ds\int_0^L ds'\left\langle \exp\left[i\mathbf{k}.\left(\mathbf{R}(s,t)-\mathbf{R}(s',0)\right)\right]\right\rangle \tag{13}$$

Here, $\mathbf{R}(s,t)$ is the chain trajectory as a function of arc co-ordinate and time, and $\mathbf{k}$ is the scattering vector of the experiment, related to the neutron wavelength and scattering angle [18]. When t=0 this expression gives the "static structure factor", measured typically by small-angle neutron scattering (SANS). At finite time the delay necessary between effectively interfering scattering events may be introduced by the technique of neutron spin-echo (NSE) [19]. Full calculation of $S(\mathbf{k},t)$ is given in [2] for the cases of both unentangled (Rouse) and entangled (reptation) dynamics. In particular, for the latter a similar one-dimensional diffusion equation is solved as for the stress relaxation, but with differing boundary conditions. Here we will discuss the limiting forms of the expression only in distinct regimes of time and scattering vector (or inverse length-scale).

2.4.1
Unentangled Motion $t<\tau_e, kR_g>>1$ (Short Timescales and Short Length Scales)

For times less than the Rouse time of an entanglement segment, τ_e and short distances, the chain behaves as if it were free since no section has moved far enough to be strongly affected by the tube constraint. The characteristic decay-rate of the scattering function at wavevector k is dominated by the Rouse-time of chain segments whose size is the order of k^{-1}, $\tau_k \sim k^{-4}$. A detailed calculation gives for $t>>\tau_k$ [2]

$$S(\mathbf{k},t)\cong S(\mathbf{k},0)\exp\left[-\frac{2}{\sqrt{\pi}}\left(t/\tau_k\right)^{1/2}\right]; \qquad \tau_k=\frac{12\zeta_0}{k_BT\mathbf{k}^4b^2}. \tag{14}$$

The form of the time-dependence can be understood from the "anomalous" diffusion of a piece of Rouse chain, which displaces in time such that $<r^2(t)>\sim t^{1/2}$ rather than $\sim t$. As a result the $exp(-k^2Dt)$ scattering from Fickian diffusers is replaced by $exp(-k^2Dt^{1/2}\tau_{mon}^{1/2})$. The initial structure factor $S(\mathbf{k},0)$ is just the static scattering function from an ideal Gaussian random walk. Known as the Debye function, at length scales well within the coil radius it is just the Fourier transform of the coulomb-like density profile of monomers on the same chain as a given monomer, and asymptotes to $12/\mathbf{k}^2b^2$.

2.4.2 *Entangled Motion $t>>\tau_e, kR_g>>1$*

For times longer than τ_e, the free Rouse motion of segments is restricted to the tube contour and eventually, for $t>\tau_R$, the structure factor is dominated by reptation. In the high wavenumber limit relative to the coil size (though still on length scales larger than the tube diameter), a simple argument again leads to the correct asymptotic result. If $\mathbf{R}(s,t)$ is still in a piece of original tube then on average it contributes to the structure factor as $S(\mathbf{k},0)$. This is true with a probability of $\mu(t)$. Otherwise it has left the original tube and cannot interfere constructively with the piece at $\mathbf{R}(s',0)$, contributing zero to the structure factor. Thus

$$S(\mathbf{k},t) \cong \frac{12}{\mathbf{k}^2b^2}\mu(t) \tag{15}$$

The general form of these predictions for the dynamic scattering function is that after an initial decay rate dependent on $\mathbf{k}$ and characteristic of free chains, a much slower decay takes over, independent of $\mathbf{k}$ but depending on the molecular weight of the labelled chain. At present the correlation times available from NSE techniques are limited to a few hundred nanoseconds. This is not long enough to probe the long-time dependence of the entangled regime at Eq. (15), but has conclusively demonstrated the cross-over from free to hindered timescales [18].

Neutron scattering can probe molecular dynamics of polymer chains at longer timescales than the upper limits of NSE by exploiting flow or deformation. In this case the equal-time (static) structure factor is measured from a partially-deuterated polymer melt deformed out of equilibrium. These experiments are hard to do because of the relatively low intensities of neutron sources. Either a steady-state shear flow must be engineered in the neutron beam, or the melt quenched rapidly below its glass transition temperature following a period of deformation. The latter technique has confirmed that $S(\mathbf{k})$ exhibits high anisotropy for low wavenumbers (large lengthscales), but that this anisotropy is lost rapidly above a characteristic wavenumber [20]. The corresponding wavelength correlates well with the tube diameter a, consistent with rheological measurements. This is expected because anisotropy on lengthscales smaller than a cor-

responds to segments of chain which are not effectively entangled. They may therefore relax to an isotropic configuration in the very short times typical of free chain segments moving by Rouse dynamics [2].

Such scattering experiments on deformed and quenched melts, while conceptually simple, pose a thorny challenge to theory when requiring quantitative interpretation. In equilibrium the scattering from a partially-labelled melt of flexible polymer chains is relatively easy to calculate using the "Random Phase Approximation" (RPA) which develops a mean-field many-body response function from the single-chain scattering functions calculated in the Gaussian limit [2, 18]. However, the RPA makes use of the equilibrium distribution of all the degrees of freedom in the system. A quenched deformed polymer melt has, by definition, some slower degrees of freedom out of equilibrium while faster ones have relaxed. Great care must be taken when calculating the response of a system with mixed annealed and quenched degrees of freedom. An extension of the RPA to cover these cases, when the quenched variables arise from the tube model, has recently been proposed [21]. Motivated by experiments on controlled-topology polymers under large extension, it predicts rather sensitive dependence of the scattering peaks on the restricted dynamics of branch points (see Sect. 6.1.2).

3 Monodisperse Star-Branched Polymers

As we conjectured in the introduction, the fundamental role of topology in this approach to entangled polymer dynamics would indicate that changes to the topology of the molecules themselves would radically affect the dynamic response of the melts. In fact rheological data on monodisperse star-branched polymers, in which a number of anionically-polymerised "arms" are coupled by a multifunctional core molecule, pre-dated the first application of tube theory in the presence of branching [22]. Just the addition of one branch point per molecule has a remarkable effect, as may be seen by comparing the dissipative moduli of comparable linear and star polymer melts in Fig. 5.

Three experimental observations are particularly striking. First, the range of relaxation times in star polymers is much broader than for monodisperse linear polymers. Rather than representing a dominant single relaxation time, the mechanical spectra require a range of comparably-weighted modes. Second, the range of timescales for this spectrum varies exponentially with the number of entanglements of the arms, M_a/M_e so that both the terminal time and viscosity of the star polymer melt shows a dependence of roughly $\exp(-\nu M_a/M_e)$ where ν is a universal constant of ~0.6. Third, the terminal time and viscosity are dependent *only* on M_a and *not* on the number of arms when the polymers are well-entangled. It is therefore possible to increase the molecular weight of a melt of star polymers by, say, a factor of ten without changing its viscosity at all, providing this is done by adding arms to the branch point. The use of highly multifunctional chlorosilane coupling agents has permitted the synthesis of star polymers with over 30 arms per molecule [23]. This independence on arm-number breaks

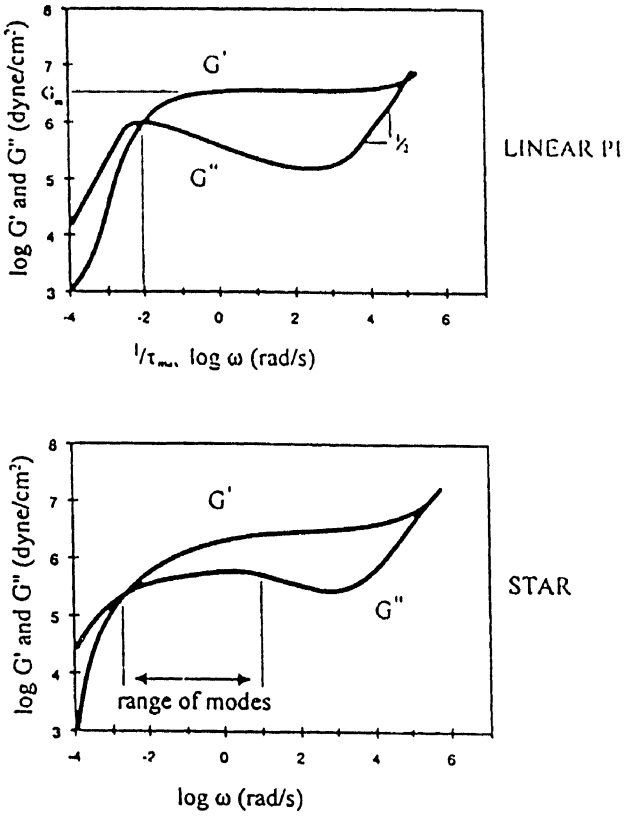

Fig. 5. The elastic modulus $G'(\omega)$ and dissipative modulus $G''(\omega)$ for linear (*top*) and three-arm-star branched (*bottom*) polyisoprene from [5]. Note the broad range of relaxation times indicated by the width of the peak in the star-polymer

down for very high numbers of arms, because overcrowding near the branch point gives a crowded "core" dominated by material from a single molecule. The cores may even order spatially within the melt, leading to new very slow modes in the rheology [23].

3.1 Tube Model for Stars in a Fixed Network

The tube model gives a direct indication of why one might expect the strange observations on star melts described above. Because the branch points themselves in a high molecular weight star-polymer melt are extremely dilute, the physics of local entanglements is expected to be identical to the linear case: each segment of polymer chain behaves as if it were in a tube of diameter a. However, in

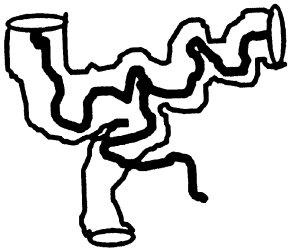

Fig. 6. Proposed mechanism of entangled dynamics of a star polymer in a melt. Retractions as shown partially renew the tube, beginning with rapid retractions near the free end and much more rarely renewing deeper parts of the molecule

this case reptation is suppressed because the diffusion of the centre of mass of a molecule along the tube formed by any two of the arms would necessitate dragging the third arm into the same tube. This is entropically unfavourable since $3kT$ of free energy (via the orientational degrees of freedom of a subchain of length M_e) would be paid for each tube segment dragged a distance a into the tube of another chain segment. Thus the branch point is effectively pinned up to very rare fluctuations of the configuration. Instead we must rely on the *fluctuations* in the length of primitive path of the star arms (which must be present due to the Rouse "breathing" modes along the tube contours) to renew the configurations of the entangled arms as in Fig. 6. Of course the actual number of monomers in the star arms does not fluctuate. Instead the motion results from the formation of *unentangled loops* of chain both within the original tube and exploring the environment around it. The high free energy of these states arises from their double-occupation of tube segments participating in the loops. Primitive path length fluctuations will lose stress contributions from each arm independently, so the stress relaxation function will not depend strongly on the numbers of arms in the star. Moreover it is not surprising that the probabilities of the largest fluctuations which completely release a star arm into a new configuration are exponentially low in the arm length. We now proceed to treat this insight slightly more quantitatively.

3.1.1
Brownian Chain Tension in a Melt and the Tube Potential

An alternative way of viewing the entropy loss on constraining entangled polymers is to see it as equivalent to a *tension* of $3kT/a$ along every entanglement segment. So the free energy change associated with doubly-occupied tube described above emerges naturally as just this tension multiplied by the distance translated curvilinearly along the tube, a. This is a very useful insight – it provides an alternative way of understanding Eq. (8) for the stress: the tension $3kT/a$ is carried by each entanglement segment of length a. The components of

the total stress are calculated by counting strands transferring tension across the corresponding planes [2].

The chain tension arises in a physical way: at timescales short enough for the tube constraints to be effectively permanent, each chain end is subject to random Brownian motion at the scale of an entanglement strand such that it may make a random choice of exploration of possible paths into the surrounding melt. One of these choices corresponds to retracing the chain back along its tube (thus shortening the primitive path), but far more choices correspond to extending the primitive path. The net effect is the chain tension sustained by the free ends.

In fact, without the inclusion of the chain-end tension, the equilibrium path-length of the chain is not maintained. We can write a potential $U(z)$ for the length of the primitive path z by including both the (quadratic) curvilinear rubber-elastic term and the (linear) end-tension term as follows:

$$\begin{aligned} U(s) &= \frac{3kT}{2Nb^2}z^2 - \frac{3kT}{a}z \\ &= \frac{3kT}{2Nb^2}\left(z-L\right)^2 + const. \end{aligned} \tag{16}$$

where $L=Nb^2/a$ is the equilibrium primitive path length of the chain. We have chosen to measure z from the branch point outwards. This quadratic potential will determine the fluctuation dynamics of an arm of an entangled star polymer: the free energy paid for a retraction which brings the entangled path length from the branch point to the free end from its equilibrium value L to some smaller value $z<L$. Whenever this happens, the subsequent equilibrium configuration will have a renewed configuration for all chain segments occupying tube whose primitive path distance from the branch point is between z and L.

3.1.2 *Approximate Theory for Stress-Relaxation in Star Polymers*

The observations above can be rapidly turned into a semi-quantitative theory for star-polymer stress-relaxation [24] which is amenable to more quantitative refinement [25]. The key observation is that the diffusion equation for stress-release, which arises in linear polymers via the passage of free ends out of deformed tube segment, is now modified in star polymers by the potential of Eq. (16). Apart from small displacements of the end, the diffusion to any position s along the arm will now need to be *activated* and so is exponentially suppressed. Each position along the arm, s, will possess its own characteristic stress relaxation time $\tau(s)$ given approximately by

$$\tau\left(s\right) = \tau_0 \exp\left(\frac{U\left(s\right)}{kT}\right). \tag{17}$$

Henceforth we take the primitive path co-ordinate $s=L-z$ from the free end inwards to the branch point so that $\tau(s)$ is an increasing function of s. The prefactor τ_0 is an inverse "attempt frequency" for explorations of the potential by the free end, and may be expected to scale as the Rouse time for the star arm (in fact this is not quite true – the actual scaling is as $M_a^{3/2}$ [25, 26]). The relaxation modulus can be calculated exactly as for linear polymers, using Eq. (11), but this time with the simple (Poisson process) expression for $p(s,t)$ from the activated diffusion picture:

$$p(s,t) = e^{-t/\tau(s)} . \tag{18}$$

The form of $p(s,t)$ is well-approximated for highly entangled arms by a step function in s: consider the form of the relaxation at any time t intermediate between the relaxation time of the first entangled segments near the end of the arm and the core-segments of the star. At t some internal segment will typically be just in the process of reconfiguration via its first "visit" by the free end. This segment will have an arc-length co-ordinate s given by $\tau(s)=t$. All segments exterior to the segment $s(t)$ are almost certain to have relaxed, because their relaxation timescales are exponentially shorter, while segments nearer to the core are conversely almost certainly unrelaxed.

In this theory the diffusion constant of the star molecule and the viscosity are both determined by the longest of the relaxation times of Eq. (17), so depend exponentially on the arm molecular weight M_a via $\tau_{\max}=\tau(L)\sim\tau_0 \exp(-U(L)/kT)\sim\tau_0 \exp(\nu' M_a/M_e)$, where τ_0 is an attempt-time for arm retractions.

This theory was able to account for both the molecular-weight scaling of the dynamic quantities D_0, η, and $\tau_{\max}$ as well as for the shape of the relaxation spectrum (see Fig. 5) apart from one important feature – the constant ν' in the leading exponential behaviour that multiplies the dimensionless arm molecular weight needed to be adjusted. This can be understood as follows. The prediction of the tube model for the plateau modulus from the stress Eq. (7) is

$$G_0 = \frac{4}{15} c_N f_{eq} L \tag{19}$$

where f_{eq} is the equilibrium tension [2]. From the definition of the entanglement molecular weight enshrined in

$$G_0 = \frac{\rho RT}{M_e} \tag{20}$$

[1] in terms of the density of entanglement strands ρ/M_e, we can deduce a quantitative relationship between a and b as $a^2=(4/5)N_e b^2$ and find from Eq. (16) that $U(L)=15N_a/8N_e$. So the tube model gives a prediction for the constant ν' of 15/8. This was in marked contrast to a value of about 0.6 required to fit experimental data [25] and taken at face value gives enormous discrepancies in predictions

for, for example, the viscosity, overpredicting values by many orders of magnitude for well-entangled stars. The resolution of this difficulty comes from recognising the importance of co-operative *constraint-release* effects in the melt. These are much more effective at accelerating relaxation away from the fixed network result in the case of branched polymers than linear polymers. This is because here constraint release acts directly against the exponentially slow retractions of the dangling arms. We now look at a method for accounting for constraint release in star polymer melts.

3.2 Tube Theory of Star Polymer Melts

3.2.1 *Approximate Theory for Constraint Release in Star Polymer Melts*

The much more significant contribution of constraint release to the dynamics of entangled star polymers in comparison to linear polymers arises from the very broad distribution of relaxation timescales we have discussed above. Fortunately, the same breadth of timescales provides a simple way of calculating the effect [27]. As a consequence of the exponential separation of relaxation timescales along a star arm, by the time that a given tube segment s in the population is relaxing, all segments of tube s' such that $s'<s$ (nearer a chain end) have renewed their configurations typically *many* times. So chain segments at s and nearer the star cores do not entangle with these fast segments at the timescale $\tau(s)$ and beyond. Alternatively we can say that the tube is widened due to this effective dilution of the entanglement network – fast-relaxing segments act as solvent for the slower relaxing ones. Such an idea applied to constraint-release in linear polymers is problematical [26, 28] because of the dominance of the single relaxation time τ_{rep}, but becomes applicable in the case of stars, and branched polymers generally. This picture of "dynamic dilution" is equivalent to an early theory for constraint release in linear polymers dubbed "double reptation" because it associated stress with binary topological contacts between chains. Such "stress points" were supposed to vanish when either chain diffuses away [29, 30]. A criterion which successfully accounts for the regimes of validity of such a simplification compares the rates of self-diffusion of monomers on chain segments relaxing on a timescale τ with the rate of tube widening given by the dilution hypothesis. If the first is greater than the second, then the diluting tube acts as the effective topological constraint, and "dynamic dilution" is valid. If not, then the chain relaxation is not impeded by the tube and the approximation fails. We revisit this physics more quantitatively in Sect. 3.2.5. when we have a few more tools to hand.

The new information necessary to make this approach quantitative is the dependence of the effective entanglement molecular weight on the concentration, ϕ of unrelaxed segments. This is known from experiments on dilution of polymer melts by theta-solvents to be approximately $M_e(\phi)=M_{e0}/\phi$, which corre-

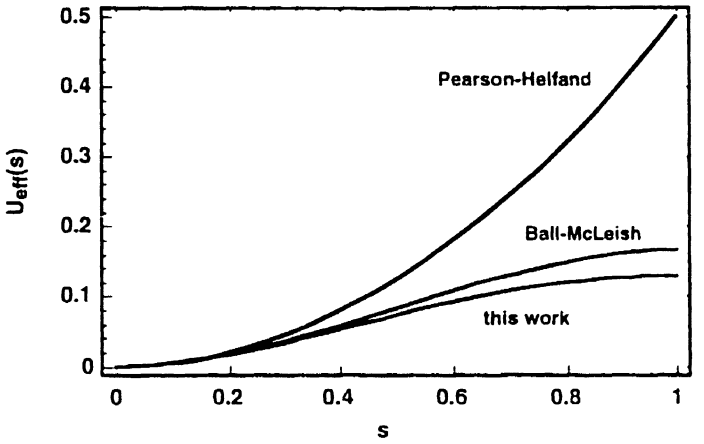

Fig. 7. The effective free-energy potentials for retraction of the free end of arms in a monodisperse star polymer melt. The *upper curve* assumes no constraint-release, the *lower two curves* take the "dynamic dilution" approximation with the assumptions $M_e \sim \phi^{-1}$ (Ball-McLeish) and $M_e \sim \phi^{-4/3}$ (Milner-McLeish)

sponds, via Eq. (20),to the approximately quadratic concentration dependence of $G_0 \sim \phi^2$ [2, 31] (but see Sect. 3.2.2. for refinements). At any stage in the relaxation dynamics of a melt of identical star polymers, therefore, when a segment s is currently relaxing for the first time, the effective entanglement molecular weight is $M_e(s)=M_{e0}/(1-s/L)$. To recompute the relaxation times $\tau(s)$ with the dynamic dilution assumption we consider the activated diffusion in a hierarchical way: to retract from s to $s+\Delta s$, the attempt frequency is $\tau(s)^{-1}$ and the barrier to diffusion is $\exp\{(-1/kT)\,[U(s+\Delta s; M_e(s))-U(s; M_e(s))]\}$ where the notation for U indicates that the running value of the entanglement molecular weight is kept. Taking the limit of Δs small gives the differential equation

$$\frac{\partial \ln \tau(s)}{\partial s} = \frac{15}{4}\frac{M_a}{M_{e0}}\frac{s}{L^2}\left(1-\frac{s}{L}\right) \tag{21}$$

where the last term arises from the "dynamic dilution" of the tube increasing the effective value of M_e [27]. Integration of this equation leads to an effective renormalisation of the potential $U(s)$ which is now a cubic in s

$$U_{eff}(s) = kT\frac{15}{4}\frac{M_a}{M_e}\left(\frac{s^2}{2L^2}-\frac{s^3}{3L^3}\right). \tag{22}$$

The terminal time and viscosity are dominated, as we saw above, by the potential at complete retraction $U_{eff}(L)$. This is now given by $15/24(M_a/M_e)$, in much closer agreement with experiments. The formula for the relaxation mod-

ulus also needs modifying since each element of chain *ds* contributing to the stress relaxation now does so in an environment diluted by (1–*s*/L), so picks up this factor within the integrand [27]. Figure 7 compares the original quadratic entropic potential of Eq. (16) with the renormalised effective potential of Eq. (22). Both the terminal time and the shape of the potential are modified, the flattening at high *s* (deep retractions) giving rise to a flatter slope in $G''(\omega)$ for the longest relaxation times.

The shape of the relaxation spectrum predicted by Eq. (22) does indeed fit rheological data on pure star melts better than the quadratic expression calculated for stars in permanent networks [27], except at high frequencies where the assumption of activated diffusion breaks down (it may easily be verified that $U_{eff}(s)<kT$ for the fraction $(M_e/M_a)^{1/2}$ of chain nearest the chain end). This and other refinements to the theory have been the subject of very recent work, to which we now turn.

3.2.2
Parameter-Free Treatment of Star Polymer Melts

The approximate treatment described above accounts rather well for the linear rheology of star polymer melts. In fact it has been remarked that the case for the tube model draws its real strength from the results for star polymers rather than for linear chains, where the problems of constraint release and breathing modes are harder to account for (but see Sect. 3.2.4.). However, there are still some outstanding issues and questions:

(1) what are the proper prefactors to the expression for $\tau(s)$ using $U_{eff}(s)$?
(2) how sensitive is the result to the exact dilution behaviour of the entanglement network?
(3) at short times, how can we account for the effect of non-activated Rouse motion on the relaxation of segments near the end of the star arms?

In particular it has been conjectured that the terminal relaxation of star polymers might be the most sensitive test of the "dilution exponent" β in $G_0 \sim \phi^{\beta}$. We noted above that values of β close to 2 are candidates, but a number of careful experiments in theta solvents suggest a mean value of nearer 2.3 [32]. A physically reasonable scaling assumption for the density of topological entanglements in a melt of Gaussian chains leads to a value of 7/3 [31].

Recent work [33] has addressed all these questions, and in particular has given a cross-over formula for $\tau(s)$ incorporating all these effects, so valid for all timescales longer than the Rouse time of an entanglement segment τ_e. The prefactor comes from a solution to the diffusion equation appropriate to the activated barrier-hopping of the star-arm free end under a steady-state flux of diffusers. The first-passage time for diffusing particles (the chain ends) can be written exactly as a quotient of integrals over the effective potential well in which they are trapped. When the renormalisation process applied to the "bare" quadratic

potential is modified for a general dilution exponent and the integrals calculated in the (appropriate) asymptotic limit of $U_{eff}>>kT$, the result is

$$\tau_a(x) \cong \tau_e\left(\frac{M_a}{M_e}\right)^{3/2}\left(\frac{2\pi^5}{15}\right)^{1/2} \frac{\exp\left[U_{eff}(xL)/kT\right]}{x\left[(1-x)^{2\alpha} + \left(\left(\frac{4M_a}{15M_e}\right)(1+\alpha)\right)^{\frac{2\alpha}{\alpha+1}}\Gamma\left(\frac{1}{\alpha+1}\right)^{-2}\right]^{1/2}} \tag{23}$$

where $x=s/L$, $\alpha=\beta-1$, and the generalised effective potential is given by

$$U_{eff}(s) = kT\frac{15N}{4N_e}\frac{1-(1-s/L)^{1+\alpha}\left[1+(1+\alpha)s/L\right]}{(1+\alpha)(2+\alpha)} \tag{24}$$

It is straightforward to check that this is equivalent to Eq. (22) in the case $\alpha=1$. However, it differs significantly in the case $\alpha=4/3$ (see Fig. 7). The Boltzmann factor in U_{eff} still dominates Eq. (23) for the first-passage times, but now the weakly s-dependent prefactor is calculated explicitly, as is its scaling with $(M_a/M_e)^{3/2}$.

Early-time motion, for segments s such that $U_{eff}(s)<kT$, is dominated by non-activated exploration of the original tube by the free end. In the absence of topological constraints along the contour, the end monomer moves by the classical non-Fickian diffusion of a Rouse chain, with spatial displacement $<r^2>\sim t^{1/2}$, but confined to the single dimension of the chain contour variable s. We therefore expect the early-time result for $\tau(s)$ to scale as s^4. When all prefactors are calculated from the Rouse model [2] for Gaussian chains with local friction we find the form

$$\tau_e(x) = \frac{225\pi^3}{256}\left(\frac{N_a}{N_e}\right)^2 \tau_R x^4 . \tag{25}$$

A cross-over formula for $\tau(s)$ covering both the early and activated timescales can be constructed with sufficient accuracy as $\tau(x)=\tau_a(x)\tau_e(x)/(\tau_a(x)\exp(-U_{eff}/kT)+\tau_e(x))$.

Finally we require an expression for the relaxation modulus consistent with the dilution hypothesis in which each tube segment relaxing its stress typically at a time $\tau(x)$ does so in a background whose effective density of entangled strands is Φ_{eff}. The appropriate general form is

$$G(t) = \int_0^1 dx \frac{dG\left(\Phi_{eff}(x)\right)}{dx} e^{-t/\tau(x)} \tag{26a}$$

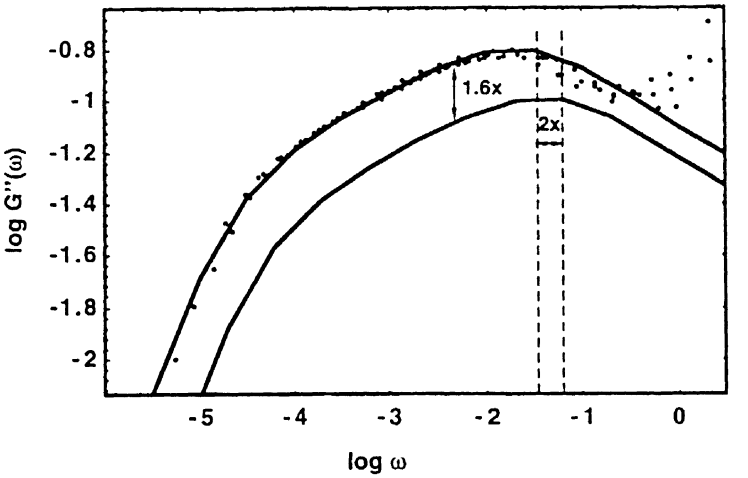

Fig. 8. Predictions of parameter-free theory for $G''(\omega)$ and data for a star polybutadiene from [33]. Small shifts in the two prefactors bring the experiments and theory into quantitative agreement over five decades in timescale. Dilution exponent $\alpha=4/3$ and $M_e=1850$

which in the specific case of monodisperse star melts, $\Phi_{eff}=(1-x)$ with $x=s/L$, becomes

$$G(t)=G_0(1+\alpha)\int_0^1 dx(1-x)^{\alpha}\exp\left[-t/\tau(x)\right] \tag{26b}$$

with notation as above.

The scheme of Eqs. (23)–(26) above allows a prediction for the relaxation spectrum of a monodisperse star melt to be made without any free parameters at all if G_o and τ_e are taken from data on linear polymers in the low and high frequency range respectively. When this is done the shape and range of relaxation times (via the rheological function $G''(\omega)$) is very well accounted for (see Fig. 8). The departure of data from theory at this level, which just concerns *entangled* modes, is delayed to frequencies higher than τ_e^{-1}, when the classical $\omega^{1/2}$ form of unhindered Rouse relaxation is both expected and seen. To achieve a quantitative fit for the entangled modes at the level of prefactors, shifts of about 1.6 in the modulus and 2 in the monomeric friction factor are required from those calculated from linear polymers. These shifts seem to be independent of polymer chemistry, and may result from the level at which constraint-release has been treated via the dilution approximation. In particular it was confirmed that the difference of just 1/3 in the candidate values for the dilution exponent can alter the terminal time of a moderately-entangled star polymer by over an order of magnitude. If this theoretical framework is correct, it therefore allows simple melt rheology to become an exceedingly accurate way to determine β. Within the

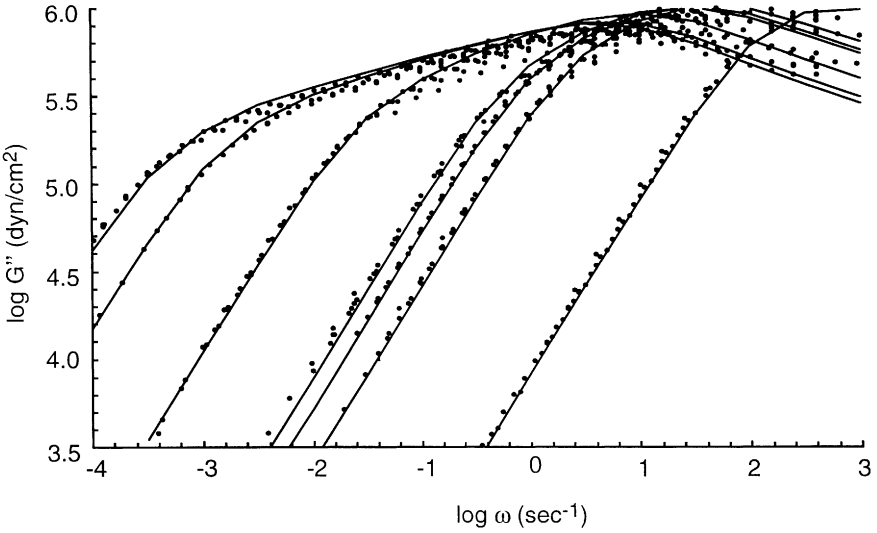

Fig. 9. Predictions of parameter-free theory for *G"(ω)* with *O(1)* corrections to G_0 and τ_e as for Fig. 8 and data for a range of 3- and 4-arm star polyisoprenes from [5]. Arm molecular weights in 10^3 g mol^{-1} are 11.4, 17, 36.7, 44, 47.5, 95 and 105. The entanglement molecular weight has been taken as 5000 g mol^{-1}

range of reported values of M_e for the range of chemistries examined [33, 34], a value of about 7/3 [30] seems to be preferred.

With this choice of β, the theoretical picture presented in this section is consistent, for example, with the range in M_a/M_e (from about 2 to about 20) explored by the polyisoprene (PI) data set of Fetters et al. [5] using a single value of M_e of 5000 g mol^{-1}. The viscosities of these melts cover five decades in magnitude yet the current theory, together with values for G_0 and τ_e consistent with data on linear PI predicts the entire range of viscoelastic spectra (see Fig. 9).

3.2.3
Single Chain Structure Factor for Star-Polymer Dynamics

The dynamic structure factor for scattering from a single chain as defined in Eq. (13) has a simple long-time form for the case of linear reptating polymers (see Eq. 15), due to the homogenous nature of the chain's orientational relaxation. The special entangled dynamics of star polymers, however, lends a little more structure to $S(\mathbf{k},t)$ [35]. The full result is relatively complex, but differs from the approximation for linear polymers as given in Eq. (15) in that the scattering within the range $R_g^{-1}<k<a^{-1}$does not follow the same time-dependence, but decays more rapidly with increasing k. This is due to two effects: the exponentially slower relaxation of deeper parts of the chain, which dominate the low-

k region, and also the continued contribution of relaxed outer parts of the chain to the low-k scattering. In particular, pairs of monomers nearby on the outer parts of the star arm, which contribute at early times to high-k scattering, contribute to lower-k scattering at longer times, when they have become part of a retracted and renewed portion of chain. The interference in the scattering amplitude is then between the former and present pieces of chain (the two copies of the outer parts of the star arm in Fig. (6). As the retractions and reconfigurations become deeper, monomer pairs which once were typically separated by short distances may approach separations of the order of the chain radius of gyration. The scattering function can be approximated by:

$$S_{star}(\boldsymbol{k},t) \cong S_{star}(\boldsymbol{k},0)(\frac{t}{\tau_R})^{-z(k)} \tag{27}$$

for $\tau_R < t < \tau_{\max}$. The scale-dependent dynamic exponent $z(k)$ is an approximately linear function of k, decreasing from 1 to 0.2 over the k-range $3R_g^{-1}$ to R_g^{-1}. Current experiments do not provide access to the timescales over which such behavior is predicted, but may do so in the future.

3.2.4 *Linear Chains Revisited – The "3.4 Law"*

Comparison of Fig. 3 (dashed line for theory) and Fig. 8 will underline our earlier remark that the tube model seems to do much better when applied to star melts than to its original goal of linear melts, at least as far as the shape of the relaxation spectra, and the dependence of the terminal times on molecular weight in concerned. However, it is clear that the physics accounted for in the previous section on star polymers represents a more complete theory than that used in Sect. 2.2 for stress relaxation by reptation in linear polymers. There only a single mode (the "centre of mass" mode) of the chain was assumed without any detailed structure coming from internal chain modes. Of course the consideration of entangled star polymers forces us to consider these modes because the reptation mode is absent. In fact, at the level we treated reptation, there is no stress relaxation in star polymers at all! This suggests that a tube theory for linear polymers which treats path-length fluctuations at the same level as we have used for stars might do more justice to the data – it would certainly do more justice to the capabilities of the model.

Doi conjectured early in the development of the tube model that path-length fluctuations would both reduce the predicted reptation time and steepen its dependence on molecular weight [36]. As we have seen for the essential path fluctuations of star polymer arms, at the Rouse time of the dangling arm, a fraction $(N_a/N_e)^{-1/2}$ of the original tube is lost by the curvilinear Rouse diffusion of the free end. At longer times the fluctuations begin to be activated by the effective path-length potential – hence the exponentially slow deeper retractions in stars. But the linear polymers will also lose entanglements from their free end in just

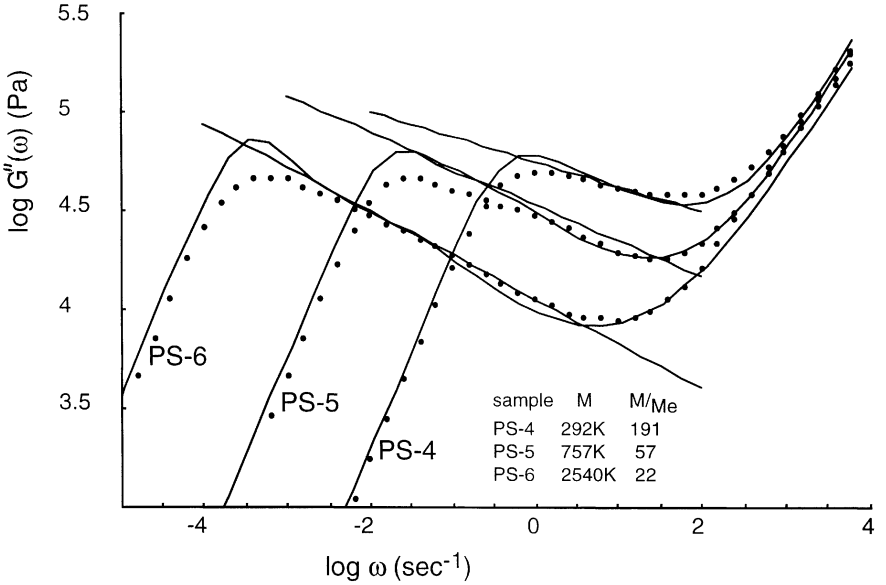

Fig. 10. Data for $G''(\omega)$ on three monodisperse linear polystyrenes from [15] with values of M/M_e of 22, 57 and 191. The theoretical curves account for path length fluctuations calculated as for star polymers [41] choosing values for G_0 and τ_e consistent with published data

the same way. This reduces the path length which the centre of mass must typically diffuse by reptation to renew the entire tube by a factor of $[1-\kappa(N_e/N)^{1/2}]$ where κ is a number of order 1. So the reasoning that led to Eq. (3) above for the reptation time now gives

$$\tau_{rep} = \tau_{mon} \frac{N^3}{N_e} \left[1 - \kappa \left(\frac{N_e}{N} \right)^{1/2} \right]^2 \tag{28}$$

Such a functional form mimics a power law of $M^{3.4}$ over a range of molecular weights up to about $100M_e$, but this is not as large as the range experimentally observed, even with a free choice for the parameter κ.

Various authors have performed numerical simulations on one-dimensional chains which possess the curvilinear Rouse modes necessary to capture path length fluctuations [37–40]. Stress is arranged to be lost from tube segments passed by either free end of the polymer – this happens in general as a combination of reptation and fluctuation. These calculations produce up to three orders of magnitude in M/M_e for which the power law $M^{3.4}$ models the viscosity dependence well, crossing over gently to the pure-reptation result of M^3 at very high molecular weights.

Rubinstein has constructed on a reptation-fluctuation approach a detailed self-consistent theory of constraint release, allowing each loss of entanglement in one chain to permit a random jump in the tube of another [37]. When this is done the form of predicted relaxation functions are in good accord with experiments. However, in monodisperse linear melts it appears that the fluctuation contribution is more important than constraint release.

Very recent work has applied the analytical form for the stress relaxation following that for star polymers developed above, but crossing over to disentanglement by reptation when this is faster than fluctuation. At earlier times another cross-over to unentangled Rouse modes on length scales smaller than a was included, again without resort to extra free parameters [41]. This approach gives a close match with experiments on monodisperse model melts. The results of the predictions for G'' are shown in Fig. 10 together with the data on linear polystyrenes (PS) from [15]. The advantage of this approach is, as in the case of star polymers, that there are no extra parameters to import into the theory – the tube diameter and monomeric friction constant invoked in the basic reptation model are sufficient for the inclusion of fluctuation and Rouse modes. The theory correctly predicts the viscosity (response to the left of the peak) and the fluctuation-dominated slope (to the right of the peak) in this range of M/M_e from 20 to 200. Note that the dependence of the effective slope of $G''(\omega)$ to the right of the peak on molecular weight is also captured. The physical reason for this is also clear: the x^4-dependence of the Rouse disentanglement times near the chain end is directly linked to a form for $G''(\omega)$ that asymptotes to $\omega^{-1/4}$ to the right of the peak if chains are long enough. The only region in which there are significant differences between theory and experiment are at the reptation time itself where the effects of constraint release by *reptation* of other chains and polydispersity are expected to be strongest. Satisfyingly, a plot of the predictions of the viscosity against molecular weight are very closely modelled by a power law with exponent 3.4 up to M/M_e of 1000, in close agreement with the data. Further careful experiments on the rheology of very high molecular weight monodisperse polymers will serve to test other consequences (such as a return to a slope of –1/2 in $G''(\omega)$ immediately to the right of the maximum for extreme values of M/M_e) of this very promising resolution of an ancient puzzle.

3.2.5
A Criterion for the Validity of Dynamic Dilution

The mathematical treatment that arises from the "dynamic dilution" hypothesis is remarkably simple – and very effective in the cases of star polymers and of *path length fluctuation* contributions to constraint release in linear polymers. The physics is equally appealing: all relaxed segments on a timescale τ are treated in just the same way: they do not contribute to the entanglement network as far as the unrelaxed material is concerned. If the volume fraction of unrelaxed chain material is Φ, then on this timescale the entanglement molecular weight is renormalised to M_e/Φ^{α} or, equivalently, the tube diameter to $a/\Phi^{\alpha/2}$. However, such a

simple approach cannot work for all cases in which constraint-release is important. In particular it fails for monodisperse chains affected by constraint-release from the *reptation* of other chains as the following rough calculation will show:

A single-mode approximation for the relaxation of entangled fraction $\Phi(t)$ by reptation is

$$\frac{\delta\Phi(t)}{\delta t} = -\frac{1}{\tau_{rep}}\Phi(t)\,. \tag{29}$$

A naïve application of dynamic dilution would introduce a dependence of the reptation time on the unrelaxed volume fraction. Since $\tau_{rep} \sim L^2 \sim (aM/M_e)^2$ this would imply the choice of $\tau_{rep}(\Phi) \sim \Phi$ in the case $\alpha=1$ for the dilution exponent. But making this substitution completely alters the relaxation function to the pathological $G(t)=G_0(1-t/\tau_{rep})^2$. A more refined treatment at the level of a proper diffusion equation retains a relaxation which is much too fast. Yet dynamic dilution works perfectly for branched polymers – why? Clearly the answer lies in the distribution of timescales for the constraint-release (CR) events. In the linear polymer case the CR events all occur on the timescale of τ_{rep}. On the other hand the vast majority of CR events that permit swelling of the tube in star polymer melts to occur on a timescale τ, themselves possess *exponentially* shorter timescales than τ.

The key issue is the following: to follow dynamics constrained by a tube dilated to diameter a at a timescale τ, a chain must be able to explore a distance perpendicular to its contour of at least a by *constraint-release Rouse* motion [26, 42]. Here entanglements on fast timescales act as effective friction-points on unrelaxed chains – an example would be self-dilute long chains in a melt of shorter chains. At the short chains' reptation time, local sections of the long chain of molecular weight M_e may "hop" a distance of order a. Such local dynamics always results in Rouse-like motion at longer length and timescales [2]. An equivalent picture is one which endows Rouse dynamics to the *tube* of the long polymers [26]. Another example is the motion of slow sections of star polymers – if they have no entanglements with equally slow or slower material, they are free to move in a local frictional environment determined by the relaxation of faster-relaxing material. In both these cases, as in ordinary unentangled Rouse chains, the perpendicular diffusion of local pieces of chain follows the sub-Fickian behaviour $\langle r^2(t)\rangle \sim t^{1/2}$. The important requirement for a piece of unrelaxed chain to feel a dilated tube is that the Rouse-like exploration of space generated by fast entanglements $\langle r^2(t)\rangle$ is *faster* than the growth of the tube diameter $a^2(t)$ through dilution by current disentanglement. So if x is some label for chain material which relaxes at time $\tau(x)$ (for example x could be, as above, the co-ordinate label of segments along the arm of a star polymer) the physical criterion for dynamic dilution can be written

$$\frac{1}{r^2(t)}\frac{dr^2(t)}{dt} > \frac{1}{a^2(\Phi(t))}\frac{d}{dt}a^2(\Phi(t)) \tag{30}$$

Using the Rouse result, the left hand side of Eq. (30) is just $1/2t$. In the case of star polymers, using the approximate result for $\tau(x)$ from Eq. (21) and the corresponding dynamic dilution result $\Phi(x)=(1-x)$ the criterion becomes

$$\frac{1}{2} > \left(\frac{4}{15}\right)\frac{1}{(1-x)^2 x}\left(\frac{M_e}{M_a}\right) \tag{31}$$

(see [42]). This is satisfied for $x>8/15(M_e/M_a)$, i.e. when the chain first feels the original undiluted tube, and for $x<1-(8M_e/15M_a)^{1/2}$. This is typically very close to the core of the star, and corresponds to a "disentanglement transition" when the tube dilates faster than the remaining unrelaxed star arm can follow it by Rouse-like constraint release. The contribution of this small amount of unrelaxed material obeying effectively unentangled dynamics near the terminal time contributes very little to the relaxation modulus.

So the criterion that the effective constraint-release must be fast enough to allow local pieces of unrelaxed chain to explore any dilated tube fully confirms the assumption of dynamic dilution for nearly the whole range of relaxation timescales exhibited by star polymers.

As a second example we can apply it to polydisperse linear polymers; the variable x becomes naturally the molecular weight of a chain reptating at time τ, and $\Phi(x)$ the integrated weight distribution function over all chains longer than x. This is just the problem addressed by the "double reptation" [29, 30] approach. Use of the general expression for $G(t)$ in Eq. (26) gives an expression identical with that derived from double reptation (simply squaring the fraction of unrelaxed material to calculate the current stress). Applying the dynamic dilution criterion Eq. (30) we find as shown in detail in [42]

$$\frac{x}{\Phi(x)}\frac{d\Phi}{dx} > -\frac{3}{2}. \tag{32}$$

So dynamic dilution is valid in linear polymers only for the case of extremely wide polydispersity in which the weight distribution is broader than that of a power-law with exponent –5/2. In particular we see that it is *not* valid for near-monodisperse linear polymers around their terminal time.

4 More Complex Topologies

The recognition of the two fundamental mechanisms of reptation and arm fluctuation for linear and branched entangled polymers respectively allows theoretical treatment of the linear rheology and dynamics of more complex polymers. The essential tool is the "renormalisation" of the dynamics on a hierarchy of timescales, as for the case of star polymers. It is important to stress that experimental checks on well-controlled architectures of higher complexity are still very few due to the difficulty of synthesis, but the case of comb-polymers is an example where good data exists [7].

4.1 Combs and H-Polymers

These polymers possess a high molecular weight "backbone" to which are attached a number, q, of side arms (see Fig. 11). The structure most amenable to our theoretical development are those in which the arms are all of the same molecular weight M_a and regularly spaced along the backbone of molecular weight M_b. We assume all molecules are identical. The case of interest to us in the context of topological interactions has both arms and backbone initially entangled. For if on the other hand $M_a/M_e<1$, the backbones behave for all times like linear polymers, with a slightly modified friction factor and entanglement length since the arms just act as diluent. However for $M_a/M_e>1$ the behaviour is predicted to be quite different [43]. Now the backbones are quite immobile for early times since the side arms behave almost like the arms of star polymers, and do not release the diffusion of their branch points until the timescale for full retraction. On the other hand the retraction of the side arms is *slower* than in a melt of stars of identical M_a because of the presence of the backbone material, which acts as permanent network for the side arms throughout their retraction. This reduces the extremely efficient process of dynamic dilution considered in the previous section, so that the effective potential for relaxation times for the arms is now

$$U_{eff}(s) = kT\frac{15}{4}\frac{M_a}{M_e}\left(\frac{s^2}{2L^2} - \phi_{arm}\frac{s^3}{3L^3}\right) \tag{33}$$

(compare Eq. 22), where ϕ_{arm} is the volume fraction of arm-material $qM_a/(qM_a+M_b)$. In this discussion we retain $\alpha=1$ for simplicity, but the more general case poses no difficulty [46]. This renormalised potential is calculated in exactly the same way as for star polymers in in Sect. 3.2.1, except that the effective entanglement molecular weight as a function of the curvilinear co-ordinate for arm retraction s is now $M_e(s)=M_{e0}/(1-\phi_{arm}s/L)$. This interpolated behaviour for retracting arms, intermediate between the star-network and star-melt cases, also arises in a blend of star polymers with long linear chains [42, 44].

Now at times $t>\tau_{arm}$, the longest retraction time of the side arms, the backbone is free to move, controlled by the effective frictional drag of the branch-

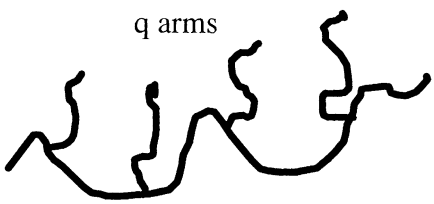

Fig. 11. The schematic structure of a comb polymer; q arms of molecular weight M_e are attached with regular spacing to a backbone of molecular weight M_b

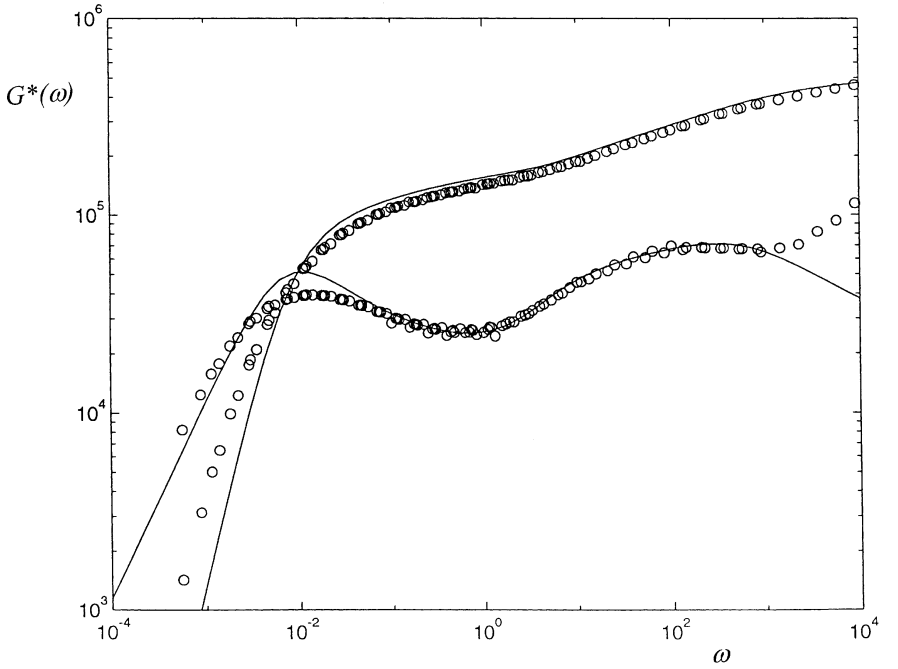

Fig. 12. The rheological functions $G'(\omega)$ and $G''(\omega)$ for an H-shaped PI of arm molecular weigh 20 kg mol^{-1} and backbone 110 kg mol^{-1} [46]. The high-frequency arm-retraction modes can be seen as the "shoulder" from $\omega \sim 10^0$ to $\omega \sim 10^3$ together with a low-frequency peak due to the "cross-bar" dynamics at $\omega \sim 10^{-2}$. The smooth curves are the predictions of a model which takes Eq. (33) as the basis for the arm-retraction times and a Doi-Edwards reptation spectrum with fluctuations for the backbone. The reptation time is correctly predicted, as is the spectrum from the arm modes, though the low frequency form is more polydisperse than the simple theory predicts

points, which typically far outweighs the monomeric frictional drag from the backbone itself. Each branch point takes a random step of size $a^\star$ with a rate $\tau_{arm}{}^{-1}$ so the effective friction constant of the branch point $\zeta_{br} \sim kT\tau_{arm}/a^{\star 2}$. Here $a^\star$ is the diluted value of the tube diameter at the relaxation time of the dangling arms. At the timescales for backbone motion, all the arm material has disentangled (typically at much shorter timescales) so, just as in the mutual dilution of star polymers, acts as unentangled solvent for the backbone. The melt thus behaves like a melt of *linear* polymers at long times, with a degree of entanglement per chain of $M_b(1-\phi_{arm})/M_e$ and a total frictional drag of $q\zeta_{br}$. In this way it is possible for a highly branched polymer to behave like a linear polymer for some range of timescales. Whether the long-time dynamics of the backbones is effectively entangled or not depends on the renormalised degree of entanglement, which is reduced as the amount of material in the side arms increases. Thus even

if the backbones are originally entangled with other molecules' arms, the final motion may be a slowed-down Rouse motion if mutual entanglements between backbones are not sufficient to force them to reptate (this is just the case of $M_b(1-\phi_{arm})/M_e \leq 1$). Both cases of renormalised Rouse and renormalised reptation have been observed in model materials [7, 42].

The simplest case of comb polymer is the H-shaped structure in which two side arms of equal length are grafted onto each end of a linear "cross-bar" [6]. In this case the backbones may reptate, but the reptation time is proportional to the *square* of M_b rather than the cube, because the drag is dominated by the dumbbell-like frictional branch points at the chain ends [45, 46]. In this case the dependence on M_b^2 is not a signature of Rouse motion – the relaxation spectrum itself exhibits a characteristic reptation form. The dynamic structure factor would also point to entangled rather than free motion.

Experiments on both combs and H-polymers show rheological spectra with two distinct regions at frequencies typical of entangled modes: a high-frequency "shoulder" attributable to the arm retractions, and a low-frequency region which may be of the form $\omega^{1/2}$ in the case of unentangled backbones, or exhibit a characteristic time via a maximum in $G''(\omega)$ for mututally entangled backbones (see Fig. 12).

Combining the predictions for the reptation time of the H cross-bar and the effective modulus when the arms are acting as solvent gives a prediction for the scaling of the viscosity of a melt of H-polymers on their structural parameters:

$$\eta_H \cong G_0 \tau_0 (1-\phi_{arm})^3 \left(\frac{M_b}{M_e}\right)^2 \exp[-2\nu \frac{M_a}{M_e}(\frac{1}{2} - \frac{\phi_{arm}}{3})] \,. \tag{34}$$

A full analytical expression for the relaxation spectrum is straightforward to calculate at the level of Sect. 3.2.1 for stars. Timescales $\tau_{arm}(s)$ and $\tau_{bb}(s)$ are calculated from the appropriate renormalised potentials for activated fluctuation, crossing over to free Rouse for the arms at short timescales. The backbone of an entangled H-polymer relaxes stress by ordinary Fickian diffusion of its extremities at the "early" times immediately following complete relaxation of the arms, because its renormalised structure is a simple dumbbell, not a Rouse chain. It has only one internal "fluctuation mode" which strongly interferes with its reptation mode at the terminal time. Such an approach has proved quantitative for linear rheological response of entangled model H-polyisoprenes (see Fig. 12). However, the terminal region is *highly* sensitive to polydispersity in the arm molecular weight. This is because the effective friction constant of the branch points (and so the reptation time of the "cross-bar") is exponentially dependent on M_a. This has a very much greater broadening effect on the relaxation spectrum than in the case of simple linear polymers.

The experiments on H-polymers confirm another aspect of the dynamic dilution theory for constraint release in branched polymers: the range of relaxation times clearly attributable to the arms of the H-polymers is typically much

wider than for a melt of star polymers whose arm molecular weight matches those of the Hs (compare the width of the "shoulder" region of $G''(\omega)$ in Fig. 12 – about three decades – with that of the second smallest star polymer in Fig. 9 – less than two decades). This is because now the slow cross-bar segments exponentially increase the slower relaxation times of the arms. They behave like a permanent network for all timescales earler than that of crossbar reptation (see Eq. 32).

4.2 Dendritic Polymers

If combs represent one extreme of the topological family of branched polymers, then another extreme is given by the case of dendritic polymers, which retain a branched structure at all timescales. The study of tree-like branched architectures is also motivated by the important commercial low density polyethylene (LDPE), which has remarkable rheological properties making it suitable for many processing operations [3].

4.2.1 *Cayley Tree*

A useful "toy" theoretical model which captures the essential features of self-entangled dendritic polymers is the monodisperse Cayley tree in which each chain segment branches with a fixed functionality z at each of its ends, except those at the extremity of the molecule (see Fig. 13). Smaller versions of these structures, too low in molecular weight to be entangled, have been synthesised and are usually referred-to as "dendrimers" [47].

The application of tube-theory incorporating a "dynamic dilution" model for constraint release proceeds as for the comb-polymers [48], but in this case there are as many distinct stages in the dynamic renormalisation of the molecular structure as there are levels of branching in the molecule. When there are many levels, a further approximation can be taken by working in discrete, rather than continuous, timescales – the relaxation times of the successive layers of branch points, τ_i. Considering the entangled segment connecting the i-th to the $(i+1)$-th level of the molecule as a star-arm retracting in an entanglement network whose concentration is at all times given by the concentration of *unrelaxed* segments, gives a recursion relation for the τ_i:

$$\tau_{i+1} \approx \tau_i \exp\left(\frac{2\nu M_x}{M_e}\left[\frac{(z-1)^i - 1}{(z-1)^N - 1}\right]\right) \tag{35}$$

where M_x is the molecular weight between the branch points and N here the number of levels in the Cayley tree. The constant ν is 15/8 as for star polymers. The z-dependent function in the square brackets of Eq. (35) is just the effective

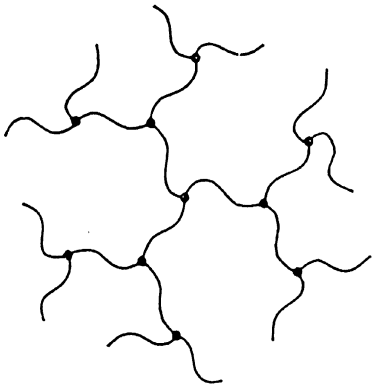

Fig. 13. The Cayley-tree model structure

concentration of entangled segments Φ_i operative at level i which dilutes the entanglement molecular weight just as for star polymers.

The hierarchy of relaxation times τ_i as a function of level i can be inverted to give an approximate form for $G(t)$ (since $G(t) \sim \Phi_i^2(t=\tau_i)$), which in the physical case of $z=2$ becomes

$$G(t) = 4G_0 \left[\ln\left(\frac{\tau_{\max}}{t} \right) \right]^{\theta} \tag{36}$$

where $\tau_{\max} \sim \tau_0 \exp(2\nu M_x/M_e)$ is the longest entangled relaxation time of the tree. θ is a "topological exponent" which in the case of the Cayley tree is 2, but assumes other values for more irregular trees (see below).

A feature of theories for tree-like polymers is the "disentanglement transition", which occurs when the tube dilation becomes faster than the arm-retraction within it. In fact this will happen even for simple star polymers, but very close to the terminal time itself when very little orientation remains in the polymers. In tree-like polymers, it is possible that several levels of molecule near the core are not effectively entangled, and instead relax via renormalised Rouse dynamics (in other words the criterion for dynamic dilution of Sect. 3.2.5 occurs before the topology of the tree becomes trivial). In extreme cases the cores may relax by Zimm dynamics, when the surroundings fail to screen even the hydrodynamic interactions between the slowest sections of the molecules.

4.2.2
Mean-Field Gelation Ensemble

Perhaps a more appealing model for a randomly branched structure such as LDPE is given by a stochastic tree in which branch points have a probability p of

occurring at the end of chain segments, and $(1-p)$ of termination [49]. This model, which leads to a naturally-polydisperse set of branched structures even when the segments between branch points are monodisperse (M_x) is also known as the Flory-Stockmayer gelation ensemble [50, 51]. It models a cross-linking ensemble of chains, but without loops, and has a gelation transition at $p=p_c=(z-1)^{-1}$, when a polymer of infinite molecular weight appears.

To model a polydisperse branched polymer melt, it suffices to keep p below p_c and to generate the concentrations of segments at each level of the disentanglement hierarchy. The term "seniority" has been coined for the effective topological level of a segment – within retraction dynamics in a polymer melt all segments of equal seniority relax on the same timescale. Conversely the concentration of segments at all higher seniorities controls the effective dilution of the entanglement network on that timescale. Because the relaxation by fluctuation of an arbitrary segment may come from either of the sub-trees it links, the seniority is controlled by the shorter of the longest paths to a free end in each sub-tree. Such a statistic can be calculated from the branching rules of any ensemble of branched polymers [49].

The result of treating the Flory-Stockmayer ensemble in this way and at the same level of approximation as that of the Cayley tree sketched in the previous section, is that a very similar relaxation spectrum to Eq. (36) is predicted, but with a value for the exponent θ of 4 rather then 2. A disentanglement transition is also found, as well as the appealing feature that at each seniority a fixed fraction of the molecules still entangled actually renormalise into *linear* polymers (like the comb topology) and relax by reptation rather than by further fluctuation [49].

The rheology of cross-linking polymer solutions and melts at the gel-point is a wide field of great interest [52] whose detail is beyond the scope of this article. However there is clear experimental evidence on the few entangled systems studied that they differ qualitatively from the universal features observed for unentangled systems at the gel point [53]. In particular, it is often reported that at the gel-point the rheology exhibits "dynamic scaling": $G(t)\sim t^{-u}$ for some dynamic exponent u. Unentangled systems follow a universal value of $u=0.67$, which can be understood via a Rouse theory for branched polymers. Scaling between cluster-size and its terminal time (which emerges from the local friction assumption), coupled with the scaling in the distribution function for cluster sizes (which is a property of both mean-field gelation and three dimensional "percolation") combine to give dynamic scaling [54]. On the other hand, there is growing evidence that for entangled systems $u=u(M_x/M_e)$ and takes in general much smaller values. Although the functional form Eq. (36) is not a power law, it may approximate closely to one over as wide a range of frequencies as used in experiments. If a power law is fitted to the exact function, the theory is then able to produce effective values for u, together with their dependence on M_x. An important prediction of such a procedure is that the exponent u should decrease as $(M_x/M_e)^{-1}$. A good deal of data on model systems is still lacking here, which would serve both to sharpen the theory of the gelation ensemble proper, and ex-

plore the appropriateness of the pre-gelation Flory-Stockmayer model for the structure of LDPE. In Sect. 6 we will see that experiments in non-linear response have begun to suggest that the approximation may be a poor one. First we examine the role of polydispersity in entanglement relaxation times in a more controlled way – via the blending of model materials of different architectures and molecular weights.

5
Experiments and Calculations on Model Blends

From the foregoing it will be clear that whenever entanglements and long chain branching are both present the dynamics in a polymer melt are highly co-operative. The orientational relaxation time of chain segments is exponentially dependent on both the contour distance to the nearest effective free end and on the effective entanglement density of its environment at all previous timescales.

A strong test of this theory is presented by a blend of two dynamically different components (but of identical local chemistry) such that the volume fraction of both is large. Two cases of especial interest suggest themselves: blends of linear with star polymers [42, 55] and blends of star polymers with widely separated molecular weights [56]. Recent work on both these systems has shed further light on the nature of co-operative constraint release and the remarkable power of the theoretical tools we now have at hand.

5.1
Star-Star Blends

A recent set of data compares the linear rheology of two monodisperse polyisoprene 3-arm stars of arm molecular weight of 28 kg mol^{-1} and 144 kg mol^{-1} together at three blend compositions [56]. The data are very remarkable: the terminal times of each component of the blend are separated by more than six decades, yet no relaxation process is identifiable with either of the two component terminal times in blends of composition 0.2, 0.5 and 0.8. Instead entirely new relaxation times emerge, between the two original terminal times, together with a great variety of relaxation spectra (see Fig. 14). Many phenomenological "blending laws" for relaxation moduli fail immediately, for they frequently work by trying to combine the two original functions $G_i(t)$ in some form at the same timescale [57]. Instead, new cooperatively determined timescales seem to arise in the blend.

Of course from a molecular point of view this is no longer surprising – we know that dynamic dilution is a highly cooperative process. However the quantitative prediction of the dynamic moduli of Fig. 14 is clearly a very demanding task for a theory with essentially no free parameters! We outline here how the tube model calculation is done in this case; for details see [56].

The initial problem arises from the fundamental "Ball-McLeish" [27] equation for the relaxation timescales along the star arms, which we write here from

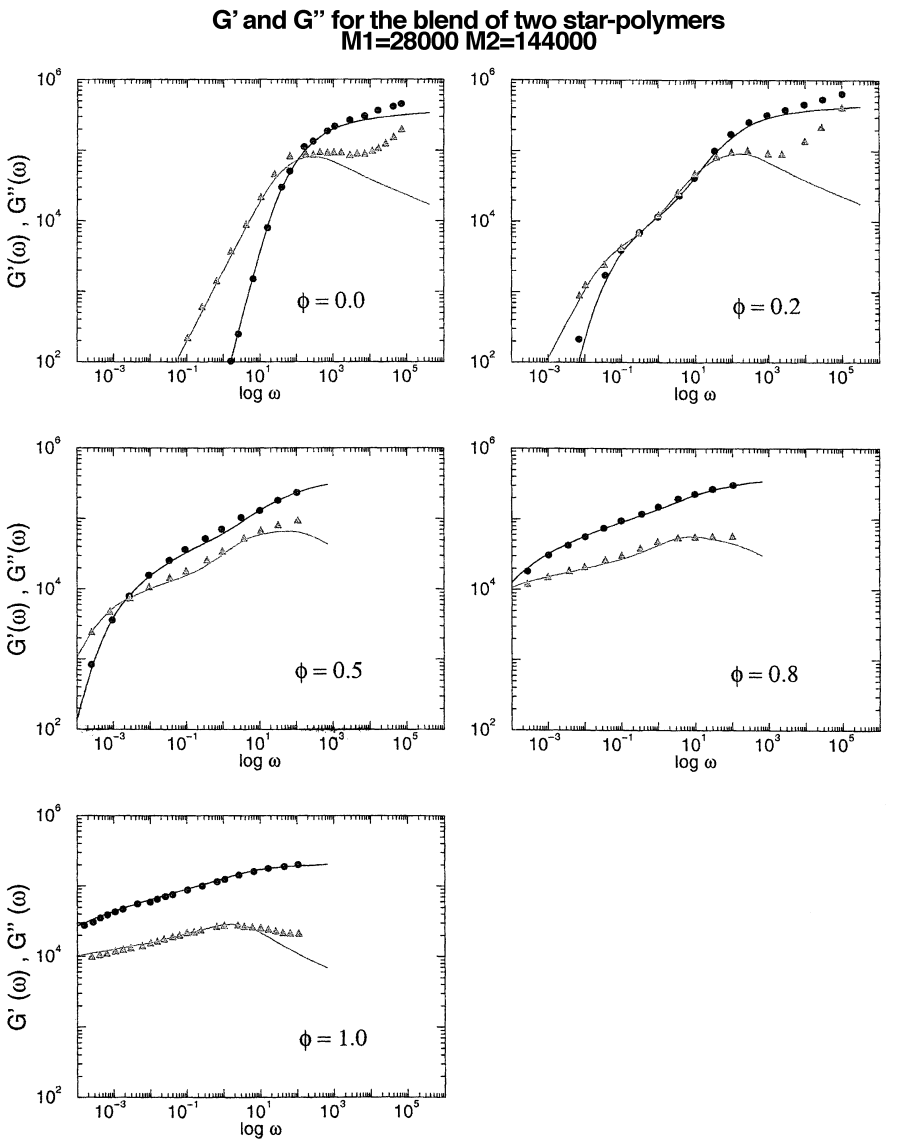

Fig. 14. Data (points) for $G'(\omega)$ and $G''(\omega)$ for a range of compositions of a blend of two polyisoprene stars of molecular weights 28 and 144 kg mol^{-1}. The fractions of the bigger star are in order 0.0, 0.2, 0.5, 0.8 and 1.0. Curves are theoretical predictions of the tube model with co-operative constraint release treated by dynamic dilution [56]. The choice of 2.0 rather than 7/3 for the dilution exponent β is compensated for by taking M_e= 5500 kg mol^{-1}

Eq. (21) in the *dimensionless* arc-length co-ordinate x for each star polymer species:

$$\frac{d\tau_i(x_i)}{dx_i} = \tau_i(x_i)\frac{15}{4}\left(\frac{M_i}{M_e}\right)x_i\Phi(x_1,x_2) \qquad i=1,2 \tag{37}$$

These two equations (one for each component) cannot be integrated simply as before because they are coupled by the dependence of the unrelaxed volume fraction Φ on both fractional primitive path coordinates x_i: $\Phi(x_1,x_2)=\phi_1(1-x_1)+\phi_2(1-x_2)$ while both stars are still relaxing. A solution is to identify a "relaxation coordinate" which is universal to both blend components. In this case, substitution of the variable $z=M_i^{1/2}x_i$ into Eq. (37) removes all explicit dependence on the arm molecular weights M_i in each equation. So z must be just such a "universal" variable (in fact such a variable can always be found – any single-valued function of the maximal free-energy explored at time t will do). Integration, taking care to respect the change in the effective entanglement network when the smaller star has completely relaxed, gives the effective potentials for each component. From this point it is straightforward to calculate the first-passage times in terms of the arclength co-ordinates, including the rapid Rouse retraction at short times, just as for the monodisperse star melt. The explicit dependence of Φ on each star's arc co-ordinate individually is used finally to calculate the relaxation modulus via the generalisation of Eq. (26):

$$G(t) = G_0\left\{2\phi_1\int_0^1 \Phi_1(x)\exp[-t/\tau_1(x)]dx + 2\phi_2\int_0^1 \Phi_2(x)\exp[-t/\tau_2(x)]dx\right\}. \tag{38}$$

To simplify the calculations the approximation $\alpha=1$ was used for the dilution exponent. Experience with monodisperse melts indicates that the effect of changing α is almost indistinguishable from an equivalent increase to the value of M_e, so the approximation was compensated for by choosing M_e=5500 kg mol^{-1}.

Results are shown against the data in Fig. 14 using parameters fixed by the chemistry and composition. The agreement is astonishingly close. The theory has predicted naturally a "motional narrowing" that arises from the blending of star polymers: while the smaller star relaxes much more slowly in the environment of the larger star arms than in its own melt, the larger star is plasticised via dynamic dilution by the smaller stars in the same blend and relaxes much faster than in its own melt. In the intermediate blend ratios, it is even possible to identify the provenance of features in the relaxation spectra by plotting the contributions from each component [56]. Checking such predictions of partial relaxation spectra would make interesting experiments on deuterated blends using IR dichroism or similar techniques.

5.2 Star-Linear Blends

Perhaps a more challenging, model system is the blend of linear and star polymers. This is a very sharp test of the physics of entanglements because typically the two fundamental processes of entanglement loss, reptation and arm fluctuation, will occur on similar timescales. We know that dynamic dilution is a valid way of treating constraint release in the presence of the second, but not the first process. What will happen in such a blend? Two data sets exist of the rheology of star-linear blends at intermediate concentrations, one for polybutadiene [58] and one for polyisoprene [42]. Both compare star polymers with linear chains of molecular weight about *twice* that of the star arm, but with different degrees of entanglement ($M_a/M_e \approx 19$ and 13 respectively). Of course the pure star melts in both cases have considerably higher viscosity than the linear melts due to their much longer terminal times. Other studies have concentrated on self-dilute stars dispersed in a linear matrix at low concentration [59,60] and have seen the expected "tube Rouse" viscoelasticity of unrelaxed star arms at long times following the reptation of the linear chains. An important observation on the higher concentration blends (both components self-entangled) is that the viscosity depends approximately exponentially on the volume fraction of star polymer from concentrations of a few percent to $\phi_{star}=1$. We now give a brief résumé of how a tube model for this system would describe the dynamics on a hierarchy of timescales.

The dynamical history of stress-relaxation in a star-linear blend begins life in just the same way as a star-star blend, because when $t<<\tau_{rep}$ the linear chain relaxation is dominated by pathlength fluctuation and behaves as a two-arm star with $M_{arm}=M_{lin}/2$. So very early Rouse fluctuation (Eq. 25) crosses over to activated fluctuation in self-consistent potentials. These are calculated via the coordinate transformation used in the star-star case above. For example, the effective potential for the star component in this regime is

$$U_{s<}(x)=\frac{15}{4}\left(\frac{M_a}{M_e}\right)\left(\frac{x^2}{2}-\frac{x^3}{3}\left(\phi_s+\phi_l\sqrt{2M_a/M_l}\right)\right) \tag{39}$$

The correction to the coefficient of ϕ_l in the dynamic dilution (cubic) term in the potential (compare Eq. 22 for the pure star case) arises from the way the difference in "arm" molecular weights affects the fraction of unrelaxed arm at the same timescale.

Unless the molecular weight of the star arm is rather low, this period of relaxation by fluctuation is generally interrupted by the reptation of the linear polymers. This happens when the centre of mass diffusion of the linear chains is able to renew the tube of all (central) portions of the chain not relaxed by the star-like modes. So the reptation time is given by

$$\tau_{rep}=\tau_e\frac{15}{4}\left(\frac{M_l}{M_e}\right)^3\left(1-x_d\sqrt{2M_a/M_e}\right)^2 \tag{40}$$

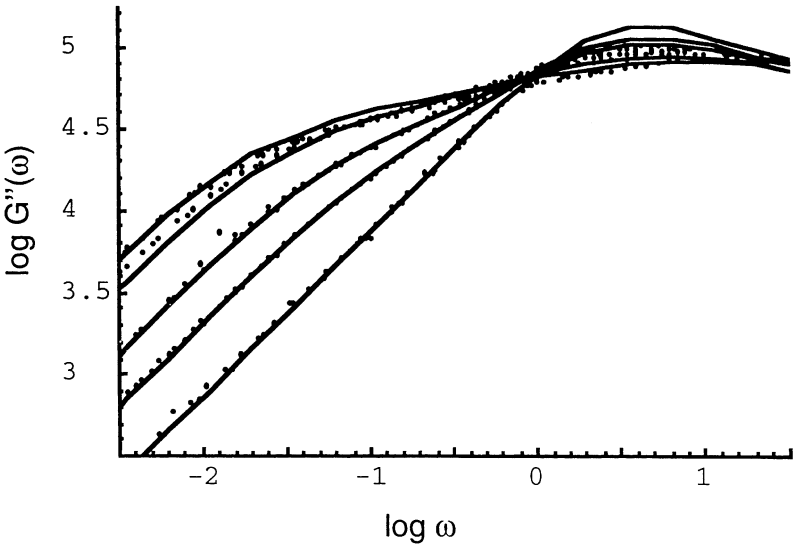

Fig. 15. Plot of $G''(\omega)$ data on PI star-linear blends superposed at 25 °C, together with theory from [42]. Fractions of star polymer ϕ_s are 0, 0.4, 0.65, 0.9 and 1.0

where the x_d is the fraction of star arm relaxed at the reptation time, itself calculated self-consistently using Eq. (40) with Eq. (39). The stress carried by the linear polymers is lost at this timescale, but equally so are the entanglements from linear chains that contributed to the tube diameter for the stars. The unrelaxed volume fraction Φ jumps suddenly from $\phi_s(1-x_d)+\phi_l(1-x_d(2M_a/M_l)^{1/2})$ to $\phi_s(1-x_d)$. This will induce an equally sudden jump in the tube diameter since $a\sim\Phi^{-\alpha/2}$. Immediately, the criterion for dynamic dilution tube retraction (Sect. 3.2.5) is violated. Now the star arms are free to relax via the "constraint release Rouse" process we have discussed before in the contexts of bimodal linear blends, comb backbones and terminal relaxation for star cores. The tube as it stood at τ_{rep} executes local Rouse hops driven by the reptation of the matrix of linear chains until a later time τ_c at which its exploration of the melt encounters the larger inflated tube created by entanglements with other star arms only. During this period of renormalised Rouse motion, the stress relaxation will be of the standard Rouse form $G(t)\sim t^{-1/2}$. If the star volume fraction is very low, the larger tube may never be encountered, but if it is, arm fluctuation resumes in a new diluted potential of

$$U_{s>}(x)=\frac{15}{4}\left(\frac{M_a}{M_e}\right)\phi_s\left(\frac{s^2}{2}-\frac{s^3}{3}\right) \tag{41}$$

This looks very similar to the pure star result, except for the dilated effective value of M_e via the ϕ_s factor. Additionally, the prefactor to the derived expression

for relaxation times $\tau(x)$ in this long-time regime needs to honour the delayed time at which dynamic dilution is regained, and so picks up an effective extra friction in this slowest regime. This extra friction just reflects the physics of the sluggish "solvent" of reptating linear chains.

The explicit appearance of the star fraction in the potential of Eq. (41) is promising – it naturally confers an exponential dependence of the terminal time and viscosity on ϕ_s as seen in the experiments. Figure 15 shows results on the PB blend for $G''(\omega)$ together with the predictions of the theory outlined above using parameters determined by synthesis and values for M_e and τ_e consistent with the literature (though again as $\alpha=1$ in this calculation a slightly higher value for M_e was used). Again the agreement is very good – if for example the intermediate constraint release Rouse process is omitted there is a substantial discrepancy. The experiments confirm an important intuition about the effective tube diameter for arm retraction: throughout the renormalised Rouse regime, arm retraction continues within the tube whose width remains as it was at τ_{rep}. This gives an insignificant contribution to stress relaxation when compared to that from the Rouse motion of the tube. Such would *not* be the case if retraction were allowed in *gradually* widening tube – this latter process would be much more effective in relaxing entanglements during the Rouse regime than the experimental data permit. But the tube diameter relevant for fluctuation is the one in which the chain has time to make unentangled loops. This takes rather longer than the time taken simply to explore the tube – so strengthening the criterion in Sect. 3.2.5 to a *strong inequality* [59].

6 Response to Large Deformations and Flows

It became clear in the early development of the tube model that it provided a means of calculating the response of entangled polymers to large deformations as well as small ones [2]. Some predictions, especially in steady shear flow, lead to strange anomalies as we shall see, but others met with surprising success. In particular the same step-strain experiment used to determine $G(t)$ directly in shear is straightforward to extend to large shear strains γ. In many cases of such experiments on polymer melts both linear and branched, monodisperse and polydisperse, the experimental strain-dependent relaxation function $G(t,\gamma)$ may be written

$$G(t,\gamma)=G(t)h(\gamma) \tag{42}$$

for all times $t>\tau_k$, a material time constant [61]. So for the longest relaxation times of the material, the non-linear viscoelastic response factorises into a time-dependence identical to that of linear deformations, and a strain-dependence $h(\gamma)$, which is known as the *damping function*. In particular, linear polymer melts have a rather weak non-linear elasticity, in which the effective modulus falls rapidly with strain in a universal way. In fact it was the success in accounting for the universal damping function that drew attention to the tube model as a

powerful simplifying tool, rather than the linear rheological response. This, as we have seen, requires a rather subtle treatment of fluctuations to operate quantitatively.

The challenge within our programme is to follow up the consequences of the tube model for the non-linear rheology of branched polymers – would such a theoretical framework lead to any understanding of the special behaviour of, for example, LDPE in complex flows? We build up our tools as before in the context of linear polymers.

6.1 Retraction on Step-Strain in the Tube Model

When large non-linear deformations are made, we need to make additional assumptions within the tube model on how the tube itself deforms with the bulk strain. The simplest, and original assumptions are that:
(i) the tube contour (primitive path) deforms affinely;
(ii) the tube diameter remains unchanged;

although other assumptions are possible [62, 63] (and see below). The first may be justified on the grounds that, by definition, the tube diameter sets the scale below which non-affine deformation of chains dominates – this concept just needs to extend into the nonlinear region. The main challenge to such an extension is the possible increased significance of elastic inhomogeneities at large strains. The second assumption is less compelling, but is motivated by the observation that the local configuration of chains is not greatly different from that at equilibrium even at large strains due to the fact that $N_e >> 1$.

When these assumptions are made, an additional mechanism for stress-relaxation arises – that of *retraction* (see Fig. 16). When a chain is embedded randomly in a deforming incompressible medium, the contour length of both chain and tube is initially increased by the rapid strain. However, when the strain stops, the stretched chain now supports a greater curvilinear tension at its centre than the equilibrium tension f_{eq} still applied to its ends by their entropic exploration of the surrounding entanglement network. So the chain retracts back along the deformed tube until its curvilinear tension returns to equilibrium, which will be achieved when it regains its equilibrium contour length. This process happens much faster than reptation for long chains because no diffusion of

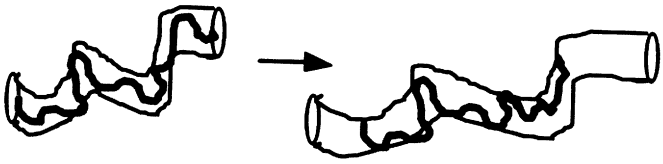

Fig. 16. Chain retraction in a tube under non-linear strain

the centre of mass of the molecule is required. Instead the retraction dynamics take the form of curvilinear Rouse motion (local friction on a connected linear object) so the contour length relaxation follows the Rouse form – $t^{-1/2}$ cut-off at the Rouse time $\tau_R \sim \tau_{mon} N^2$.

We now use this to calculate the stress in the melt *after* the retraction has occurred. The deformation is described by the tensor **E** defined so that an arbitrary vector **v** in the material is deformed affinely into the vector **E.v**. For example, in simple shear of shear strain γ, and in uniaxial extension of strain ε, the tensor **E** takes the forms

$$\begin{pmatrix} 1 & \gamma & 0 \\ 0 & 1 & 0 \\ 0 & 0 & 1 \end{pmatrix} \qquad \begin{pmatrix} \varepsilon & 0 & 0 \\ 0 & \varepsilon^{-1/2} & 0 \\ 0 & 0 & \varepsilon^{-1/2} \end{pmatrix}$$

When applying Eq. (7) to calculate the stress, the length of an entanglement strand is increased by a factor $|\mathbf{E.u}|$ where **u** is the unit vector along the strand. This needs to be inserted inside the average over all initial orientations **u**. The unit vector itself changes naturally only in direction to $\mathbf{E.u}/|\mathbf{E.u}|$. The other modification is to the concentration of entanglement strands c_a. The retraction process means that the same proportion of original entanglement strands are lost as the length retracted, so c_a is reduced along each chain by the factor $<|\mathbf{E.u}|>^{-1}$. Note that we may pre-average because a well-entangled chain explores all orientations in its tube segments.

The final result for the stress-tensor is that

$$\boldsymbol{\sigma} = kT\, c_{eq}\, \mathbf{Q}(\mathbf{E}) \tag{43}$$

where c_{eq} is the equilibrium value of c_a and the geometric tensor **Q** is defined by the orientational averages over the unit vector **u**:

$$\mathbf{Q} = \frac{1}{\left\langle |\mathbf{E.u}| \right\rangle} \left\langle \frac{\mathbf{E.u}\,\mathbf{E.u}}{|\mathbf{E.u}|} \right\rangle \tag{44}$$

The averages may be written in spherical polar co-ordinates as angular integrals, which are simple to evaluate numerically, and in some cases have analytic forms.

6.1.1 *Properties of the Q-Tensor and Consequences*

In the two classic viscometric deformations of simple shear and extension, the appropriate components of **Q** have very different behaviour. For small shear strains, the shear stress depends on the component Q_{xy}, which has the linear asymptotic form $4\gamma/15$. This prefactor is the origin of the constant ν in the tube potential of Sect. 3.For large strains, however, $Q_{xy} \sim \gamma^{-1}$, and therefore predicts strong shear-thinning. Physically this comes from the entanglement loss on re-

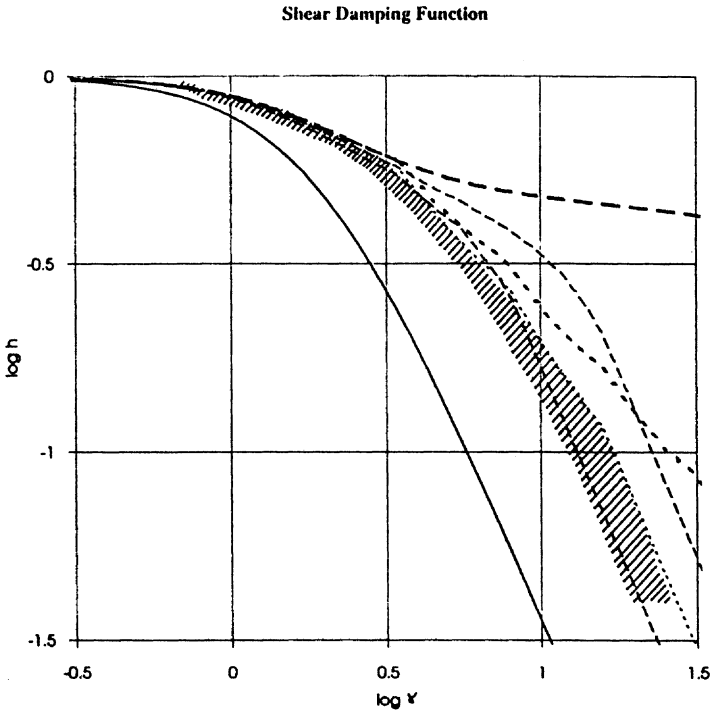

Fig. 17. Damping functions in shear from the tube model for linear polymers (*lowest curve*) and various branched architectures. In the cases of comb and tree, the *lower curves* give the case of the structure with four levels of branching, the *upper* the limit of large structures hatched area covers published results on LDPE

traction and the alignment of the remaining tube segments into the plane of the shear – away from the "x-y" direction in which they contribute maximally to the shear stress. In extension the relevant experimental component is the difference $Q_{xx}-Q_{yy}$. This is linear with extensional strain ε at low strain, but in this geometry asymptotes to a constant (15/4) at high strains because segments orient into the direction in which they contribute to the stress.

The behaviour of the **Q**-tensor in shear gives directly the damping function from its definition in Eq. (42) so that $h(\gamma)=(15/4)Q_{xy}(\gamma)/\gamma$. This function is plotted in the usual convention in Fig. 17. It is very close to results on monodisperse entangled solutions and melts [64].

6.1.2 *Damping Functions for Branched Polymers*

The process of chain retraction can be applied to more complex topologies of entangled polymers under the same assumptions discussed for linear polymers

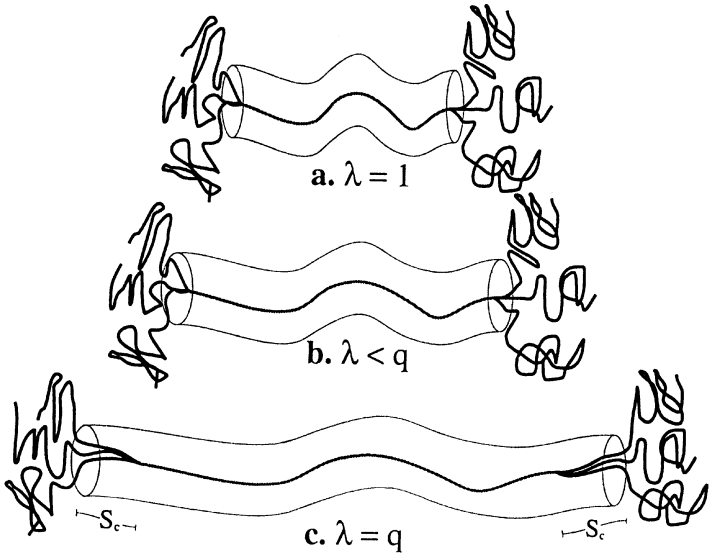

Fig. 18a–c. Tube-model diagrams of the low-frequency model for the "pom-pom" architecture: **a** the unstretched molecule; **b** under deformation such that the cross-bar has been stretched by a factor less than the number of arms; **c** under deformation such that the backbone has been stretched by a factor greater than the number of arms, initiating "branch-point-withdrawal"

[65]. In the case of star polymers retraction may proceed just as for linear chains, and the damping function is expected to be of the universal "Doi-Edwards" type. This has been confirmed experimentally [61]. However for polymers with higher levels of branching the situation is different. In spite of being stretched along its contour by a large bulk strain, a segment one level further into a branched molecule than the outermost arms cannot in general retract, because this would mean drawing those outer segments into its tube. It may only do this when its tension exceeds the sum of the (equilibrium) tensions in the impeding arms – a criterion only met beyond a critical strain. This strain will be proportional to the number of arms attached at the outermost branch point, because of the Hookean elastic response of the chain's entropic tension. This process is illustrated in Fig. 18 for a polymer composed of two three-arm stars joined by a long linear "cross-bar". When the tension in the cross-bar is increased via a bulk strain to the sum of the equilibrium tensions of the dangling arms, and not before, the arm configuration may be partially collapsed and the branch points withdrawn into the tube originally occupied by the cross-bar.

In a manner akin to the hierarchical relaxations in a highly branched polymer, this new form of retraction via "branch point withdrawal" also happens hi-

erarchically, though as a function of strain rather than time. A segment two levels into the molecule may only retract when its tension exceeds that of all the first level segments attached to it, and so on. As a consequence of this balance of entropic tensions, the strain at which any segment withdraws its outermost branch point (and so the functional form it contributes to the strain dependence) just depends on the number of free ends at the edge of the tree it is connected to that withdraws first (we recall that any segment in a branched polymer is connected to two trees). This statistic (of the lesser number of free ends of the two trees) has been termed the "priority" distribution [65], in analogy with the "seniority" distribution which controls the relaxation times. In general a branched molecule has different seniority and priority distributions – a knowledge of the former is required to predict the linear stress-relaxation function, of the latter to predict the non-linear strain response. A general formula giving the damping function in terms of the priority distribution of an arbitrary branched melt is given in [65].

Predictions of the damping function (defined now as the effective modulus after all rapid (Rouse) retractions have occurred) for both Cayley tree and comb architectures are shown alongside the Doi-Edwards function in Fig. 17. It is immediately apparent that the damping functions are only "universal" for a particular topology of polymer, and may eventually be useful in characterising branched melts. Results on LDPE are also shown, indicating that the structure is more likely to be tree-like than comb-like within this picture. Though very appealing, this is probably pushing the tube model as far as one ought to, if not a little further.

An important, and startling, prediction is that for most monodisperse branched structures, time-strain factorability will be lost. Hence the careful definition of the damping function we adopted above. As we already saw for the related H-polymer structure, a melt of the model polymer in Fig. 18 will behave as a diluted and slowed down system of entangled *linear* chains at times much longer than the longest relaxation time of the arms. So the non-linear response in step strain at these timescales must be described by the (much more thinning) Doi-Edwards damping function! The strain response exhibits a higher effective modulus at short times than at long times in nonlinear step strain.

Very recent experiments on H-polymer melts have confirmed this expectation [46], together with a subtle and interesting feature: the *stretch* relaxation time depends itself rather strongly on strain. The higher the strain, the sooner is the transition from a rubbery to a Doi-Edwards strain thinning. For high strains beyond the level at which branch point withdrawal occurs this is not difficult to understand as the dangling segments which control the effective drag on the branch points are smaller. However, even at smaller strains the branch point will tend to withdraw the dangling arms by up to one entanglement length. This is not a minor perturbation to the effective drag on the branch point because of its exponential dependence on the dangling primitive path length (the underlying dynamics are those of an entangled star arm). This partial retraction is however the sort of assumption that requires more than rheological measurement to con-

firm satisfactorily. In this case, small angle neutron scattering on quenched strained samples was able to contribute direct structural evidence that small translational rearrangements of branch points do occur for all strains [46].

Given the clear observation of non-factorable $G(t,\gamma)$ in model monodisperse branched polymers, the puzzle which then arises is to explain why the highly branched LDPE *does* exhibit time-strain factorability. Experiments and calculations on branched melts with controlled polydispersity will be the next stage, since it is known that summing the response of intrinsically-nonfactorable rheological models with a sufficiently broad range of relaxation times can lead to an overall response that is indistinguishable from a factorable one [66]. This would explain the factorable behaviour of LDPE.

6.1.3 *Strain Dependence of the Tube*

It is of interest to think about relaxing the assumptions (i) and particularly (ii) introduced at the beginning of Sect. 6.1, although hard experimental tests for specific assumptions of the deformation of the tube constraint itself can never be confined to rheology alone, but will involve at least careful analysis of neutron-scattering experiments [46, 63]. Not only might the tube diameter depend on the local strain, the localising field described by the tube may well take on an anisotropy consistent with the symmetry of the bulk strain. For discussions of how tube variables deform with strain see [67, 68]

Reasons have been advanced for both an increase and a decrease of the tube diameter with strain. A justification of the former view might be the retraction process itself [38]. If it acts in a similar way to the dynamic dilution and the effective concentration of entanglement network follows the retraction then $c_{eff} \sim <|\mathbf{E.u}|>^{-1}$ so that $a \sim <|\mathbf{E.u}|>^{1/2}$. On the other hand one might guess that at large strains the tube deforms at constant tube volume La^2. The tube length must increase as $<|\mathbf{E.u}|>$, so from this effect $a \sim <|\mathbf{E.u}|>^{-1/2}$. Indeed, Marrucci has recently proposed that both these effects exist and remain unnoticed in step strain because they cancel [69]! Of course this is far from idle speculation because there is another situation in which such effects would have important consequences. This is in conditions of continuous deformation, to which we now turn.

6.2 Constitutive Equations for Continuous Flow

The step-strain experiments discussed above furnish the simplest example of a strong flow. Many other flows are of experimental importance: transient and steady shear, transient extensional flow and reversing step strains, to give a few examples. Indeed the development of phenomenological constitutive equations to systematise the wealth of behaviour of polymeric liquids in general flows has been something of an industry over the past 40 years [9]. It is important to note that it is not possible to derive a constitutive equation from the tube model in

closed form without making rather uncontrolled mathematical assumptions – indeed this suggests that the space of non-Newtonian constitutive behaviour is rather larger than that spanned by compact sets of differential or integral equations. However, the behaviour of the tube model for linear polymers in steady shear flow has recently become very important in the study of "living" polymers (whose chains continually break and reform in dynamic equilibrium), and in particular wormlike surfactant micelles [70, 71]. A further challenging area is in the special elongational behaviour of highly branched polymers [3].

6.2.1
Linear Polymers in Continuous Flow

The essential picture of stress arising from occupied and deformed tube segments carries over naturally to the case of continuous flow. Tube segments are born at chain ends, are carried by diffusion along the chain during which time they are stretched and oriented, and die when they are passed again by a chain end. Thus to calculate the stress a knowledge of the survival probability function *p(s,t)* just as in Eq. (11) is required in the form of *p(s,t,t')*, the probability that a segment born at time *t'* still exists at time *t* at contour co-ordinate *s* along the occupying chain. Equation (9) for *p* is now modified by the *convection* of the chain past the tube segment by the flow as well as by the curvilinear diffusion. We assume that the flow rates are less than the inverse retraction time so that the chain length is constant. If *v(s)* is the relative velocity of tube and chain (due to the extension of the tube by the flow past the constant-length chain), then Eq. (9) becomes

$$\left[\frac{\partial}{\partial t} - D_c\frac{\partial^2}{\partial s^2} + v(s,t)\frac{\partial}{\partial s}\right]p(s,t,t') = 0 \tag{45}$$

where *v(s,t)* arises from the extension rates of all the segments from the centre of the chain to the point *s*. If any segment has an orientation **u** then its local rate of increase in length if deformed affinely in the flow is **K:uu** where **K** is the velocity gradient tensor. So *v(s,t)* in Eq. (45) is itself given by

$$v(s,t) = \int_0^s ds'\,\mathbf{K}(t):\int \mathbf{u}(s')\mathbf{u}(s')f(\mathbf{u},s',t)d^2\mathbf{u} \tag{46}$$

The probability distribution *f(***u***,s,t)* for the local segment distribution is related to the contribution from the ensemble of segments at *s* to the total stress. It is calculated self-consistently from the survival probability function by letting the surviving tube segments be deformed by the total deformation tensor over their lifetimes, **E***(t,t')*:

$$f(u,s,t) = \int_{-\infty}^{t} dt\int d^2\mathbf{u}'\,\delta(\mathbf{u}-\mathbf{u}')\mathbf{E}(t,t').\mathbf{u}'\frac{\partial}{\partial t'}p(s,t,t') \tag{47}$$

The stress tensor can now be written as

$$\sigma(t) = \frac{15}{4} G_0 \frac{1}{L} \int_{-L/2}^{L/2} ds \int d^2\mathbf{u}\,\mathbf{uu}\, f(\mathbf{u},s,t) \tag{48}$$

This full set of self-consistent equations is clearly very difficult to solve, even numerically. However, good approximations of closed integral type have been proposed. These essentially ignore the *s*-dependence of the survival and orientation functions, which makes them a *physically* appealing approach in the case of wormlike surfactants [71, 72]. For ordinary monodisperse polymers the following approximate integral constitutive equation results:

$$\sigma = \frac{15}{4} G_0 \int_{-\infty}^{t} dt' \left(\frac{\partial}{\partial t'} \mu_{DE}(t-t') \right) \mathbf{Q}(\mathbf{E}(t,t')) \tag{49}$$

where $\mu_{DE}(t)$ is the Doi-Edwards relaxation function of Eq. (12). The remarkable feature shared by this constitutive set and its approximations is that the stress in steady shear is non-monotonic. This has been used to explore the unstable and inhomogenous flows in both Poiseuille ("spurt effect") [73] and Couette ("shear-banding") [71, 74] flows. The non-monotonic behaviour in ordinary polymer melts is still debated, but it now seems clear that this phenomenon does exist in entangled solutions of living polymers, thanks to flow-field visualisation by NMR-imaging [75] and birefringence [76]. The consequences of such a constitutive instability for an apparent multiplicity of possible bulk flow fields under the same imposed conditions still represents a severe current challenge to theory [77].

If the ideas of Marrucci [69] are correct and the non-monotonic predictions of the simple Doi-Edwards theory need to be modified in the case of polymer melts (for a recent development see [78]), then an explanation will be required for the apparent difference at high shear rates between melts and wormlike micelle solutions. There is also evidence that ordinary entangled polymer solutions do exhibit non-monotonic shear-stress behaviour [79]. As in the field of linear deformations, it may be that a study of the apparently more complex branched polymers in strong flows may shed light on their deceptively simple linear cousins.

6.2.2
Constitutive Equations for Branched Polymer Melts

A current challenge for molecular rheology is the continuous flow of highly branched polymers [3, 66]. The central issue is that in both uniaxial and planar extensional flows, LDPE is strain-hardening [12] (stress grows faster than linearly with strain over some range of strain and time in a time-dependent flow), while retaining a softening characteristic in shear. It has proved impossible to fit

simultaneously all the flow behaviour of LDPE with existing integral-type phenomenological constitutive equations (of similar form to Eq. 49 above), even qualitatively [80]. This is because such equations rely on employing restrictive functionals of the flow history to calculate the stress, considered as the primary dynamic variable. Although this approach guarantees frame-invariance by making their kernel functions depend only on invariants of the strain history; planar extension and shear possess the same invariant structure arising from the 2-dimensionality of the flows. However, the insights of the special molecular features of long-chain-branched polymers under high strain, and in particular the delayed retraction and branch-point withdrawal processes, make a molecular approach doubly appealing.

Very recently, the continuous flow theory of this section and the theory for branched molecules in Sect. 4 have been combined in a constitutive theory for a class of model branched polymers related to the H-structure, but now with an arbitrary number of arms, q, attached at each end of a cross-bar [81] (Fig. 18). For a wide range of flow rates, the cross-bar may be oriented and stretched, while the dangling arms remain isotropic due to their much faster relaxation dynamics. Thus important contributions to the stress arise only from the cross-bars. However the arms play an important role: when the cross-bar becomes highly stretched as in an extensional flow, branch-point withdrawal diminishes the size of the frictional "blob" of dangling arms, which in turn reduces very rapidly the effective frictional drag of the branch points. The result, after some simplification, is that the average stretch of the cross-bar, $\lambda(t)$, and its averaged orientation-tensor, $\mathbf{S}(t)$, each follow coupled dynamic equations, with a characteristic relaxation time for each: τ_s and τ_b respectively [45]. These may be thought-of as the Rouse and reptation time for the cross-bars as renormalised linear polymers.

$$\begin{aligned} &\frac{\partial}{\partial t}\lambda = \lambda(\mathbf{K}:\mathbf{S}) - \frac{1}{\tau_s}(\lambda - 1) \\ &\mathbf{S}(t) = \int_{-\infty}^{t} \frac{dt}{\tau_b(t')} \exp\left\{\int_{t'}^{t} (t'')\right\} \mathbf{Q}(t,t') \end{aligned} \tag{50}$$

The relaxation times vary with time itself only when the backbone becomes full-stretched (λ=q), and then in such a way as to maintain this maximum stretch until the flow no longer tends to stretch the molecules further. The history of relaxation time τ_b needs to be taken into account in the integral part of the dynamic equations, just as for wormlike micelles [72]. The stress itself is a function of both molecular variables:

$$\boldsymbol{\sigma}(\mathrm{t}) = (15/4) G_0 \, \phi_b^2 \, \lambda^2(t) \, \mathbf{S}(t) \tag{51}$$

with corrections arising from the configuration of the dangling arms in a more refined version [81]. In the set of Eqs. (50) and (51) we have the pleasing structure of a stress calculated at each time from a number of molecular variables,

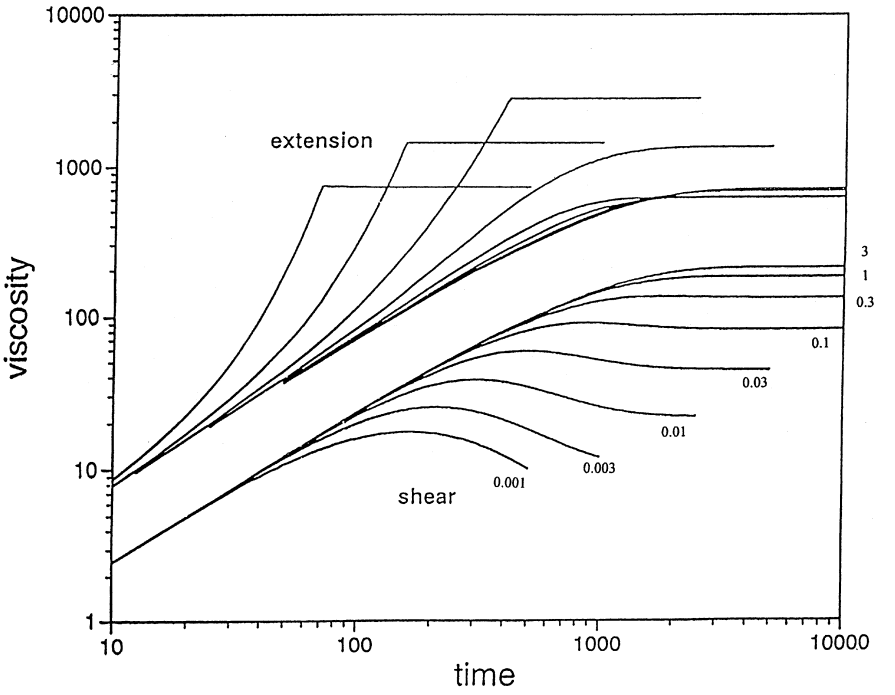

Fig. 19. a Predicted "startup-flow" in extension and shear for the constitutive equation derived for a "pom-pom" polymer with q=5. Stress divided by the strain-rate is plotted (so that early time response is rate-independent) against time after initiation of the flow for a range of dimensionless rates from 0.001 to 3. Both axes are logarithmic

each following their own (coupled) dynamics. This feature gives such a constitutive formulation the same qualitative features of extensional and shear flows of LDPE (see Fig. 19), and succeeds in combining extreme shear-softening in shear together with large strain hardening in extension. Moreover the three important geometries of flow are correctly ordered, with both planar and uniaxial extension exhibiting similar behaviour, while shear belongs with the data in a special class of its own.

How has the molecular model managed to escape from the straightjacket of frame-invariance which seemed to force the most general phenomenologies to predict similar responses in planar extension and shear? The answer lies in the separation of timescales: the molecular picture does not see the stress itself as a fundamental variable, but reveals it as the natural product of a scalar and tensor (the latter of unit trace) with the physical interpretations of segmental stretch and orientation respectively. It is then possible to endow these two variable with *different* relaxation times; the tradition in phenomenological theories has been to treat the stress tensor as a whole, possessing a single relaxation time. Moreover, it is the *entangled* nature of the high-priority segments which provides the

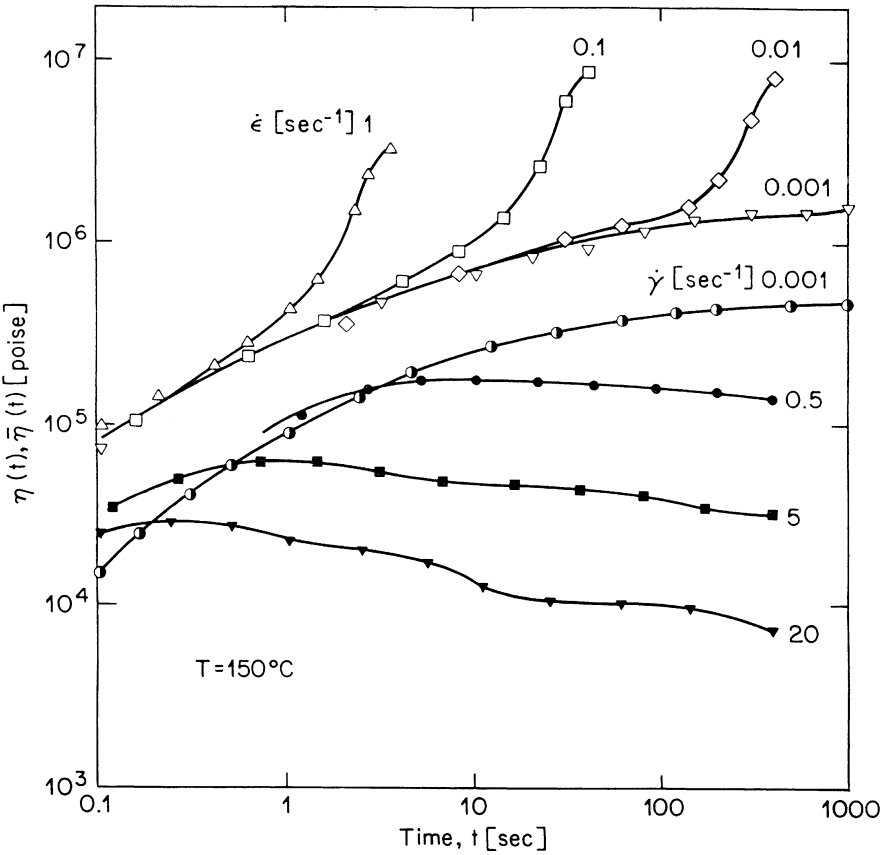

Fig. 19. b Experimental results in startup flow in shear and extension on branched LDPE from Meissner [3]. The qualitative nature of the response in the two flows is remarkably similar to the pom-pom model in (a)

separation in timescales. When the cross-bar of the model molecule is only one entanglement long, τ_s and τ_b become equal, and the model is indistinguishable from simple "elastic dumbbell" [9] theories, except for the existence of a maximum permitted stretch. However, as the degree of entanglement increases, so does the ratio τ_b/τ_s since the former arises from reptation – a diffusive motion in the tube, and the latter from forced drag, a Rouse motion. More complex topologies of branched polymer will have the orientation of "deep" segments (of high priority) controlled by activated diffusion like star-arms, which will lead to an even sharper separation in timescales as a function of degree of entanglement.

Initial indications are that a multi-mode version of Eqs. (50) and (51) can be useful at a quantitative level in modelling an extensively-investigated LDPE for all geometries of flow [82]. Matching only the linear viscoelastic relaxation spectrum, and adding a segment priority distribution consistent with that derived

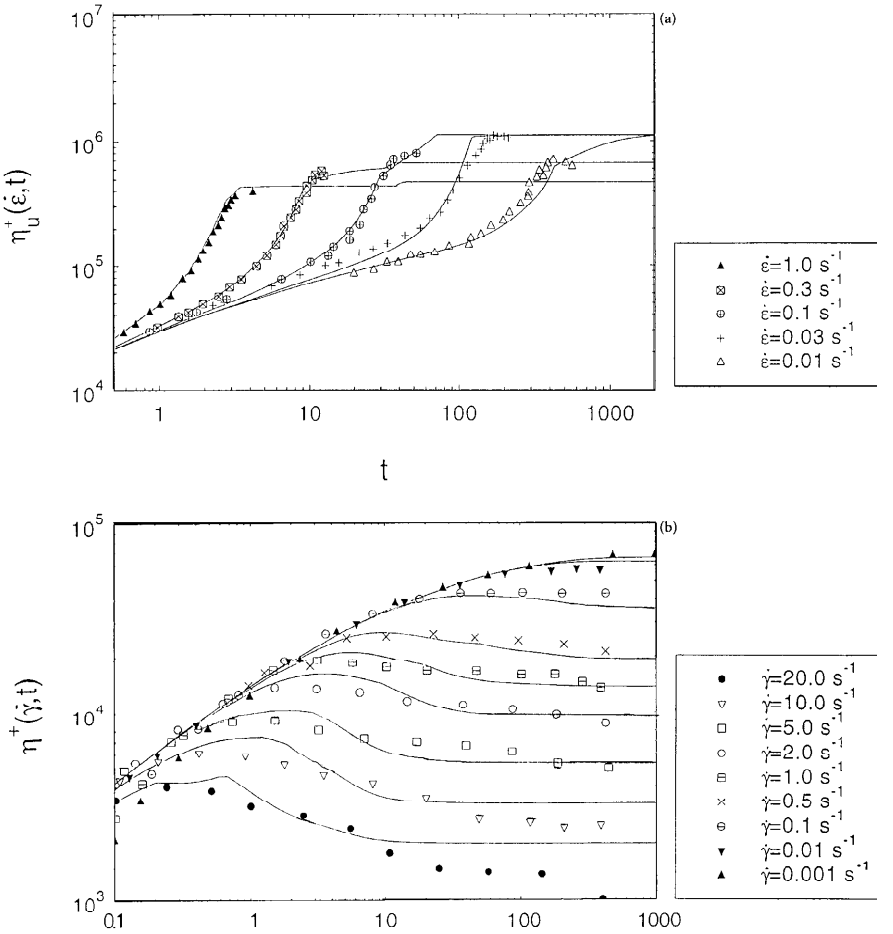

Fig. 20a,b. Transient data in: **a** extension; **b** shear on LDPE from [81] modelled with a multimode version of the "pom-pom" constitutive equation. The linear modes (of weights and relaxation times τ_b) have been "decorated" with the structure of pom-pom elements (adding values of τ_s and q to each mode)

theoretically from a random branching model [65] (which gives $f(m) \sim m^{-2}$) already gets the shape of the time-dependent hardening in extension correct over extension rates which vary over three orders of magnitude. As the segment priority increases, so the ratio of timescales for stretch and orientation approaches unity. This is also anticipated physically as a consequence of the greater dynamic dilution of the slowest relaxing segments – they possess a higher effective value of M_e at the timescales of their own relaxation than are the faster segments. Naturally, there is as good an agreement with the data in planar as in uniaxial flows but an unassured surprise is that the entire field of transient shear data is cor-

rectly predicted by such a model after all choice of free parameters has been exhausted (see Fig. 20). It is too early to say how far such a quantitative programme can be taken, or whether a more nuanced theory of coupled interactions between segments at different priorities within the same molecule will be essential.

6.2.3 *Molecular Constitutive Equations for Polymer Melts in Viscoelastic Flow Solvers*

The constitutive behaviour discussed above in both weak and strong flows is nonetheless restricted to "simple flows" in which the deformation rate tensor is spatially uniform. Many important rheological applications of polymer melts of course arise in flows that are far from simple: converging flows into dies, helical flows in extruders, free-surface flows as in fibre or film production. A molecular theory for rheological response is a necessary, but not sufficient, tool for predicting and controlling the effect of molecular variables on complex flow phenomena. A good example is found in the famous vortex growth in branched polymer melts seen in Fig. 1. Another level of calculation is required, that takes the *local* physics embodied in a molecular constitutive equation and computes the consequences under the additional imposition of conservation of mass and momentum together with the boundary conditions of a complex flow. This is not the place to review the great range of methods which have been used to attack this challenging problem of *non-Newtonian* fluid mechanics, particularly as most of this work has been directed to the solution of phenomenological models (but see e.g. [83]). However, there have recently been a number of considerable advances in a particularly appropriate type of flow solver for molecular approaches, namely *Lagrangian* solvers [84–86]. Rather than discretise the spatial domain by a fixed grid, the lattice of finite elements moves and deforms with the flow. Careful application of this technique seems to permit the attainment of high deformation rates (in terms of the fluid relaxation time) without numerical instability, and compares well with fixed-grid methods. A great advantage is that its data structure is easily adapted to carry physical "hidden" variables (such as the orientation and stretch of the pom-pom molecules) on the co-moving fluid elements themselves.

Of course it would be desirable to avoid all mathematical coarse-graining of a constitutive equation in such an approach, carrying tiny Brownian simulations of actual polymer molecules along with the flow. However this is numerically prohibitive in computer time in the case of polymer melts. Some remarkable progress has been made in the case of model polymer *solutions* [87], where the molecules can be suitably sparsely spread in the flow. Conversely, large simulations have been made of ensembles of linear entangled polymers [88], but these, while impressive, have barely reached fractions of the reptation time of their model polymers. While providing useful numerical calculations of the properties of the effective entanglement tubes, the regime of viscoelastic flow is still quite out of reach.

So in the world of polymer melts, the intermediary of a constitutive equation, or equation set, albeit molecularly derived, would seem unavoidable at present. The success of the branched-polymer model discussed above would suggest that

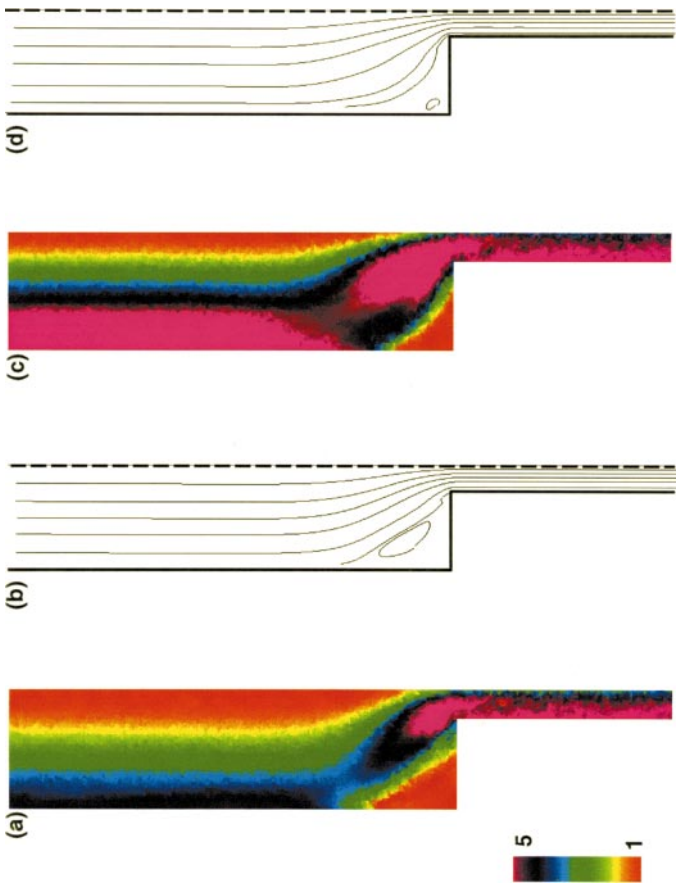

Fig. 21a–d. Flow from startup into a 4:1 contraction computed for the "pom-pom" model with fixed total and cross-bar molecular weight and Weissenberg number (dimensionless deformation rate) of 3[(a) and (b)] and 8 [(c) and (d)]. (a) and (c) show (colour coded) the level of dimensionless stretch of the pom-pom cross-bar, λ. (b) and (c) show the respective streamlines. Note the "spur" of preoriented material joining the wall to the funnel and the reduction of the corner vortex at high flow rates when extension thinning sets in. (Computations courtesy of Dr. T. M. Nicholson)

the pom-pom Eqs. (50) and (51), with their physical branching parameter q, would be good candidates for an attempt at contraction flow computations in Lagrangian solvers. This has been attempted very recently, and has indeed discovered a strong growth of recirculating vortices in a contraction flow [89]. Figure 21 shows streamlines and a representation of the spatial field of molecular stretch, λ, for a 4:1 contraction flow of a five-armed "pom-pom" melt. Not only do we see vortex growth, but it becomes apparent that the high extensional hardening of the stretching molecular cross-bars is responsible for it. Interest-

ing transient overshoots in stretch are also predicted, as are initially counter-intuitive predictions for the off-axis position of the maximum molecular stretches. The latter phenomenon has actually been seen in birefringence measurements in flowing polymer melts [90]. Via the molecular model we see that it arises from the pre-orientation of molecules near the wall by the shear flow there, which predisposes them to very rapid stretching by the extensional flow into the contraction. This combination of steady shear and extension is more effective at stretching the cross-bar segments than the centreline history of benign convection followed by brief but rapid extension. Clearly there is a need at this point to apply hard tests to such calculations in complex flows in the same way that has been possible in simple flows. The constraint here is really the double one of restrictions in the quantities of well-characterised model materials *vs* the engineering challenge of miniaturising flow devices. Progress on both fronts may soon lead to a capability to perform some remarkable experiments of this type.

7 Conclusions

This is probably a good point to conclude our account of this story to date. We have made one iteration of a loop in the qualitative comparison of Figs. 1 and 20. Clearly there is a long way to go before we can apply these tools and ideas to a stochastically-branched and polydisperse polymer melt. However, the molecular approach to the dynamics of entangled polymers outlined here has proved remarkably fruitful, and has accounted for a very wide range of phenomena, some initially very puzzling. The central role of molecular topology continues to grow in its appeal. There are still many open challenges of which a few might be the following questions.

(i) Is the prediction of a stress-maximum in the shear flow of linear (and some branched) polymers pathological in the case of melts, and if so what is the correct molecular physics that is missing? What is the role of tube deformation?
(ii) Are our conjectures about the validity of dynamic dilution for constraint release valid, and how should they generalise to non-linear flows?
(iii) Is the extension to non-linear flows of branched polymers outlined here valid and what experimental tests of it are the best to devise? Can the level of quantitative success enjoyed by the tube model in linear deformation be extended to highly non-linear deformations?

Finally, there lies the obvious challenge of employing these ideas in the design of future commercial polymers. If this is at all successful in the future, and it will only be so in an atmosphere of open partnership of industrial and academic scientists and engineers, it will have proved a very satisfying and complex example of the interaction of pure and applied science, as well as of physics, chemistry and engineering.

8 References

1. Ferry JD (1986) Viscoelastic properties of polymers. Wiley, New York
2. Doi M, Edwards SF (1986) The theory of polymer dynamics. Oxford
3. Meissner J (1975) Pure Appl Chem 42:551–574
4. Quack G, Hadjichristidis N, Fetters LJ, Young RN (1980) Ind Eng Chem Prod Res Dev, 1 9:587
5. Fetters LJ, Kiss AD, Pearson DS, Quack GF, Vitus FJ (1993) Macromolecules 26:647
6. (a) Roovers J (1984) Macromolecules 17:1196; (b) Hakiki A, Young RN, McLeish TCB (1996) Macromolecules 29:3639
7. Roovers J, Graessley WW (1981) Macromolecules 14:766
8. (a) Struglinski MJ, Graessley WW (1985) Macromolecules 18:2630; (b) Struglinski MJ, Graessley WW (1986), Macromolecules 19:1754; (c) Struglinski MJ, Graessley WW, Fetters LJ (1988) Macromolecules 21:783
9. Larson RG (1988) Constitutive equations for polymer melts and solutions. Butterworths, Boston
10. Feigl K, Oettinger H-C (1994) J Rheol 38:847
11. Bernstein B, Kearsley EA, Zapas LJ (1963) Trans Soc Rheol 7:391
12. Laun HM, Schuch H (1989) J Rheol 33:119
13. de Gennes PG (1971) J Chem Phys 44:572
14. Tirrell M (1984) Rubber Chem Technol 57:523
15. Baumgartel M, Schausberger A, Winter HH (1990) Rheol Acta 29:400
16. Rubinstein M, Colby RH (1988) J Chem Phys 89:5291
17. Cates ME (1987) Macromolecules 20:2289
18. Higgins JS, Benoit H (1995) Neutron scattering of polymers. Oxford
19. (a) Higgins JS, Roots JE (1985) J Chem Soc, Faraday Trans II 81:757; (b) Ewen B, Richter D (1997) Adv Polym Sci 134:1
20. Muller R, Pesce JJ, Picot C (1993) Macromolecules 26:4356
21. Read D (1997) PhD thesis, University of Leeds
22. Utracki LA, Roovers J (1973) Macromolecules 6:366
23. (a) Roovers J (1991) Macromolecules 24:5895; (b) Vlassopoulos D, Pakula T, Fytas G, Roovers J, Karatasos K, Hadjichristidis N (1997) Europhys Lett 39:617
24. (a) de Gennes PG (1975) J Phys (Paris) 36:1199; (b) Doi M, Kuzuu NY (1980) J Polym Sci, Polym Lett Ed 18:775
25. Pearson DS, Helfand E (1984) Macromolecules 19:888
26. Marrucci G (1985) J Polym Sci Polym Phys Edn 23:159
27. Ball RC, McLeish TCB (1989) Macromolecules 22:1911
28. Viovy JL, Rubinstein M, Colby RH (1991) Macromolecules 24:3587
29. (a) des Cloizeaux J (1988) Europhys Lett 5:437; (b) des Cloizeaux J (1991) Macromolecules 23:3992
30. Tsenoglou C (1988) J Polym Sci: Part B: Polym Phys 26:2329
31. Colby RH, Rubinstein M (1990) Macromolecules 23:2753
32. Adam M, Delsanti M (1984) J Phys Fr 45:1513
33. Milner ST, McLeish TCB (1997) Macromolecules 30:2159
34. Fetters LJ, Lohse DJ, Richter D, Witten TA, Zirkel A (1994) Macromolecules 27:4639
35. Clarke N, McLeish TCB (1993) Macromolecules 26:5264
36. Doi M (1983) J Polym Sci Polym Phys Edn 21:667
37. Rubinstein M (1987) Phys Rev Lett 59:1946
38. Deutsch JM, Madden TL (1989) J Chem Phys 91:3252
39. O'Connor NPT, Ball RC (1992) Macromolecules 25:5677
40. Ketzmerick R, Öttinger H-C (1989) Continuum Mech Thermodyn 1:113
41. Milner ST, McLeish TCB (1998) Phys Rev Lett

42. Milner ST, McLeish TCB, Johnson J, Hakiki A, Young RN (1998) Macromolecules
43. Yurasova TA, McLeish TCB, Semenov AN (1994) Macromolecules 27:7205
44. McLeish TCB, O'Connor KP (1993) Polymer 34:2998
45. McLeish TCB (1988) Macromolecules 21:1062
46. McLeish TCB, Allgaier J, Bick DK, Bishko G, Biswas P, Clarke N, Groves DJ, Hakiki A, Heenan R, Johnson JM, Kant R, Read D, Young RN (1998) (in preparation)
47. Boris D, Rubinstein M (1996) Macromolecules 29:7251
48. McLeish TCB (1988) Europhys Lett 6:511
49. Rubinstein M, Zurek S, McLeish TCB, Ball RC (1990) J Phys (Paris) 51:757
50. Flory PJ (1953) Principles of polymer chemistry. Cornell University Press, Ithaca, New York
51. Stockmayer WH (1944) J Chem Phys 38:355
52. Lairez D, Adam M, Emery JR, Durand D (1992) Macromolecules 25:286
53. Mours M, Winter HH (1996) Macromolecules 29:7221
54. Rubinstein M, Colby R (1990) In: Ohta M (ed) Space-time organisation in molecular systems. Springer, Berlin Heidelberg New York
55. Struglinski MJ, Graessley WW, Fetters LJ (1988) Macromolecules 21:783
56. Blottière B, McLeish TCB, Hakiki A, Young RN, Milner ST (1998) Macromolecules
57. Utracki LA (1989) Polymer alloys and blends. Hanser
58. Struglinski MJ, Graessley WW, Fetters LJ (1988) Macromolecules 21:783
59. Roovers J (1987) Macromolecules 20:148
60. Watanabe H, Yoshida H, Kotaka T (1988) Macromolecules 21:2175
61. Osaki K (1993) Rheologica Acta 32:429
62. Wagner M (1994) J Rheol 38:655
63. Straube E, Urban V, Pyckhout-Hinzen W, Richter D, Glinka CJ (1995) Phys Rev Lett 74:4464
64. Osaki K, Nakamura H, Kurata M (1982) Macromolecules 15:1068
65. Bick DK, McLeish TCB (1996) Phys Rev Lett 76:2587
66. Larson RG (1987) J Non-Newt Fluid Mech 23:249
67. Read D, McLeish TCB (1997) Macromolecules 30:6376
68. Rubinstein M, Panyukov S (1997) Macromolecules 30:8036
69. Marrucci G (1996) J Non-Newt Fluid Mech 62:279
70. Cates ME (1990) J Phys Chem 94:371
71. Spenley NA, Cates ME, McLeish TCB (1993) Phys Rev Lett 71:939
72. Cates M (1997) In: McLeish T (ed) Theoretical challenges in the dynamics of complex fluids. Kluwer, Dordrecht
73. (a) McLeish TCB, Ball RC (1986) J Polym Sci Polym Phys Edn 24:1735; (b) McLeish TCB (1987) J Polym Sci Polym Phys Edn 25:2253
74. Berret J-F, Porte G, Decruppe J-P (1997) Phys Rev E, 55:1669
75. Britton MM, Callaghan PT (1997) Phys Rev Lett 78:4930
76. Berret JF, Roux DC, Porte G (1994) J Phys II 4:1261
77. Olmsted PD, Lu C-YD (1997) Phys Rev E 56:56
78. Mead DW, Doi M, Larson RG (1998) Macromolecules (submitted)
79. Vinogradov G (1973) Rheol Acta 12:273
80. Samurkas T, Larson RG, Dealy JM (1989) J Rheol 33:559
81. McLeish TCB, Larson RG (1998) J Rheol 42:81–110
82. Inkson N, Harlen OG, McLeish TCB (1998) J Rheol (submitted)
83. Denn MM (1990) Annu Rev Fluid Mech 22:13
84. Rasmussen HK, Hassager O (1993) J Non-Newt Fluid Mech 46:63
85. Yuan XF, Ball RC, Edwards SF (1993) J Non-Newt Fluid Mech 46:331
86. Harlen O, Rallison JM, Szabo P (1995) J Non-Newt Fluid Mech 60:81
87. Öttinger H-C (1995) Stochastic processes in polymer fluids. Springer, Berlin Heidelberg New York
88. Kremer K, Grest G (1995) In: Binder K (ed) Monte Carlo and MD simulations in polymer science. Oxford

89. Bishko G, McLeish TCB, Harlen OG, Larson RG (1997) Phys Rev Lett 79:2452
90. Ahmed R, Liang RF, Mackley MR (1995) J Non-Newt Fluid Mech 59:129

Received: June 1998